Valorisation of recycled glass: novel catalytic routes for water purification

Thesis submitted to the University of Sheffield for degree of Doctor of Philosophy in Science

Mengyuan Qian

Department of Chemistry

July 2024

Authors Declaration

I, the author, confirm that the Thesis is my own work. I am aware of the University's Guidance on the Use of Unfair Means (www.sheffield.ac.uk/ssid/unfair-means). This work has not been previously been presented for an award at this, or any other, university.

Acknowledgement

Abstract

This research made an extensive use of Catalytic Wet Peroxide Oxidation (CWPO) techniques by using recycling glass as a catalyst for the abatement of organic pollutants namely phenol, ibuprofen, benzyl alcohol and 1-phenylethanol to CO_2 and water or by selectively oxidizing them.

Based on the composition of recycled glass, other than main compositions, it also contains metal compounds such as MnO_2 or Cr_2O_3 and Fe_2O_3 about 1 wt.%, which fall in the range of other metal-doped catalysts. Experiments showed that Fe^{3+} has the largest activity in triggering the generation of ·OH in comparing to Cr^{3+} and Mn^{2+}. ICP showed negligible fluctuations between samples made it a robust catalyst system, and the glass colour and feedstock variability will not influence the catalyst performance. XPS results revealed that more Fe is distributed at the surface (0.5 at.%) rather than the bulk (0.1 at.%), this reflects the iron propensity to readily oxidize facilitates migration of Fe from the bulk to the surface as Fe_2O_3 over time.

This study successfully demonstrated the concept of using of recycled glass (green and brown) containing Fe^{3+} centres as a heterogeneous catalyst for phenol and ibuprofen oxidation by CWPO. The results have indicated that decreasing the size of the glass particles leads to increased phenol conversion and carbon dioxide production with the size range of 0.1 - 0.5 mm showing the best catalytic activity. It enables the possibility of a scale-up application in the industry. As a result, the performance of recycled glass can be comparable and promising (i.e., 100% phenol and ibuprofen conversion and 20% CMB, low metal leaching (less than 0.2 wt.%)) to industrial catalyst, namely Fe/ZSM-5 under appropriate reaction conditions (increased mass and longer reaction time) for an overall much lower (about 3000 times) cost. This approach closes the material loop through high-value recycling, further extending the life cycle of these resources and as such reduces the need of new input of energy demanding raw materials.

Although the selective oxidation of benzyl alcohol and 1-phenylethanol was not fully achieved, these results represent a valuable fundamental investigation, providing key insights to guide future optimisation of reaction conditions and improvements in selectivity.

This research marks a significant step forward in sustainable water treatment technologies by using waste materials in innovative ways. This approach not only addresses critical environmental issues but also aligns with the global shift towards a circular economy. The

Abstract

findings have promising implications for both water management and chemical manufacturing industries, offering a cost-effective, sustainable, and scalable solution to some of the most pressing environmental challenges of our time.

Thesis Content

List of Abbreviations

Activated Carbon	————	AC
Advanced Oxidation Processes	————	AOPs
Acetophenone	————	AP
Benzoic Acid	————	BA
Benzaldehyde	————	BzH
Biological Oxygen Demand	————	BOD
Circular Economy	————	CE
Carbon Mass Balance	————	CMB
Chemical Oxygen Demand	————	COD
Catalytic Wet Peroxide Oxidation	————	CWPO
1,2-Dichloroethane	————	1,2-DCE
Dichloromethane	————	DCM
Dimethyl Sulfoxide	————	DMSO
Emerging Organic Contaminants	————	EOCs
Environmental Protection Agency	————	EPA
Equation	————	Eq.
External Standard Method	————	ESTD
Food and Agriculture Organization	————	FAO
High Performance Liquid Chromatography	————	HPLC
Ibuprofen	————	IBU
Inductively Coupled Plasma Optical Emission Spectroscopy	————	ICP-OES
Inductively Coupled Plasma	————	ICP
Inductively Coupled Plasma Mass Spectrometry	————	ICP-MS
Internal Standard Method	————	ISTD

Abbreviations

Liquid Crystal Display	———————	LCD
Membrane Bioreactor	———————	MBR
Metal: substrate molar ratio	———————	M:S
Nuclear Magnetic Resonance	———————	NMR
National Pollutant Release Inventory	———————	NPRI
Nonsteroidal Anti-inflammatory Drugs	———————	NSAIDs
1-Phenylethanol	———————	1-PEA
Potential of Hydrogen ($-\log_{10}[\mathrm{H}^+]$)	———————	pH
Persistent Organic Pollutants	———————	POPs
Propylene Oxide and Styrene Monomer	———————	POSM
Pharmaceuticals and Personal Care Products	———————	PPCPs
quantitative Nuclear Magnetic Resonance	———————	qNMR
Radiofrequency	———————	RF
Scanning Electron Microscope	———————	SEM
Signal-to-noise Ratio	———————	SNR
Styrene and Propylene Oxide	———————	SPO
Triethanolamine	———————	TEA
2,2,6,6-Tetramethylpiperidine-1-oxyl	———————	TEMPO
Trifluoroacetic Acid	———————	TFA
Total Organic Carbon	———————	TOC
Ultraviolet	———————	UV
Ultraviolet-visible	———————	UV-Vis
United Nations	———————	UN
US Environmental Protection Agency	———————	USEPA
Wet Air Oxidation	———————	WAO

Abbreviations

World Health Organization	————————	WHO
Wastewater Treatment Plants	————————	WWTPs
X-ray Photoelectron Spectroscopy	————————	XPS
X-ray Diffraction	————————	XRD
X-ray Fluorescence	————————	XRF

Chapter 1 Introduction

1.1 Global freshwater deficiency crisis

Water is fundamental for life on Earth. It is essential to sustainability in energy and food production, healthy ecosystems, and the survival of the human race. However, the world's freshwater supplies are becoming increasingly limited due to the growing human population and, in turn, the increase in demand for the use of natural resources. This poses a challenge as society must balance commercial demands with the need to conserve water resources to satisfy a growing global population.[1] The disposal of large amounts of untreated wastewater into rivers, lakes, aquifers and coastal waters is causing a deterioration in the quality of freshwater resources. According to the United Nations (UN), 2 million metric tonnes of sewage and other effluents are discharged into water bodies every day. Freshwater shortage has been reported for approximately one-sixth of the world's population.[2] This resource deficiency promotes the spread of serious human diseases and affects water quality. Therefore, it has become one of the main challenges that our society is facing in the 21st Century. Urgent action is required, especially when human health is threatened, food production is limited, ecosystem functions are weakened, and even economic growth is hampered or impeded. Providing safe fresh water for all is a complex task that has been extensively researched for decades. Various processes and measures have been developed to address this issue.[3]

Ranked second only to fresh drinking water, access to a secure food supply is crucial. Agriculture is undeniably a core part of the global economy. Crops and livestock farming provide a significant amount of nutrients for humanity. However, their production requires substantial resources such as water, energy, and land.[4] The current world population exceeds 7.8 billion and is increasing by more than 330 thousand per day. The United Nations has projected a global population of approximately 10 billion people by 2057.[5] Due to this population growth, there will be a further and considerable reduction in water availability per person, which will cause stress to the biodiversity of the universal ecosystem. The Food and Agriculture Organization (FAO) reports that despite an increase in production every year, food supplies (cereal grains) per capita have declined due to the growth in human population and the lack of fresh water and cropland. Agriculture is the largest consumer of clean water resources, using approximately 70% of fresh water worldwide.[6] For comparison, producing 1 kg of cereal grain requires about 1000 litres of water, while 1 kg of beef requires up to 40,000 litres of water.[4]

In light of these challenges, an increasing number of countries are turning to regenerated

water, which is treated wastewater that has been deemed suitable for a new use, as an alternative means of securing and enhancing agricultural yields. Regenerated water offers an opportunity to replace finite freshwater resources for uses that do not require the same level of quality as drinking water. To reduce the cost of high-quality water treatment, the 'fit-for-purpose' approach has been established, which involves setting water-quality objectives based on the end user's requirements. Reused water applications have the potential to benefit agricultural and landscape irrigation, industrial regeneration, ground water recharge, and ecological purposes. [7] This approach aligns with various legislations and guidelines, such as the WHO's guidelines for using wastewater in agriculture and aquaculture.[8] Agriculture remains the most common application for regenerated water.[5] Therefore, a reliable water supply is essential to alleviate the pressure and uncertainties of clean water scarcity. As an example, in Australia, the benefits of reusing water have become apparent in the agricultural sector despite the scarcity of freshwater.[9] Another example is Singapore's water purification program includes five "NEWater" purification plants that meet approximately 40% of the nation's water needs.[10]

Despite the benefits of regenerated water for food supply, to have sustainable agriculture remains a significant challenge. Agriculture must maintain adequate food supply while also addressing potential environmental, socioeconomic, and human health impacts in accordance with national plans. The terrestrial ecosystem plays a crucial role in the water cycle (Figure 1.1) by vegetation transpiring into the atmosphere. This accounts for approximately 64% of all precipitation that returns to the land globally.[11] Additionally, the water absorbed by plants eventually returns to the atmosphere as surface or ground water, despite some loss through evaporation. In summary, agriculture can both contribute to and suffer from water pollution. However, poor agricultural practices can lead to the transfer of toxic contaminants and the deposition of pollutants into surface and subterranean water sources. This can result in soil degradation, salinization, and waterlogging of irrigated land. It is then important to implement sustainable agricultural practices to prevent these negative impacts on the environment as agriculture relies on a symbiotic relationship between land and water. As the FAO (1990a) makes quite clear, "... appropriate steps must be taken to ensure that agricultural activities do not adversely affect water quality so that subsequent uses of water for different purposes are not impaired".[6]
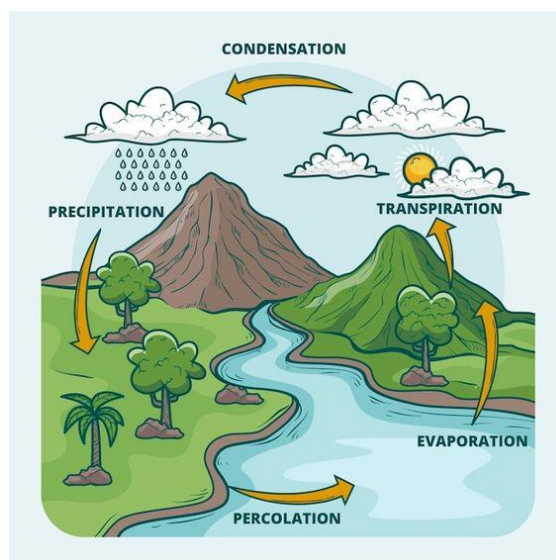
Figure 1.1 Schematic of water cycle. Reproduced from Freepik with permission[12] It is a continuous process in which water evaporates from the Earth's surface, condenses in the atmosphere as clouds and returns to the surface as precipitation, while also moving through living organisms and groundwater.

1.2   Organic contaminants of emerging concern

Despite the critical scarcity of freshwater resources, the practice of irrigation is further complicated by concerns over the use of regenerated water. This water often contains organic contaminants that pose significant threats to human health and environmental integrity. Emerging organic contaminants (EOCs) have been identified in groundwater sources impacted by agricultural and urban activities. These contaminants include a wide range of compounds, including pesticides and their degradation products, pharmaceuticals, industrial chemicals, personal care products, fragrances, water treatment by-products, flame retardants, surfactants, and lifestyle substances such as caffeine and nicotine. Wastewater containing inadequately treated chemicals, which are identified as being of high concern under the European chemicals regulation REACH,[13] contribute to the contamination of crops. These chemicals can accumulate in the edible parts of fruit and vegetables when used for irrigation, posing a risk to both consumers and agricultural workers.[14,15] The increasing recognition of these substances, previously undetected or considered insignificant, as significant threats to aquatic ecosystems and human health, underlines the urgent need for preventive measures to prevent their entry into the food chain. As a result, there is an urgent need for strict regulation of agricultural irrigation practices to mitigate chemical hazards. This scenario places water managers in a challenging position, with the dual objectives of increasing food production and reducing water waste and pollution, all in the context of adapting to climate change.

With increasing concern about water quality, particularly in the context of agricultural irrigation,

the detection of emerging organic contaminants (EOCs) such as anti-inflammatory drugs (ibuprofen and diclofenac), caffeine and phenol has become more widespread. These substances are of particular concern because of their high toxicity, strong corrosivity, unpleasant odours and slow biodegradability, which have significant adverse effects on both human health and ecological systems. This situation highlights the urgent need for effective management strategies to manage the presence of EOCs and minimise their adverse effects on irrigation water quality and the overall health of ecosystems. Furthermore, in anticipation of new environmental standards being introduced for an expanded list of EOCs in the near future, it is crucial to deepen our understanding of their environmental behaviour. Such knowledge is essential for the development of informed policies and practices to protect water resources and ensure sustainable agricultural practices in the face of these emerging challenges.

Phenol, an organic pollutant, has received considerable attention as a priority toxic pollutant, recognised by the US Environmental Protection Agency (EPA) since 1977 and listed as a pollutant in Canada's National Pollutant Release Inventory (NPRI) since 1995. Its prominence in scientific and regulatory studies is due not only to its inherent toxicity and widespread occurrence in industrial activities (plastics and resins production, petrochemicals, pharmaceuticals, herbicides and pesticides, dyes and pigments), but also to its role as an intermediate (petroleum refining, coal gasification, chlorinated phenols) or by-product in the oxidation of higher molecular weight aromatic compounds (polycyclic aromatic hydrocarbons).[16] It is estimated that over 10 million metric tonnes of phenol are released into the environment each year.[17] In view of these considerations, phenol is often used as a model pollutant in research focused on organic wastewater treatment strategies. Its chemical properties, particularly its stability and persistence due to its aromatic nature, pose challenges in its removal, transformation and disposal. Consequently, in this thesis, phenol is used as a benchmark contaminant for initial studies, which will form the basis for subsequent investigations of other organic contaminants such as ibuprofen, benzyl alcohol and 1-phenylethanol (Figure 1.2).
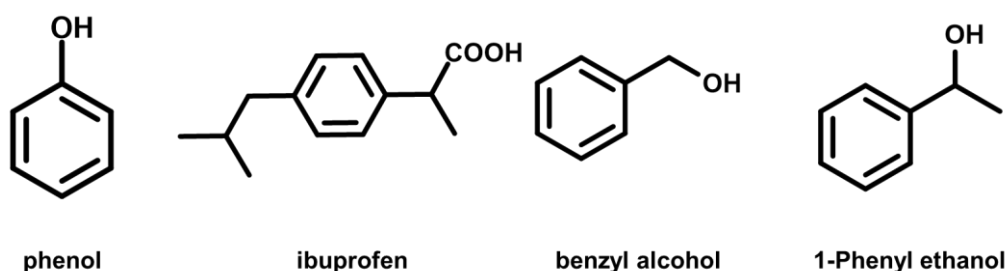
Figure 1.2 Molecular structures of phenol, ibuprofen, benzyl alcohol and 1-phenylethanol.

1.3   Methods of removing organic contaminants in wastewater

Plants are often used to concentrate and isolate contaminants due to their widespread growth and ability to absorb chemicals from the atmosphere, water, and soil. However, consumption of contaminated plants either by humans or animals or other species may pose a potential health risk that has not yet been fully understood. Therefore, due to a rapidly increasing population and prolonged droughts and floods caused by the depletion of water resources, freshwater has become a scarce resource in many parts of the world. There is a pressing need to develop cost-effective and efficient materials and methods to remove contaminants from wastewater in order to address the challenge of supplying an adequate amount of clean water. This section outlines some widely used technologies that have been introduced in recent decades for water purification.

1.3.1   Biological treatment technologies

Biodegradation is the process by which microorganisms, fungi, and enzymes break down pollutants in the environment into smaller, and most often fewer toxic compounds. This process occurs naturally, but in recent decades it has also been applied deliberately in wastewater treatment to ensure clean water resources. Biological methods have received more attention than chemical and physical methods due to their apparent economic and ecological advantages.[18] The effectiveness of biodegradation, however, depends on the nature of the contaminants.[19] However, persistent organic pollutants (POPs) and xenobiotic organic contaminants, such as heterocyclic compounds and pharmaceuticals, are resistant to most biological treatments due to their high bioaccumulation and bio-toxicity properties. These substances can only be degraded chemically; either aerobically anaerobically.[20]

1.3.1.1 Aerobic biodegradation

On the other hand, organic pollutants can be efficiently degraded under aerobic conditions with the help of aerobic bacteria. These bacteria use enzymes which are part of the oxygenase family to oxidize pollutants and produce energy during cellular respiration. The activated sludge reactor and membrane bioreactor (MBR) are common types of aerobic biodegradation reactors.[21]

Activated sludge is a wastewater treatment process that utilises air and a biological floc consisting of bacteria and protozoans. It is important to note that this process should be objectively evaluated for its effectiveness in treating sewage and industrial wastewater. This technique can efficiently eliminate organic, nitrogenous substances and phosphate from polluted water sources when sufficient oxygen is introduced with proper hydraulic retention

time. However, wastewater often lacks oxygen or has a limited amount of it, leading to a common issue known as sludge bulking. This issue can have a negative impact on the quality of the effluent after treatment.[22] While the addition of oxygen through aeration equipment can improve the oxidation efficiency of biological treatment systems, the capital and operating costs associated with such equipment may outweigh its benefits, especially for smaller treatment facilities. In addition, the excess biomass produced by an activated sludge process requires proper handling and disposal, which can be a significant economic burden. Sludge management, including dewatering, stabilisation and final disposal or reuse, is often a major part of the total operating costs of wastewater treatment plants. If not properly managed, the accumulation and disposal requirements for this excess sludge can reduce the feasibility and sustainability of activated sludge systems.

Compared to the sludge technique, MBR is less dependent on oxygen in the water. It is widely used for industrial wastewater treatment. MBR has similarities to activated sludge, but the use of a membrane makes the whole process significantly more effective.[23] However, membrane fouling during the treatment process adversely impacts the performance of MBR.[24] This leads to a significant increase in trans-membrane pressure, prolonging the hydraulic resistance time and increasing energy consumption. Eventually, the treatment and replacement of uncleaned membranes will result in increased operational costs.[25]

1.3.1.2 Anaerobic biodegradation

Anaerobic digestion is a process in which microorganisms decompose biodegradable substances without the presence of oxygen. These processes have often been criticised for being slow and inefficient.[26] However, it is important to note that they can regenerate energy when reducing Chemical Oxygen Demand (COD) and Biological Oxygen Demand (BOD). In addition, organic contaminants (e.g., polycyclic aromatic hydrocarbons and diethylhexyl phthalate[27,28]) with high molecular weight are difficult to decompose using aerobic processes, but can be decomposed using anaerobic bacteria. Anaerobic treatments are highly effective in addressing high loads of small degradable organic molecules, such as effluents from sugar, food, and paper industries.[29] Therefore, research and applications of anaerobic mineralization remain important for contaminated water treatment.

1.3.2 Physical treatment technologies

Adsorption technology has been applied to wastewater treatment as a cleaner purification and separation technique with high efficiency. This process is mainly achieved through the contaminant (adsorbate) in the effluent and its solid adsorbent, which then physically removes the pollutant from the contaminated water matrix. The effectiveness of adsorption is highly

dependent on the performance of the material used as adsorbent, which has to be porous, possess large surface areas (200-2000 m^2 g^{-1} [30]) and can selectively retain molecules on the solid surface. Adsorption has been widely used for removing metals (lead, cadmium, and mercury)[31,32] and both coloured (textile dyes)[33] and colourless (phenolic compounds, pesticides, and pharmaceutical residues)[34] organic contaminants.

Adsorption can be classified into two types: physisorption and chemisorption. The main difference between them is that physisorption involves van der Waals forces, while chemisorption involves a stronger interaction in the energy range of chemical bonds. Physisorption does not involve electron exchange and occurs quickly due to the easy working conditions, requiring, practically, no activation energy. In contrast if chemisorption occurs the process may be irreversible.

Activated carbon (AC) is the most used material for wastewater treatment. It can be prepared from various sources, including peat, black ash, and charcoal. Different preparation methods result in two main physical forms of activated carbon: granular or powder, which are used in adsorption columns or during batch filtration, respectively.[35,36] The high internal surface area and pore volume of AC make it an excellent adsorbent, as well as a good catalyst, or support. [37]

Some disadvantages of AC are its high regeneration costs,[38] non-selectivity, and lower thermal stability. Zeolites, a large group of minerals that contain hydrated aluminosilicates of sodium, potassium, calcium and barium, are a valid alternative as a substitute adsorbent.[39] They can be easily dehydrated or rehydrated and are widely used in applications such as adsorbents, ion-exchangers, molecular sieves or catalysts. The exceptional adsorptive properties of zeolites are due to their chemical composition, which provides a vast effective surface area.[40] Some commonly used synthetic zeolites include MCM-22, ZSM-5,[41,42] BETA[43] and Y[44]. Synthetic zeolites have been shown to outperform natural zeolites in eliminating ink, dyes and contaminants from wastewater.[45,46]

1.3.3 Chemical treatment technologies

Although biological processes work in certain context, the efficiency of the processes, such as activated sludge and MBR, in removing a broad range of emerging organic contaminants from effluents after treatment has been called into question.[47–49] Treatment technologies such as activated carbon oxidation, nanofiltration, and reverse osmosis membranes, which were originally introduced, are not sufficient for treating synthetic and complicated contaminated water containing personal care products, pharmaceuticals, surfactants, various industrial additives, and multiple chemicals. Furthermore, studies have shown that physicochemical

processes such as flocculation,[50] coagulation,[51] or lime softening[52] though effective for the removal of metals, are ineffective in removing pharmaceuticals. Therefore, traditional water treatment technologies are outdated for efficiently removing a wide range of toxic organic contaminants.

Chemical oxidation technologies are a more advanced method compared to previous ones. This methodology uses oxidants such as H_2O_2, O_3, ClO_2 and $KMnO_4$ to decompose organic pollutants into less hazardous compounds or transform them into forms that are easier to treat. However, the degradation effectiveness of processes that use oxidants like hydrogen peroxide without a catalyst is low. Advanced oxidation processes (AOPs) use the principle of utilizing the greater reactivity of hydroxyl radicals to boost the overall efficiency of the oxidation process. AOPs hold great promise for the development of technologies for wastewater treatment. For instance, they have been utilised in applications to degrade and mineralise organic contaminants, such as pharmaceuticals (e.g. carbamazepine, benzocaine, diclofenac, and ibuprofen),[53] agrochemicals (e.g. triallate, triclosan, and oxadiazon),[54] and phenolic substances (e.g. phenol and chlorophenols).[55–57] These processes are considered sustainable as long as they are less expensive than those that require demanding reaction conditions and additional post-treatment for used catalysts, such as contaminated activated carbon.[58] Several technologies fall into this category, including Fenton and derived reactions, photo-Fenton, wet oxidation, ozonation, and photocatalysis, which all use different sources of radicals.[56,59–62]

1.3.3.1 Wet Air Oxidation and Catalytic Wet Air Oxidation

Wet air oxidation (WAO) is a technique for reducing pollutants that involves using air or pure oxygen as an oxidant to treat contaminated water. This method is used when the water is either too dilute in contaminants for incineration or too concentrated for biological treatment. The Zimmermann-designed WAO was first introduced in the late 1950s, with initial applications at Zimpro (now Siemens Water Solutions).[63] The oxidation reactions typically occur at temperatures ranging from 150 °C to 320 °C and at pressures of 10 to 220 bar. The working conditions are determined by the targeted contaminations; for example, higher temperatures require higher pressure to maintain a liquid phase in the system. These demanding conditions result in increased treatment costs. In addition, the WAO process alone cannot completely mineralise organic pollutants. Small molecular intermediates, such as methanol, ethanol and acetic acid, are resistant to further oxidation. Therefore, an additional step after pre-treatment WAO is necessary. Catalytic wet air oxidation not only requires milder operating conditions, but also facilitates further mineralisation of the intermediates with the help of catalysts. Although the cost of the process depends on the wastewater conditions, catalytic wet air oxidation is generally less expensive than non-catalytic WAO (50% less).[64–66]

Heterogeneous catalysts, including metal oxides containing noble metals, have received significant attention for reducing the cost of post-treatment separation steps.[67,68]

1.3.3.2 Oxidation using hydrogen peroxide

Hydrogen peroxide is an environmentally friendly oxidant that can effectively oxidise organic contaminants in a cost-effective manner, it can decompose to ultimately generate water, the greenest solvent and by-product. It acts as a powerful oxidation reagent during a reaction, where $\cdot OH$ has a standard reduction potential of 2.80 V (Eq. 1.1) which is higher than H_2O_2 itself (Eq. 1.2). Direct oxidation of many organic substances in waste effluents is possible. Hydrogen peroxide is an effective disinfectant and pre-oxidising agent for drinking water due to its slow decomposition rate under mild processing conditions. This allows the hydrogen peroxide to remain active and effective for a longer period, thus enabling a prolonged activity and gradual oxidation throughout the treatment process. H_2O_2 can decompose into highly reactive hydroxyl radicals ($\cdot OH$) as shown in Equation 1.3. However, this same slow decomposition rate can be disadvantageous when attempting to remove organic substances from wastewater, as the goal is to rapidly degrade organic pollutants. Therefore, a faster decomposition rate of hydrogen peroxide is preferred to ensure efficient and effective oxidation and removal of organic substances. In order to generate hydroxyl radicals at the requisite rate for the large-scale abatement of pollutants, it is necessary to employ either UV radiation or a catalyst. The Catalytic Wet Peroxide Oxidation process is then employed, which involves catalysing the oxidation process with catalysts. Reactions can occur at mild conditions like at atmospheric pressure within a temperature range of 20-80°C.

$$\cdot OH + e^- \rightarrow OH^- \ (2.80 \text{ V}) \qquad \text{(Eq. 1.1)}$$
$$H_2O_2 + 2H^+ + 2e^- \rightarrow 2H_2O \ (1.78\text{V}) \qquad \text{(Eq. 1.2)}$$
$$H_2O_2 \rightarrow 2\cdot OH \qquad \text{(Eq. 1.3)}$$
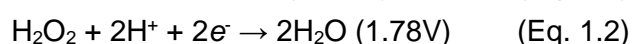
1.3.3.3 Fenton reaction

Fenton oxidation process with Fe^{2+} as the catalyst and H_2O_2 as the oxidant, is a core theme of research and the most popular technique. This process is attractive due to the abundance of non-toxic iron and the ease of handling and decomposition of H_2O_2 into environmentally friendly products, namely water and oxygen. As compared to other AOPs, Fenton's reagent requires relatively milder operating conditions (100°C, ambient pressure) and a simple experimental set-up compared to other oxidation techniques. Therefore, the degradation of refractory organic compounds such as drugs has always been considered to be most sustainable and ideal through this process.[76]

The generation of hydroxyl radicals in situ from the decomposition of hydrogen peroxide is the

key to the Fenton reaction, as these radicals are highly unstable and reactive oxidising agents capable of oxidising organic and inorganic compounds. Fenton's reagent has been extensively studied in recent decades since its proposal in 1894.[69] Fenton discovered that ferrous ions have interesting oxygen transfer properties that promote the oxidation of tartaric acid by hydrogen peroxide. This process produces hydroxyl radicals with high oxidation ability through catalytic H_2O_2 decomposition with the assistance of Fe(II). Fenton's process (Figure 1.3) involves the reaction between the oxidant H_2O_2 and the catalyst iron ions, resulting in the formation of highly active radicals, primarily the ·OH radicals with a reduction potential of 2.8 V.
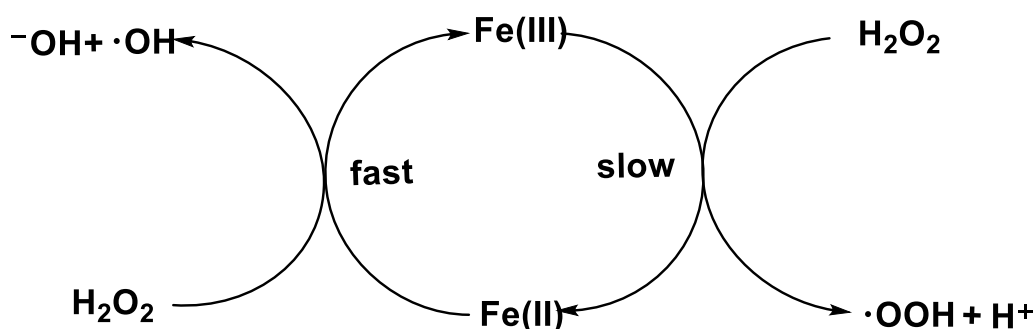
Figure 1.3 Fenton's process involves the fast reaction between the oxidant H_2O_2 and the Fenton's reagent Fe^{2+}, resulting in the formation of highly active radicals, primarily the ·OH radicals with an oxidation potential of 2.8 V. A slower reaction between Fe^{3+} with an extra H_2O_2 to regenerate Fenton's reagent: Fe^{2+}

Equation 1.4 and Equation 1.5 demonstrate this process. The catalyst iron (II) is regenerated at the end of the process.

$$H_2O_2 + Fe^{2+} \rightarrow Fe^{3+} + HO^- + \cdot OH \quad \text{(Eq. 1.4)}$$
$$Fe^{3+} + H_2O_2 \rightarrow Fe^{2+} + \cdot OOH + H^+ \quad \text{(Eq. 1.5)}$$
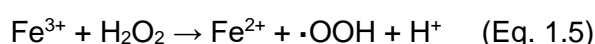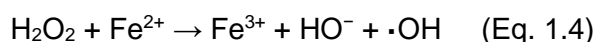
The reaction occurs at a very high rate ($k = 70 \text{ M}^{-1} \text{ s}^{-1}$)[70] at 25 °C and triggers a series of chain reactions. This is due to the interaction between ferrous iron and hydrogen peroxide, which leads to the formation of hydroxyl radicals as hydrogen peroxide is converted.

The Fenton-like reaction (Eq. 1.5,[70–73]) reduces the ferric ions produced in the reaction by excess hydrogen peroxide, regenerating ferrous ions and maintaining an efficient cyclic mechanism. Large amounts of reactive radicals such as ·OH and ·OOH are produced as a result of the first two reactions (Eq. 1.4 and Eq. 1.5). Organic pollutants can be attacked by these radicals, and broken down into smaller molecules, oxygenated chemicals or even CO_2 and H_2O. It is worth noting that the Fenton reaction (Eq. 1.4, k = 63-76 $M^{-1}s^{-1}$ [72,74]) is generally faster than the Fenton-like reaction (Eq. 1.5, $k = 1.0 \times 10^{-3}$ - 1.0×10^{-2} $M^{-1}s^{-1}$ [72,74]). Furthermore, hydroperoxyl radicals ($E^0(\cdot OOH/H_2O_2)$ = 1.50 V) are less reactive than hydroxyl radicals

$((E^0(\cdot OH/H_2O) = 2.73$ V$))$.[72,74,75]

When free radicals react with ferric ions (Eq. 1.6), they can reduce Fe^{3+} back to Fe^{2+}, creating a cycle between these two ion forms and indicating a potential Fenton-like process (Fe^{3+}/H_2O_2 system). However, ferrous ions can also react with the free radicals produced in Equation 1.4 and Equation 1.5, which reduces the number of available free radicals (Eq. 1.7 and Eq. 1.8).

$$Fe^{3+} + \cdot OOH \rightarrow Fe^{2+} + H^+ + O_2 \qquad \text{(Eq. 1.6)}$$
$$Fe^{2+} + \cdot OH \rightarrow Fe^{3+} + HO^- \qquad \text{(Eq. 1.7)}$$
$$Fe^{2+} + \cdot OOH \rightarrow Fe^{3+} + HOO^- \qquad \text{(Eq. 1.8)}$$
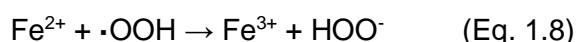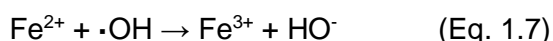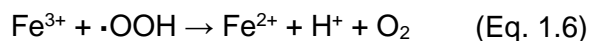
Furthermore, the radicals produced by the Fenton and Fenton-like reactions can react with each other or with excess hydrogen peroxide in the solution. This further reduces the number of free radicals by scavenging. The overall result of these reactions is the decomposition of hydrogen peroxide into molecular oxygen and water, as shown below:

$$2\,H_2O_2 \rightarrow 2\,H_2O + O_2 \qquad \text{(Eq. 1.9)}$$
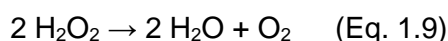
Moreover, the model indicates that a proportion of H_2O_2 would be consumed, irrespective of the presence or absence of an organic molecule to be oxidised. This would result in the wastage of oxidant H_2O_2 and, consequently, an unnecessary increase in cost.

For our aims, the production of hydroxyl radicals is essential throughout the entire process. The chain initiation phase is where most of these hydroxyl radicals, the most active species for pollutant degradation in the Fenton reaction, are created (Eq. 1.4). The catalytic cycling of iron between its Fe^{3+} and Fe^{2+} forms is a major factor in the Fenton system's ability to produce extremely potent $\cdot OH$ radicals.

1.3.3.4 Homogeneous and heterogeneous Fenton reaction

Conventional Fenton reactions using H_2O_2 together with iron (II) salt, soluble in water, produce $\cdot OH$ as a homogeneous catalytic reaction. However, the pH range is narrow (optimum pH ca. 3), and has to be controlled strictly. A lower pH (pH=2.5) may cause a scavenging of $\cdot OH$ radicals available for substrate due to the presence of H^+ and the formation of $[Fe(H_2O)_6]^{2+}$. Moreover, a more stable ion $[H_3O_2]^+$ can form and reduce the reactivity of H_2O_2 with Fe^{2+}. At a higher pH (>4) Fe^{2+} will be precipitated out of the reaction system in the form of FeO(OH), inhibiting both the production of $\cdot OH$ radicals and the regeneration of Fe^{2+}.[74] Besides, oxidation potential of $\cdot OH$ will decrease with increasing pH.[77] Also, decomposition of H_2O_2 into O_2 and H_2O is accelerated at extreme pH values (highly acidic or highly alkaline) where it is more susceptible to dissociation and subsequent decomposition.[75,78] Furthermore,

additional separation procedures would be necessary for the removal of residual iron following treatment, which could potentially result in the leaching or discharge of iron into the environment. This would result in an increase in the overall treatment cost due to the high consumption of hydrogen peroxide and the necessity for iron removal steps. This would increase the treatment cost due to the high consumption of hydrogen peroxide.[79]

Table 1.1 Comparison of homogeneous and heterogeneous catalyst.[80,81]

Aspect	Homogeneous Catalysts	Heterogeneous Catalysts
Catalyst Recovery	Difficult to separate from the reaction mixture.	Easier to recover and reuse due to their solid form.
Operational pH Range	Optimal activity at acidic conditions around pH 3.	Can operate over a broader pH range, including near-neutral pH conditions.
Reaction rate	Generally faster due to better solubility and reactivity of the catalyst.	May be slower due to mass transfer limitations and lower surface area activity.
Cost	Lower upfront cost but may require more reagents to maintain pH.	Higher upfront cost but more cost-effective in the long term due to catalyst reuse.
Environmental Impact	Generates more sludge and requires disposal of used catalyst.	Generates less waste and the catalysts are often more environmentally friendly.
Application Flexibility	Limited by the need for strict pH control and catalyst recovery challenges.	More versatile, can be used in a wider range of applications including those with higher pH levels.
Catalyst Stability	Catalysts can degrade over time, requiring replacement.	Typically more stable and can be used for extended periods.
Selectivity	High selectivity in reactions due to controlled conditions.	Selectivity can be engineered by modifying the catalyst surface.
Ease of Handling	Handling and operation can be challenging due to corrosive conditions.	Generally safer and easier to handle due to solid form and less corrosive nature.
Scale-up Potential	Scale-up can be challenging due to the need for specialized equipment.	Easier to scale up due to robustness and ease of catalyst separation.

To overcome the inherent drawbacks of homogeneous systems for our intended applications, heterogeneous catalytic Fenton reactions were and are considered as a practical and promising alternative. Immobilizing the active metals like transition metal cations, mainly Fe ions, have been investigated and developed as heterogeneous catalysts. Nevertheless, depending on specific applications and requirements, other transition metals such as Cu, Mn, Co, Ni, and Ti can also be utilized. Compared to homogeneous processes, employing a heterogeneous catalyst in the Fenton reaction offers several advantages (Table 1.1). These include ease of recovery and reuse, as well as the stabilization of active sites, making them particularly valuable for chemical reactions in hostile environments. Due to these benefits, heterogeneous catalysts are fundamental to over 80% of current bulk chemical processes in

the chemical and petrochemical industries. [82] Specifically, in the Fenton process, they enable operations under more extreme conditions (broader pH range, higher temperatures) and allow for the straightforward recovery, regeneration, and reuse of the catalyst.

The preparation of solid catalysts requires a deliberate choice of support. Currently, the most ideal candidates are zeolites.[83–85] Other supports, such as pillared clays,[86] activated carbon,[87] alumina,[88] silica,[89] and mesoporous molecular sieves,[90] have also been investigated previously. However, these catalysts have limitations, such as the leaching process of the active phase, which is common during oxidation at the optimum pH of 3 for homogeneous Fenton reactions. In the case of zeolites, the leaching phenomenon of iron was detected below a pH value of 5. An inverse correlation between pH and leaching was observed. However, no significant increase in activity was observed under neutral conditions. Although pillared clays showed a similar leaching trend, they are more stable with high total organic carbon (TOC) reduction even at an operating pH of 5.[91]

1.4 Phenol as a benchmark contaminant

Phenolic compounds are a diverse group of organic chemicals characterised by the presence of one or more hydroxyl groups (OH) directly attached to one or more of its aromatic ring structure. Phenol, the simplest member of this category, serves as the foundation for all subsequent homologues within this group. Each variant is essentially a modification or extension of the basic phenolic structure. For example, bisphenol, 4-tert-octylphenol, and 2,4,6-trichlorophenol are all well-studied to be present in aquatic environments. Phenols are important in household products and as intermediates in industrial synthesis processes. For example, hydroquinone, which is synthesised from phenol, acts as a reducing agent in photographic developers. This process converts exposed silver bromide crystals into black metallic silver.

Phenols are structurally similar to alcohols, but they can form stronger hydrogen bonds, making them more soluble in water (over 90 g L^{-1} at room temperature) and resulting in higher boiling points (>180 °C). This highlights the potential risks it poses to water safety. They can exist as either colourless liquids or white solids at room temperature and are known for their potential toxicity and caustic properties.

1.4.1 Sources of phenolic compounds in water

The presence of phenol in water can be attributed to two main sources: natural occurrences and anthropogenic (man-made) activities. Naturally occurring phenol comes from the decomposition of dead plants and animals in water. This process, which is part of the natural

carbon cycle, contributes to the background levels of phenol found in aquatic environments. On the other hand, anthropogenic activities contribute, and to a much larger extent, the presence of phenol in water through discharges from various sources, including industrial operations, agricultural practices, domestic and municipal wastewater. These anthropogenic contributions significantly increase phenol levels in aquatic environments above natural background levels, posing potential risks to water quality and ecosystem health.

1.4.1.1 Natural sources

Many terrestrial and aquatic plant species contain phenolic chemicals. Some are created in plant hemicellulose by irradiating amino acids with UV light. For instance, it is well known that willow bark has a specific concentration of salicylic acid.[92] In addition, benzene, commonly found in organic wastes, can undergo metabolic degradation to produce phenol.[93] Phenol is produced as a metabolic waste product, mainly through the conversion of tyrosine in the digestive tract, in the human body and animals.[94] Moreover, microbial fermentation of plant extracts can lead to the production of various phenolic compounds, as demonstrated in a study where Lentinus edodes fermented cranberry pomace, resulting in the formation of ellagic acid.[95] These are all the possible ways that directly and/or indirectly introduce phenolic compounds into the water bodies eventually. However, the environmental impact of naturally occurring phenol is minor compared to man-made phenol due to much lower production levels, which will be discussed in the next session.

1.4.1.2 Anthropogenic sources

Phenolic compounds play diverse roles in everyday human activities. Phenol is widely used in various industries, particularly in the chemical sector for the synthesis of derivatives such as alkylphenols, cresols, aniline and resins.[96] Phenol is also used in the oil, gas and coal industries.[97] Moreover, phenolic resins are primarily used in the construction, woodworking and appliance industries to meet a wide range of requirements.[98,99] Industrial processes such as wood distillation, chlorine-based water disinfection, cooking and paper production all contribute to the formation of chlorophenols.[100] In addition, some of these chemicals are released into the atmosphere by vehicular activities and subsequently washed into water bodies by rainwater, further contributing to pollution. Thus, industrial activities that directly or indirectly discharge phenol-containing effluents into water bodies contribute to water pollution.

Besides industrial waste, the use of pesticides, insecticides and herbicides in agriculture is a major source of water pollution with phenolic compounds. Due to the biodegradation of some pesticides, phenol and some chlorophenols like 2-chlorophenol, 2,4-dichlorophenol and some catechol are normally detected in the aquatic environment.[101,102] Herbicides, fungicides and

pesticides, as well as their degradation by-products, are transported into water bodies via agricultural run-off.

In addition to the industrial and agricultural sectors, domestic and municipal sources also contribute to the discharge of phenol into water.[24,103,104] Phenol is used in a wide range of products, from disinfectants to medical supplies. Household products such as soaps, perfumes, paints and varnishes are often discharged directly into municipal sewers, resulting in phenol contamination of nearby waterways.[105,106] Municipal waste is a significant contributor to phenol emissions, mainly through wastewater treatment plants and landfill leachate. For example, p-cresol is known to originate from incineration residues, while compounds such as bisphenol A and 4-tert-butyl-phenol have been identified from the fly ash produced during the incineration process.[107]

The direct or indirect release of effluents and/or discharges from anthropogenic activities into water bodies and atmosphere results in their significant contamination with phenolic compounds (10 g L^{-1}).[108]

1.4.2 Impact of phenol on health and environment

The release of phenol into the environment poses a range of risks to human health, animal welfare, plant life, and aquatic organisms. Normally, the concentrations of phenol in uncontaminated natural water sources, such as lakes or rivers, resulting from metabolic processes, range from 0.01 to 1.0 µg L^{-1} which is not harmful to the environment. In contrast, in industrial wastewater, phenol concentrations can reach levels as high as 10 g L^{-1}, which is over 100 million times higher than those found in natural water bodies.[108,109] Upon entering the environment, phenol rapidly degrades in the air within 1-2 days (half-life about 15 h), yet persists for at least a week in water and biodegrades in soil rapidly (half-life generally < 5 days).[110] This indicates significant toxicity and phenol has been listed as one of the priority pollutants by US Environmental Protection Agency (USEPA) and Canada National Pollutant Release Inventory (NPRI), i.e., the concentration of phenol in surface water must not exceed 1 ppb (also known as µg L^{-1}) according to the water purity regulations established by the USEPA.[111] However, the toxicity threshold for phenol exposure in both humans and animals has been found to range between 9 and 25 mg L^{-1}.[112] The high standard of phenol discharge was mainly due to its high reactivity where it is easily interact or react with compounds like inorganic matter or microorganism present in water body.[113] Moreover, there is also concern that certain bacteria capable of degrading non-ionic surfactants may transform phenol into derivative compounds, such as alkyl phenol, which are more harmful than the original substance, i.e., under anaerobic conditions, nonylphenol polyethoxylated, a type of surfactant,

degrades into nonylphenol or nitro phenol.[114]

Phenol is classed as a hazardous material that can cause acute and chronic health effects. Prolonged exposure may result in symptoms such as abnormal breathing, tremors, and coma. Lethal doses, estimated based on body weight, can cause respiratory arrest.[115,116] For an adult with 70 kg body weight, range of 1024 mg L^{-1} are considered lethal.[117] Some chronic effects including sudden weight loss, vertigo and anorexia are reported as well.[24] When phenol enters the human body, it undergoes metabolic processes that result in the formation of reactive intermediates, such as quinone moieties.[118,119] These intermediates can form covalent bonds with proteins, which may affect human health.[120] Phenol derivatives, including chlorophenols, chlorocatechols, and methylphenols, have been found to have toxic effects (concentration dependent) on humans. Bisphenol A and alkylphenols are compounds that have the potential to disrupt the endocrine system, affecting the mammary glands in both humans and animals.[121] Long-term exposure to phenol through inhalation and dermal contact can cause cardiovascular diseases. Phenol is known to cause significant irritation to human skin, eyes, and mucous membranes. Acute toxicity symptoms include irregular breathing, muscle weakness, tremors, loss of coordination, convulsions, coma, and potentially respiratory arrest at lethal doses. Ingestion of liquid products containing concentrated phenol can result in severe gastrointestinal damage, which may be fatal.[122]

The toxicity of a chemical substance to living organisms is commonly characterized by the median lethal concentration (LC50) and median effect concentration (EC50) values. Across all organisms, the LC50 and EC50 values for phenol ranged from 0.26 to 2200 mg L^{-1}, representing 3 orders of magnitudes or more of difference.[109] For example, a freshwater fish like a carp, has been identified as highly sensitive to phenol, with a 96-hour LC50 value of 1.6 mg L^{-1}.[123] The opossum shrimp was found to be the most susceptible to phenol among marine organisms, with a 96-hour LC50 of 0.3 mg L^{-1}.[124] In addition, phenol has been shown to have a negative impact on growth. For instance, fish exposed to pentachlorophenol have experienced disrupted growth, resulting in reduced weight.[125] Feeding was significantly reduced at phenol concentrations ranging from 3 to 4 mg L^{-1}. This reduction may have contributed to the observed decrease in weight gain in fish exposed to phenol. A study on fish embryo development found that 2,4-dichlorophenol and pentachlorophenol (at concentrations of 8 and 24 mg L^{-1}, respectively) impeded the development of fathead minnow fish embryos when the phenol level in the surrounding medium exceeded the stipulated amount.[126] The build-up of organic toxins in these organisms presents a considerable risk to associated food webs and can have a negative impact on the entire aquatic ecosystem.

1.4.3 Reaction pathways of phenol mineralization

The reaction pathway for phenol decomposition is influenced by catalysts (e.g., active species) and reaction conditions (e.g., pH), resulting in highly complex actual reaction pathways.

Numerous routes for phenol oxidation have been proposed.[72,127–131] Variations in reaction pathways in the literature stem from different active species (e.g., Cu,[127] Fe[130]), oxidants (e.g., H_2O_2,[127] O_2[132]), and reaction conditions (e.g., acidic medium[127] or basic medium[128]), all of which impact the mechanism and intermediates formed during oxidation. Often proposed methods begin with the hydroxylation of phenol to hydroquinone and catechol in tandem, and then these dihydroxybenzenes are oxidized to benzoquinones. After that, the quinone intermediates break down into short-chain acids like formic and acetic acids, which finally form CO_2 and water. Reaction circumstances have a significant impact on the details of the oxidation pathway, specifically the ring-opening of quinone intermediates and the subsequent generation of acid. It is well acknowledged that acids like acetic and formic acids, as well as CO_2, are the end products of phenol oxidation and are resistant to further oxidation. To improve the selectivity for innocuous products like CO_2 and lower the toxicity of the reaction mixture, it is essential to understand the phenol oxidation route and identify intermediates. This is because some intermediates, such hydroquinone and p-benzoquinone, are more hazardous than phenol itself.[133,134]

1.5 Ibuprofen as a representative of pharmaceutical contaminant

As introduced in Section 1.2 of this chapter, there is a growing concern regarding 'emerging micropollutants', such as pharmaceuticals and personal care products (PPCPs). These contaminants appear in effluent at low concentrations (μg L^{-1} or ng L^{-1}) and are highly toxic to the environment despite their low concentrations. More attention has been paid to groups of analgesics and nonsteroidal anti-inflammatory drugs (NSAIDs) because of their massive consumption, which results in their high presence in surface and ground waters.[135] Among these drugs, ibuprofen (which will be abbreviated as IBU in this thesis work, Figure1.4), is one of the most popular and widely prescribed drugs for fever, headache, muscle pain, and is the second most frequently detected pharmaceutical in the environment worldwide.[136] Ibuprofen inhibits the enzyme cyclooxygenase, which converts arachidonic acid into cyclic endoperoxides. These endoperoxides are then transformed into prostaglandins and thromboxanes, which act as mediators of inflammation. By inhibiting cyclooxygenase activity and the subsequent synthesis of prostaglandins, ibuprofen effectively reduces the release of substances and mediators involved in inflammation. This inhibition prevents the activation of nociceptors, which are responsible for the perception of pain.[137] The daily dosage of ibuprofen

ranges from 600 to 1200 mg per day. In the USA, UK and Poland, approximately 300, 160 and 60 metric tonnes of ibuprofen are consumed annually respectively.[138,139] The World Health Organization (WHO) marked ibuprofen as an 'Essential Drug' in 2010.[140]
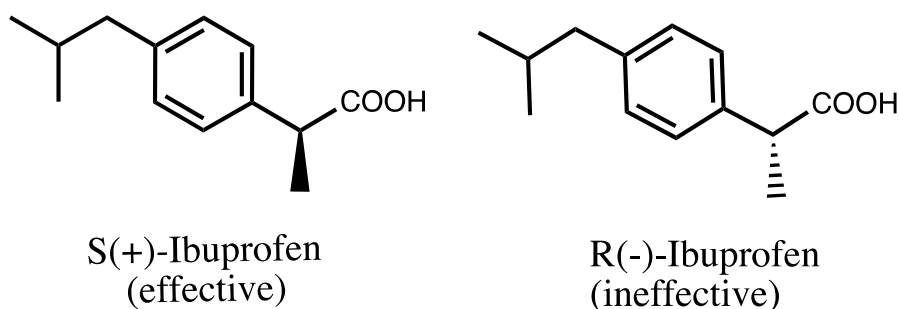
Figure 1.4 Structural formula of Ibuprofen enantiomers. Ibuprofen is a racemic mixture of two enantiomers, S(+)-ibuprofen and R(-)-ibuprofen. The majority of the effects of racemic ibuprofen are elicited by S(+)-ibuprofen. The drug is sold as a 50:50 mixture of the two forms as it is the easiest way to manufacture this compound.

Ibuprofen has a very low solubility in water (20 mg L^{-1}) with a chemical structure of 2-(4-isobutylphenyl) propanoic acid. Like all other NSAIDs, it is administered as a racemic mixture of R(-)- and S(+)-enantiomers (Figure 1.4). It contains an aromatic ring as does phenol, with isobutyl substitutions and propanoic acid. The pharmacologic activity is largely due to the S(+)-IBU[141] enantiomer, however, in the liver, the enzyme α-methylacyl-coenzyme A racemase can convert about 50-65% of R(-)-IBU to S(+)-IBU via an acyl-CoA thioester.[142,143]

1.5.1 The presence of ibuprofen in the environment

In Great Britain, ibuprofen has a predicted no-effect concentration of 0.01 μg L^{-1}.[144] Reports suggest that its concentration levels vary across different countries and depend on the type of environmental sample analysed. In aquatic environmental samples, ibuprofen concentrations are typically measured in μg L^{-1}. Various concentrations of these substances have been detected in effluents in China, Korea, Sweden, and the UK, ranging from 0.004 to 600 μg L^{-1}.[145] Ibuprofen concentrations in wastewater samples have been reported at varying levels: of 45, 1, 6 or 700-1700 μg L^{-1} in Canada, South Africa, Belgium, and Pakistan, respectively.[146,147] In surface waters, average concentrations were 1, 8, 1400. 1-67, and 15-410 μg L^{-1} for Canada, France, China, Greece, and Korea, respectively.[145,148] In Europe, the concentration of ibuprofen in groundwater has been found to range from 3 μg L^{-1} to 400 μg L^{-1}.[145]

The concentrations of Ibuprofen in environmental sludge samples vary significantly between South Africa (9 μg kg^{-1}) and Pakistan (2000-6000 μg kg^{-1}),[149] indicating the impact of each country's management or regulatory practices on their ecosystems and toxicity levels.

Additionally, soil samples had widely varying ibuprofen concentrations ranging from 320-610 µg kg^{-1} in particular, a concentration of 0.2 µg L^{-1} was detected in agricultural soil that had been irrigated with to wastewater containing pharmaceuticals.[150,151]

Furthermore, transformation products of ibuprofen have been identified in influents of wastewater treatment plants, with concentrations about 20 µg L^{-1} for carboxyibuprofen, 1100 µg L^{-1} for 1-hydroxyibuprofen, and 8 µg L^{-1} for 2-hydroxyibuprofen (Figure 1.5).[152] A wastewater treatment plant in Girona, Spain reported maximum influent concentrations of 14 µg L^{-1} for ibuprofen, 6 µg L^{-1} for 1-hydroxyibuprofen, 94 µg L^{-1} for 2-hydroxyibuprofen, and 40 µg L^{-1} for carboxyibuprofen, while effluent samples showed maximum levels of 2 µg L^{-1} for ibuprofen, 1µg L^{-1} for 1-hydroxyibuprofen, 6 µg L^{-1} for 2-hydroxyibuprofen, and 11 µg L^{-1} for carboxyibuprofen. The Ter River was found to contain high concentrations of certain compounds, including carboxyibuprofen up to 4 µg L^{-1}.[153]
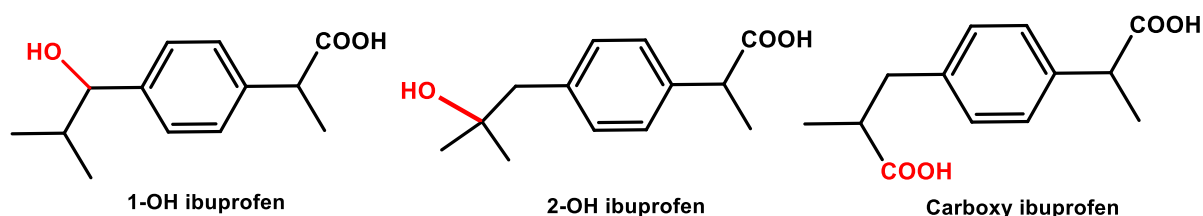
Figure 1.5 Chemical structures of 1-hydroxyibuprofen (1-OH ibuprofen), 2-hydroxyibuprofen (2-OH) ibuprofen and carboxyibuprofen.

1.5.2 Contamination routes of ibuprofen to the environment

The high usage of ibuprofen is considered an environmental risk due to the vast annual production of NSAIDs in the world (annual prescriptions in the United States are estimated to be around 70 million, in Canada around 10 million and in the UK around 20 million).[154] Ibuprofen can be introduced into the environment through two main pathways, leading to its accumulation in different environmental matrices: 1) ibuprofen that is metabolized by humans or animals is primarily expelled into community water systems, resulting in its accumulation in aquatic ecosystems or soil substrates; 2) unused or expired medications. These are often disposed of in domestic or industrial waste containers and subsequently find their way into municipal waste systems, posing a latent risk of soil contamination.

1.5.2.1 Metabolized ibuprofen

Ibuprofen can enter the environment in its original form or as a modified derivative resulting from the organism's metabolism. The modified forms of ibuprofen are released into the environment through excretion in urine or faeces after consumption by humans or animals.

The main route for eliminating ibuprofen from humans involves a two-step process that produces a glucuronic acid conjugate. This is achieved through the formation of carboxyl IBU and hydroxyl metabolites of R(-)- and S(+)- IBU via oxidative metabolism in the hepatocyte with the aid of cytochrome P450 enzymes (CYPs).[141] The major primary metabolites found in urine are 17 carboxyl IBU and hydroxyl metabolites 2-hydroxyibuprofen (2-OH IBU), which account for approximately 37% and 25% of the administered dose, respectively. In addition to ibuprofen, 1-hydroxyibuprofen (1-OH IBU) and 3-hydroxyibuprofen (3-OH IBU) have been identified, although in very small concentrations (Figure 1.6). The carboxyl and hydroxyl metabolites of IBU do not appear to have any pharmacological activity. Therefore, IBU is almost entirely metabolized, with little unchanged drug detected in the urine. The human body metabolizes IBU (10%-15% of an IBU dose) through a direct one-step route to form glucuronic acid conjugate. This process occurs via the uridine 5′diphosphoglucuronosyltransferases (UGTs), resulting in the formation of IBU-acyl glucuronides.[155] Up to 15% of IBU (24 metric tonnes per year in the UK) is excreted from the body as either its original form or its metabolites, which are released into the environment. Figure 1.6 illustrates the accepted biotransformation pathway of IBU in the human body.[156] However, ibuprofen in wastewater is transformed into more toxic intermediate compounds during chlorination process in treatment plants,[157] including 1-(4-isobutylphenyl)-1-ethanol, 4-isobutyricbenzaldehyde,[158] 2-[4-(1-hydroxyisobutyl)phenyl] propionic acid, 1-ethyl-4-(1-hydroxy) isobutylbenzene, 4-ethylbenzaldehyde, and 4-ethylphenol.[159]

In addition, ibuprofen's use in veterinary medicine contributes to environmental dispersion. After being ingested, the substance is excreted onto the land through animal urine or faeces, thus increasing its presence in the environment.
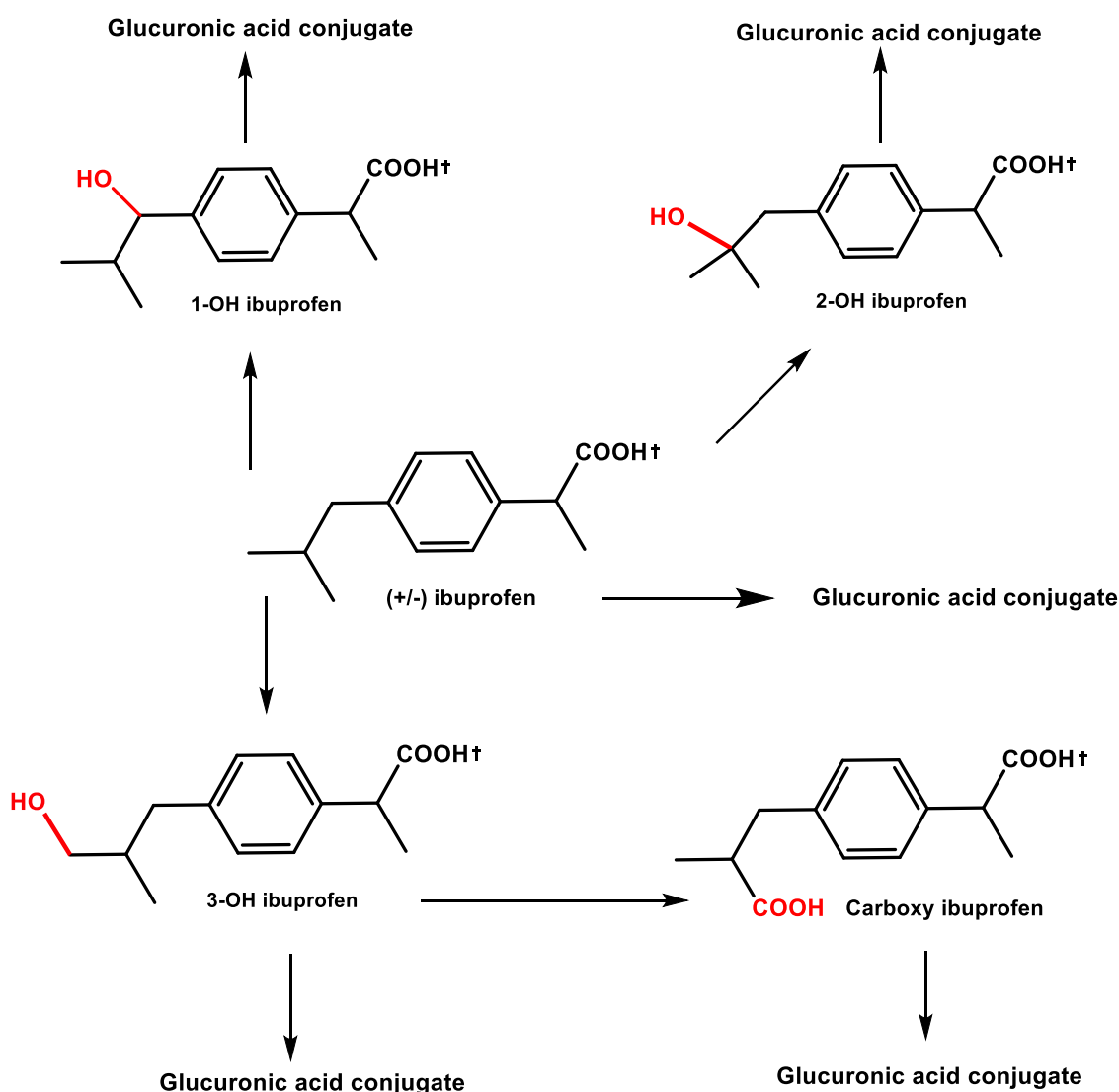
Figure 1.6 Biotransformation of ibuprofen. † = sites of glucuronidation. Primary elimination route is to form carboxy IBU and hydroxy metabolites (2-hydroxyibuprofen) via oxidative metabolism as major products, and then to form glucuronic acid conjugate; secondary elimination route is direct glucuronidation to IBU-acyl glucuronides.

1.5.3 Impact of ibuprofen on environment

The widespread use of ibuprofen and other pharmaceuticals has raised concerns about their impact on the environment. Research on the toxicity of ibuprofen in living organisms has been limited, with most studies focusing on its potential harm to aquatic life.[160] Ibuprofen's properties, including its high lipophilic degree and low biodegradability, make it likely to accumulate in the environment.[161] Furthermore, the biological activity of the substance suggests that it may have harmful effects on various aquatic species.

Exposure to ibuprofen at concentrations harmful to organisms results in a variety of effects. Acutely, high concentrations of ibuprofen above 100 mg L^{-1} may cause damage. Sub-lethal

effects can occur at concentrations between 10 and 100 mg L^{-1}. In natural ecosystems, concentrations of ibuprofen range from 0.2 to 8.0 µg L^{-1}. Chronic exposure of aquatic animals to ibuprofen over long periods can have serious consequences, including cytotoxic and genotoxic effects, increased oxidative stress at the cellular level, and negative effects on growth, reproductive capacity and behaviour. These phenomena have been documented using both in vivo and in vitro experiments that mimic ibuprofen-contaminated ecosystems.[160]

Studies have shown that ibuprofen, when biotransformed in organisms, can produce intermediates that are more toxic than ibuprofen itself.[140] For example, ibuprofen can disrupt cell division and chromosome pairing.[162] In zebrafish exposed even to environmental concentrations (0.1-11 µg L^{-1}), ibuprofen altered antioxidant systems, affected liver proteins and altered blood protein and enzyme levels.[163] Bivalve molluscs, indicators of water quality, showed biochemical and cellular changes after 14 days at 0.8 µg L^{-1} ibuprofen.[164] In oryzias latipes, a fish common in rice paddies, marshes and tide pools in Asia, a concentration of 0.1 µg L^{-1} affected reproduction and induced vitellogenin in males,[165] whereas the water flea daphnia magna exposed to 1-4 µg L^{-1} ibuprofen throughout their life cycle showed changes in growth, maturation and reproduction.[166]

The toxic effects of ibuprofen have also been observed in plant species; for example, in the legume cowpea exposure to ibuprofen resulted in reduced shoot and root lengths, reduced fresh and dry weights, reduced leaf area and reduced levels of chlorophyll a and b, carotenoids, total chlorophyll, minerals (K and Mg), glutathione reductase and soluble proteins. At the same time, there was an increase in Ca and Mn concentrations, increased sodium translocation from roots to shoots and increased levels of H_2O_2, malondialdehyde and antioxidant enzymes such as superoxide dismutase, catalase and ascorbate peroxidase.[167]

The toxicity of ibuprofen affects a wide range of organisms, highlighting the need for vigilant monitoring of ibuprofen-contaminated environments to accurately assess its toxicological effects on communities. This information is essential for the development of regulatory measures or innovative technologies aimed at reducing the presence of ibuprofen and minimising its environmental impact.

1.5.4 Mineralization pathway of ibuprofen

Persistent pollutants have adverse effects on plant and aquatic environments.[165,168,169] Ibuprofen is one such pollutant that cannot be fully removed from sewage using traditional biological treatment methods. As a result, wastewater treatment plants (WWTPs) mainly use advanced oxidation processes (AOP) to treat effluent containing emerging and non-biodegradable contaminants (Table 1.2). However, these processes result in the formation of

various metabolites that may have higher or indefinite toxicity compared to the parent compounds. e.g., 4-isobutylphenol, hydratropic acid, 4-(1-carboxyethyl) benzoic acid, 4-ethylbenzaldehyde, 2-[4-(1-hydroxy-2-methylpropyl) phenyl] propanoic acid, 1-(4-isobutylphenyl)-1-ethanol, 4-acetylbenzoic acid, 1-isobutyl-4-vinylbenzene and 4-isobutylacetophenon.[159] Therefore, it is important to develop more efficient processes that can either mineralise Ibuprofen to a maximum extent or to by-products/intermediates of reduced toxicity compared to the parent ibuprofen molecule.

Table 1.2 Selected advanced treatment methods used in Ibuprofen removal.

Treatment	IBU decomposition %	Ref
Coagulation-flocculation	12	170
Ozonation/AOP	34	145
Ozonation/AOP	100(10 min), 100 (30 min)	145
Membrane processes	7	145,171
Membrane processes	> 99	145,172
Membrane bioreactor (MBR)	~ 100	145,173
Membrane bioreactor (MBR)	97	174
Activated sludge with high nitrifying activity in sequencing batch reactor (SBR)	76	175
Fenton oxidation	97	176
Photo-Fenton	93	177

1.6   Potential application of glass in fine chemical synthesis

Besides total oxidation applications, selective oxidation plays a central role in organic synthesis,[178] and there is a high demand in the chemical industry for environmentally friendly, efficient and selective oxidation methods.[179] In particular, the selective oxidation of alcohols is a key transformation in the production of fine chemicals.[180] In this thesis work we considered the applicability of glass in the oxidation of phenol and ibuprofen-like compounds. Alcohols such as benzyl alcohol and 1-phenylethanol, both of which have a single aromatic ring, were chosen as initial subjects. The focus is on their oxidation products, specifically benzaldehyde and acetophenone (Figure 1.7), to assess the effectiveness of glass-based catalysts in these reactions.
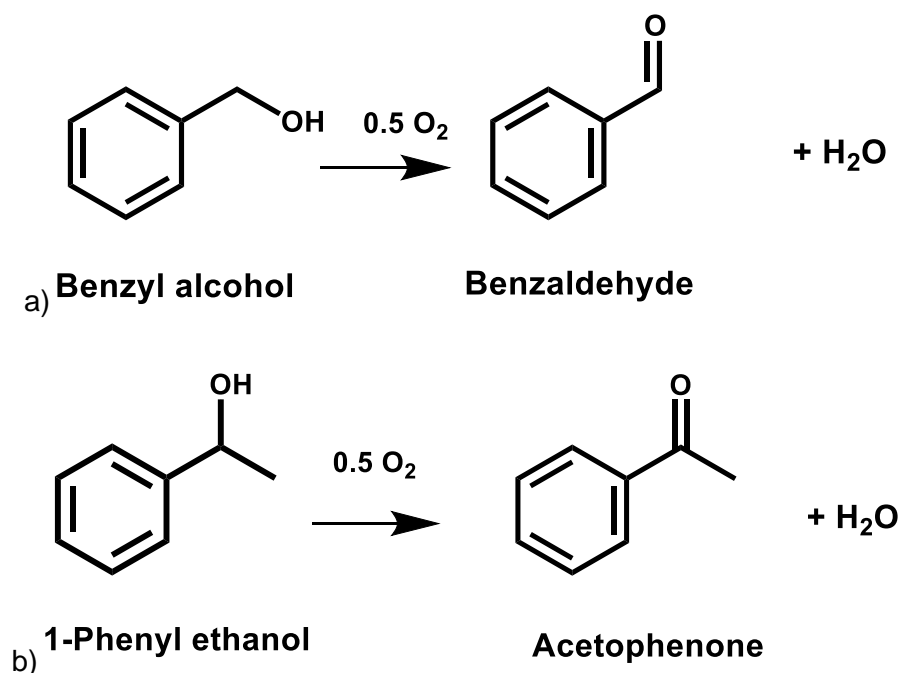
Figure 1.7 The oxidation of a) benzyl alcohol to benzaldehyde and b) 1-phenylethanol to acetophenone using molecular oxygen shows their structural similarity to phenol and ibuprofen, both of which have an aromatic group.

Benzaldehyde (BzH) occupies a prominent position within the family of aromatic aldehydes due to its wide range of uses as a raw material. It is used in a wide range of industries as a basic component in the manufacture of perfumes, beverages, pharmaceutical intermediates and many other products.[181–183]

Traditionally, the synthesis of benzaldehyde (BzH) has been achieved through the hydrolysis of benzyl chloride or the vapour/liquid phase oxidation of toluene. The hydrolysis route often resulted in the production of chlorinated by-products and toxic acids, which posed significant challenges for industrial applications.[184,185] Meanwhile, the vapour-liquid oxidation method faced limitations due to harsh reaction conditions and low selectivity.[186] In recent years, the industry has increasingly adopted benzyl alcohol oxidation as a method for BzH production, attracted by its controllable conditions and high yield.[184,185]

Acetophenone, also known as methylphenyl ketone, acetylbenzene or hypnone, is the simplest ketone with both aromatic (phenyl) and aliphatic (methyl) functional groups. Characterised by a sweet, pungent aroma, acetophenone is widely used as a fragrance component in soaps, detergents and perfumes. It is also used as an industrial solvent and as a key intermediate in manufacturing processes in the pharmaceutical and resin industries.[187]

The oxidation of alcohols to aldehydes or ketones, which serve as intermediates in the synthesis of pharmaceuticals, agrochemicals or perfumes, is a key reaction in synthetic

organic chemistry. Potassium permanganate ($KMnO_4$)[188] and dichromate ($K_2Cr_2O_7$),[189] known for their strong oxidising properties, are commonly used as oxidants in this process. However, these oxidants are not without drawbacks, as their use can lead to environmental problems and increased costs. Green oxidants, particularly H_2O_2[190] and O_2,[191–193] have attracted considerable interest for their environmentally friendly properties in oxidation reactions. Despite their appeal, it's important to note that O_2 and H_2O_2 inherently have minimal activity and require activation by additional materials to effectively enhance their oxidative performance. This need for activation underlines the ongoing research and development efforts to identify and utilise catalysts or systems that can efficiently harness the potential of these green oxidants in various chemical processes.

Recognised for their non-toxicity, abundance and biocompatibility, iron-based metals have attracted considerable interest from the scientific community.[194,195] A series of iron catalysts, including $FeBr_3$, Fe_2O_3 and $Fe_2(SO_4)_3$, have been reported by Zhang et al.[196] to exhibit effective catalytic performance in the oxidation of benzylamine to imine under air atmosphere, highlighting the potential of these iron-based catalysts in facilitating environmentally friendly chemical transformations.

As a result, the structural similarity and importance of alcohol oxidation products led to an extension of research into the use of Fe-containing glass in this area.

To understand what makes glass potentially a good heterogeneous catalyst in water treatment applications and selective oxidation in fine chemical synthesis, the next section introduces the properties of glass, in particular its composition and chemical durability.

1.7   Glass as a potential catalyst in oxidation reactions

Glass is one of the most useful materials in manufacturing industries because of its versatility in producing a variety of items for household and industrial use. The presence of glass in modern day-to-day life is very common. It is used for the manufacture of lenses, glasses, windowpanes, and containers for the packaging sector like bottles, jars, and much more. It is a transparent material produced by melting a mixture of materials such as silica (SiO_2), soda ash (Na_2CO_3), and limestone ($CaCO_3$) at high temperature (1400°C) followed by cooling where solidification occurs without crystallization. The first glass was said to be discovered by accident where cooking pots melted with sand from the beach, a clear liquid was formed. By another definition of the American Society for Testing and Materials dated 1945, "*Glass is an inorganic product of fusion which has been cooled to a rigid condition without crystalizing.*"[197]

1.7.1 Vitreous silica (SiO_2)

Vitreous silica (SiO_2) is the simplest silicate glass composed of silicon and oxygen, the two most ubiquitous elements in the earth's crust (Table 1.3).[198] The properties such as hardness, optical properties can be used as foundation of other silicate glasses. Properties like viscosity and thermal expansion, electrical conductivity are strongly dependent on glass compositions.

Table 1.3 The relative abundance of elements in the earth's crust illustrates the common availability of Vitreous silica.

Rank	Element	% of Earth's crust
1	Oxygen	46.1
2	Silicon	28.2
3	Aluminium	8.2
4	Iron	5.6
5	Calcium	4.1
6	Sodium	2.3
7	Magnesium	2.3
8	Potassium	2.0
9	Titanium	0.5
10	Hydrogen	0.1
	Other elements	0.5
	total	100.0

Vitreous silica is one of the purest materials that can be purchased commercially. It is sometimes referred to as silica glass, fused quartz, or just quartz. It is used in the fabrication of furnaces and crucibles for high-temperature operations, especially semiconductor manufacturing. Moreover, it finds application in the manufacturing of lamp envelopes, electrical transducers, insulators, and optical parts such as prisms, lenses, and telescope mirrors. The remarkable qualities of the material, such as its high purity, outstanding thermal stability, low susceptibility to thermal shock, low electrical conductivity, good chemical durability, and broad optical transparency, are responsible for these applications.

Silicon tetrachloride ($SiCl_4$) is hydrolysed or oxidized in the vapour phase to produce very pure vitreous silica. It is placed on a revolving air-cooled aluminium mandrel or a substrate of heated sand after being combined with oxygen and natural gas in a burner.

Like all silicates, vitreous silica is mostly composed of silicon-oxygen tetrahedra. A three-dimensional network is created by connecting these tetrahedra at their corners with additional

tetrahedra (Figure 1.8). There is no long-range order in the structure beyond a few tetrahedra, but it does have order on the short range (one or two tetrahedral coordination spheres around a central one). In macroscopic terms, silica is an amorphous solid, and the best way to represent this structure is as a random network.
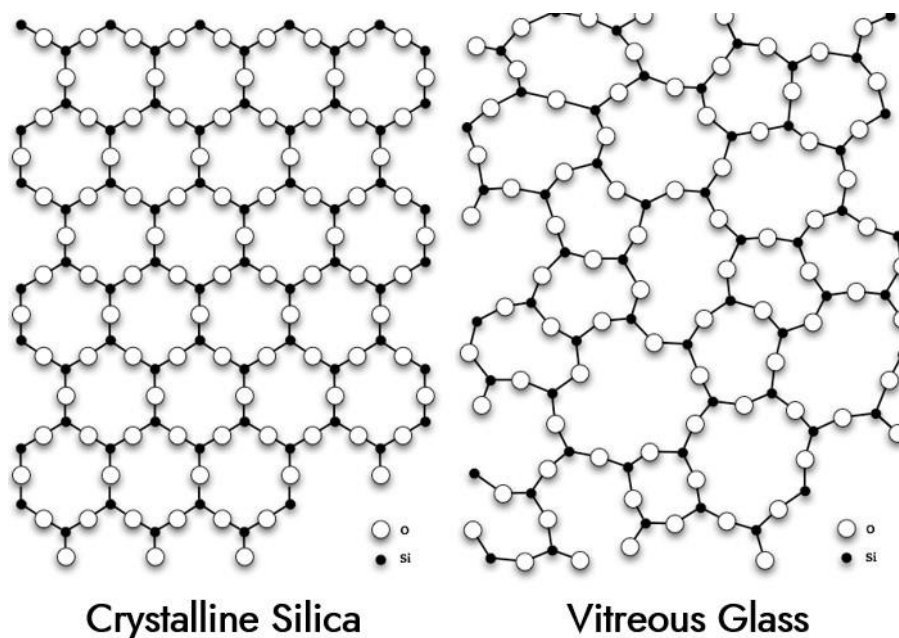
Figure 1.8 Structure of crystalline silica and vitreous glass.[198] It has a basic structure unit of vitreous silica is the silicon-oxygen tetrahedron, as in all silicates Unlike crystalline silica, however, there is no long range order to these silica tetrahedra, hence it is referred to as being in the glassy, or vitreous state.

1.7.2 Multicomponent commercial glasses

Synthetic glass, which has a history of at least 5,000 years, is made from a mixture of sand, ash and limestone heated to around 1400°C to form soda-lime glass. By incorporating various oxides into the melt, a wide range of commercial glasses can now be produced, including Pyrex borosilicate, potash-soda-lead, lime-magnesia aluminosilicate, sodium borosilicate and E-glass. Soda-lime glass is widely used for containers, windows, lamps, lenses and tableware. Pyrex borosilicate is used in car headlights, cookware and laboratory equipment. Potash-soda-lead glass is used in lamp tubes and seals, while lime-magnesia aluminosilicate is used in cookware and for sealing molybdenum. Sodium borosilicate glass is used to seal tungsten and molybdenum and E-glass is used for insulation, polymer composites and fabrics.

These glasses contain mainly silica (SiO_2: 54-81%) with varying amounts of other oxide components like boric oxide (B_2O_3: 5-24%), sodium oxide (Na_2O: 1-15%), calcium oxide (CaO: 7-21%), aluminium oxide (Al_2O_3: 1-17%), as well as minor oxide species such as lead oxide (PbO), potassium oxide (K_2O) and magnesium oxide (MgO) incorporated into the overall glass

matrix composition, rather than present as discrete phases (Table 1.4). These additives adjust specific properties but exist in different forms to the glass network. Sodium, for example, is introduced as Na_2O but exists as dispersed Na^+ ions, requiring charge balancing by disrupting the network bonds. This modification reduces network connectivity, affects melting point, viscosity and electrical conductivity, introduces 'non-bonding oxygen' and significantly affects glass properties.

Table 1.4 Average composition of some representative commercial silicate glasses (wt.%). They mainly contain Silica, soda and aluminium oxide, with many minor additions to improve the properties of melting and forming.

Glass type	SiO_2	B_2O_3	Na_2O	K_2O	MgO	CaO	PbO	Al_2O_3
Soda-lime	73		15		4	7		1
Pyrex borosilicate	81	13	14					2
potash-soda-lead	62		7	7			22	2
lime-magnesia aluminosilicate	61	5	1		7	8		17
sodium borosilicate	68	24	6					2
E fibre glass	54	8	1		1	21		15
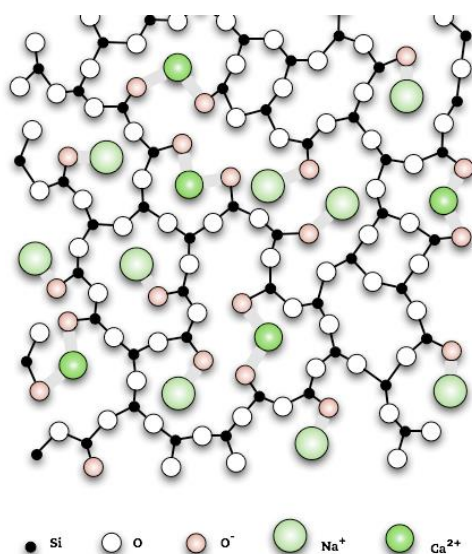
Figure 1.9 Modified network by intermediates, where ions randomly dispersed throughout the glass-forming network, network bond is then disrupted resulting in non-bonding oxygen.[199]

Soda-lime glass, pyrex borosilicate glass and vitreous silica glass are the most common types of glass, available in various shapes and sizes for retail purchase. Of these, soda-lime silicate (sodium-calcium silicate) glass is the predominant form, accounting for 90% of all glass applications and representing the most common type of glass produced historically and in modern times. Ancient glass compositions always included oxides of sodium, calcium and silicon due to their affordability, chemical durability and ease of melting and forming. The basic composition of soda-lime glass is typically about 70% silica (SiO_2), 15% soda (Na_2O), 10%

combined calcium oxide (CaO) and magnesium oxide (MgO), and 5% other oxides. Various minor additions improve the melting and forming properties (Figure 1.9): soda acts as a flux, lime as a stabiliser, alumina increases chemical resistance and reduces crystallisation, borates facilitate processing and reduce thermal expansion, zinc oxide lowers melting temperatures, and arsenic and antimony oxides are used for fining, i.e. removing bubbles. Due to its relatively low softening temperatures, soda-lime glass is often referred to as 'soft' glass.

1.7.3 Chemical durability of glass

Silicate glasses are among the most chemically inert materials commercially available. At temperatures below 300 °C they exhibit negligible reactions with liquids or gases, but they can react with water. Only at elevated temperatures do they react with gaseous hydrofluoric acid, producing volatile SiF_4. In addition, at temperatures above 1200°C, silicate glasses can react with strong reducing agents such as hydrogen or graphite.

The interaction of alkali silicate glasses with water is complex and involves at least two distinct processes: ion exchange between alkali ions in the glass and hydronium ions from the water, and dissolution of the glass in the liquid water. Consequently, the rate at which water corrodes silicate glass is influenced by several factors, including the pH of the solution (significant increase of dissolution rate at pH >8),[200] the volume of solution in contact with the glass, the concentration of the solution and the composition of the glass itself.

At extreme pH (pH >8), when exposed to water, alkali silicate glass undergoes ion exchange, whereby alkali ions from the glass exchange with hydronium ions in the water, resulting in the formation of NaOH, which dissolves and increases the alkalinity of the water. The rate of this exchange is also determined by the rate at which ions interdiffuse within the glass matrix, a process that is highly dependent on the composition of the glass. For example, the addition of calcium oxide to sodium silicate glass increases its durability. This process is negligible especially at pH 3-5. At elevated temperatures of approximately 500°C in the presence of an aqueous solution or overheated steam, the surface of glass undergoes dissolution through a series of hydrolysis reactions that break down the silicon-oxygen (Si-O) network. Initially, a gel-like layer forms on the glass surface due to the hydrolysis of Si-O bonds by water molecules. As the hydrolysis reactions continue, the glass network structure is progressively degraded, ultimately leading to the formation of silicic acid (Eq. 1.10 H_4SiO_4):

$$2\,H_2O + SiO_2 \rightarrow H_4SiO_4 \quad (Eq.\ 1.10)$$
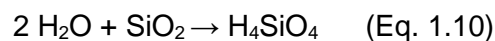
The hydrated surface of alkali silicate glass can either retain the structure of its dry counterpart,

thereby improving durability, or it can transform into a less dense structure that allows faster ion transport. The inclusion of alumina in the glass mitigates this transformation tendency, which correlates with its ability to minimise bulk phase separation. Binary alkali silicate glasses, characterised by a higher sodium content, are particularly susceptible to water attack, necessitating the addition of lime or magnesium to improve durability. As a result, commercial soda-lime glasses containing these additives retain their unaltered surfaces and exhibit improved durability.

Commercial soda-lime glass often contains alumina (Al_2O_3), which is known to improve the durability of the glass. The optimum addition of a few percent of alumina significantly increases durability by minimising the tendency to develop a transformed layer. Similarly, the addition of higher-value oxides such as titanium dioxide and zirconium dioxide further improves durability. Incorporating a second alkali oxide, such as calcium, into sodium silicate glass also improves durability, particularly when the molar ratio of alkali ions approaches equality. This improvement is due to the 'mixed alkali' effect, which reduces the mobility of one alkali ion in the presence of another, thereby increasing the durability of the glass.

1.7.4 Glass recycling

The surge in demand for glass products has led to a significant increase in waste glass, which is an ideal candidate for recycling.[201] Recycling glass not only saves energy, but is also in line with growing environmental awareness, highlighting the importance of integrating waste glass into various applications. As a result, post-consumer waste glass has become a significant component of the solid waste stream, putting additional pressure on landfills burdened with waste glass. Despite the growth of glass container recycling in many countries, logistical challenges, such as the cost of transporting collected glass to recycling facilities, hinder its efficient reuse in new products.[202] According to UK Statistics on Waste, as of 2020, the UK produced 2.4 million metric tonnes of glass packaging waste in 2017, achieving a recycling rate of 68%, slightly above the EU target of 60% and an increase of 0.6% on 2016.[203] Recycled glass is used in construction materials such as mortar, cement, concrete and blocks.[204,205]

However, a significant proportion of waste glass remains either in landfill or in storage, awaiting economically viable recycling opportunities. The potential of glass recycling to reduce energy consumption, raw material uses and wear and tear on production machinery underlines the urgent need to increase recycling efforts and meet current demand.

1.7.5 Glass in Fenton reaction

As mentioned in Section 1.3.3.3, the Fe^{2+} and Fe^{3+} ions have an excellent ability to promote the decomposition of hydrogen peroxide into hydroxyl radicals, which is critical to ensure the efficiency of an overall Fenton reaction. Zeolites, often analysed as catalyst supports in CWPO, are characterised by their hydrated crystalline aluminosilicate composition, derived from either natural or synthetic sources.[206] In contrast, soda-lime glass, which is inherently amorphous, often contains a small percentage of Al_2O_3 to increase its durability. With similar composition to zeolite, green beer glass bottles with ferric oxide content (more than 0.1 wt.% loading) could potentially be used as a heterogeneous catalyst, and they could help to remove various NSAIDs such as ibuprofen in wastewater. The total iron content of the glass was analysed by inductively coupled plasma optical emission spectroscopy (ICP-OES). The working hypothesis in this thesis work is that glass containing iron can be used as a substitute for iron-containing zeolite, which gives excellent performance in the Fenton reaction,[207–209] because a small amount of iron ion is able to generate the hydroxyl radical responsible for the oxidation of pollutants. This is because although iron-containing zeolite has been shown to be efficient as a catalyst in the Fenton reaction, it is rather expensive to scale up. An alternative is needed to offset the cost. Several studies have reported the synthesis of zeolite from waste materials containing silica and alumina,[210,211] and one reported synthesis from glass used in LCD panels.[212] Waste glass (£20 per tonne for green glass[213]) is much cheaper than zeolite (£700 per kg) because it comes from packaging such as beer bottles.

Recycled glass is available in large quantities and is relatively inexpensive, so recycling the used glass after the catalyst can be achieved at a lower cost than post-treating the zeolite. It can also form part of the circular economy (Section 1.8). In addition, experiments within the research group on similar organic pollutants, which are often treated by the Fenton reaction, have shown some promise. The use of ferrous glass, especially in the range of 4 mm to 0.1 mm, for water treatment applications has not been widely explored. Therefore, with the abundance in the waste sector, recycled ferrous glass could become a more economical and sustainable heterogeneous catalyst.

1.8 Waste management - Circular Economy

This concept utilises a circular economy approach. Approximately 2,500 million metric tonnes of waste were generated from household and economic activities in the EU. Of this waste, 47% was landfilled, 37% underwent recycling, and 10% was backfilled and the rest was incinerated.[214] In 2019, the European Union's ecological footprint exceeded the planet's ecosystems' capacity, as commented by a French member of the Green group. This suggests

that if global consumption matched the level of the EU, it would require the resources of 2.8 Earths to sustain such consumption.[215] The report highlights the prevalence of built-in product obsolescence and the lack of access to spare parts, warranty information, and repair options. This encourages consumers to buy new products instead of repairing existing ones. i.e., 59% of consumers are unaware that the legal minimum warranty period in the EU is two years.

1.8.1 Importance and Benefits of Circular Economy

The circular economy (CE) is a model of production and consumption that prioritises sharing, leasing, reusing, repairing, refurbishing, and recycling existing materials and products to extend their life cycle as much as possible and ultimately closing the loop of materials through high-value recycling efforts.[216–219] In practice, this model involves the minimisation of waste. When a product reaches the end of its life, its materials are recycled and reused, generating additional value within the economy. This approach represents a notable departure from the traditional linear economic model, which follows a take-make-consume-dispose pattern and relies on the abundance of low-cost, readily available resources and energy

Recent initiatives in South Korea, China, the United States, and Europe are promoting circular economies through remanufacturing and reuse. The EU Horizon 2020 program's 2014 circular-economy call for proposals and the European Commission's Circular Economy Package are significant steps towards this goal. The Ellen MacArthur Foundation has been raising awareness of this issue since 2010. Examples of circular economy implementation include eco-industrial parks like Kalundborg Symbiosis in Denmark and companies such as Xerox and Caterpillar. These companies are moving towards a model of selling services over goods, which aims for broader market adoption.

Adopting a circular economy provides three main benefits: environmental protection, reduced dependence on raw materials, and job creation while saving consumers money. Firstly, sustainable resource use practices can reduce biodiversity loss by minimizing the exploitation of natural resources and reducing disruptions to landscapes and habitats. Furthermore, prioritising the development of more efficient and sustainable products from the outset can lead to a reduction in total annual greenhouse gas emissions. Industrial processes and waste management contribute to 9% and 3% of the EU's greenhouse gas emissions, respectively. The design phase of a product is crucial as it influences over 80% of the product's environmental impact. For instance, in Europe, each individual generates 180 kg of waste packaging, emphasising the necessity for enhanced design and production processes.

Secondly, recycling raw materials can help to mitigate supply risks, including price volatility and import dependency. This is particularly crucial for critical raw materials required in

producing technologies vital for achieving climate goals, such as batteries and electric engines. The expanding global population increases the demand for raw materials, which poses a challenge due to the finite supplies available. This leads to some EU countries depending on imports for these essential resources. According to Eurostat data, the EU imports approximately half of the raw materials it consumes. Although the total trade value of raw materials with the rest of the world has almost tripled since 2002, the EU still has a trade deficit of €36 billion in 2021 as it imports more than it exports.[220]

Thirdly, transitioning to a circular economy is projected to enhance competitiveness, foster innovation, stimulate economic growth, and generate employment opportunities.[216] It is estimated that this transition will create 700,000 jobs within the European Union by 2030. Redesigning materials and products for circular use is expected to catalyse innovation across various economic sectors. Furthermore, this transition offers the potential for consumers to access more durable and innovative products, which could enhance their quality of life and result in long-term financial savings.

1.8.2 Difficulties in Waste Management towards Circular Economy

Conventional linear economic models, which are characterized by a 'take-make-dispose' approach, generate approximately two billion metric tonnes of municipal waste worldwide annually. The global material footprint has increased by 70% over the past two decades, indicating a significant escalation in resource consumption. Given these circumstances, it is evident that there is an urgent need to transition to a circular economy. However, currently, the global economy is estimated to be less than 10% circular,[221,222] with linear material flows being the prevailing mainstream approach.[218,219] Recent research has shown that there has been only a slight shift from a linear and moderately recycling system towards a more circular use of materials.[222–224] However, current waste management practices do not fully support the concept of a Circular Economy, and there is a need to identify new solutions for treating and utilizing waste effectively.[225,226] Waste management is acknowledged as a crucial factor in the transition towards a Circular Economy.[123,124] The key principles of CE involve using design to eliminate waste, regenerating biological materials, and restoring technological materials, which are at the heart of this research project.[227]

1.8.3 Application of Circular Economy in Water Purification

The application of circular economy principles to water purification involves creating systems that maximise water reuse, minimise waste, and enhance resource recovery. This approach redefines traditional water treatment processes, focusing on the recovery and regeneration of water, energy, and materials. Advanced treatment technologies can convert wastewater into

high-quality water suitable for various purposes, including agricultural irrigation, industrial processes, and even potable water supply. These systems can also recover valuable by-products such as phosphorus and nitrogen, which can be used as fertilisers, and capture energy through biogas production from organic matter in the wastewater.[228–231] Additionally, to minimize waste from water purification via CWPO, recycled glass can be included in the loop as a potential catalyst (Section 1.7.5), which can also be reused after purification process in construction or packaging. By integrating these principles, water purification is transformed from a process of removing contaminants to a platform for resource recovery. This aligns with the circular economy's goal of closing loops, reducing environmental impact and benefiting agricultural irrigation. The result is a more sustainable, efficient, and resilient water management system that conserves precious water resources.

1.9   Project aims

With the background and context outlined, the research presented in this thesis is aimed at the development of an innovative catalyst derived from recycled glass, which contains Fe^{3+} centres within the particle size range of 4 mm to 0.1 mm. This catalyst will be used to efficiently remove contaminants, specifically phenol and ibuprofen, from water via catalytic wet peroxide oxidation. In addition, the project will investigate the catalyst's effectiveness in the selective oxidation of fine chemicals, including benzyl alcohol and 1-phenylethanol. The overall aim is to embody the principles of the circular economy by reusing abundant waste materials, thereby increasing their value and lifetime through application in water purification. This approach not only promotes the reuse of treated water for irrigation, but also closes the material loop through high-value recycling initiatives, further extending the life cycle of these resources and as such diminishes the need of new input of energy demanding raw materials.

The aims for this research project are:

(i) to evaluate the feasibility and efficiency of using recycled glass containing Fe^{3+} as a heterogeneous catalyst for the decomposition of phenol. This study considers the effect of variation of several parameters, including the size of the glass beads, the molar ratio of metal to substrate (M:S), and the reaction time of this abatement process.

(ii) to develop a straightforward method for identifying all, or most, intermediates formed during the oxidation of ibuprofen, with particular emphasis on toxic aromatic intermediates. This evaluates the effectiveness of the catalyst in removing toxic water contaminants by Catalytic Wet Peroxide Oxidation (CWPO) using High Performance Liquid Chromatography (HPLC), in order to extract parameters like conversion selectivity and carbon mass balance that are

needed to explore the potential of using recycled glass as a heterogeneous catalyst for the removal of ibuprofen using the CWPO technique.

To reach these aims it was necessary to identify a suitable ^{1}H-NMR technique for the analysis of benzyl alcohol and 1-phenylethanol, together with their potential oxidation products. This will facilitate the investigation of the effectiveness of recycled glass as a catalyst in the partial oxidation of benzyl alcohol and 1-phenylethanol, using either air or molecular oxygen. Within this scope, the study will use different systems, including a plug flow reactor and a static pressurised reactor.

1.10 Reference

(1)   Gleick, P. H. *Science*, 2003, **302**, 1524-1528.

(2)   McGinnis, R. L. and Elimelech, M. *Environmental Science & Technology*, 2008, **42**, 8625-8629.

(3)   Shannon, M. A.; Bohn, P. W.; Elimelech, M.; Georgiadis, J. G.; Mariñas, B. J.; Mayes, A. M. *Nature*, 2008, **452**, 301-310.

(4)   Gadanakis, Y.; Bennett, R.; Park, J.; Areal, F. J. *Agricultural Water Management*, 2015, **160**, 22-32.

(5)   United Nations, The United Nations World Water Development Report 2023: Partnerships and Cooperation for Water. UNESCO, Paris.

(6)   FAO. *Water for Sustainable Food and Agriculture*; FAO: Rome, Italy, 2016.

(7)   Helmecke, M.; Fries, E.; Schulte, C. *Environmental Sciences Europe*, 2020, **32**, 4.

(8)   WHO, UNEP, Guidelines for the safe use of wastewater, excreta and greywater, Excreta and greywater use in agriculture, 2006, **4**.

(9)   Lazarova, V.; Asano, T.; Bahri, A.; Anderson, J. *Milestones in Water Reuse*, 1st ed.; IWA Publishing, 2013.

(10)   PUB   NEWater | *PUB,   Singapore's   National   Water   Agency*. https://www.pub.gov.sg/Public/WaterLoop/OurWaterStory/NEWater (accessed 2024-01-29).

(11)   Pimentel, D.; Berger, B.; Filiberto, D.; Newton, M.; Wolfe, B.; Karabinakis, E.; Clark, S.; Poon, E.; Abbett, E.; Nandagopal, S. *BioScience*, 2004, **54**, 909–918.

(12)   Free Vector | *Hand drawn water cycle. Freepik*. https://www.freepik.com/free-vector/hand-drawn-water-cycle_19058832.htm (accessed 2024-06-29).

(13)   *EUR-Lex - 02006R1907-20140410 - EN - EUR-Lex*. https://eur-lex.europa.eu/legal-content/EN/TXT/?uri=CELEX:02006R1907-20140410 (accessed 2024-01-30).

(14)   Denora, M.; Candido, V.; Brunetti, G.; De Mastro, F.; Murgolo, S.; De Ceglie, C.; Salerno, C.; Gatta, G.; Giuliani, M. M.; Mehmeti, A.; Bartholomeus, R. P.; Perniola, M. *Frontiers in Plant Science*, 2023, **14**, 1238163

(15)   González García, M.; Fernández-López, C.; Polesel, F.; Trapp, S. *Environmental Research*, 2019, **172**, 175-181.

(16)   Sun, Z.; Chu, L.; Wang, X.; Fang, G.; Liu, C.; Chen, H.; Gu C.; Gao, J. *Environmental Science & Technology*, 2023, **57**, 11967-11976.

(17)   Alshabib, M.; Onaizi, S. A. *Separation and Purification Technology*, 2019, **219**, 186-207.

(18)   Kanaujiya, D. K.; Paul, T.; Sinharoy, A.; Pakshirajan, K. *Current Pollution Reports*, 2019, **5**, 112-128.

(19)   Leahy, J. G.; Colwell, R. R. *Microbiological reviews*, 1990, **54**, 305-315.

(20)   Scott, J. P.; Ollis, D. F. *Environmental Progress*, 1995, **14**, 88-103.

(21)   Sipma, J.; Osuna, B.; Collado, N.; Monclús, H.; Ferrero, G.; Comas, J.; Rodriguez-Roda, I. *Desalination*, 2010, **250**, 653-659.

(22)   Low, E. *Water Research*, 2000, **34**, 3204-3212.

(23)   Milla, T. Starch-Based Biopolymers in Municipal Sludge Treatment Processes, (Master thesis, University of Aalto) 2024

(24)   Villegas, L. G. C.; Mashhadi, N.; Chen, M.; Mukherjee, D.; Taylor, K. E.; Biswas, N. *Current Pollution Reports*, 2016, **2**, 157-167.

(25)   Umar, M.; Roddick, F.; Fan, L. *Critical Reviews in Environmental Science and Technology*, 2015, **45**, 193-248.

(26)   Zupanc, M.; Kosjek, T.; Petkovšek, M.; Dular, M.; Kompare, B.; Širok, B.; Blažeka, Ž.; Heath, E. *Ultrasonics Sonochemistry*, 2013, **20**, 1104-1112.

(27)   Liang, L.; Song, X.; Kong, J.; Shen, C.; Huang, T.; Hu, Z. *Biodegradation*, 2014, **25**, 825-833.

(28)   Boll, M.; Geiger, R.; Junghare, M.; Schink, B. *Environmental Microbiology Reports*, 2020, **12**, 3-15.

(29)   Zheng, C.; Zhao, L.; Zhou, X.; Fu, Z.; Li, A. *Water Treatment*, 2013, **11**, 250-286.

(30)   Rajan, M. J.; Anish, C. I.; Rajan, M. J.; Anish, C. I. Role of Activated Carbon in Water Treatment. In *Water Quality - New Perspectives*; IntechOpen, 2022.

(31)   Hegazi, H. A. Removal of Heavy Metals from Wastewater Using Agricultural and Industrial Wastes as Adsorbents. *HBRC Journal*, 2013, **9**, 276-282.

(32)   Renu; Agarwal, M.; Singh, K. *Journal of Water Reuse and Desalination*, 2017, **7**, 387-419.

(33)   Khamparia, S.; Jaspal, D., *Handbook of Environmental Materials Management,* Springer, 2018, 1-14.

(34)   Al-Qodah, Z. *Water Research*, 2000, **34**, 4295-4303.

(35)   Koumanova, B.; Allen, S. J. *Journal of the University of Chemical Technology and Metallurgy*, 2005, **40**, 175-192.

(36)   Dąbrowski, A.; Podkościelny, P.; Hubicki, Z.; Barczak, M. *Chemosphere*, 2005, **58**, 1049-1070.

(37)   Moreno-Castilla, C.; Rivera-Utrilla, J. *MRS Bulletin*, 2001, **26**, 890-894.

(38)   Lu, P. J.; Lin, H. C.; Yu, W. T.; Chern, J. M. *Journal of the Taiwan institute of chemical engineers*, 2011, **42**, 305-311.

(39)   Pérez-Botella, E.; Valencia, S.; Rey, F. *Chemical Review*, 2022, **122**, 17647-17695.

(40)   Ruthven, D. M. *Chemie Ingenieur Technik*, 2011, **83**, 44-52.

(41)   de Magalhães, L. F., da Silva, G. R., & Peres, A. E. C. *Adsorption Science & Technology*, 2022, 1-26.

(42)   Zhang, J.; Wei, J.; Song, Z.; Song, J.; Wang, Y.; Pan, L.; Ding, G. *Journal of Environmental Engineering*, 2023, **149**, 05023004.

(43)   Lu, T.; Yan, W.; Xu, R. *Inorganic Chemistry Frontiers*, 2019, **6**, 1938-1951.

(44)   Rahman, M. M.; Awang, M. B.; Yusof, A. M. *Australian Journal of Basic and Applied Sciences*, 2012, **6,** 50-54.

(45)   Cramer, A. J.; Cole, J. M. *Journal of Materials Chemistry A*, 2017, **5**, 10746-10771.

(46)   Meteš, A.; Kovačević, D.; Vujević, D.; Papić, S. *Water Research*, 2004, **38**, 3373-3381.

(47)   Ozaki, H. *Proceedings of the Regional Symposium on Membrane Science and Technology*, 2004, 21-24.

(48)   Servos, M. R.; Bennie, D. T.; Burnison, B. K.; Jurkovic, A.; McInnis, R.; Neheli, T.; Schnell, A.; Seto, P.; Smyth, S. A.; Ternes, T. A. *Science of The Total Environment*, 2005, **336**, 155-170.

(49)   Urase, T.; Kikuta, T. *Water Research*, 2005, **39**, 1289-1300.

(50)   Petrovic, M.; Diaz, A.; Ventura, F.; Barceló, D. *Environmental Science & Technology*, 2003, **37**, 4442-4448.

(51)   Ternes, T. A.; Meisenheimer, M.; McDowell, D.; Sacher, F.; Brauch, H.-J.; Haist-Gulde, B.; Preuss, G.; Wilme, U.; Zulei-Seibert, N. *Environmental Science & Technology*, 2002, **36**, 3855-3863.

(52)   Westerhoff, P.; Yoon, Y.; Snyder, S.; Wert, E. *Environmental Science & Technology*, 2005, **39**, 6649-6663.

(53)   Valcárcel, Y.; Martínez, F.; González-Alonso, S.; Segura, Y.; Catalá, M.; Molina, R.; Montero-Rubio, J. C.; Mastroianni, N.; López de Alda, M.; Postigo, C.; Barceló, D. *Environment International*, 2012, **41**, 35-43.

(54)   Silva, A. M. T.; Zilhão, N. R.; Segundo, R. A.; Azenha, M.; Fidalgo, F.; Silva, A. F.; Faria, J. L.; Teixeira, J. *Chemical Engineering Journal*, 2012, **184**, 213-220.

(55) Babuponnusami, A.; Muthukumar, K. *CLEAN - Soil, Air, Water*, 2011, **39**, 142-147.

(56) Rey, A.; Faraldos, M.; Casas, J. A.; Zazo, J. A.; Bahamonde, A.; Rodríguez, J. J. *Applied Catalysis B: Environmental*, 2009, **86**, 69-77.

(57) Kuśmierek, K. *Reaction Kinetics, Mechanisms and Catalysis*, 2016, **119**, 19-34.

(58) Chatzisymeon, E.; Foteinis, S.; Mantzavinos, D.; Tsoutsos, T. *Journal of Cleaner Production*, 2013, **54**, 229-234.

(59) Pignatello, J. J.; Oliveros, E.; MacKay, A. *Critical Reviews in Environmental Science and Technology*, 2006, **36**, 1-84.

(60) Skoumal, M.; Rodríguez, R. M.; Cabot, P. L.; Centellas, F.; Garrido, J. A.; Arias, C.; Brillas, E. *Electrochimica Acta*, 2009**, 54**, 2077-2085.

(61) Scheers, T.; Appels, L.; Dirkx, B.; Jacoby, L.; van Vaeck, L.; van der Bruggen, B.; Luyten, J.; Degrèv, J.; van Impe, J.; Dewil, R. *Desalination and Water Treatment*, 2012, **50**, 189-197.

(62) Méndez-Arriaga, F.; Esplugas, S.; Giménez, J. *Water Research*, 2008**, 42**, 585-594.

(63) Siemens AG. Zimpro ® Wet Air Oxidation System : Innovative Technologies for Difficult Waste Water Treatment Problems. *Water Solutions*, 2013.

(64) Boucher, V.; Beaudon, M.; Ramirez, P.; Lemoine, P.; Volk, K.; Yargeau, V.; Segura, P. A. *Environmental Science: Water Research & Technology*, 2021, **7**, 1301-1314.

(65) Li, D.; Wang, D.; Jiang, Z. *Current Organocatalysis*, 2020, **7**, 199-211.

(66) Hu, L.; Guo, N.; Hu, M.; Yan, Z.; Gao, R.; Ma, J.; Hu, Y.; Peng, L. *IOP Conference Series: Earth and Environmental Science*, 2020, **512**, 012036.

(67) Besson, M.; Descorme, C.; Bernardi, M.; Gallezot, P.; Di Gregorio, F.; Grosjean, N.; Pham Minh, D.; Pintar, A. *Environmental Technology*, 2010, **31**, 1441-1447.

(68) Grosjean, N.; Descorme, C.; Besson, M. *Applied Catalysis B: Environmental*, 2010, **97**, 276-283.

(69) Fenton, H. J. H. *Journal of the Chemical Society Transactions*, 1894, **65**, 899-910.

(70) Bokare, A. D.; Choi, W. *Journal of Hazardous Materials*, 2014, **275**, 121-135.

(71) Babuponnusami, A.; Muthukumar, K. *Journal of Environmental Chemical Engineering*, 2014, **2**, 557-572.

(72) Thomas, N.; Dionysiou, D. D.; Pillai, S. C. *Journal of Hazardous Materials*, 2021, **404**, 124082.

(73) Neyens, E.; Baeyens, J. *Journal of Hazardous Materials*, 2003, **98**, 33-50.

(74) Bokare, A. D.; Choi, W. *Journal of Hazardous Materials*, 2014, **275**, 121-135.

(75) Ghernaout D.; Elboughdiri N.; Ghareba S. *Open Access Library Journal*, 2020, **7**, 1-26.

(76) Pérez, M.; Torrades, F.; Domènech, X.; Peral, J. *Journal of Chemical Technology & Biotechnology*, 2002, **77**, 525-532.

(77) Zhang, M.; Dong, H.; Zhao, L.; Wang, D.; Meng, D. *Science of The Total Environment*, 2019, **670**, 110-121.

(78) Matavos-Aramyan, S.; Moussavi, M. *International Journal of Environmental Sciences & Natural Resources*, 2017, **2**, 115-132.

(79) Barrault, J.; Bouchoule, C.; Tatibouët, J.-M.; Abdellaoui, M.; Majesté, A.; Louloudi, I.; Papayannakos, N.; Gangas, N. H. *Studies in Surface Science and Catalysis*, 2000, **130**, 749-754.

(80) Mirzaei, A.; Chen, Z.; Haghighat, F.; Yerushalmi, L. *Chemosphere*, 2017, **174**, 665-688.

(81) Nidheesh, P. V. *RSC Advances*, 2015, **5**, 40552-40577.

(82) Van Santen R. A. *Modern heterogeneous catalysis: an introduction*. John Wiley & Sons, 2017.

(83) Adityosulindro, S.; Julcour, C.; Barthe, L. *Journal of Environmental Chemical Engineering*, 2018, **6**, 5920-5928.

(84) Arimi, M. M. *Progress in Natural Science: Materials International*, 2017, **27**, 275-282.

(85) Oliveira, J. S. de; Mazutti, M. A.; Urquieta-González, E. A.; Foletto, E. L.; Jahn, S. L. *Materials Research*, 2016, **19**, 1399-1406.

(86) Moma, J.; Baloyi, J.; Ntho, T. *RSC Advances*, 2018, **8**, 30115-30124.

(87) Iwanow, M.; Gärtner, T.; Sieber, V.; König, B. *Beilstein Journal of Organic Chemistry*, 2020, **16**, 1188–1202.

(88) Trueba, M.; Trasatti, S. P. *European Journal of Inorganic Chemistry*, 2005, **17**, 3393-3403.

(89) Cuzzola, A.; Bernini, M.; Salvadori, P. *Applied Catalysis B: Environmental*, 2002, **36**, 231-237.

(90) Ivanova, I. I.; Kuznetsov, A. S.; Yuschenko, V. V.; Knyazeva, E. E. *Pure and Applied Chemistry*, 2004, **76**, 1647-1657.

(91) Catrinescu, C.; Teodosiu, C.; Macoveanu, M.; Miehe-Brendlé, J.; Le Dred, R. *Water Research*, 2003, **37**, 1154-1160.

(92) Davidson R S. *Journal of Photochemistry and Photobiology B: Biology*, 1996, **33**, 3-25.

(93) R Rappaport, S. M.; Kim, S., Lan; Q., Li; G., Vermeulen; R., Waidyanatha; S., Rothman, N. *Chemico-biological interactions*, 2010, **184**, 189-195.

(94) Tsuruta, Y.; Watanabe, S.; Inoue, H. *Analytical Biochemistry*, 1996, **243**, 86-91.

(95) Vattem, D. A.; Shetty, K. *Process Biochemistry*, 2003, **39**, 367-379.

(96) Careghini, A.; Mastorgio, A. F.; Saponaro, S.; Sezenna, E.; *Environmental Science and Pollution Research,* 2015, **22**, 5711-5741.

(97) Bruce, R. M.; Santodonato, J.; Neal, M. W. *Toxicology and Industrial Health*, 1987, **3**, 535-568.

(98) Takeichi, T.; N. Furukawa. 2012, 723-751.

(99) Fabris, H. J.; Knauss, W. G. *Comprehensive Polymer Science and Supplements* 1989, 131-177.

(100) Paasivirta, J.; Heinola, K.; Humppi, T.; Karjalainen, A.; Knuutinen, J.; Mäntykoski, K.; Särkkä, J. *Chemosphere*, 1985, **14**, 469-491.

(101) Badanthadka, M.; Mehendale, H. M. *Encyclopedia of Toxicology (Third Edition),* 2014, 896-899.

(102) Lee, H.-B.; Weng, L.-D.; Chau, A. S. Y. *Journal of Association of Official Analytical Chemists*, 1984, **67**, 1086-1091.

(103) Bevilaqua, J. V.; Cammarota, M. C.; Freire, D. M. G.; Sant'Anna Jr., G. L. *Brazilian Journal of Chemical Engineering*, 2002, **19**, 151-158.

(104) Mu'azu, N. D.; Jarrah, N.; Zubair, M.; Alagha, O. *International Journal of Environmental Research and Public Health*, 2017, **14**, 1094.

(105) Kwon, K.-D.; Jo, W.-K.; Lim, H.-J.; Jeong, W.-S. *Environmental Science and Pollution Research*, 2008, **15**, 521-526.

(106) Pivnenko, K.; Pedersen, G. A.; Eriksson, E.; Astrup, T. F. *Waste Management*, 2015, **44**, 39-47.

(107) Kurata, Y.; Ono, Y.; Ono, Y. *Journal of material cycles and waste management*, 2008, **10**, 144-152.

(108) Krastanov, A.; Alexieva, Z.; Yemendzhiev, H. *Engineering in Life Sciences*, 2013, **13**, 76-87.

(109) Duan, W.; Meng, F.; Cui, H.; Lin, Y.; Wang, G.; Wu, J. *Ecotoxicology and environmental safety*, 2018, **157**, 441-456.

(110) US Department of health and human servies. Public Health Service, *Agency for Toxic Substances and Disease Registry*. 2008.

(111) Sun, X.; Wang, C.; Li, Y.; Wang, W.; Wei, J. *Desalination*, 2015, **355**, 68-74.

(112) Pedlosky, J. *Journal of Fluid Mechanics*, 1981, **102**, 169-209.

(113) Friedrich, L. C.; Machulek Jr, A.; Silva, V. D. O.; Quina, F. H. *Scientia Agricola*, 2012, **69**, 347-351.

(114) Montgomery-Brown, J.; Reinhard, M. *Environmental Engineering Science*, 2003, **20**, 471-486.

(115) Gupta, S.; Ashrith, G.; Chandra, D.; Gupta, A. K.; Finkel, K. W.; Guntupalli, J. S. *Clinical Toxicology*, 2008, **46**, 250-253.

(116) National Research Council; Division on Earth; Life Studies, Board on Environmental Studies; Committee on Toxicology; Committee on *Acute Exposure Guideline Levels. Acute Exposure Guideline Levels for Selected Airborne Chemicals*. National Academies Press (US) 2010, **8**.

(117) Villegas, L. G. C.; Mashhadi, N.; Chen, M.; Mukherjee, D.; Taylor, K. E.; Biswas, N. A Short Review of Techniques for Phenol Removal from Wastewater. *Current Pollution Reports*, 2016, **2**, 157-167.

(118) Anku, W. W.; Mamo, M. A.; Govender, P. P.; Anku, W. W.; Mamo, M. A.; Govender, P. P. *Phenolic compounds-natural sources, importance and applications*, 2017, 419-443.

(119) Schweigert, N.; Zehnder, A. J. B.; Eggen, R. I. L. *Environmental Microbiology*, 2001, **3**, 81-91.

(120) Rohn, S. *Food Research International*, 2014, **65**, 13-19.

(121) Muñoz-de-Toro, M.; Markey, C. M.; Wadia, P. R.; Luque, E. H.; Rubin, B. S.; Sonnenschein, C.; Soto, A. M. *Endocrinology*, 2005, **146**, 4138-4147.

(122) Calabrese, E. J.; Kenyon, E. M. *Air Toxics and Risk Assessment*; Lewis Publishers: United States, 1991.

(123) Verma, S. R.; Tonk, I. P.; Gupta, A. K.; Saxena, M. *Water Research*, 1984, **18**, 111-115.

(124) Jeong-Seon, K. I. M.; Pyung, C. *Korean Journal of Fisheries and Aquatic Sciences* 1995, **28**, 87-97.

(125) Saha, N.; Bhunia, F.; Kaviraj, A. *Bulletin of environmental contamination and toxicology*, 1999, **63**, 195-202.

(126) Li, E.; Bolser, D. G.; Kroll, K. J.; Brockmeier, E. K.; Falciani, F.; Denslow, N. D. *Aquatic Toxicology*, 2018, **201**, 66-72.

(127) Santos, A.; Yustos, P.; Quintanilla, A.; Rodrıguez, S.; Garcıa-Ochoa, F. *Applied Catalysis B: Environmental*, 2002, **39**, 97-113.

(128) Santos, A.; Yustos, P.; Quintanilla, A.; Garcıa-Ochoa, F. *Applied Catalysis B: Environmental*, 2004, **53**, 181-194.

(129) Alejandre, A.; Medina, F.; Fortuny, A.; Salagre, P.; & Sueiras, J. E. *Applied Catalysis B: Environmental*, 1998, **16**, 53-67.

(130) Zazo, J. A.; Casas, J. A.; Mohedano, A. F.; Gilarranz, M. A.; Rodríguez, J. J. *Environmental science & technology*, 2005, **39**, 9295-9302.

(131) Liotta, L. F.; Gruttadauria, M.; Di Carlo, G.; Perrini, G.; Librando, V. *Journal of hazardous materials*, 2009, **162**, 588-606.

(132) *(*Quintanilla, A.; Casas, J. A.; Mohedano, A. F.; & Rodríguez, J. J. *Applied Catalysis B: Environmental*, 2006, **67**, 206-216.

(133) Santos, A.; Yustos, P.; Quintanilla, A.; García-Ochoa, F.; Casas, J. A.; Rodríguez, J. J. *Environmental science & technology*, 2004, **38**, 133-138.

(134) Sadana, A.; Katzer, J. R. *Industrial & Engineering Chemistry Fundamentals*, 1974, **13**, 127-134.

(135) Raitano, G.; Goi, D.; Pieri, V.; Passoni, A.; Mattiussi, M.; Lutman, A.; Romeo, I.; Manganaro, A.; Marzo, M.; Porta, N.; Baderna, D.; Colombo, A.; Aneggi, E.; Natolino, F.; Lodi, M.; Bagnati, R.; Benfenati, E. *Environment International*, 2018, **119**, 275-286.

(136) Weber, F.-A.; Aus Der Beek, T.; Carius, A.; Grüttner, G.; Hickmann, S.; Ebert, I.; Hein, A.; Küster, A.; Rose, J.; Koch-Jugl, J.; Stolzenberg, H.-C. *Environmental Toxicology and Chemistry*, 2014, **35**, 823-835.

(137) Jan-Roblero, J.; Cruz-Maya, J. A. *Molecules*, 2023, **28**, 2097.

(138) Marchlewicz, A.; Guzik, U.; Wojcieszyńska, D. *Water, Air, & Soil Pollution*, 2015, **226**,

(139) Marchlewicz, A.; Guzik, U.; Wojcieszyńska, D. *Water Air Soil Pollut*, 2015, **226**, 355.

(140) Parolini, M.; Binelli, A.; Provini, A. *Ecotoxicology and Environmental Safety*, 2011, **74**, 1586-1594.

(141) Davies, N. M. *Clinical Pharmacokinetics*, 1998, **34**, 101-154.

(142) Lloyd, M. D.; Yevglevskis, M.; Lee, G. L.; Wood, P. J.; Threadgill, M. D.; Woodman, T. J. *Progress in Lipid Research*, 2013, **52**, 220-230.

(143) Woodman, T. J.; Wood, P. J.; Thompson, A. S.; Hutchings, T. J.; Steel, G. R.; Jiao, P.; Threadgill, M. D.; Lloyd, M. D. *Chemical Communications*, 2011, **47**, 7332.

(144) Boxall, A. B. A.; Keller, V. D. J.; Straub, J. O.; Monteiro, S. C.; Fussell, R.; Williams, R. J. *Environment international*, 2014, **73**, 176-185.

(145) Luo, Y.; Guo, W.; Ngo, H. H.; Nghiem, L. D.; Hai, F. I.; Zhang, J.; Liang, S.; Wang, X. C. *Science of The Total Environment*, 2014, **473-474**, 619-641.

(146) Guerra, P.; Kim, M.; Shah, A.; Alaee, M.; Smyth, S. A. *Science of the Total Environment*, 2014, **473-474**, 235-243.

(147) Vergeynst, L.; Haeck, A.; De Wispelaere, P.; Van Langenhove, H.; Demeestere, K. *Chemosphere*, 2015, **119**, S2-S8.

(148) Almeida, B.; Kjeldal, H.; Lolas, I.; Knudsen, A. D.; Carvalho, G.; Nielsen, K. L.; Barreto Crespo, M. T.; Stensballe, A.; Nielsen, J. L. *Biodegradation*, 2013, **24**, 615-630.

(149) Matongo, S.; Birungi, G.; Moodley, B.; Ndungu, P. *Chemosphere*, 2015, **134**, 133-140.

(150) Vazquez-Roig, P.; Andreu, V.; Blasco, C.; Picó, Y. *Science of The Total Environment*, 2012, **440**, 24-32.

(151) Ashfaq, M.; Nawaz Khan, K.; Saif Ur Rehman, M.; Mustafa, G.; Faizan Nazar, M.; Sun, Q.; Iqbal, J.; Mulla, Sikandar. I.; Yu, C.-P. *Ecotoxicology and Environmental Safety*, 2017, **136**, 31-39.

(152) Aymerich, I.; Acuña, V.; Barceló, D.; García, M. J.; Petrovic, M.; Poch, M.; Rodriguez-Mozaz, S.; Rodríguez-Roda, I.; Sabater, S.; von Schiller, D.; Corominas, Ll. *Water Research*, 2016, **100**, 126-136.

(153) Ferrando-Climent, L.; Collado, N.; Buttiglieri, G.; Gros, M.; Rodriguez-Roda, I.; Rodriguez-Mozaz, S.; Barceló, D. *Science of The Total Environment*, 2012, **438**, 404-413.

(154) Lin, J.; Zhang, Y.; Bian, Y.; Zhang, Y.; Du, R.; Li, M.; Tan, Y.; Feng, *Science of The Total Environment*, 2023, **904**, 166897.

(155) Rudy, A. C.; Knight, P. M.; Brater, D. C.; Hall, S. D. *The Journal of pharmacology and experimental therapeutics*, 1991, **259**, 1133-1139.

(156) Kepp, D. R.; Sidelmann, U. G.; Hansen, S. H. *Pharmaceutical research*, 1997, **14**, 676-680.

(157) Cao, F.; Zhang, M.; Yuan, S.; Feng, J.; Wang, Q.; Wang, W.; Hu, Z. *Environmental Science and Pollution Research*, 2016, **23**, 12303-12311.

(158) Rácz, G.; Csenki, Z.; Kovács, R.; Hegyi, Á.; Baska, F.; Sujbert, L., Szende, B. *Pathology & Oncology Research*, 2012, **18**, 579-584.

(159) Zheng, B. G.; Zheng, Z.; Zhang, J. B.; Luo, X. Z.; Wang, J. Q.; Liu, Q.; Wang, L. H. *Desalination*, 2011, **276**, 379-385.

(160) Parolini, M.; Binelli, A. *Ecotoxicology*, 2012, **21**, 379-392.

(161) Oliveira, L. L. D.; Antunes, S. C.; Gonçalves, F.; Rocha, O.; Nunes, B. *Ecotoxicology and Environmental Safety*, 2015, **119**, 123-131.

(162) Kayani, M. A., Parry, J. M., Vickery, S., & Dodds, P. F. *Environmental and molecular mutagenesis*, 2009, **50**, 277-284.

(163) Falfushynska, H.; Poznanskyi, D.; Kasianchuk, N.; Horyn, O.; Bodnar, O. *Bull Environ Contam Toxicol*, 2022, **109**, 1010-1017.

(164) Martyniuk, V.; Gylytė, B.; Matskiv, T.; Khoma, V.; Tulaidan, H.; Gnatyshyna, L.; Stoliar, O. *Ecotoxicology*, 2022, **31**, 1369-1381.

(165) Han, S.; Choi, K.; Kim, J.; Ji, K.; Kim, S.; Ahn, B.; Yun, J.; Choi, K.; Khim, J. S.; Zhang, X.; Giesy, J. P. *Aquatic Toxicology*, 2010, **98**, 256-264.

(166) Adamczuk, M. *Science of The Total Environment*, 2022, **848**, 157783.

(167) Wijaya, L.; Alyemeni, M.; Ahmad, P.; Alfarhan, A.; Barcelo, D.; El-Sheikh, M. A.; Pico, Y. *Plants (Basel)*, 2020, **9**, 1473.

(168) Gonzalez-Rey, M.; Bebianno, M. J. *Environmental Toxicology and Pharmacology*, 2012, **33**, 361-371.

(169) Wang, L.; Peng, Y.; Nie, X.; Pan, B.; Ku, P.; Bao, S. *Comparative Biochemistry and Physiology Part C: Toxicology & Pharmacology*, 2016, **179**, 49-56.

(170) Suarez, S.; Lema, J.; OMIL, F. *Bioresource Technology*, 2009, **100**, 2138-2146.

(171) Jermann, D.; Pronk, W.; Boller, M.; Schäfer, A. I. *Journal of Membrane Science*, 2009, **329**, 75-84.

(172) Sahar, E.; David, I.; Gelman, Y.; Chikurel, H.; Aharoni, A.; Messalem, R.; Brenner, A. *Desalination*, 2011, **273**, 142-147.

(173) Trinh, T.; van den Akker, B.; Stuetz, R. M.; Coleman, H. M.; Le-Clech, P.; Khan, S. J. *Water Science and Technology*, 2012, **66**, 1856-1863.

(174) Tadkaew, N.; Hai, F. I.; McDonald, J. A.; Khan, S. J.; Nghiem, L. D. *Water Research*, 2011, **45**, 2439-2451.

(175) Kruglova, A.; Kråkström, M.; Riska, M.; Mikola, A.; Rantanen, P.; Vahala, R.; Kronberg, L. *Bioresource Technology*, 2016, **214**, 81-88.

(176) Hussain, S.; Aneggi, E.; Briguglio, S.; Mattiussi, M.; Gelao, V.; Cabras, I.; Zorzenon, L.; Trovarelli, A.; Goi, D. *Journal of Environmental Chemical Engineering*, 2020, **8**.

(177) Monteiro, R. T.; Santana, R. M. da R.; Silva, A. M. R. B. da; Lucena, A. L. A. de; Zaidan, L. E. M. C.; Silva, V. L. da; Napoleão, D. C. *Revista Eletrônica em Gestão, Educação e Tecnologia Ambiental*, 2018, **22**, 3.

(178) Sheldon, R. Metal-Catalyzed Oxidations of Organic Compounds: Mechanistic Principles and Synthetic Methodology Including Biochemical Processes; *Elsevier*, 2012.

(179) Hajimohammadi, M.; Safari, N.; Mofakham, H.; Deyhimi, F. *Green chemistry*, 2011, **13**, 991-997.

(180) Tojo, G.; Fernandez, M. I. *Oxidation of Alcohols to Aldehydes and Ketones: A Guide to Current Common Practice*; Springer Science & Business Media, 2006.

(181) J. Jachuck, R. J.; K. Selvaraj, D.; S. Varma, R. *Green Chemistry*, 2006, **8**, 29-33.

(182) Ragupathi, C.; Judith Vijaya, J.; Narayanan, S.; Jesudoss, S. K.; John Kennedy, L. *Ceramics International*, 2015, **41**, 2069-2080.

(183) Zhu, S.; Cen, Y.; Yang, M.; Guo, J.; Chen, C.; Wang, J.; Fan, W. *Applied Catalysis B: Environmental*, 2017, **211**, 89-97.

(184) Datta Mal, D.; Khilari, S.; Pradhan, D. *Green Chemistry*, 2018, **20**, 2279-2289.

(185) Lu, C.; Hu, J.; Meng, Y.; Zhou, A.; Zhang, F.; Zhang, Z. *Chemical Engineering Research and Design*, 2019, **141**, 181-186.

(186) Miao, C.; Zhao, H.; Zhao, Q.; Xia, C.; Sun, W. *Catalysis Science & Technology*, 2016, **6**, 1378-1383.

(187) Sanders, H. J.; Keag, H. F.; McCullough, H. S. *Industrial and Engineering Chemistry*, 1953, **45**, 2-14.

(188) Mahmood, A.; Robinson, G. E.; Powell, L. *Organic Process Research & Development*, 1999, **3**, 363-364.

(189) Thottathil, J. K.; Moniot, J. L.; Mueller, R. H.; Wong, M. K. Y.; Kissick, T. P. *The Journal of Organic Chemistry*, 1986, **51**, 3140-3143.

(190) Cánepa, A. L.; Elías, V. R.; Vaschetti, V. M.; Sabre, E. V.; Eimer, G. A.; Casuscelli, S. G. *Applied Catalysis A: General*, 2017, **545**, 72-78.

(191) Yu, H.; Peng, F.; Tan, J.; Hu, X.; Wang, H.; Yang, J.; Zheng, W. *Angewandte Chemie*, 2011, **17**, 4064-4068.

(192) Yuan, Z.; Liu, B.; Zhou, P.; Zhang, Z.; Chi, Q. *Catalysis Science & Technology*, 2018, **8**, 4430-4439.

(193) Chen, C.-T.; Nguyen, C. V.; Wang, Z.-Y.; Bando, Y.; Yamauchi, Y.; Bazziz, M. T. S.; Fatehmulla, A.; Farooq, W. A.; Yoshikawa, T.; Masuda, T.; Wu, K. C.-W. *ChemCatChem*, 2018, **10**, 361-365.

(194) Martín, S. E.; Suárez, D. F. *Tetrahedron Letters*, 2002, **43**, 4475-4479.

(195) Hu, Y.; Chen, L.; Li, B. *Catalysis Communications*, 2018, **103**, 42-46.

(196) Zhang, E.; Tian, H.; Xu, S.; Yu, X.; Xu, Q. *Organic. Letter*, 2013, **15**, 2704-2707.

(197) Jiang, Z.-H.; Zhang, Q.-Y. *Progress in Materials Science*, 2014, **61**, 144-215.

(198) Lichtenstein, L. The Structure of Two-Dimensional Vitreous Silica, (Dissertation, University of Berlin), 2012.

(199) Brown, L.; Hayes, J. *Molecular Engineering - Perfecting Glass Composition*. Glassflake. https://www.glassflake.com/blog/2021/07/05/molecular-engineering-perfecting-glass-composition (accessed 2024-03-01).

(200) Bansal, N. P.; Doremus, R. H. *Handbook of Glass Properties*; Elsevier, 2013.

(201) Kaza, S.; Yao, L.; Bhada-Tata, P.; Van Woerden, F. *What a Waste 2.0: A Global Snapshot of Solid Waste Management to 2050*; The World Bank, 2018.

(202) Corinaldesi, V.; Nardinocchi, A.; Donnini, J. *European Journal of Environmental and Civil Engineering*, 2016, **20**, s140-s151.

(203) DEFRA. UK Statistics on Waste Key Points Data Revisions in This Update : 2020, **3**, 1-19.

(204) Kou, S. C.; Poon, C. S. *Cement and Concrete Composites*, 2009, **31**, 107-113.

(205) Rashad, A. M. *Construction and Building Materials*, 2014, **72**, 340-357.

(206) Derouane, E. G.; Lemos, F.; Naccache, C.; Ribeiro, F. R. Zeolite Microporous Solids: Synthesis, Structure, and Reactivity; *Springer Science & Business Media*, 2012.

(207) Gonzalez-Olmos, R.; Martin, M. J.; Georgi, A.; Kopinke, F.-D.; Oller, I.; Malato, S. *Applied Catalysis B: Environmental*, 2012, 125, 51–58.

(208) Perisic, D. J.; Gilja, V.; Stankov, M. N.; Katancic, Z.; Kusic, H.; Stangar, U. L.; Dionysiou, D. D.; Bozic, A. L. *Journal of Photochemistry and Photobiology A: Chemistry*, 2016, 321, 238–247.

(209) Yang, X.; Cheng, X.; Elzatahry, A. A.; Chen, J.; Alghamdi, A.; Deng, Y. *Chinese Chemical Letters*, 2019, **30**, 324-330

(210) Murayama, N.; Yamamoto, H.; Shibata, J. *International Journal of Mineral Processing*, 2002, **64**, 1-17.

(211) Sugano, Y.; Sahara, R.; Murakami, T.; Narushima, T.; Iguchi, Y.; Ouchi, C. *ISIJ International*, 2005, **45**, 937-945.

(212) Tsujiguchi, M.; Kobashi, T.; Oki, M.; Utsumi, Y.; Kakimori, N.; Nakahira, A. *Journal of Asian Ceramic Societies*, 2014, **2**, 27-32.

(213) Tomić, T.; Schneider, D. R. *Journal of Environmental Management*, 2020, **267**, 110564.

(214) Hidalgo, D.; Martín-Marroquín, J. M.; Corona, F. *Renewable and Sustainable Energy Reviews*, 2019, **111**, 481-489.

(215) *WWF EU Overshoot Day Report*, 2019

https://awsassets.panda.org/downloads/wwf_eu_overshoot_day___living_beyond_nature_s_limits_web (accessed 2024-06-29).

(216) *Circular economy: definition, importance and benefits. Topics | European Parliament.* https://www.europarl.europa.eu/topics/en/article/20151201STO05603/circular-economy-definition-importance-and-benefits (accessed 2024-02-25).

(217) Djuric Ilic, D.; Eriksson, O.; Ödlund (former Trygg), L.; Åberg, M. *Journal of Cleaner Production*, 2018, **182**, 352-362.

(218) Govindan, K., & Hasanagic, M. I*nternational Journal of Production Research*, 2018, **56**, 278-311.

(219) Taelman, S. E.; Tonini, D.; Wandl, A.; Dewulf, J. *Sustainability*, 2018, **10**, 2184.

(220) *Extra-EU trade of raw materials tripled since 2002*.
 https://ec.europa.eu/eurostat/web/products-eurostat-news/-/ddn-20220425-1   (accessed 2024-06-29).

(221) Brown, A.; Haas, D. W.; Laubscher, M.; Pallecchi, A.; Reh, F.; Rietveld, E.; Soezer, A.; van, K. *Circular economy foundation*. 2018, **1**.

(222) Haas, W.; Krausmann, F.; Wiedenhofer, D.; Heinz, M. *Journal of Industrial Ecology*, 2015, **19**, 765-777.

(223) Mayer, A.; Haas, W.; Wiedenhofer, D.; Krausmann, F.; Nuss, P.; Blengini, G. A. *Journal of industrial ecology*, 2019, **23**, 62-76.

(224) Silva, A.; Rosano, M.; Stocker, L.; Gorissen, L. *Waste Management*, 2017, **61**, 547-557.

(225) Zhang, A.; Venkatesh, V. G.; Liu, Y.; Wan, M.; Qu, T.; Huisingh, D. *Journal of Cleaner Production*, 2019, **240**, 118198.

(226) Fellner, J., Lederer, J., Scharff, C., & Laner, D. *Journal of Industrial Ecology*, 2017, **21**, 494-496.

(227) The circular economy | *Nature*. https://www.nature.com/articles/531435a (accessed 2024-02-26).

(228) Sengupta, S.; Nawaz, T.; Beaudry, J. W. *Current Pollution Reports*, 2015, **1**, 155-166.

(229) Fang, C.; Zhang, T.; Li, P.; Jiang, R.; Wu, S.; Nie, H.; Wang, Y. *Journal of environmental sciences*, 2015, **29**, 106-114.

(230) Hou, H.; Li, Z.; Liu, B.; Liang, S.; Xiao, K.; Zhu, Q.; Hu, S.; Yang, J.; Hu, J. *The Science of the total environment*, 2019, **704**, 135274.

(231) Shepherd, J. G.; Sohi, S.; Heal, K. *Water Research*, 2016, **94**, 155-165.

Chapter 2 Experimental

This chapter explains the experimental framework, including the materials and equipment used for testing and analysing catalysts, the synthesis (zeolites) and characterization of the catalyst (zeolites and glass), the execution of catalyst tests, and the chemical analysis used to characterize reaction mixtures.

2.1   Materials and methods

All reagents were used as received without any further purification, unless otherwise specified in the text. For all purity values, it refers to mass % unless otherwise specified in the text.

2.1.1 Preparation of inorganic catalysts

2.1.1.1 Zeolites

The materials and chemicals used for catalysts preparation include zeolite NH_4-ZSM-5 (surface area 425 $m^2 g^{-1}$, SiO_2: Al_2O_3 mole ratio 23:1, Alfa Aesar), Iron (III) nitrate nonahydrate (Fe $(NO_3)_3 \cdot 9H_2O$, 99+% purity, Acros).

2.1.1.2 Recycled glass

The recycled glass comes from two main sources (Table 2.1): glass recycling company, namely GTS (Rotherham, UK), and consumer-level recycling from grocery stores. The glass recycled from stores includes a variety of brands and colors, such as Green and Brown glass from brands like Thirsty and Becks, and Transparent glass from Vinho Verde.

Table 2.1 Sources of recycled glass samples with their glass code, respective iron content (wt.%) and their colours. Iron content measured by ICP-OES (section 2.3.2).

Glass code	Iron content wt.%	Source of glass	Colour of glass
G1	0.23	GTS	green
G2	0.33	Becks	green
G3	0.25	Thirsty	brown
G4	0.07	Vinho Verde	transparent
G5	0.05	Gallo	transparent

2.1.2 Materials for catalyst tests

Phenol (C_6H_6O, MW: 94.11 g mol^{-1}, 99%, Acros), iron(II) sulfate heptahydrate ($FeSO_4 \cdot 7H_2O$, MW: 278.01 g mol^{-1}, >99.0%, Acros), benzyl alcohol (C_7H_8O, MW:108.14 g mol^{-1}, 99%, Acros), iron (III) nitrate nonahydrate ($Fe(NO_3)_3 \cdot 9H_2O$, MW: 404.00 g mol^{-1}, >99%, for analysis, Acros),

TEMPO ($C_9H_{18}NO$, MW:156.25 g mol^{-1}, 98%, Merck), ibuprofen (IBU, $C_{13}H_{18}O_2$, MW: 206.28 g mol^{-1}, 99.1%, ApexBio), hydrogen peroxide 30% w/w (H_2O_2, MW: 34.01 g mol^{-1}, VWR), 1-phenylethanol ($C_8H_{10}O$, MW: 122.167 g mol^{-1}, 97%, Alfa Aesar), Pressurized oxygen (O_2, MW: 16 g mol^{-1}, 99.5% v/v, BOC), SNOOP® Liquid Leak Detector (Merck).

2.1.3 Materials for analysis

2.1.3.1 For the quantification and identification of phenol and its degradation products

Acetonitrile (C_2H_3N, MW: 41.05 g mol^{-1}, HPLC grade, Sigma-Aldrich), *p*-benzoquinone ($C_6H_4O_2$, MW: 108.10 g mol^{-1}, ≥ 99.5%, Sigma-Aldrich), oxalic acid dihydrate ($C_2H_2O_4 \cdot 2H_2O$, MW: 126.07 g mol^{-1}, ≥ 99.0%, Sigma-Aldrich), malonic acid ($C_3H_4O_4$, MW: 104.06 g mol^{-1}, ≥ 99.95%, Sigma-Aldrich), maleic acid ($C_4H_4O_4$, MW: 116.10 g mol^{-1}, ≥ 99.0%, Sigma-Aldrich), hydroquinone ($C_6H_6O_2$, MW: 110.11 g mol^{-1}, 99.5%, Acros), catechol ($C_6H_6O_2$, MW: 110.11 g mol^{-1}, >99%, Acros), formic acid (CH_2O_2, MW: 46.03 g mol^{-1}, 99%, Acros), fumaric acid ($C_4H_4O_4$, MW: 116.07 g mol^{-1}, >99%, Acros), acetic acid ($C_2H_4O_2$, MW: 60.05 g mol^{-1}, 100%,VMR), orthophosphoric acid (H_3PO_4, MW: 98.00 g mol^{-1}, 85%, VWR).

2.1.3.2 Quantification and identification of ibuprofen and its degradation products

Trifluoroacetic acid (TFA, $C_2HF_3O_2$, MW: 114.02 g mol^{-1}, HPLC grade, Sigma-Aldrich), acetonitrile (C_2H_3N, MW: 41.05 g mol^{-1}, Sigma-Aldrich) and 2-[4-(1-hydroxy-2-methylpropyl)phenyl]propionic acid ($C_{13}H_{18}O_3$, MW: 222.28 g mol^{-1}, >98%, HPLC grade, Sigma-Aldrich), 4-isobutylacetophenone (4-IBAP, $C_{12}H_{16}O$, MW: 176.27 g mol^{-1}, >97%, Alfa Aesar), (±)-2-phenylpropionic acid ($C_9H_{10}O_2$, MW: 150.17 g mol^{-1}, >98%, Alfa Aesar). 4-acetylbenzoic acid ($C_9H_8O_3$ MW: 164.16 g mol^{-1}, 96%, Fluorochem), 4-iso-butylbenzoic acid ($C_{11}H_{14}O_2$ MW: 178.23 g mol^{-1}, 95%, Fluorochem), 4-ethylbenzaldehyde ($C_{11}H_{14}O_2$ MW: 134.17 g mol^{-1}, 95%, Fluorochem), 1-(4-iso-butylphenyl)ethanol ($C_{12}H_{18}O$, MW: 178.27 g mol^{-1} ≥97%, Fluorochem) and 4-Ethylbenzaldehyde ($C_9H_{10}O$, MW: 134.18 g mol^{-1}, Fluorochem), 1-oxo-ibuprofen ($C_{13}H_{16}O_3$, MW: 220.3 g mol^{-1}, ≥ 98%, Cayman), oxalic acid ($C_2H_2O_4$, MW: 90.03 g mol^{-1}, Sigma-Aldrich).

2.1.3.3 For the determination of the concentration of H_2O_2 in the aqueous samples by iodometry

Potassium iodide (KI, MW:166 g mol^{-1}, 99+%, Acros). Sodium thiosulfate ($Na_2O_3S_2$, anhydrous, for analysis, MW: 158.1 g mol^{-1}, 99%, Fisher Scientific), starch soluble (Alfa Aesar, $C_6H_{10}O_5X$), sulfuric acid (H_2SO_4, MW: 98.08 g mol^{-1}, conc: ≥97.5%), potassium dichromate ($K_2Cr_2O_7$, MW:

294.18 g mol^{-1}, ≥99.0%, Sigma-Aldrich).

2.1.3.4 For the quantification and identification of benzyl alcohol, 1-phenylethanol and their oxidation products

Benzaldehyde (C$_7$H$_6$O, MW: 106.12 g mol^{-1}, 99.5%, Fluorochem), benzoic acid (C$_7$H$_6$O$_2$, MW: 122.12 g mol^{-1}, 99%, Acros), dimethylsulfoxide-d$_6$ (C$_2$D$_6$OS, MW: 84.17 g mol^{-1}, 99.8%, Eurisotop). 2-Propanol (C$_3$H$_8$O, MW: 60.1 g mol^{-1}, HPLC grade, 99.9%, Sigma Aldrich), Acetophenone (C$_8$H$_8$O, MW: 120.15 g mol^{-1}, 99%, Sigma Aldrich).

2.1.4 Experimental apparatus for catalyst test

The following apparatus were used for catalyst preparation: stirrer hotplate (Asynt, IKA RCT) drying oven (Genlab, Mino 30/F/DIG,) from, muffle oven (Carbolite, CWF 11/14), universal oven (Memmert, UN30), ball miller (Retsch, PM100, milling balls: steel, 20 mm).

The following in part custom made experimental apparatus was used for the catalytic tests via Fenton reaction: glass reactor (custom-made, volume: 100 mL, A in Figure 2.1), stirrer hotplate with a thermocouple (D&E in Figure 2.1, Asynt), custom-made alumina block (diameter: 16 cm, C in Figure 2.1).
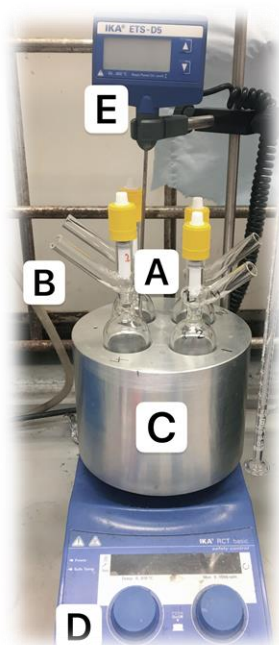
Figure 2.1 Batch reactor used for Fenton reaction under endogenous pressure. **A**: custom-made glass reactor (volume: 100 mL), **B**: side arm **C**: four-holes aluminum block; **D**: stirrer/hotplate; **E**: calibrated thermometer.

The following equipment were used for aerobic catalyst tests: stirrer hotplate (Asynt, IKA RCT) ,

25 mL two-neck round bottom flask, equipped with condenser, steel needles, thermal mass flow controller (Brooks instrument Figure 2.2), Radley reactor (Figure 2.3) equipped with 50 mL ACE round bottom flasks (diameter: 50 mm), air compressor (OL197/10RC ProTech 06254, SIPUK), pump tube (L/S 25, 15.2 m, Master Flex®).
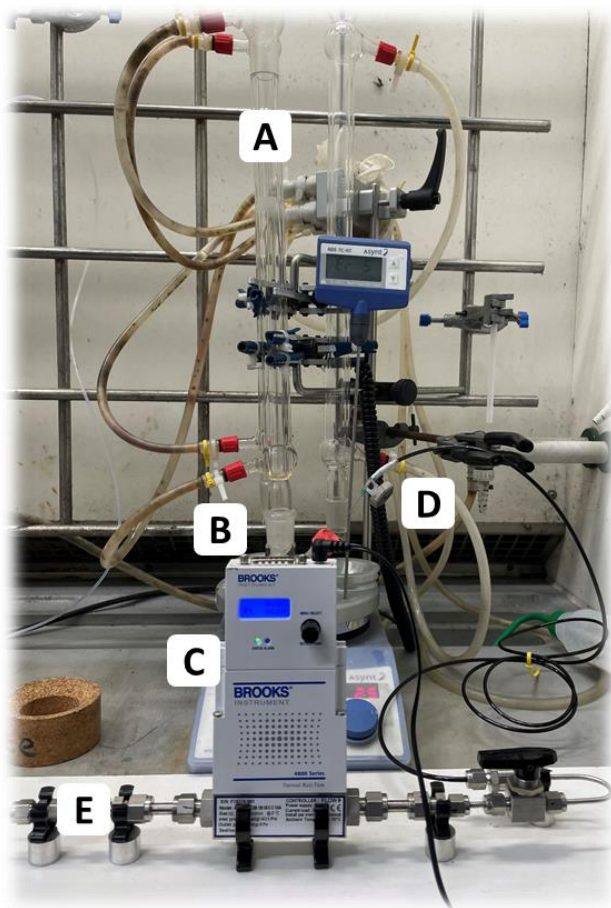
Figure 2.2 The aerobic reactions were conducted in a batch reactor under endogenous pressure, allowing for the flow of air or oxygen. **A**: condenser with a 25 mL two-neck glass reactor with a stirring bar, substrate, and catalyst, **B**: mass flow controller, **C**: stirrer hotplate, **D**: steel needle to feed of reagent.
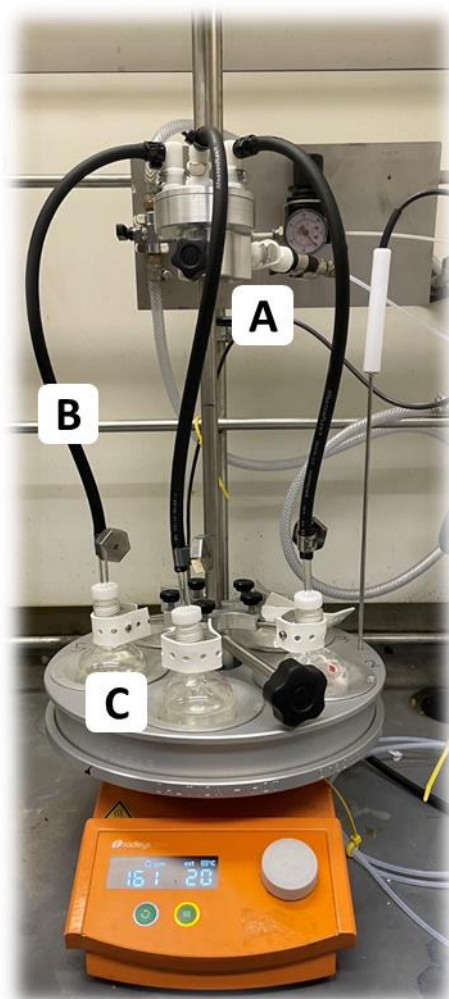
Figure 2.3 Radley set up was used for pressurized aerobic reaction at a pressure gauge up to 2 bar. **A**: Air or molecular oxygen source, **B**: pump tube, to the **C**: 50 mL round bottom flask (ACE) which contains substrate, catalyst and a stirrer.

The following equipment were used for sample analysis: Mini-Centrifuges (SCILOGEX D1008), ^{1}H-NMR (Bruker Advance III 400 spectrometer) equipped with a probe (5 mm PABBO BB/19F-1H/D-GRD), pH meter (Accumet AB150, Fisher Science), HPLC (Shimadzu, prominence Liquid Chromatograph) equipped with a C18 Waters XBridge column (C18, 4.6×250 mm) and a Shimadzu UV detector (CBM-20A), ICP-OES (Agilent, 4500 spectrometer).

2.2　Synthesis and preparation of catalysts

2.2.1　Zeolite Fe/ZSM-5

Wet impregnation protocol was used for the preparation of iron supported zeolite catalyst. It is a process that involves bringing a solid into contact with a liquid phase containing a metal precursor, followed by the removal of the excess liquid through evaporation. This process results in the concentration of the metal precursor, which facilitates the deposition of metal species either on the surface of the solid or within its pores, depending on the material's pore structure. The anchoring of active species onto the solid's surface via wet impregnation, during the deposition, is generally attributed to intermolecular forces, such as Coulomb forces, van der Waals forces, or hydrogen bonds.[1] A typical wet impregnation process is shown in Figure 2.4.
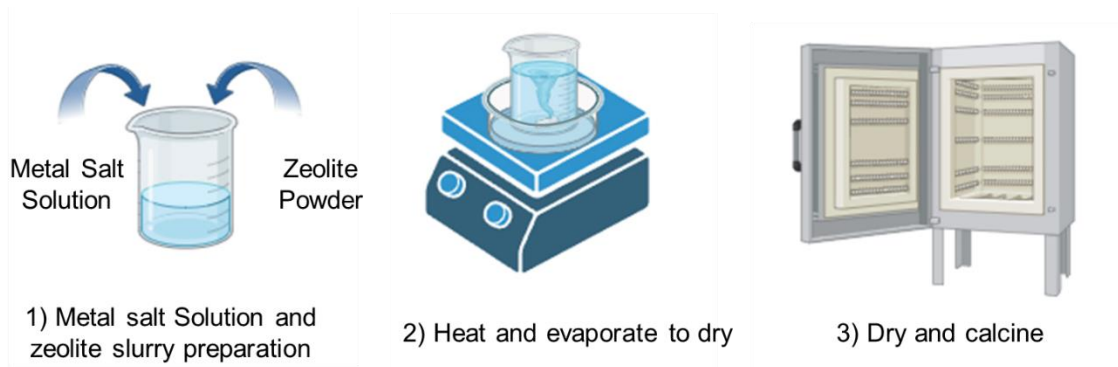
Figure 2.4 Schematic diagram of metal-supported catalyst preparation by wet impregnation in three steps. The concentration of metal salts decides the metal loading of the WI catalyst. Adopted from[2] with permission.

This protocol is known for its robustness to changes of preparation parameters, as well as its simplicity as it requires no complex equipment or procedures, making it cost-effective for various laboratories. Furthermore, it enables an accurate control over metal content by adjusting its concentration. However, reports indicate that it may results in an uncontrolled distribution of metal sites within the pores and on the external surface of the framework. This is primarily due to the lack of specific interactions between the metal and the zeolite.[3] Additionally, this technique often leads to the formation of large metal particles due to agglomeration.[4] Despite these limitations, wet impregnation makes it a preferred method for synthesising Fe/ZSM-5 catalysts and its widespread adoption due to the simplicity and cost-effectiveness it offers. Typically, this procedure is supplemented by a post-reduction step, which commonly employs H_2 gas or $NaBH_4$ in solution to modify the oxidation state of the deposited metal species.[5]

Iron supported zeolite catalyst (1 wt.% loading for the metal dopant) was prepared by using wet impregnation protocol with $Fe(NO_3)_3 \cdot 9H_2O$ as the precursor. NH_4/ZSM-5 was calcined prior to use to obtain H/ZSM-5 (temperature ramping rate of 20 °C min^{-1}, calcination temperature of 550 °C, and calcination time of 4 h). A solution of 25 mL $Fe(NO_3)_3 \cdot 9H_2O$ was prepared, the mass of $Fe(NO_3)_3 \cdot 9H_2O$ calculated according to a loading of 1 wt.% for 2 g of catalyst was added into an aqueous slurry containing H/ZSM-5 under stirring, and heated in an oil bath at 80 °C until dryness. The sample was then transferred into a drying oven at 120 °C for 16 h, recovered and calcined by using the same calcination process as described above.

2.2.2 Preparation of recycled glass for catalytic tests

Recycled glass bottles were washed with a detergent (Alconox, Sigma-Aldrich) and rinsed with de-ionised water; they were then dried in the oven before being calcined in a muffle oven operating in static air at a temperature of 550 °C for 4 h (temperature ramp rate: 20 °C min^{-1}) to burn any residual contaminant. Glass samples were initially crushed between diameters of 7 and 2 mm. The pieces of glass were milled into seven size-fraction by using mechanical sieves: <0.1 mm, 0.1-0.2 mm, 0.2-0.5 mm, 0.5-1 mm, 1-1.4 mm, and 1.4-2 mm, and > 2 mm.

2.3 Characterisation of the recycled glass

The following analytical techniques, including X-ray photoelectron spectroscopy (XPS), and inductively coupled plasma optical emission spectroscopy (ICP-OES), are suitable to determine the elemental composition of the recycled glass at surface and bulk level.

2.3.1 X-ray photoelectron spectroscopy (XPS)

X-ray photoelectron spectroscopy (XPS) is one of the most widely used near surface analysis techniques (penetration depth 1-10 nm) which provides both elemental and chemical state information. When a beam of X-ray crosses a sample, some rays pass through while others are absorbed, causing interactions at the atomic level. This absorption leads to phenomena such as scattering, electron release, the production of fluorescent X-rays and photoelectrons emission (Figure 2.5).
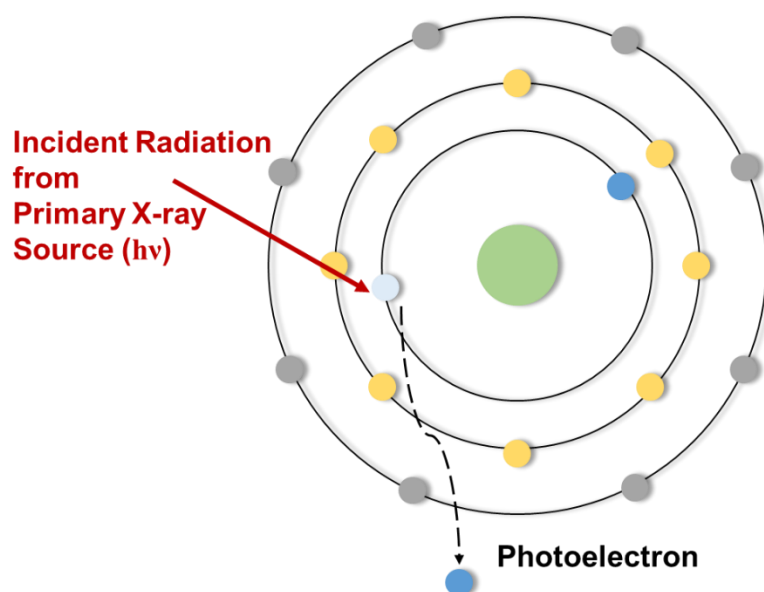
Figure 2.5 Schematic of the photoemission process involved in XPS surface analysis.[6] An electron can be ejected when an atom or molecule absorbs an X-ray photon. The surface elements and chemical states can be identified by detecting the kinetic energy (Ek) of the emitted electrons.

The kinetic energy (E_K) of the ejected photoelectrons is related to the electron binding energy (E_b), as shown in the Einstein's photoelectric equation (Eq. 2.1[6,7]), whereas E_b reflects the type and valence of the elements in the tested sample.

$$E_\mathrm{k} = hv - E_b - \varphi \qquad \text{(Eq. 2.1)}$$

Where:

E_k is the kinetic energy of emitted electron

E_b is the binding energy of the emitted electron

h is Planck's constant

v is the frequency of incident X-ray

φ is the work function of the spectrometer

Within this framework, the technique is capable of: 1) identifying all elements except hydrogen and helium; 2) determining chemical bonding states; and 3) providing depth information on the nanometer scale.[8] The mechanism by which this is achieved involves the behavior of photoelectrons, which are susceptible to scattering and absorption by the atoms that make up the sample. In particular, only those photoelectrons originating near the surface of a material are able to escape the material without being back-scattered or absorbed. As a result, the typical depth of analysis provided by X-ray photoelectron spectroscopy (XPS) is limited to less than 10 nanometers. This characteristic makes the technique exceptionally sensitive not only to surface layers but also to any contamination present.

XPS analyses were performed using a Kratos Axis Ultra-DLDspectrometer. Samples were

examined using a micro-focused monochromatic Al X-ray source operating at 72 W in the '400 micron spot' mode. This mode produces an elliptical X-ray spot approximately 400 × 600 microns in size. Data acquisition was performed using pass energies of 150 eV for survey scans and 40 eV for high resolution scans, with step sizes of 1 eV and 0.1 eV respectively.

Data analysis was performed using CasaXPS version 2.3.24, following calibration of the data set against the lowest binding energy component of carbon (C 1s), which was assigned a value of 284.8 eV.

2.3.2 Inductively coupled plasma optical emission spectroscopy (ICP-OES)

ICP-OES is an analytical technique that can be used to accurately determine the amount of elements in trace amount in a range of ppb (part per billion) or ppt (part per trillion) from both liquid and solid sample matrices. The technique is based on the detection of photons emitted by atoms and ions excited in a radiofrequency (RF) discharge. Solid samples are often pre-treated with acid for a digestion process into liquid solution before analysing.[9] The samples are first ionised by a plasma, which itself is an ionised gas composed of positive-charged ions and unbounded electrons.[10] Unlike other type of ionisation sources such as electrospray, where only small amount of energy is imparted to the samples, ICP technique is able to practically atomize a sample. The so-called ICP torch is usually an assembly of three concentric fused-silica tubes (Figure 2.6).[11] These are frequently referred to as the outer, intermediate, and inner gas tubes. A water-cooled, three-turn copper coil, called the *load coil*, surrounds the end of the torch and is connected to an RF generator. Argon gas (0.5 -1.5 L min^{-1}) delivers the sample aerosol to the central channel of the plasma. High-voltage discharge is applied to generate a portion of argon ions and electrons which are then accelerated and collide with other argon atoms to produce further ions and electrons. This propagation is called ICP, a large amount of heat will be released which is able to reach 10,000 Kelvin.[11] Once within the plasma, samples undergo desolvation, vaporisation, atomisation and ionisation. The extent of ionisation depends on both: temperature of the plasma and the ionisation potential of the element. As argon has almost the highest first ionisation potential (15.7 eV),[12] which makes ICP able to measure most of the elements. The relaxation of these excited states results in the emission of photons, the wavelength of each photon being specific to the type of atom or ion, allowing elemental identification. The number of photons is directly related to the concentration of the element in the sample.
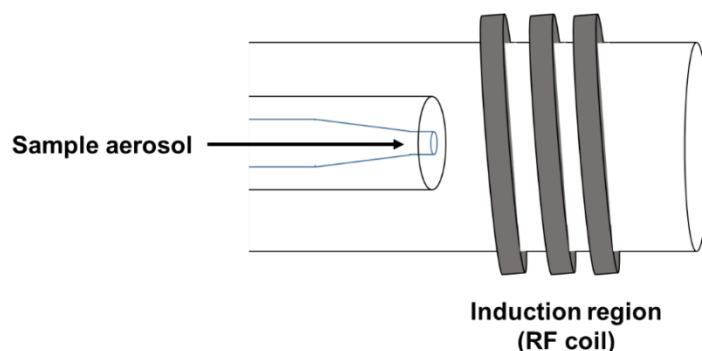
Figure 2.6 Schematic diagram of an ICP assembly showing the three concentric tubes composing the torch, the RF coil, the different plasma regions the carried by the inner argon flow. Regenerated from.[11]

Multielement metal content determinations were carried out using HP/Agilent 5800 ICP-OES instrument via appropriate calibration curves. Glass samples (0.1 g) were dissolved in HF and *aqua regia* (volume ratio HNO_3: HCl=1:3) within Teflon autoclaves and left the sample to mineralize overnight. Prior to analysis, the mixture was diluted with deionized water and neutralised to pH around 3 with NaOH. 5 mL of the supernatant was submitted for ICP analysis.

2.4   Catalytic tests

2.4.1   Phenol oxidation by Fenton reaction as benchmark

A phenol stock solution (1 g L^{-1}) was prepared by dissolving a specified amount (1 g) of the solid reagent in deionised water (1 L). Catalytic tests for phenol oxidation were carried out in a 100 mL stoppered glass batch reactor (Figure 2.1) at specified temperature and stirring conditions. The reactor was charged with a specified amount of catalyst (typically 1 to 3 mg) and 50 mL of phenol solution, then heated to the target temperature at a rate of 200 °C min^{-1} using an Asynt stirrer-hotplate inside an aluminium block at atmospheric pressure. Upon reaching the desired temperature, H_2O_2 was introduced to initiate the reaction, which was later stopped using an ice bath to maintain consistent reaction times. The mixtures were centrifuged to remove the solid catalyst from the liquid phase, followed by HPLC analysis to assess phenol degradation and identify reaction by-products.

In a typical experiment, a certain amount of catalyst (recycled glass, 0.1 g, Fe content: 0.07-0.3 wt.%, with metal to substrate molar (M:S) ratio of 100) was added in 50 mL of phenol solution (1 g L^{-1}) in a glass batch reactor. When the reaction mixture, with continuous stirring (500 rpm), reached and stabilized at a temperature of 80 °C, a stoichiometric amount of H_2O_2 (phenol:H_2O_2 molar ratio of 1:14, 844 µL, H_2O_2 30% w/w) was added into the solution to start

a Fenton reaction. Catalytic tests were carried out for 30 min to 12 h with a 4 h reaction time typically used unless otherwise specified under endogenous pressure, and then the reaction was quenched by inserting the reactor in an ice-water bath.

A stoichiometric ratio of phenol to H_2O_2 was set as 1:14 for complete oxidation of phenol to CO_2 and H_2O, as shown in Equation 2.2.

$$C_6H_6O + 14 H_2O_2 \rightarrow 6 CO_2 + 17 H_2O \quad \text{(Eq. 2.2)}$$

2.4.2 Ibuprofen oxidation by Fenton reaction

An ibuprofen stock solution (20 mg L^{-1}) was prepared by dissolving a specified amount (20 mg) of the solid reagent in deionised water (1 L).

In a typical experiment, a certain amount of catalyst (recycled glass, 0.1 g, Fe content: 0.07-0.3 wt.%, with M:S of 100) was added in 50 mL of ibuprofen solution (20 mg L^{-1}) in a glass batch reactor. When the reaction mixture, with continuous stirring (500 rpm), reached and stabilized at a temperature of 80 °C, a stoichiometric amount of H_2O_2 is needed to start mineralizing ibuprofen to CO_2 and H_2O (ibuprofen:H_2O_2 molar ratio of 1:33, 17.4 µL, H_2O_2 30% w/w) was added into the solution to start a Fenton reaction. Catalytic tests were carried out from 4 to 24 h, with a 4 h reaction time typically used unless otherwise specified under endogenous pressure. The post-treatment of reaction mixture follows Section 2.4.1.

A stoichiometric ratio of ibuprofen to H_2O_2 was set as 1:33 for complete oxidation of ibuprofen to CO_2 and H_2O, as shown in Equation 2.3.

$$C_{13}H_{18}O_2 + 33 H_2O_2 \rightarrow 13 CO_2 + 42 H_2O \quad \text{(Eq. 2.3)}$$
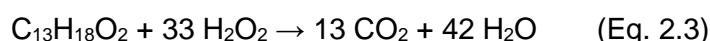
2.4.3 Benzyl Alcohol oxidation by Fenton reaction

A benzyl alcohol stock solution (1 g L^{-1}) was prepared by dissolving a specified amount (0.5 g) of the liquid reagent in deionised water (0.5 L).

In a typical experiment, a certain amount of catalyst (recycled glass, 0.02 g, Fe content: 0.07-0.3 wt.%, M:S of 100) was then added into 10 mL benzyl alcohol (1 g L^{-1}) in a glass batch reactor (Figure 2.1). H_2O_2 was added to start the reaction (molar ratio: 17, volume: 180 µL, H_2O_2 30% w/w) for 4 to 24 h at 80°C. Post reaction treatment follows Section 2.4.1 with ^{1}H-NMR as characterization method.

A stoichiometric ratio of benzyl alcohol to H_2O_2 was set as 1:17 for complete oxidation of

ibuprofen to CO_2 and H_2O, as shown in Equation 2.4.

$$C_7H_8O + 17\ H_2O_2 \rightarrow 7\ CO_2 + 21\ H_2O \qquad \text{(Eq. 2.4)}$$

2.4.4 Mechanistic study investigation in the oxidation of benzyl alcohol

A certain amount of recycled glass (**G3**, Fe content: 0.2 wt.%, 0.02 g, glass size: <0.1 mm, 0.1-0.2 mm, 0.2-0.5 mm, 0.5-1 mm, M:S ratio 1:100) was added into 10 mL of BnOH (1 g L^{-1}) and TEMPO (BnOH: TEMPO 1:100, 1:10 and 1:4) in the glass batch reactor (Figure 2.1), and heated with continuous stirring until 80°C, after stabilization was achieved, different amount of H_2O_2 (BnOH:H_2O_2 molar ratio 1:1, 1:2, 1:20 and 1:40) was then added and the reaction continued for 24 hours. Post reaction treatment follows Section 2.4.1 with ^{1}H-NMR as characterization method.

2.4.5 Benzyl alcohol oxidation by molecular oxygen

2.4.5.1 Aerobic oxidation by using a pressurised system

A certain amount of recycled glass catalyst (**G1 to G4,** 0.01 to 0.4 g, Fe content: 0.07-0.3 wt.%, glass size: <0.1 mm M:S 1:100 to 1:5) was introduced into 10 mL of BnOH water solution (1 g L^{-1}) in a 50 mL ACE round bottom flask. The reaction vessels were then pressurized at 1 or 2 bar of molecular oxygen (A pressure gauge is a pressure measured as a difference with respect to the surroundings) by using a Radley set-up (Figure 2.3). The sealed system was tested from gas leakage by using snoop liquid before increasing to desired temperature (80 to 100°C). When the system was stabilised at the set temperature and pressure, the reaction was then carried out for 24 hours with continuous stirring, and cooled down to 30 °C before disconnecting from the set up. Post reaction treatment followed 2.4.1 with ^{1}H-NMR as characterization method.

2.4.5.2 Aerobic oxidation by insufflating O_2

A certain amount of recycled glass catalyst (**G1 to G4**, 0.01 to 0.4 g, Fe content: 0.07-0.3 wt.%, glass size: <0.1 mm M:S 1:100 to 1:5) was introduced in 8 mL of BnOH water solution (1 g L^{-1}) in a 25 mL two-necked round bottom flask. The flask was fitted with a condenser and sealed at the neck with a rubber stopper (Figure 2.2). Oxygen was then introduced into the solution by insufflation, using a mass flow controller with the flow rate set at 5 mL min^{-1}. A needle was used to introduce the oxygen into the solution through the neck of the flask. The reaction was started when the temperature was stabilised at the desired temperature (80 to 100°C) and was then carried out for 4 h. The post reaction treatment follows Section 2.41 with ^{1}H-NMR as the characterisation method.

2.4.6 1-phenylethanol oxidation by Fenton reaction

A 1-phenylethanol stock solution (1 g L^{-1}) was prepared by dissolving a specified amount of the liquid reagent in deionised water and storing it away from light.

Reaction set-up, condition, post reaction treatment all follow Section 2.4.3, with a stoichiometric amount of H$_2$O$_2$ (molar ratio: 20, 186 µL) added.

A stoichiometric ratio of 1-phenylethanol to H$_2$O$_2$ was set as 1:20 for complete oxidation of ibuprofen to CO$_2$ and H$_2$O, as shown in Equation 2.5.

$$C_8H_{10}O + 20\ H_2O_2 \rightarrow 8\ CO_2 + 25\ H_2O \qquad \text{(Eq. 2.5)}$$

2.4.7 1-phenylethanol Oxidation by molecular oxygen

As per Sections 2.4.5.1 and 2.4.5.2.

2.5 Characterization of reaction mixtures

In order to determine the performance of the catalyst, reaction mixtures at selected reaction times t, were characterized via different techniques. For mixtures that can lead to a large number of intermediates and unknown products, a characterization method capable of both resolution of the single components and quantification of these components is necessary. To this scope, high performance liquid chromatography (HPLC) was chosen to quantify the extent of phenol and ibuprofen decomposition, as well as to identify any potential products or by-product that could be generated. In the case of benzyl alcohol and 1-phenylethanol, proton nuclear magnetic resonance (NMR) was a faster and yet appropriate methodology for both qualitative and quantitative purposes.

For all Fenton reactions where H$_2$O$_2$ was used as oxidizing or mineralizing agent, iodometry was used to determine the amount of H$_2$O$_2$ after any reaction.

2.5.1 High Performance Liquid Chromatography (HPLC)

High performance liquid chromatography (HPLC) is an analytical technique used to separate (or in chromatographic terms: resolve), identify and possibly quantify each component in a mixture. It is known as one of the most common methods used in environmental applications such as detection of phenolic compounds and bio-monitoring of pollutants.[13,14] As HPLC is a tool that can be used for both separation and purification of compounds, a number of studies have applied HPLC as their primary step for the study and identification of phenol and

ibuprofen containing mixtures.[15–19]

The separation principle of HPLC is based on the distribution of the analyte (sample) between a mobile phase (eluent: typically, a mixture of solvents e.g., water, acetonitrile) and a stationary phase (column packing material: typically, a granular substance made of solid, or a liquid supported on a solid i.e. silica, polymers). Depending on the chemical structure of the analyte, the molecules are slowed down as they pass through the stationary phase.[20] The specific intermolecular interactions between the molecules of a sample and the packing material define their time "on-column". Therefore, different components of a sample will be eluted at different times (retention time). This results in the separation of the sample components. A detection unit (e.g. UV/Vis detector in this case) detects the analytes after leaving the column. The signals converted and recorded by a data management system (computer software) and then and then displayed in a chromatogram (Figure 2.8). After passing through the detector unit, the mobile phase can be subjected to additional detector unit, a fraction collection unit or to the waste.

There are two main modes of liquid chromatography: normal phase and reversed phase. In normal phase, the stationary phase is polar and the mobile phase is non-polar. In reversed phase, which is more commonly used, the stationary phase is non-polar and the mobile phase is polar/aqueous. For the analysis in this thesis, which are predominantly aqueous, reversed phase chromatography will be employed using a C18 non-polar stationary phase.

In general, an HPLC system contains the following modules: a solvent reservoir, a pump, an injection reservoir, an injection valve (most often via a loop), a column, a detector unit and a data processing unit (Figure 2.7). The analyte (sample) is delivered to the eluent by the injection valve. The solvent (eluent) is pumped through the system at high pressure (up to 400 atmospheres [21]) and constant speed (range of a few mL min^{-1}). To minimise drift and noise in the detector signal, a constant and pulseless flow from the pump is essential.
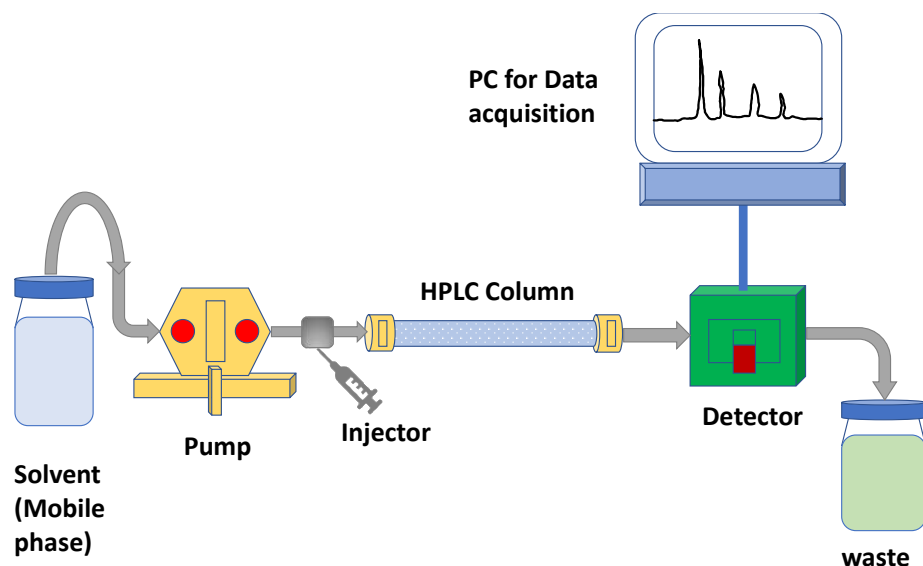
Figure 2.7: Diagram of HPLC instrument,[20] it includes a pump to pressurize solvent mixtures which act as the mobile phase, a sample injector (syringe, sampling loops or autosampler system) to introduce the sample to the column, an HPLC column to separate the components, and a detector for identify these products based for example on their absorbance. The data was transferred to a workstation on computer for data acquisition.
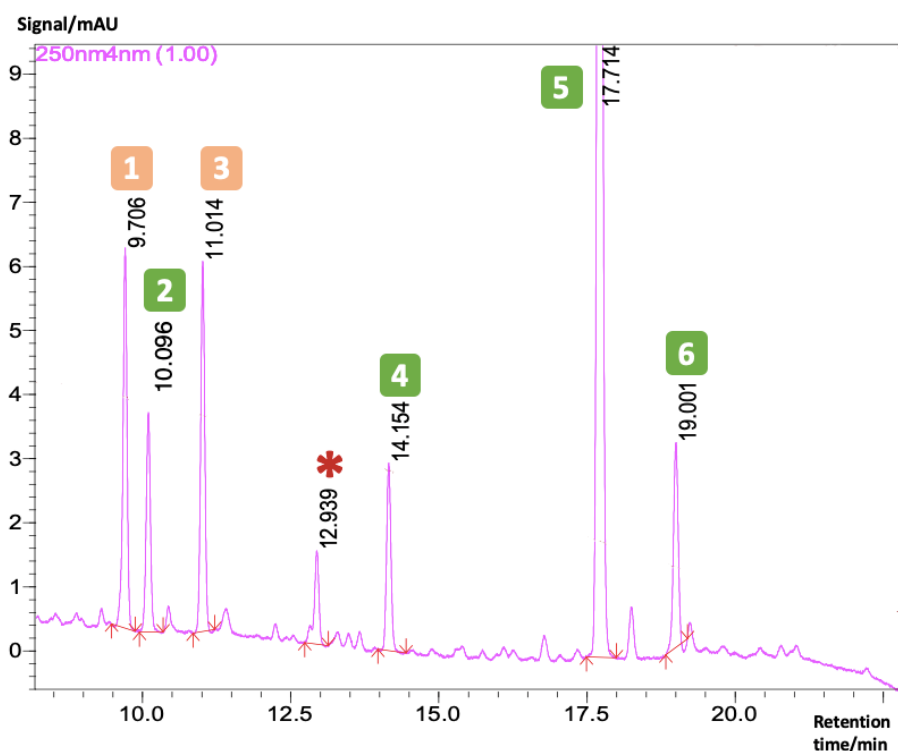
Figure 2.8: A chromatogram of ibuprofen degradation with stoichiometric amount of H_2O_2 and iron nitrate (metal to substrate ratio (M:S) of 100), data collected at 250 nm. y-axis represent the signal (mAU) collected by UV detector, x-axis represents retention time (min). Several products were identified based on the standard sample numbered according to their retention time. Some of the identified products (green) are 2: 4-acetylbenzoic acid (10.1 ± 0.1 min), 4: 1-oxo IBU (14.2 ± 0.1min), 5: ibuprofen (17.7 ± 0.2 min), 6: 4-isobutylacetophenone (19.00 ± 0.2 min). Two unknown products (orange) were detected at 1: 9.7 ± 0.1 min; 3 11.01 ± 0.1 min. One uncertain substance was detected at 12.9 ± 0.1min (red star).

A representative chromatogram (for the specific case of ibuprofen degradation) is shown in Figure 2.8. The x-axis refers to the retention time, typically expressed in minutes, which indicates the time taken for each component to pass through and exit the column. The y-axis is in milli-absorbance units (mAU) when a UV-vis detector has been used. From this chromatogram, the components can be identified by comparing the retention time with a sample used as a reference standard (most often the pure component), and the concentration of each component is obtained by integrating the areas of the chromatographic peaks based on the use of calibration curves to determine response factors.

Before any calibration curve is made, it is important to first determine a suitable wavelength to be used for the UV detector, as different compounds may have their highest absorbance at different wavelengths depending on their own structure, which will severely affect the response factor of the calibration curve. The response factor (RF) is the slope of a calibration curve, also corresponds to the sensitivity of a method, and it is defined as the ratio of the detector response (usually a signal in mV or mA) to the amount (concentration) of analyte in the calibration curve and standard. It should be noted though that if the UV detector is coupled to a chromatograph than the signal is generally taken as the peak area for that compound. The steeper the slope of this ratio, the higher the response factor, and the better and more sensitive the calibration curve.

The typical HPLC conditions used in this thesis is as follows: HPLC chromatograph (SHIMADZU prominence LC-20AD XR) equipped with a UV-vis photo diode array detector at a wavelength of 270 nm for phenol and a range from 200 nm for ibuprofen. The column used was a WATERS XBridge® C18 column 5 µm, 4.6 mm × 250 mm. For phenol and its products, acetonitrile and 0.1% orthophosphoric acid solution with ratio of 30%/70% (V/V) were used as mobile phase with a flow rate of 1 mL min^{-1}, the injection volume was 5 µL. For ibuprofen and its products, the flow rate was 1 mL min^{-1} and the injection volume was 50 µL by a loop. The gradient used was: 20 min = 95% B, 5% A, 30 min = 95% B, 5% A, 31 min = 5% B, 95% A, 40 min = 5% B, 95% A, where A is 0.1% trifluoroacetic acid (TFA), and B is acetonitrile.

After a catalytic test was completed, about 1.5 mL of reaction mixture was transferred into an HPLC sample vial. Once the instrument was ready for injection (stabilisation of the pump under the chosen method at around 2.5k psi for 10 mins), a blank test without sample would be done before any samples. When all analysis were completed, data analysis (see Section 4.2) for qualification and qualification was carried out.

2.5.2 Quantification of compounds by means of calibration curves

In order to carry out reliable quantification of analytes by HPLC analysis, accurate calibration

using standards is required. There are two commonly used quantitation methods: 1) External Standard Method (ESTD): A series of calibration standards at different known concentrations are analysed. The instrument response (e.g. peak area) is plotted against a concentration to generate a calibration curve, which is then used to determine unknown sample concentrations. 2) Internal Standard Method (ISTD): A known amount of an internal standard compound is added to both the samples and calibration standards. The ratio of analyte signal to internal standard signal is used for quantitation, thus allowing to correct for injection errors.[22–24]

For HPLC applications, either the external standard method or internal standard method can be used as required to ensure reliable quantification of the samples, though the internal standard approach can improve accuracy by accounting for variations in injection volume.

Regardless of which calibration is used, it should also be noted that quantitative information in chromatography is obtained by integration of chromatographic peaks: the peak height, and the peak area. Both types of signals provide a measurement of the response of the detector for a given compound. Though peak highest can practically be used only in the presence of highly sharp and symmetric peaks. In this thesis, peak areas were chosen as a consistent quantification measurement method.

As summarized in Figure 2.2, the external standard method was chosen for chromatographic analysis in this work. Due to the high number of samples required for analysis, the external standard approach is much faster than the internal standard method, which requires identifying and adding a suitable internal standard compound to each sample - a tedious process. While the internal standard method can provide higher accuracy by accounting for any injection inconsistencies, this advantage is less critical for the chromatographic analysis. However, for the NMR data analysis (Section 2.5.3.2), the internal standard method was employed to improve quantitative accuracy by using an internal reference to correct for potential variations during NMR measurements. Overall, the external standard method was more practical for efficient chromatographic analysis of the numerous samples, while the ISTD approach was beneficial for the NMR quantification.

Table 2.2 Comparison of two different calibration methods: External Standard (ESTD) and the Internal Standard (ISTD) method.

Calibration method	Advantages	Disadvantages
External Standard (ESTD)	1. Simple to perform 2. Can be applied to a wide variety of methods	It is greatly affected by the stability of the chromatographic detector system and any potential chromatographic impurities in the injection.
Internal Standard (ISTD)	1. Commonly used for highly complex matrices where the matrix itself can affect the detection system (e.g. food extracts or petroleum mixtures) 2. Compensate for any losses during filtration or extraction	Selection requirements are strict, hence it's both time consuming and high demanding: 1. Must be different than the sample, well resolved and must not elute where any sample peaks could be expected. 2. Must have a similar linear response as the sample (Inject a fixed volume/concentration) 3. Available in a high purity form from multiple commercial sources. 4 Must be stable and not react with the sample or mobile phase solution.

2.5.3 Nuclear Magnetic Resonance (NMR)

2.5.3.1 Theory of NMR

Nuclear magnetic resonance is a spectroscopy that relies on the interaction between an external electromagnetic radiation and atomic nuclei to generate information regarding the nature of these nuclei, their amounts and the neighbouring surrounding atoms or functional groups.[25] A nucleus with an odd atomic number contains a half-integer nuclear spin (I), for instance: ^1H, ^{13}C, ^{15}N, ^{19}F and ^{31}P. A nucleus with both an odd proton number and odd neutron number contains a whole-integer nuclear spin (I), for instance: ^2H, ^{10}B and ^{14}N. By virtue of spin selection rules, only when $I \neq 0$, atomic nuclei can be detected by NMR spectroscopy.[26]
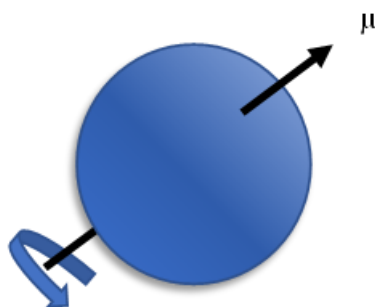
Figure 2.9 A graphical depiction of a spinning nucleus along its own axis, possessing an angular moment P and a magnetic moment μ.

The spinning charged nucleus generates its own magnetic field, and possess an angular momentum, P and a magnetic moment, μ (Figure 2.9), where γ is the gyromagnetic ratio,

value depends on the isotope (Eq.2.6).

$$\mu = \gamma \times P \quad \text{(Eq. 2.6)}$$

NMR-active nuclei with $I = \frac{1}{2}$ will align with an external magnetic field $\mathbf{B_0}$ in 2 orientations: parallel (lower energy level) or anti-parallel (highest energy level) the applied field $\mathbf{B_0}$. The different between the two energy levels, ΔE, depends on the external magnetic field that applied and the gyromagnetic ratio, and will in turn impacts the detection capabilities of the technique (Figure 2.10). When the nuclei are irradiated with a radio wave (in MHz range) with appropriate frequency, transitions between two spin levels will be triggered, so as the orientation change of nuclear spins, this energy absorption is called the magnetic resonance.[27]
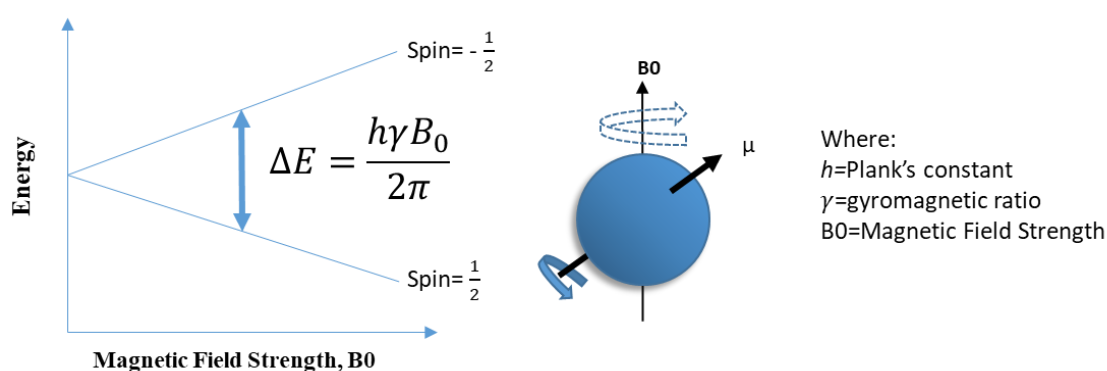
Figure 2.10 Left: a plot showing the correspondence between the energy different, ΔE between the two spin states and the magnetic field strength, $\mathbf{B_0}$ that applied to this NMR-active nuclei. Right: in an applied magnetic field $\mathbf{B_0}$, a nucleus is spinning along its own axis as the same time performing a processional motion (orbit) along the direction of $\mathbf{B_0}$.
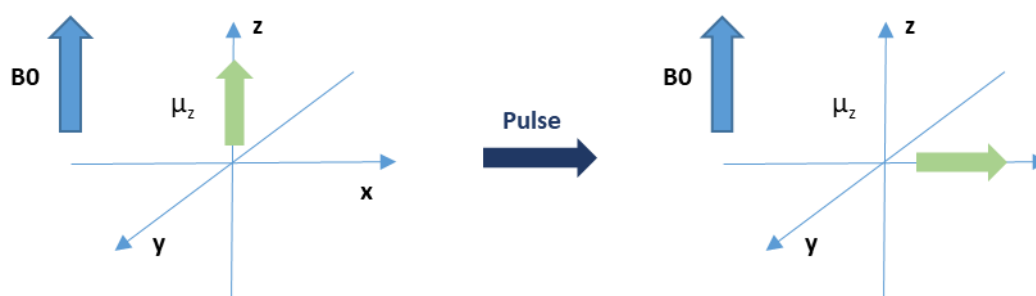
Figure 2.11 A simplified scheme showing the transformation of magnetization (green) from z direction to the xy plane with the introduction of a magnetic pulse (dark blue) with a similar frequency but a perpendicular orientation as the applied magnetic field $\mathbf{B_0}$ (blue). A relaxation process will then be observed and recorded as NMR signal.

The precession movement creates a parallel (μ_z) and a perpendicular (μ_{xy}) component of magnetic vector associated with the nuclear magnetic dipoles, in the absence of extra disturbance, $\mu_{xy}=0$. Moreover, μ_z cannot be accurately measured due to the strong applied magnetic field in the same direction. Hence, a magnetic pulse (with similar frequency but

perpendicular direction to B_0) is always introduced to reach resonance and transfer μ_z to μ_{xy} (Figure 2.11). Afterwards, a relaxation process can be observed, energy emitted as radiofrequency will be recorded as free induction decay by detector. An NMR spectrum with intensities vs frequencies will be generated by the technique.

Figure 2.12 A simplified schematic diagram of a classic NMR instrument. The sample tube (orange) was inserted into a magnetic field B_0 generated by the magnet around it (light blue). A radiofrequency (RF) transmitter introduces pulses to create magnetization transformation as demonstrated in Figure 2.11. a detector records the absorption from the relaxation process and transfer it into NMR signal. An NMR spectrum will then be generated with intensity in the y axis and chemical shifts in the x axis (Figure 2.13).

A simplified schematic diagram of a classic NMR instrument is shown in Figure 2.12, where the sample tube was inserted into a magnetic field that aligns with the nuclear spins of the atoms in the sample tube. Moreover, there is another series of magnetic coils around the sample tube which are used to provide the radiofrequency pulses and then NMR signal will be detected and collected by the recorder.

Figure 2.13 Benzaldehyde: ^{1}H-NMR (400 MHz, DMSO-d6), a: δ ppm 9.99 (s, 1H), b: 7.90 (d, 2H), d: 7.70 (t, 1H), c: 7.60 (t, 2H)

Figure 2.13 is a typical ^{1}H-NMR spectrum of benzaldehyde. The y-axis is the intensity of the signal, the x-axis is the chemical shifts of the peaks and it relates to the chemical environment of the protons. The peaks area corresponds to the number of atomic nuclei that form this signal, this means peaks from protons **b** and **c** should have two times the peak area of those for protons **a** and **d**.

2.5.3.2 NMR analysis protocol

200 µL of reaction mixture was mixed with 15 µL of diluted 2-propanol (0.2 mol mL^{-1} in DMSO-d6) as internal standard and 500 µL of DMSO-d6 as NMR solvent into a small vial for through mix, it was then transferred into NMR sample tube for analysis. Analysis was carried out by using a Bruker Advance III HD spectrometer at 400MHZ. The ^{1}H-NMR was optimized by using a water suppression method and collecting an average of around 128 scans per spectrum.

With internal calibration method (ISTD) used, the concentration of any analyte (C_X) will be as follows Equation 2.7:

$$C_X = \frac{A_X \times C_{IS}}{RF \times A_{IS}} \quad \text{(Eq. 2.7)}$$

where:

C_X is the concentration of analyte

A_X is the peak area of the analyte

C_{IS} is the concentration of the internal standard

A_{IS} is the peak area of the internal standard

RF is the response factor of the analyte

2.5.4 H₂O₂ determination in reaction mixtures

A number of methods can be used to determine the amount of H₂O₂ in a mixture, especially aqueous. This is either at the beginning of a reaction or at its end, and in turn to determine also the H₂O₂ conversion as complementary to the conversion or degradation of an organic substrate.[28] These may include: titanium oxalate[29] (spectrophotometric), peroxidase enzyme catalyzer,[30] cobalt bicarbonate method,[31] permanganate titration[32] and iodometric back-titration.[33] While some techniques like permanganate and cobalt bicarbonate assays have seen use in water treatment applications, iodometric back-titration is less susceptible to interference from organic compounds.

2.5.4.1 Theory of iodometric back-titration

The amount of H₂O₂ was quantified by iodometry.[33,34] This approach relies on the quantitative reduction of H₂O₂ by iodide under acidic conditions (Eq. 2.8), with the liberated iodine being titrated against a thiosulfate solution (Eq. 2.9).

$$H_2O_2 + 2KI + H_2SO_4 \rightarrow I_2 + K_2SO_4 + 2H_2O \quad \text{(Eq. 2.8)}$$

$$I_2 + 2Na_2S_2O_3 \rightarrow Na_2S_4O_6 + 2NaI \quad \text{(Eq. 2.9)}$$
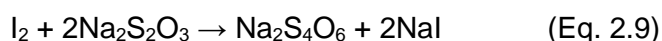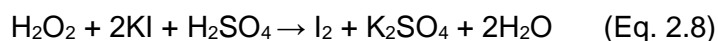
1 or 2 mL of reaction mixture solution, 1 mL KI (100 g L⁻¹) and 1 mL H₂SO₄ (10%, m/m) was pipetted into the iodine flask, the mixture was then placed in a dark place for 10 min [35,36] until a yellow solution was obtained. The sample solution was titrated with Na₂S₂O₃ (0.001 mol L⁻¹) until the solution became pale yellow. A few drops of starch solution (10 g L⁻¹) was added to indicate the colour change (from pale yellow to blue). More Na₂S₂O₃ (0.001 mol L⁻¹) was added until the blue colour disappeared. The volume (V$_{Na2S2O3}$) of Na₂S₂O₃ solution at the end point of titration was recorded, then the concentration of H₂O₂ calculated following the formula (Eq. 2.10):

$$X_{(H_2O_2)} = \frac{C_{(corrected\ Na_2S_2O_3)} \times (V_{(Na_2S_2O_3)} - V_{(Blank)}) \times R_D}{2 \times V_{(H_2O_2)}} mol L^{-1} \quad \text{(Eq. 2.10)}$$

where:

$X_{(H_2O_2)}$ is the concentration of hydrogen peroxide in the reaction mixture.

$C_{(corrected\ Na_2S_2O_3)}$ is the concentration of standard sodium thiosulfate used for titration after standardization (Appendix A1.1)

$V_{(Na_2S_2O_3)}$ is the volume of $Na_2S_2O_3$ used for titration

$V_{(Blank)}$ is the volume of $Na_2S_2O_3$ used for blank titration (Appendix A1.2)

R_D is the dilution factor

$V_{(H_2O_2)}$ is the volume of reaction mixture

2.5.4.2 Preparation of reagents

For 10 g L^{-1} starch solution: 0.5 g of soluble starch was weighed and mixed with 5 mL of water thoroughly. After that, 100 mL of boiled water was slowly added into the mixture and kept boiling for another 2 min before it was cooled down naturally to room temperature for later use. The starch solution was made freshly on the titration day.

For 100 g L^{-1} KI solution: 10.00 g of KI was weighed precisely and dissolved and then made up to 100 mL by deionized water in volumetric flask.

For 10 % H_2SO_4 (m/m) solution: 60 mL of H_2SO_4 was measured and poured into a beaker, 700 mL of water was slowly added with constant mixing. When the mixture was cooled down to room temperature, it was made up to 1000 mL using volumetric flask.

For 0.1 M of $Na_2S_2O_3$ standard solution: 16 g of sodium thiosulfate was mixed with 0.2 g of sodium carbonate in 1000 mL recently boiled and cooled water in volumetric flask.

2.5.5 Determination of metal leaching

Through the use of a calibration dilution procedure with standards made from stock solutions containing 1000 ppm of metal standards, calibrated to 10 ppb, ICP-OES was utilized to test the metal leaching of the catalyst during the reaction. The concentrations of metal ions in the samples were computed using a calibration graph. A 5 mL sample of the reaction mixture was obtained for the leaching tests following the reaction.

2.5.6 Acidity measurements

The final acidity of reaction mixtures was measured via a pH meter after each catalyst tests, the result was used as a supplementary data to monitor the extent of water purification.

The electrode of the pH meter (Accumet AB150, Fisher Scientific) was first calibrated for more accurate pH determination using standard buffer solutions of pH 4.01, 7.00 and 10.01. The electrode was first rinsed with deionised water and wiped dry before immersion in each buffer solution to allow the readings to stabilise for 3 minutes before accepting each calibration step.

This procedure was critical to the accuracy of subsequent pH measurements of the sample solutions. After calibration, the electrode was rinsed again, dried and then immersed in the sample and readings taken once stabilised. Each sample reading was taken three times to minimise errors.

2.5.7 Calculation of conversion and selectivity

The performance of the catalyst in both Fenton reaction for phenol and ibuprofen and aerobic oxidation for benzyl alcohol and 1-phenylethanol are mainly based on substrate conversion, extent of mineralization, observed selectivity and yield of the products.[37–40]

Absolute conversion is defined as the ratio (usually expressed in percentage) between the numbers of moles of reactant that has been consumed during the reaction versus the initial amount of reagent. It is used to monitor the degradation extent of phenol and ibuprofen at each stage of the reaction, therefore we can determine how much of the organic pollutant is converted to intermediate products. It can be calculated by the following Equation 2.11:

$$C_{abs} = \frac{n_{R,R}}{n_{R,O}} \times 100\% \quad \text{(Eq. 2.11)}$$

where:

C_{abs} is absolute conversion

$n_{R,R}$ is the number of mole of reactant consumed during the reaction

$n_{R,O}$ is the initial number of mole of reactant at reaction time zero.

Mineralization is defined as the fraction of the reactant that is completely oxidized to CO_2 and H_2O. It is calculated by carbon mass balance (Eq. 2.12). This value, is useful at it helps to assess if there is any unknown intermediate formed or gives the amount of CO_2 formed at each stage of the reaction.

$$CMB = \frac{\sum nP_i}{\sum nR_j} \times 100\% \quad \text{(Eq. 2.12)}$$

where:

CMB is carbon mass balance

n is the number of carbon in one molecule

P_i is different degradation products detected

nR_j is the initial number of carbon present in the reaction at time zero and corresponding to the number of carbon moles per mole of reagent.

The H_2O_2 consumption ($X_{H_2O_2}$) can be calculated as:

$$X_{H_2O_2} = \frac{C_{o,H_2O_2} - C_{f,H_2O_2}}{C_{o,H_2O_2}} \times 100\% \quad \text{(Eq. 2.13)}$$

where:

$X_{H_2O_2}$ is H$_2$O$_2$ consumption during the reaction

C_{o,H_2O_2} and C_{f,H_2O_2} is the initial and final concentration of H$_2$O$_2$ in the reaction mixture determined by iodometry titration (see Section 2.5.4).

The observed, molar, selectivity (S_i) is defined as the molar ratio between the number of mole of the interested product n_i and the sum of all the number of mole of all the products detected in the reaction mixtures:

$$S_i = \frac{n_i}{\sum n_j} \times 100\% \quad \text{(Eq. 2.14)}$$

where:

S_i is the observed selectivity of the interested product

n_i is the number of mole of the interested product

n_j is the sum number of mole of all the products present in the final reaction mixture.

The yield Y_i, of an interested product is calculated by combining Equation 2.11, Equation 2.12 and Equation 2.14 to form Equation 2.15 as follows:

$$Y_i = C_{abs} \times \frac{S_i}{100} \times \frac{CMB}{100} \times 100\% \quad \text{(Eq. 2.15)}$$

2.6   Reference

(1)   Haber, J.; Block, J. H.; Delmon, B. Manual of Methods and Procedures for Catalyst Characterization (Technical Report). **1995**.

(2)   Zhou, C. Zeolite Catalysts for Water Treatment: Catalytic Wet Peroxide Oxidation (CWPO) of Phenol (Doctoral dissertation, University of Sheffield), 2021.

(3)   Kosinov, N.; Liu, C.; Hensen, E. J.; Pidko, E. A. *Chemistry of Materials*, 2018, **30**, 3177-3198.

(4)   Yan, P.; Mensah, J.; Adesina, A.; Kennedy, E.; & Stockenhuber, M. *Applied Catalysis B: Environmental*, 2020, **267**, 118690.

(5)   Naghash, A. R.; Etsell, T. H.; Xu, S. *Chemistry of materials*, 2006, **18**, 2480-2488.

(6)   Watts, J. F., *Vacuum*,1994, **45**, 653-671.

(7)   Chastain, J., & King Jr, R. C. *Perkin-Elmer Corporation*, 1992, **40**, 221.

(8)   Andrade, J. D. X-Ray Photoelectron Spectroscopy (XPS). In *Surface and Interfacial Aspects of Biomedical Polymers: Volume 1 Surface Chemistry and Physics*; Andrade, J. D., Ed.; Springer US: Boston, MA, 1985; 105-195.

(9)   Montaser, A. Inductively Coupled Plasma Mass Spectrometry; *John Wiley & Sons*, 1998.

(10)   Novaes, C. G.; Bezerra, M. A.; Silva, E. G. P. da; Santos, A. M. P. dos; Romão, I. L. da S.; Neto, J. H. S. *Microchemical journal*, 2016, **128**, 331-346.

(11)   Hou, X.; Amais, R. S.; Jones, B. T.; Donati, G. L. Inductively Coupled Plasma Optical Emission Spectrometry. In *Encyclopedia of Analytical Chemistry; Meyers*, R. A., Ed.; Wiley, 2016; 1-25.

(12)   Weitzel, K.-M.; Mahnert, J.; Penno, M. *Chemical Physics Letters*, 1994, **224**, 371.

(13)   Puttaswamy, N.; Saidam, S.; Rajendran, G.; Arumugam, K.; Gupton, S.; Williams, E. W.; Johnson, C. L.; Panuwet, P.; Rajkumar, S.; Clark, M. L.; Peel, J. L.; Checkley, W.; Clasen, T.; Balakrishnan, K.; Barr, D. B. *Journal of Chromatography B*, 2020, **1154**, 122284.

(14)   Saeed, A. M.; Ibrahim, D. H.; Al–Latief, H. A. W. A. RP *Journal of Physics: Conference Series. IOP Publishing*, 2020, **1660**, 012020.

(15)   Yargeau, V.; Sabri, N.; Hanna, K. *Science of the total environment*, 2012, **427-428**, 382-389.

(16)   Caviglioli, G.; Valeria, P.; Brunella, P.; Sergio, C.; Attilia, A.; Gaetano, B. *Journal of pharmaceutical and biomedical analysis*, 2002, **30**, 499-509.

(17)   Yargeau, V.; Danylo, F. *Water Science & Technology*, 2015, **72**, 491-500.

(18)   Skoumal, M.; Rodríguez, R. M.; Cabot, P. L.; Centellas, F.; Garrido, J. A.; Arias, C.; Brillas, E. *Electrochimica Acta*, 2009, **54**, 2077-2085.

(19)   Hussain, S.; Aneggi, E.; Briguglio, S.; Mattiussi, M.; Gelao, V.; Cabras, I.; Zorzenon, L.; Trovarelli, A.; Goi, D. *Journal of Environmental Chemical Engineering*, 2020, **8**.

(20)   Janson, J. C.; Jönsson, J. A. *Methods of Biochemical Analysis*, 2011, **54**, 25-50.

(21)   Juliane, B; Mareike , M,; Kate , M; © *KNAUER,* VSP0019.

(22)   Oliveira, E. C. de; Muller, E. I.; Abad, F.; Dallarosa, J.; Adriano, C. *Quimica   Nova*, 2010, **33**, 984-987.

(23)   McNally, M. E.; Usher, K.; Hansen, S. W.; Amoo, J. S.; Bernstein, A. P.; *LCGC International*, 2015, **33**, 40-46.

(24)   Pigini, D.; Cialdella, A. M.; Faranda, P.; Tranfo, G. *Rapid Communications in Mass Spectrometry*, 2006, **20**, 1013-1018.

(25)   Atta-ur-Rahman. *Nuclear Magnetic Resonance*; Springer US: New York, NY, 1986.

(26)   Morris, G. A. Atta-Ur-Rahman. *Magnetic Resonance in Chemistry*, 1987, **25**, 375-375.

(27)   Freeman, R. *Magnetic Resonance in Chemistry and Medicine*; Oxford University Press: Oxford, New York, 2003.

(28)   USP technologies. *Analytical Methods for Hydrogen Peroxide for Product Assay*. https://www.h2o2.com/technical-library/default.aspx?pid=67&name=Analytical-Methods-for-H2O2 (accessed 2024-02-19).

(29)   Marković, M.; Jović, M.; Stanković, D.; Kovačević, V.; Roglić, G.; Gojgić-Cvijović, G.; Manojlović, D. *Science of the Total Environment*, 2015, **505**, 1148-1155.

(30)   Chang, Q.; Deng, K.; Zhu, L.; Jiang, G.; Yu, C.; Tang, H. *Microchimica Acta*, 2009, **165**, 299-305.

(31)   Belhateche, D.; Symons, J. M. *Journal - American Water Works Association*, 1991, **83**, 70-73.

(32)   Huckaba, C. E.; Keyes, F. G. T. *Journal of the American Chemical Societ*y, 1948, **70**, 1640-1644.

(33)   Liang, C.; He, B. A *Chemosphere*, 2018, **198**, 297-302.

(34)   Kieber, R. J.; Helz, G. R. *Analytical Chemistry*, 1986, **58**, 2312-2315.

(35)   Shen, W.; Ichihashi, Y.; Okumura, M.; Matsumura, Y. *Catalysis Letters*, 2000, **64**, 23-25.

(36)   Cheng, Z. *Physical Testing and Chemical Analysis part B Chemical analysis,* 2003, **39**, 404-405.

(37)   Nidheesh, P. V. *RSC Advances*, 2015, **5**, 40552-40577.

(38)   Adityosulindro, S.; Julcour, C.; Barthe, L. *Journal of Environmental Chemical Engineering*, 2018, **6**, 5920-5928.

(39)   Ros, D.; Gianferrara, T.; Crotti, C.; Farnetti, E. *Frontiers in Chemistry*, 2020, **8,** 810.

(40)   Thao, N. T.; Nhu, N. T.; Lin, K.-S. *Journal of the Taiwan Institute of Chemical Engineers*, 2018, **83**, 10-22.

Chapter 3 Phenol oxidation by catalytic wet peroxide oxidation

3.1   Overview

Since the mid-1970s, phenol was listed by US Environmental Protection Agency and Canada National Pollutant Release Inventory,[1] as one of the major toxic pollutants from rivers, lakes or reservoirs. Due to its wide use in industrial processes like pharmaceuticals, chemicals, textiles, wood, automotive and personal care products,[2–6] the existence of phenol, phenol intermediates or by-products during oxidation of higher molecular aromatic compounds has resulted in more than 10 million tons of phenol discharge per year in the environment.[7] This discharge of phenol without proper treatment poses a significant risk to aquatic life and human health, even at very low concentrations (2 µg L^{-1}).[8] Rivers or lakes around chemical industries can even reach up to 10 g L^{-1} that largely exceeds the restricted limit by regulation (ranging from 0.5 ppb to 0.5 ppm).[9,10]   In addition phenol can also occur naturally in water bodies through the decomposition of organic matter with a range of 0.01-1 µg L^{-1} Addressing this issue is crucial to safeguarding the health of our water resources and the well-being of both aquatic life and humans.

While chemical degradation provides an efficient option for removing high levels of phenol, there are trade-offs to consider. For example, these methods can rapidly break down phenol even at concentrations up to 15 g L^{-1}. However, chemical degradation relies on the use of harsh oxidizing agents, which can be hazardous and require careful handling. As such, more research is needed to refine chemical degradation approaches to be greener and more sustainable for large-scale use.

Among chemical methods, advanced oxidation processes (AOPs) are rapid and effective for decomposing organic pollutants in wastewater. These processes use reactive oxygen species to destroy pollutants. Hydrogen peroxide generates reactive hydroxyl radicals ($\cdot$OH), which degrade organic compounds like phenolic compounds, pesticides, herbicides, pharmaceuticals, and personal care products. The hydroxyl radical has a high reduction potential of 2.80 V and a short half-life of 10^{-9} s, primarily utilizing a radical decomposition route.[11] The Fenton reaction, using Fe^{2+} to activate hydrogen peroxide, is a widely used AOP due to its affordability and low operating requirements, such as ambient pressure and temperatures below 100°C.[12]

With its aromatic structure being difficult to be degraded and decomposed to less or non-toxic species, phenol is often selected as a model aromatic pollutant for the studies of water purification.[13–16] In view of this, we will also consider the degradation of phenol in order to

compare the efficacy of new catalytic materials, or the innovative use of materials not currently used for catalysis like recycled glass, for the degradation of this compound and to have a large literature data set to compare with.

In this context, and in the search for sustainable catalysts for the catalytic AOPs of organic pollutants, iron-modified zeolites such as Fe/ZSM-5 have attracted substantial attention due to their high activity, selectivity, thermal stability, and eco-friendly properties.[11,17] However, these materials are expensive (around £1,000 per kg). Recycling and regeneration of spent zeolite catalysts is laborious, often requiring high temperature treatment to burn residues that would quench the microporous activity of these catalysts, thus motivating the exploration of alternatives such as recycled waste glass, which naturally contain also Fe active centres.

In fact the well-established nature of Fenton reaction, which dates back to 1894,[18] and the significant amount of research conducted on its degradation capabilities[19–23] together with research within the group shows this is a potentially efficient route for the abatement of organics.[24]

In view of these factors, this chapter will: 1) describe and assess hydrogen peroxide thermal decomposition under our experimental conditions by iodometry; 2) carry out control tests of phenol oxidation using CWPOs; 3) assess the feasibility of the using of ferric and ferrous ions towards phenol decomposition by changing different parameters such as glass bead sizes, metal to substrate (M:S) molar ratio and reaction time; 4) propose a plausible phenol decomposition pathway compatible with our and literature data; 5) investigate the efficiency of Fe^{3+} containing recycled glass heterogeneous catalyst for phenol oxidation; 6) provide a comparison between the capabilities of recycled glass versus established zeolite based catalysts for phenol oxidation.

3.2   Hydrogen peroxide thermal decomposition

Hydrogen peroxide can provide $\cdot OH$ radicals during Fenton reaction, in fact ultimately it is due to these $\cdot OH$ species that the decomposition of the organic substrate occurs. However, undesired thermal decomposition of hydrogen peroxide under heating can occur and will produce water and molecular oxygen.[25] The latter can also serve as a source of molecular oxygen, which may oxidize organic compounds. However, we did not detect decomposition of phenol under reaction conditions studied (reaction time of 4 hours at 80 °C, endogenous pressure and a stirring rate of 500 rpm). These tests are of relevance because if the decomposition of H_2O_2 is uncontrolled it can cause this oxidising agent to be depleted without attacking the organic substrate. This would hence result in an overestimation of H_2O_2

consumption towards the organic degradation, or in other terms, not all H_2O_2 would be used for the degradation of the organic contaminant but would result in a non-fruitful thermal degradation unless the molecular O_2 generated in the process can also oxidise the organic compound (see control tests Section 5.6 in Chapter 5 for this important reactivity aspect). Therefore, it is important to obtain accurate H_2O_2 consumption and thus correctly evaluate the efficiency of H_2O_2 and performance of the catalyst.

In this context, there are three common titrimetric methods, namely: iodometry, permanganometry and cerimetry that are often used for batch-to-batch testing since 2000 to date to measure the concentration of hydrogen peroxide in reaction mixtures.[26–28] Iodometry is one of the most used method for hydrogen peroxide quantification (about half of the literature is related to this method), which is due to its high accuracy in detecting H_2O_2 at relatively low concentration (< 0.4 mM).[29] In iodometry, H_2O_2 typically oxidises iodide ions to form I_2, which is titrated with a standard solution of thiosulfate (Eq. 3.1 and Eq. 3.2).

$$H_2O_2 + 2KI + H_2SO_4 \rightarrow I_2 + K_2SO_4 + 2H_2O \quad \text{(Eq. 3.1)}$$
$$I_2 + 2Na_2S_2O_3 \rightarrow Na_2S_4O_6 + 2NaI \quad \text{(Eq. 3.2)}$$
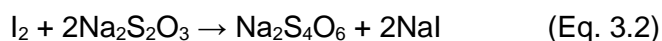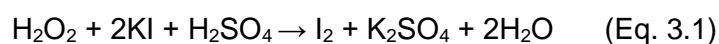
This sequence of reactions represents a back-titration, as such it is important to accurately control the amount of potassium iodide (KI) and reaction time for this redox reaction, which in turn will result in complete reduction of H_2O_2 in the first step and ensure the correct estimation of H_2O_2 concentration.[30] Therefore, we will: 1) investigate how KI concentration and titration time in the redox reaction (Eq. 2.7) effect the iodometry accuracy in determining H_2O_2 concentration in water; and 2) Determine the extent of H_2O_2 thermal decomposition under the our experimental conditions.

3.2.1 Effect of KI concentration on iodometry method accuracy

Aqueous solutions at a known concentration of H_2O_2 (3 mM) were prepared to mimic the actual reaction mixture. Two distinct concentrations in excess of KI (20 and 100 g L^{-1}) were used for redox step to investigate and isolate the impact on the iodometry results at a designed redox reaction time (10 mins) in darkness.
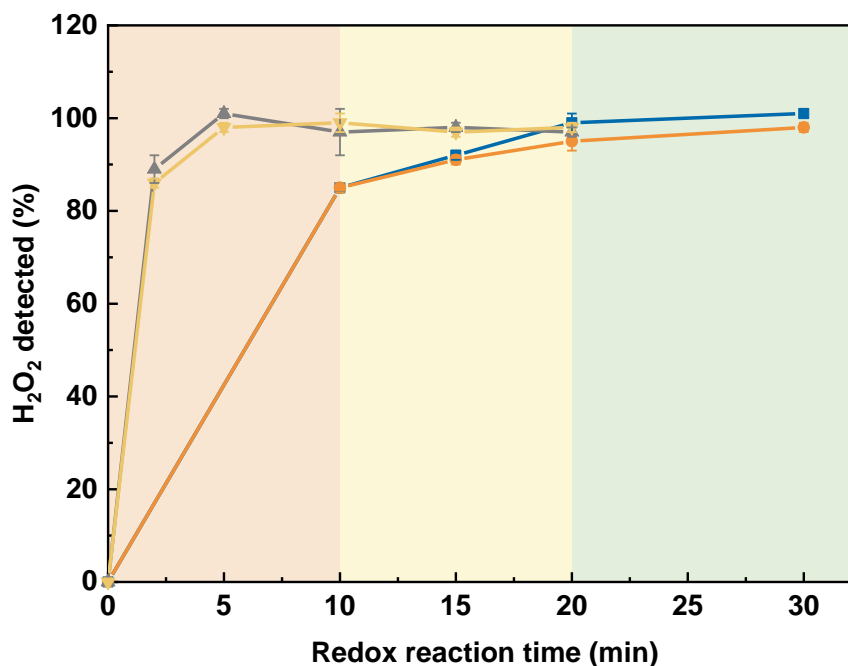
Figure 3.1 H_2O_2 detected (%) in H_2O_2 water solution, before and after 4 h thermal treatment (80 ˚C) determined by Iodometry, with two different KI concentrations (20 and 100 g L^{-1}) and different H_2O_2–KI redox reaction time (2 min to 30 min). Before thermal treatment: 20 g L^{-1} KI: ■, 100 g L^{-1} KI: ▲. After thermal treatment: 20 g L^{-1} KI: ■, 100 g L^{-1} KI: ▼. Orange area (■): comparison of H_2O_2 detected during current reaction time (10 mins); Yellow area (■): H_2O_2 detected after 20 min redox reaction; Green area (■): H_2O_2 detected after 300 min redox reaction. KI concentration of 100 g L^{-1} gave an accurate titration result after 5 min, while 20 g L^{-1} needs 20 mins. The thermal decomposition of H_2O_2 was not significant after 4 hours thermal treatment and can be neglected.

The results in Figure 3.1 illustrate that when 100 g L^{-1} of KI were used (before ▲ and after ▼ thermal treatment), a 10 mins time was sufficient for the redox reaction between H_2O_2 and KI to reach completion at room temperature. It is important to conduct the reaction in the darkness to avoid photolysis of iodine which may lead to side reactions and altering the concentration of iodine. This can disrupt the redox equilibrium and accuracy of the titration results. In contrast, after 10 min reaction between H_2O_2 and KI, H_2O_2 detected using 20 g L^{-1} of KI (85%) was significantly lower than that using 100 g L^{-1} (97%) of KI, despite a 30 times molar ratio excess amount of KI as compared to H_2O_2 being used in both case (Figure 3.1 orange area). This observation could be attributed to the lower concentration of KI (30 times molar ratio excess) in the solution, which might affect the rate of the reaction between H_2O_2 and KI. Hence, 10 mins redox reaction in dark resulted in a solution containing residual H_2O_2. This hypothesis could be supported by the circumstance of the solution turning back to dark blue within 30 seconds after the endpoint, indicating the formation of more I_2 (and hence I_3^-),[29] the formation of starch-iodine complex at a longer time (longer than 30s) will also cause a dark blue formation. As a result, for a 10-min reaction time, the amount of I_2 formed and later determined with $Na_2S_2O_3$ will be less than expected, leading to a negative discrepancy. In

contrast, using the higher concentration of KI (30 times molar ratio excess), the solution remained transparent for at least 1 minute after the endpoint indicating a complete conversion of H_2O_2. However, reaction time is also another factor to be considered for complete reaction. Hence, 100 g L^{-1} KI allows for accurate detection of H_2O_2 within 10 mins, while 20 g L^{-1} KI results in an underestimate under the same conditions. But longer titration reaction times may improve results at lower KI levels. Due to the large amount of sample to be tested, 100 g L^{-1} KI was chosen to reduce the reaction time to 10 min.

3.3 Effect of reduction time on iodometry method accuracy

To test the assumption, various reaction times ranging from 2 minutes to 30 minutes were investigated for each KI concentration. For the concentration at 100 g L^{-1} (Figure 3.1 grey curves), the amount of H_2O_2 detected reached a plateau after approximately 5 minutes, with results that were compatible with 100%, indicating that all the H_2O_2 was completely converted to H_2O. As expected, the plateau was only reached at around 20 minutes when using 20 g L^{-1} of KI (blue curves), with a value compatible with 100%. Hence, the complete reaction of H_2O_2 required 20 minutes for the 20 g L^{-1} concentration.

Within a set time frame (10 mins in our case), the completeness of the redox reaction between H_2O_2 and KI is largely affected by changing KI concentration. Adequate reaction time of at least 20 minutes can compensate for any concentration differences in the results. However, considering the large number of H_2O_2 determinations required for this thesis work, a higher KI concentration and shorter reaction time are preferred to enhance efficiency. Therefore, a trade-off parameter for the first step of iodometry method will be excess amount of 100 g L^{-1} of KI and a redox reaction time of 10 minutes to achieve an accurate result.

3.3.1 Relevance of H_2O_2 thermal decomposition in water

To verify the effect of thermal treatment on H_2O_2 after 4-hour reaction at 80 °C, and in turn its possible decomposition, blank tests of H_2O_2 water solutions (endogenous and 500 rpm) were performed. Iodometry titration was done with two different KI concentrations at their respective appropriate redox reaction time. Regardless of the KI concentration used, the detected amounts of H_2O_2 (or H_2O_2 consumption) were found to be statistically (98% vs 100%) identical that is within the experimental error with the initial amount of H_2O_2 that was introduced into the batch system. As can be seen in Figure 3.1: grey/yellow and orange/blue, that is, compare H_2O_2 consumptions before and after a 4-hour thermal treatment. This indicates that the consumption of H_2O_2 due to thermal decomposition was negligible which will not affect the degradation reaction in the absence of a catalyst.

3.4 Effects of Fe centres on phenol catalytic wet peroxide oxidation

The standard Fenton process uses Fe^{2+} and H_2O_2 as oxidant to form $\cdot OH$ radicals that is effective for most of the organic contaminants with a reaction constant as fast as 10^6 - 10^9 mol^{-1} s^{-1} (10^6-10^{12} times faster than ozone, which is another commonly used oxidant).[31] Fenton reaction with Fe^{2+} and H_2O_2 is regarded as a powerful technique for water purification in this section work. In fact, under the reaction conditions employed in this study, Fe^{2+} can be oxidized to the most stable oxidation state as Fe^{3+}. However though at a much lower rate Fe^{3+} can be converted to Fe^{2+} (Eq. 3.3 and Eq. 3.4), thus forming a catalytic cycle. In view of this, the Fenton system allows that either Fe^{2+} or Fe^{3+} theoretically initiate the reaction. For this reason subsequent, investigations will be performed on heterogeneous catalysts such as Fe/ZSM-5 and iron-containing recycled glass, where Fe^{3+} will be present in the form of Fe_2O_3. Thus, using Fe^{3+} in homogeneous phase (aquo complex form dissolved $Fe(NO_3)_3$) will provide some insights into the reactivity of this species. Though as of now disregarding the potential effects that leached species from the catalysts at this stage of the project.

$$Fe^{2+} + H_2O_2 \rightarrow Fe^{3+} + HO^- + \cdot OH \qquad k_1 = 70 \text{ M}^{-1}\text{s}^{-1} \qquad \text{(Eq. 3.3)}$$

$$Fe^{3+} + H_2O_2 \rightarrow Fe^{2+} + \cdot OOH + H^+ \qquad k_2 = 0.001\text{-}0.01 \text{ M}^{-1}\text{s}^{-1} \qquad \text{(Eq. 3.4)}$$
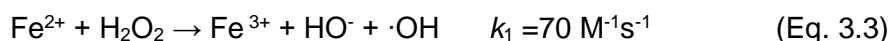
3.4.1 Comparison between Fe^{2+} and Fe^{3+} as catalyst

In this view, the effect of using Fe^{2+} or Fe^{3+} was investigated by alternating M:S ratio. Specifically, two iron salts, $FeSO_4 \cdot 7H_2O$ (Fe^{2+}) and $Fe(NO_3)_3 \cdot 9H_2O$ were chosen to conduct the comparison tests with different M:S molar ratios (1:50, 1:100 and 1:200) under identical reaction conditions, with all other parameters held constant: 50 mL (1 g L^{-1}) of phenol water solution, p = endogenous, 80°C, reaction time: 4 h, M:S molar ratio of 1:100, phenol:H_2O_2 molar ratio = 1:14.
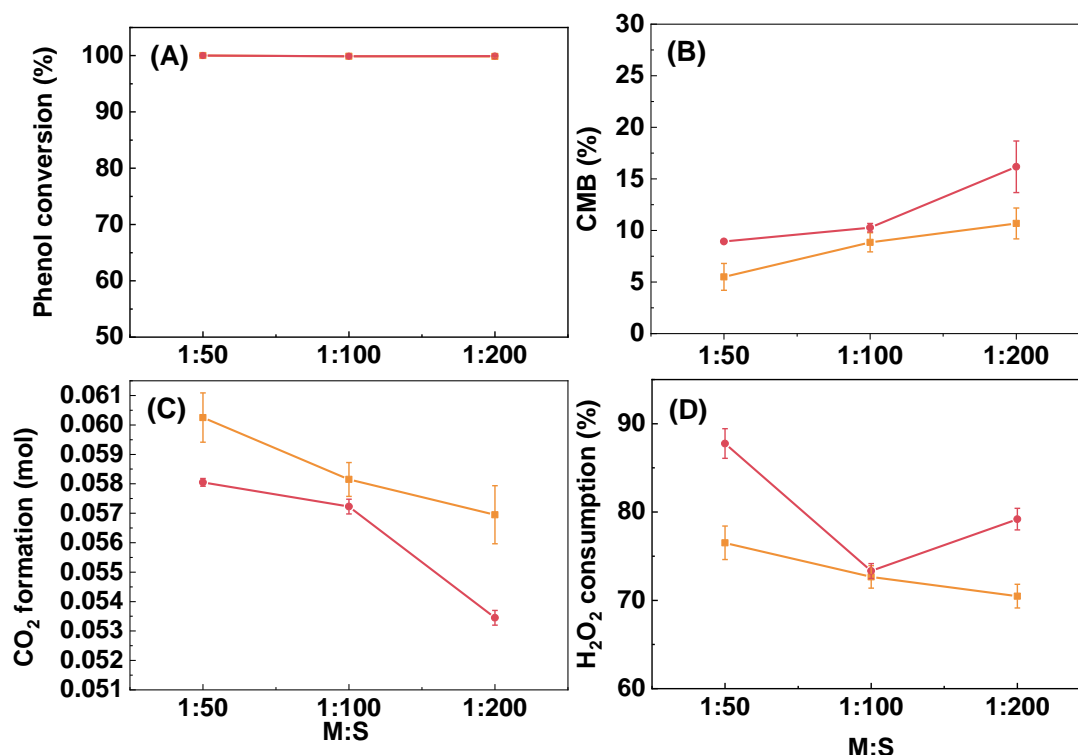
Figure 3.2 Comparison of (A) phenol conversion; (B) carbon mass balance; (C) CO_2 formation and; (D) H_2O_2 Decomposition; for phenol oxidation reactions catalysed by differing metal salts at different M:S ratios. Reaction conditions: 50 mL of phenol (1 g L^{-1}), $FeSO_4 \cdot 7H_2O$ (Fe^{2+} ●) and $Fe(NO_3)_3 \cdot 9H_2O$ (Fe^{3+} ●), M:S=1:50, 1:100 and 1:200, PhOH:H_2O_2=1:14 (stoichiometric amount towards mineralization), p = endogenous, 80°C, 4 h, 500 rpm.

The results of the three different M:S ratios (1:50, 1:100 and 1:200) in Figure 3.2 reveal disparities in the carbon mass balance (CMB%) and hydrogen peroxide consumption of the two iron catalysts, $FeSO_4 \cdot 7H_2O$ (Fe^{2+}) and $Fe(NO_3)_3 \cdot 9H_2O$ (Fe^{3+}). Despite achieving 100% phenol conversion in all three M:S ratios, Fe^{3+} leads to higher hydrogen peroxide consumption with lower CO_2 formation (lower CMB%) compared to Fe^{2+}. This difference could be due to the fact that Fe^{3+} does not generate hydroxyl radicals directly, thereby requiring additional steps (Eq. 3.3 and 3.4) and consumption of H_2O_2 to convert to Fe^{2+} for the formation of hydroxyl radicals in the Fenton-like reaction, thus lower mineralization was achieved. Hence, during the 4-hour reaction period, a minor variation was observed with respect to the formation of CO_2 and consumption of H_2O_2. However, over a longer reaction time, this discrepancy may become negligible. These considerations are important because in the Fenton scheme, the metal catalyst (Fe species in our case) is not responsible for the attack of the organic substrate and mineralization but for the attack on H_2O_2 to generate ·OH species that then lead to the attack of the organic substrate and mineralization. As such, it was proved that only minor variance was discovered when using Fe^{3+} to initiate Fenton reaction as compared to traditional Fe^{2+} within the current time frame (4 h). These promising and convincing results provided a

strong basis to start further investigation on the Fenton system by using $Fe(NO_3)_3 \cdot 9H_2O$ (Fe^{3+}) as catalyst, and in turn to explore the possibility application of heterogeneous catalysts containing Fe_2O_3.

3.4.2 Control tests on the active centres for phenol oxidation by Fenton reaction

Control experiments were performed under the same conditions (500 rpm, 80°C, 4 h) to evaluate the individual effects of the Fe^{3+} catalyst ($Fe(NO_3)_3 \cdot 9H_2O$ at M:S ratio 1:100) and the H_2O_2 oxidant (stoichiometric amount with respect to mineralization Equation 3.5) (i.e., Fe^{3+} and H_2O_2, as catalyst and oxygen source to form CO_2 and H_2O, respectively) on phenol oxidation. This was done to understand the mechanism of the Fenton reaction by investigating the contributions from each component separately, before studying their combined effect.

$$C_6H_5OH + 14\ H_2O_2 \rightarrow 6\ CO_2 + 17\ H_2O \quad \text{(Eq. 3.5)}$$
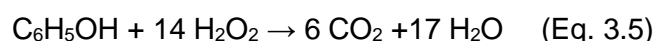
To assess the extent of the reaction, quantitative and qualitative analysis of the reaction mixtures were performed using HPLC, which was used to determine potential aromatic and aliphatic intermediates. Additionally, the absolute conversion, that is the one relying on the consumption of phenol only, regardless of any product that may be formed, and carbon mass balance were calculated to quantitatively evaluate the reaction (Figure 3.3).
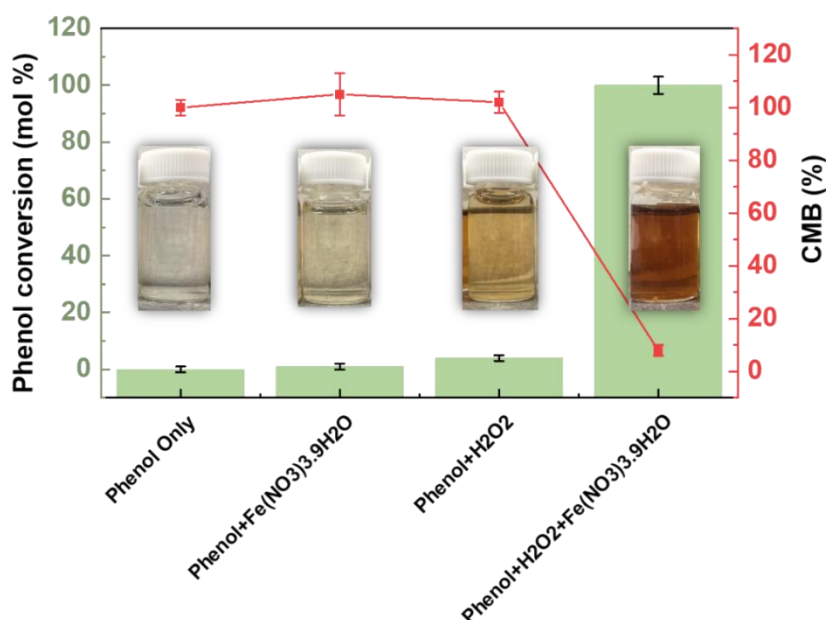
Figure 3.3 Phenol Conversion (●) and Carbon Mass Balance (■) of three different blank tests and one Fenton reactions were quantified using HPLC. Reaction conditions: 50 mL of phenol (1 g L^{-1}) water solution, $Fe(NO_3)_3 \cdot 9H_2O$, M:S=1:100, $PhOH:H_2O_2$=1:14, p = endogenous, 80°C, 4 h, 500 rpm. The colour of the reaction mixtures in the figure indicates the extent of the reaction, with the samples progressing from left to right as follows: phenol only, phenol with $Fe(NO_3)_3 \cdot 9H_2O$, phenol with H_2O_2, and phenol with both $Fe(NO_3)_3 \cdot 9H_2O$ and H_2O_2.

No significant phenol conversion was observed in the control tests containing either phenol alone (0 ± 1%) or $Fe(NO_3)_3 \cdot 9H_2O$ and phenol (1 ± 1%). This result highlights the difficulty in initiating phenol oxidation through the Fenton reaction without H_2O_2. The correspondent HPLC chromatograms (Figure 3.4 a, b) showed no detectable product detected under our HPLC conditions in the presence of phenol only and only trace amounts of oxalic acid observed in the presence of $Fe(NO_3)_3 \cdot 9H_2O$. This also consistent with the corresponding reaction mixture colours displayed in Figure 3.3.

When a stoichiometric amount of hydrogen peroxide was added to phenol under the same reaction conditions, but in the absence of Fe species, a slight increase in phenol conversion (4 ± 1%) was observed. HPLC analysis revealed the presence of only a few aromatic intermediates, including hydroquinone, p-benzoquinone, catechol, and a small amount of maleic acid, as well as residual hydrogen peroxide (Figure 3.4 c). This residual activity is attributed to the thermal decomposition of hydrogen peroxide into hydroxyl radicals (·OH) at 80°C via homolytic cleavage, which initiates the oxidation of phenol.[32,33] However, as previously discussed in Section 3.2.1, hydrogen peroxide is relatively stable under these reaction conditions with a maximum of 3% decomposition, which may have contributed to the trace phenol conversion and formation of the three aromatic intermediates.

Last but not the least, the presence of $Fe(NO_3)_3 \cdot 9H_2O$ led to activation of hydrogen peroxide and subsequent full conversion of phenol (100 ± 3%) and low CMB% (8 ± 2%) into a variety of end products. This observation highlights a high level of selectivity mostly towards CO_2 formation with the formation of intermediate carboxylic acids such as oxalic acid, formic acid, malonic acid, maleic acid, and fumaric acid (Figure 3.4 d). This outcome supports the proposed hypothesis of the Fenton process, wherein ferric ions (Fe^{3+}) in the presence of hydrogen peroxide generates ferrous ions (Fe^{2+}), which in turn drives the decomposition of hydrogen peroxide and the formation of hydroxyl radicals, resulting in an increased rate of phenol oxidation, hence an efficient mineralization of the reactant.
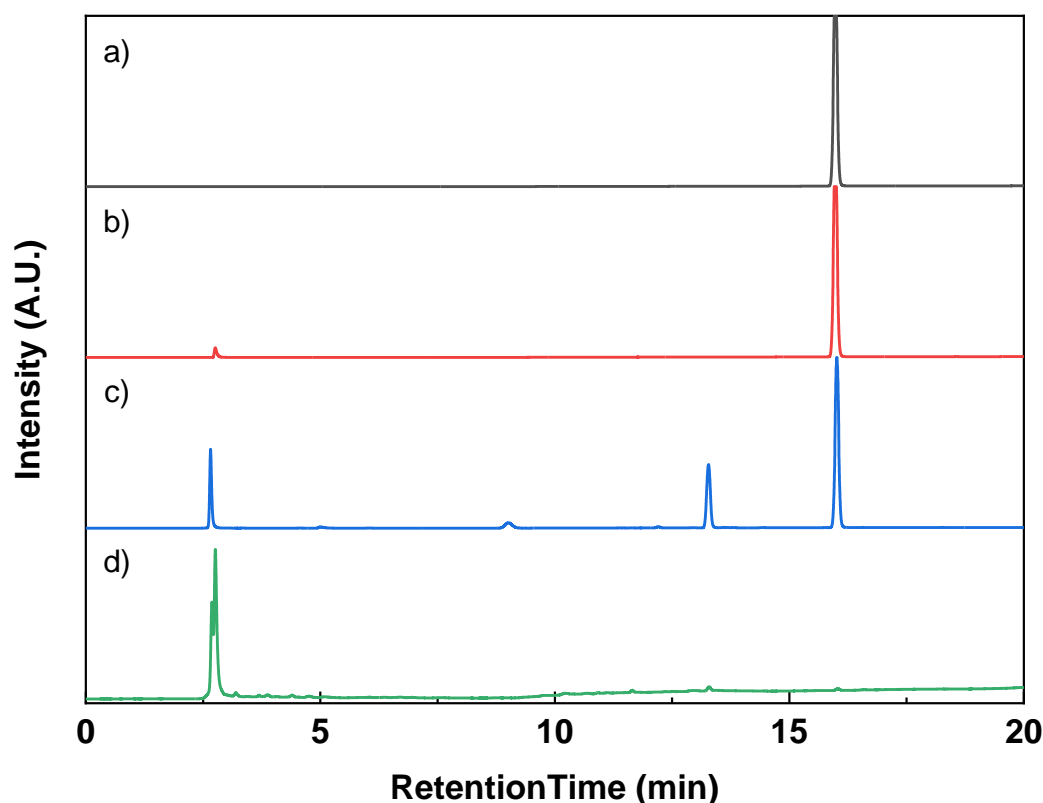
Figure 3.4 Chromatograms of four control tests collected at a wavelength of 200 nm. a) only phenol was present (●) peak at 16.0 mins; b). phenol with $Fe(NO_3)_3 \cdot 9H_2O$ (●); c). phenol with H_2O_2 (●) and d) phenol with both $Fe(NO_3)_3 \cdot 9H_2O$ and H_2O_2 (●). Reaction conditions: 50 mL (1 g L^{-1}) of phenol, $Fe(NO_3)_3 \cdot 9H_2O$, M:S=1:100, PhOH:H_2O_2=1:14, p = endogenous, 80°C, 4 h, 500 rpm. Only a phenol peak was detected at 16.0 min. HPLC condition: H_3PO_4 solution (0.1% (v/v)) and acetonitrile as dual mobile phases with acetonitrile percentage of 2% from 0-5 min, 2%-70% from 5-20 min, 2 % from 20-30 min and injection volume 5 μL.

The presence of a stoichiometric amount of hydrogen peroxide, led to a nearly a full mineralization of phenol was achieved as indicated by the CMB value (8 ± 2%), that is more than 92% of phenol was converted into CO_2 and H_2O. This result is also evidenced by HPLC chromatogram and highlights no phenol (expected retention time 16 mins) was detected. However, in order to have a complete mineralization the reaction time should be incremented and inefficiencies in the oxidation ability of H_2O_2 were also attributed to concurrent undesired side reactions, that result in the formation of hydroperoxyl radicals (·OOH) that diminish the oxidizing capabilities of the system. Additionally, the self-termination of the generated radicals (Eq. 3.6 and Eq. 3.7) results in radical scavenging, further reducing the efficacy of H_2O_2 as an oxidant, thereby incurring increased costs for the corresponding process.

$$·OH + ·OH \rightarrow H_2O_2 \qquad (Eq.\ 3.6)$$
$$·OOH + ·OOH \rightarrow H_2O_2 + O_2 \qquad (Eq.\ 3.7)$$
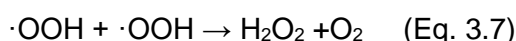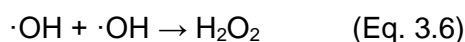
On the other hand, the introduction of ferric ions (Fe^{3+}) greatly enhances the production of

hydroxyl radicals leading to a marked increase in the rate of phenol oxidation and thus demonstrating the efficacy of the Fenton system. It has been observed that utilization of stoichiometric amounts of hydrogen peroxide does not result in full mineralization of the substrate, this has also to do with the oxidation efficiency of H_2O_2, as not all ·OH radicals will attack the substrates but may invariably terminate on the wall of the reaction vessel, or as explained above, not all H_2O_2 decomposition processes lead to ·OH.

3.5   Proposed phenol degradation pathway

The focus of research in CWPO studies primarily centres on the removal of pollutants and high total organic carbon total organic carbon degradation. However, a thorough understanding of reaction mechanisms and pathways is equally indispensable for the optimization of reaction conditions and the development of catalysts that are highly efficient and especially if to be suitable for industrial applications. As investigated by Zhou,[34] the traditionally proposed Fenton process involves over 20 chemical reactions, with the widely recognised central reaction being the "Fenton reaction" (Eq. 3.3). The generation of hydroxyl radicals is a critical component throughout the process. These hydroxyl free radicals, recognised as the most reactive species for the degradation of pollutants in the Fenton reaction, are primarily generated from Eq. 3.3, which serves as the chain initiation step. The effectiveness of the Fenton system in producing the active ·OH radical oxidant is significantly influenced by the catalytic cycling of iron between its Fe^{3+} and Fe^{2+} states. The reaction system then proceeds to the chain propagation step for the organic substrate R-H (Eq. 3.8).

$$RH + ·OH \rightarrow R· + H_2O   \text{(Eq. 3.8)}$$
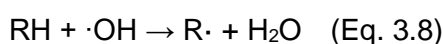
In the initial stage of the phenol oxidation process, ·OH radicals can attack the phenol molecule at either the *ortho* or *para* positions, resulting in the formation of catechol and hydroquinone, respectively. Subsequent oxidation without ring-opening leads to the production of p-benzoquinone and o-benzoquinone, which contribute to the characteristic brownish colour observed. As the oxidation process continues, the formation of carboxylic acid by-products such as maleic acid, fumaric acid, oxalic acid, formic acid, and acetic acid occurs through ring-opening reactions at various positions (Figure 3.5). These findings are consistent with previous studies by Zhu et al.[35] Liotta et al.[36] and Gerginova et al.[37] However, it is worth noting that some of the potential intermediate products may not have been detected or quantified due to their short lifetimes or low concentrations, leading to a degree of uncertainty in the calculation of carbon mass balance.

Additionally, examining the resulting toxicity of the solution is imperative, as incomplete oxidation can exacerbate environmental impacts. The aromatic intermediates exhibited higher

toxicity than phenol itself, with hydroquinone being most toxic.[38] Furthermore, interactions between copper leached from catalysts and intermediates like catechol, hydroquinone, and p-benzoquinone can induce synergistic effects, amplifying overall toxicity and warranting careful evaluation.[38] High oxalic acid concentrations are also undesirable because insoluble complexes formed with metal catalysts may cause leaching, reducing heterogeneous catalyst reusability.[39,40] Therefore, to mitigate unintended consequences, complete conversion of aromatics to carboxylic acids, followed by total mineralization, is highly recommended to avoid catalyst deactivation, metal leaching, and toxic or acidic effluents.
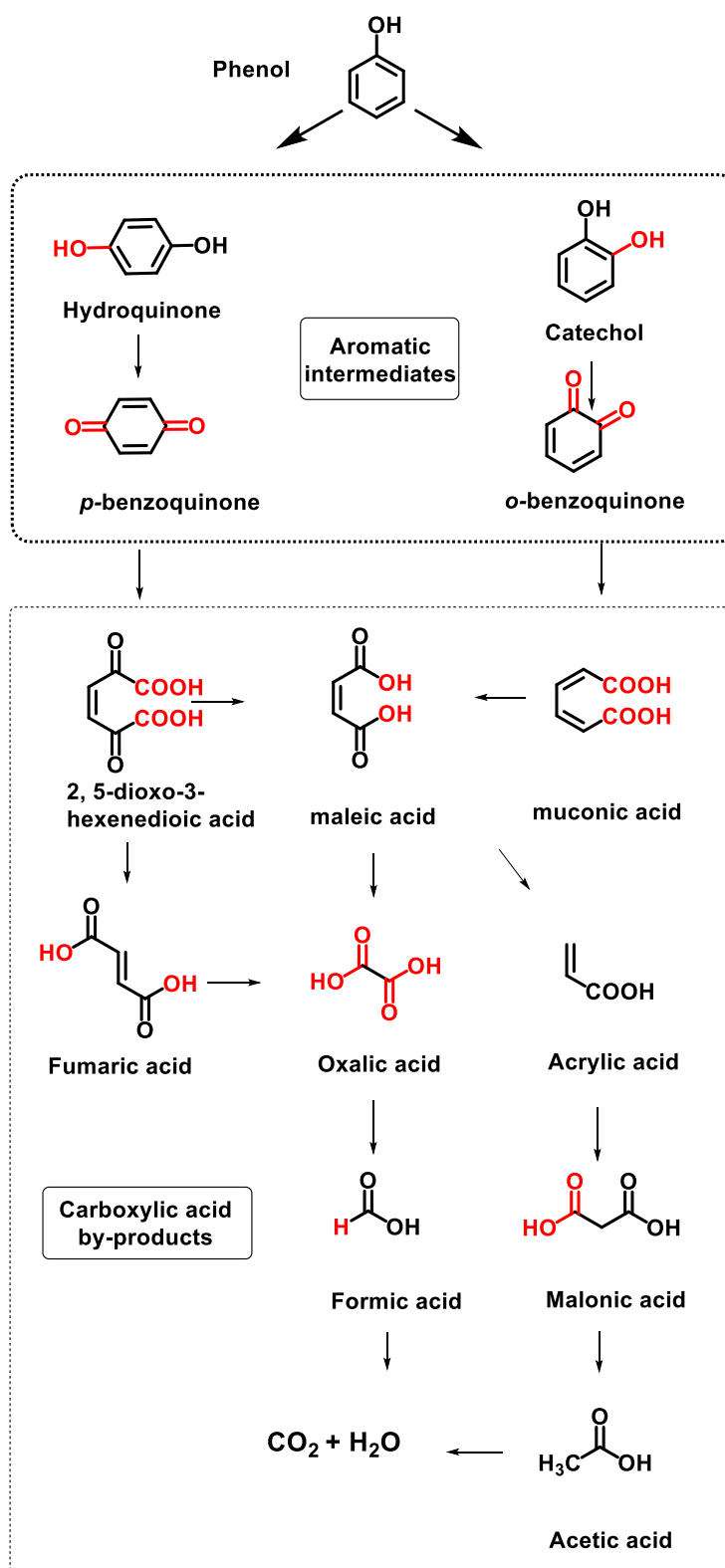
Figure 3.5 Reaction intermediates[36,41] of phenol degradation via CWPO. Phenol is oxidised to several hydroxylated aromatic intermediates: (aromatics, top) catechol, hydroquinone, p-benzoquinone and o-benzoquinone, which are further oxidised to a complex mixture of carboxylic acids (ring opening, bottom): maleic acid, fumaric acid, oxalic acid, formic acid, and acetic acid, before final mineralization to carbon dioxide and water.

3.6   Recycled glass as heterogeneous catalysts on phenol catalytic wet peroxide oxidation

The utilization of iron salts, $FeSO_4 \cdot 7H_2O$ and $Fe(NO_3)_3 \cdot 9H_2O$, as catalysts in the Fenton reaction previously discussed is referred to as a homogeneous Fenton process, because these salts are soluble in the reaction medium, water, in our case and has been proven to be effective. The iron ions in the reactions are readily accessible in water, that promotes the degradation of phenol in wastewater to occur quickly.[42] However, the Fenton reaction, regardless of whether it is homogeneous or heterogeneous, requires strict pH control, typically within a range of 2.5 to 4.0.[43,44] If the pH falls below 2.5, especially if in the presence of inorganic acids, e.g. HCl these may form covalent Fe species that inhibits the Fenton cycle,[45,46] Furthermore, the presence of high concentration of H^+, an increased scavenging effect of $\cdot OH$ and H^+ will occur, also, the more stable intermediate like $H_3O_2^+$ will be produced, making it challenging to react with Fe^{2+}, up to the point the Fenton process is completely inhibited. Conversely, if the pH exceeds 5-6, precipitation or formation of $Fe(OH)_3$ sludge may occur, impeding the recovery and recyclability of the catalyst, leading to an increase in the operational cost,[47] thus, this is inherently a major challenge to have a Fenton process at neutral pH.

The strict dependency on pH can, to some extent be mitigated by the use of heterogeneous Fe species. For example, catalysts Fe_2O_3, Fe/ZSM-5, $ZnFe_2O_4$-C_3N_4, have been shown to be effective in mediating Fenton-like reactions within a broader pH range of 3.0 to 5.0.[48-49] Some studies have even reported successful reactions at pH values as low as 2[50] and as high as 7[51] the latter a real challenge in this area of research. The immobilization of Fe^{3+} species within the catalyst structure and pore/interlayer space prevents, or at least mitigate, the precipitation of iron hydroxide and allows the catalyst to maintain its ability to generate hydroxyl radicals from H_2O_2. The major advantage in the use of heterogeneous catalyst though is that, the solid catalyst materials can be easily recovered. Other than the conventional heterogeneous catalysts, like Fe doped zeolites, a new material, recycled glass that containing essential Fe^{3+} for Fenton reaction was studied to aim for a greener (circular economy) and cheaper alternative.

Therefore, the work in this section will: 1) describe and assess the properties of recycled glasses that related to Fenton reaction; 2) identify the active species participating in the phenol decomposition process by conducting metal activity control tests.

3.6.1 Advantages of recycled glass for the Fenton reaction

Glass is utilized for various purposes such as packaging, container glass, and bulb glass. The

high demand for glass products has resulted in a substantial amount of waste glass, which represents a significant portion of the solid waste stream. While recycled glass has been effectively used for construction materials, such as mortar, cement, concretes, and blocks,[52,53] a significant amount of the waste glass is either stockpiled or landfilled, awaiting a more profitable use in a robust recycled glass market, which is not currently being met. Recycling glass can help eliminate the energy consumption, raw materials, and machinery wear and tear associated with the production of new glass. The typical composition of glass for packaging consists of about 70% silica (SiO_2), 13% sodium oxide (Na_2O), and 10% calcium oxide (CaO), which account for 93% of its overall composition.[54] Other metal compounds, such as Fe_2O_3, MnO_2 and Cr_2O_3, constitute the remaining 7% of the composition which is within the range of other metal-doped catalysts (1%). The most noticeable characteristic of a glass object is its colour, which is determined by the metal compounds that absorb different wavelengths of light (Figure 3.6). Table 3.1 summarizes the metal compounds responsible for the various coloured glasses.

Recycled glass from packaging (mostly the brewage sector) was chosen as a potential catalyst for the following reasons: 1) it contains iron oxide, which is a highly efficient metal for promoting Fenton or Fenton-like processes as discussed previously. The iron content varies based on the glass colour, and it is comparable (0.1 to 1 wt.%) to other reported catalyst materials.[55] 2) In addition, waste glass, which is derived from products like beer bottles, is much less expensive (ca. £15-25 per tonne for green glass) than zeolite (e.g., H/ZSM-5 at £700-1000 per kg). 3) Recycled glass is readily available in large quantities and is relatively inexpensive, making it more cost-effective to recycle used glass after it has served as a catalyst than to post-treat used zeolite. 4) The used/spent glass can always be recycled again for other applications. 5) Prior preliminary lab-scale experiments conducted within the research group have demonstrated promising performance of iron-containing recycled glass for water treatment, especially with particle sizes ranging from 4 mm to 0.1 mm. This provides motivation to further explore the potential of recycled glass as a sustainable catalyst in the bench scale experiments undertaken in this work.

The use of recycled glass for water decontamination exemplifies a circular economic model, whereby the waste from one industry is utilized as an input for another, generating value and reducing environmental impacts. Specifically, recycled glass serves as an inexpensive and sustainable catalyst for water treatment, while the purified water helps alleviate scarcity, enabling productive use for agriculture. This approach embodies key circular economy principles including waste valorisation, resource optimization, and regeneration of natural systems. Overall, repurposing recycled glass to catalyse water purification closes material

loops, creates economic value, and benefits the environment - core aims of a circular system. Therefore, it is of great potential to investigate recycled iron-containing glass that is abundant, sustainable, and cost-effective for applications like CWPO, something which to be best of our knowledge has never been attempted before this current study.

Table 3.1 Metals or elements used to impart colour to glass sorted according to visible light spectral except brown as an exception. Adapted from[56]

Species	Colour
Selenium Oxide	Reds
Sulphur	Yellow-Amber
Cadmium Sulfide	Yellow
Uranium Oxide	Fluorescent Yellow, Green
Iron Oxide	Greens and Browns
Chromic Oxide	Emerald Green
Cobalt Oxide	Blue-Violet
Nickel Oxide	Violet
Manganese Dioxide	Purple
Carbon Oxides	Amber-Brown
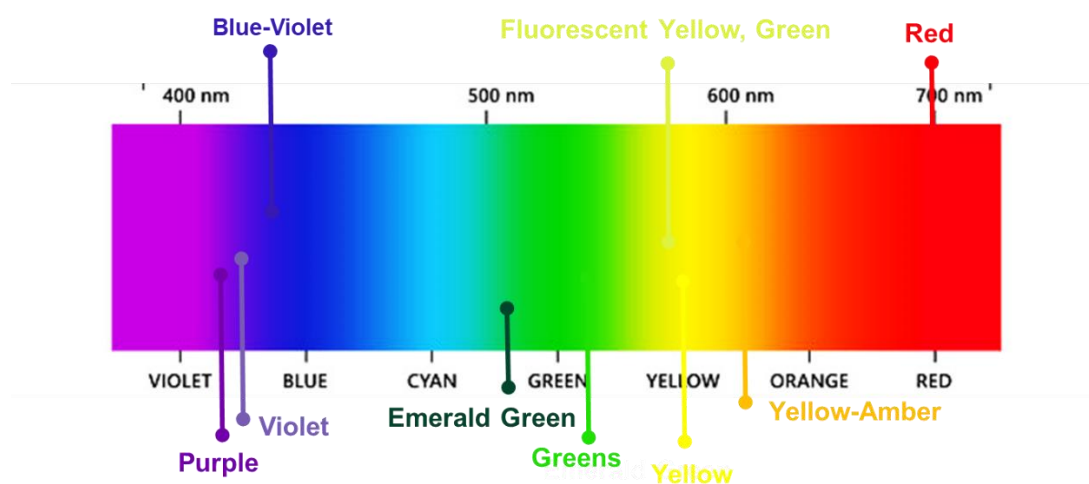
Figure 3.6 Colours of glass imparted to different metals sorted according to visible light spectral except brown as an exception. Adapted from[56]

Recycled glass bottles are typically subjected to a washing process with detergent (sodium dodecyl sulphate) before being heated at 550 °C in static air for 4 h to remove any organic contaminants and then crushed or milled and afterwards sieved to isolate into desired sizes for use in further reactions.

With regard to the selection of a calcination temperature of 550 °C, this is selected mainly on the ground to burn any organic contaminant[57] it should be noted that although pure SiO_2 has a melting point in the range of 1200 °C, the presence of Na_2O and CaO to form soda-lime glass networks with tetrahedral structures introduces ionic bonds that disrupt the rigid SiO_2 covalent structure, which reduces the melting point of glass but also make it a soft and malleable material from ca.700°C   Which is then a further reason to select calcination temperatures below this threshold.

3.6.2 Characterization of recycled glasses

It is well known that compositional aspects can exert a profound influence on catalytic outcomes.[58–60] In view of this glasses of different colours underwent comprehensive characterization employing inductively coupled plasma analysis (ICP-OES: Table 3.2) to determine their bulk composition, and X-ray photoelectron spectroscopy (XPS: Table 3.3 to analyse their surface composition. It is important to highlight that, to the best of our knowledge, there has been no prior investigation into such characterizations conducted within recycled glass matrices. This unexplored area of research holds significant potential in facilitating the utilization of recycled glass as a catalyst, thereby opening new routes for this kind of innovative applications.

Table 3.2 Elemental analysis (wt.%) of pre-recycled coloured glasses. Glass pre-treated with a two-step protocol involving HF and *aqua regia*. Mineralized mixture analysed via ICP-OES.

Sample	Fe	Cr	Mn	Si	Na	Ca	Mg	K	O
Green	0.27	0.14	0.10	28.3	8.6	6.8	1.2	0.63	59.7
Amber	0.23	0.03	0.03	28.2	8.1	6.7	1.0	0.58	53.9
Brown	0.26	0.03	0.03	32.6	8.5	6.9	1.1	0.62	48.6

Table 3.3 Surface Composition Analysis (at.%) of Recycled Green, Brown, and Transparent Glasses via X-ray Photoelectron Spectroscopy.

Sample	Fe	Si	Ca	Na	Mg	K	O
Recycled GTS Green	0.49	39	3.8	9.6	0.9	0.6	46
Recycled GTS brown	0.39	37	4.7	10	1.3	1.0	46
Recycled GTS transparent	0.23	39	2.5	9.3	0.4	2.2	47

Elemental analysis was performed on 12 samples across three colours (green, amber and brown), revealing a consistent composition (Table 3.2). Silicon was present at 30 wt.%, followed by sodium (8 wt.%) and calcium (7 wt.%), with no significant variations above 0.01 wt.% observed between batches of different colours.

The reproducible glass composition, devoid of major fluctuations between samples, is an important attribute for a robust catalyst system. The minimal elemental variations imply consistent performance can be expected independent of glass colour or feedstock variability, though this requires experimental validation. Overall, the preliminary elemental analysis indicates recycled soda-lime glass is a promising sustainable catalyst in terms of compositional reliability.

XPS confirm the presence of Fe as Fe_2O_3 equivalent like component at the surface of the recycled glass samples, with green glass exhibiting the highest Fe content. Consequently, green glass would be expected to demonstrate the greater and reproducible catalytic activity batch-to-batch. It is important to note the different scales used - elemental analysis in wt.% and XPS in at.%. By converting wt.% to at.%, the bulk glass contains approximately 0.1 at.% of Fe, while the surface shows 0.5 at.% of Fe. Considering the maximum possible surface Fe concentration is 1 at.% if all Fe resided exclusively at the surface, the bulk and surface measurements align well in this case.

The relatively larger abundance of Fe species on the surface rather than in the bulk, reflects the iron propensity to readily oxidize facilitates migration of Fe from the bulk to the surface as Fe_2O_3 over time. In contrast, Cr and Mn did not exhibit surface enrichment, remaining undetectable by XPS (Table 3.3).

While Fe^{2+} has been established as an effective Fenton catalyst, other transition metals like Mn and Cr that exhibit multiple oxidation states have also shown catalytic promise under certain conditions.[44,61] Notably, the green glass contains minor MnO and Cr_2O_3 equivalent like components in the bulk. However, the lack of detectable Mn and Cr by XPS does not definitively indicate their absence at the glass surface, in the sense that this could be below a relative detection limit for this technique. Though this observation is true for any experimental method.

As recycled glass contains a variety of metal oxide components, it is important to assess how compositional variations between different glass sources may affect their catalytic performance. While iron is expected to play a dominant role due to its known activity, the potential contributions or interactions of other metals such as manganese and chromium cannot be ignored. Control experiments using metal salts would help to investigate the effects of different metal cations present in the Fenton reaction.

3.6.3 Metal activity control tests for recycled glasses

As mentioned above, control tests were performed using three other metal salts, namely

$FeSO_4 \cdot 7H_2O$, $Cr(NO_3)_3 \cdot 9H_2O$ and $Mn(NO_3)_2 \cdot 4H_2O$, the activity of them were then compared with the result with $Fe(NO_3)_3 \cdot 9H_2O$ as a reference. The results of phenol conversion, carbon mass balance, and hydrogen peroxide consumption were recorded and presented in Figure 3.7.
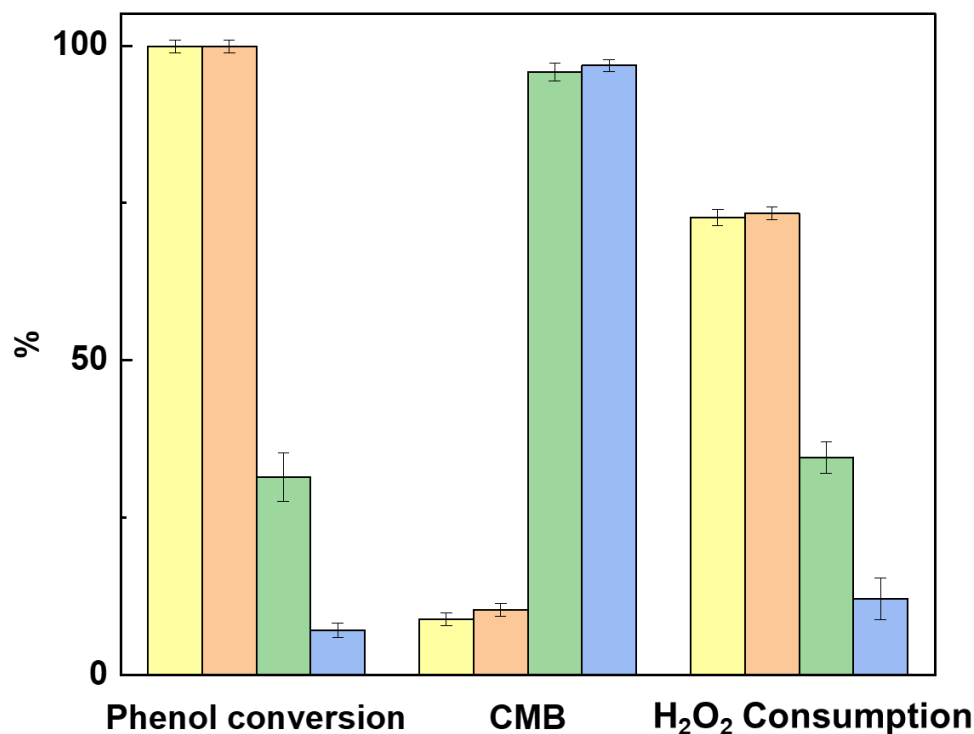
Figure 3.7 Comparison of phenol conversion, carbon mass balance and H_2O_2 consumption for phenol oxidation reactions catalysed by differing metal salts. Reaction conditions: 50 mL of phenol (1 g L^{-1}), $FeSO_4 \cdot 7H_2O$ (Fe^{2+}: ●), $Fe(NO_3)_3 \cdot 9H_2O$ (Fe^{3+}: ●), $Cr(NO_3)_3 \cdot 9H_2O$ (Cr^{3+}: ●) and $Mn(NO_3)_2 \cdot 4H_2O$ (Mn^{2+}: ●), M:S=1:100, PhOH:H_2O_2=1:14 (stoichiometric amount towards mineralization), p = endogenous, 80°C, 4 h, 500 rpm.

As shown in previous experiments, both $FeSO_4 \cdot 7H_2O$ and $Fe(NO_3)_3 \cdot 9H_2O$ rapidly and effectively catalysed phenol oxidation, achieving full conversion within 4 hours under the specified conditions (80°C, stoichiometric H_2O_2). This further verifies iron's efficacy in activating the Fenton process and enabling the interconversion between Fe^{2+} and Fe^{3+} (Eq. 3.3 and 3.4).

In contrast, the alternative metals, $Mn(NO_3)_2 \cdot 4H_2O$, exhibited negligible activity and $Cr(NO_3)_3 \cdot 9H_2O$ exhibited much lower activity under identical conditions. The minimal reactivity of Mn and Cr suggests that despite their presence in recycled glass, these species do not substantially contribute to catalytic performance, which in this case is a desired properties thus meaning that even if the amount of these metals should change, this should not have an appreciable effect of the final catalytic activity.

This is a significant finding in terms of recycled glass as a practical catalyst. Despite batch-to-batch variability in glass feedstock, the consistently high activity of iron across all samples implies compositional fluctuations in minor components have minimal impact on performance. This reproducibility and apparent insensitivity to changes in non-essential metals are critical attributes that distinguish recycled glass as a robust sustainable catalyst versus an unpredictable waste material. The reliability provides a foundation for implementation and process scale-up.

This indicates that the recycled glass catalyst activity is primarily dictated by the iron content, with other metals playing a minimal role. The reliability despite variability in glass feedstock enhances the viability of recycled glass as a sustainable catalyst for scaled-up water treatment processes.

3.6.4 Activity control tests for mixed recycled glasses

As recycled glass is selected at random from a recycling facility, and it could not be otherwise, this may have the implication of a non-uniform chemical composition of the starting material, with potential implications for batch-to-batch variability and thus scaling up recycled glass as a catalyst and, in turn, our approach.

To evaluate the effects of any disparities in recycled glass composition, a randomized selection of glass containers was sampled from diverse batches, colours, and manufacturers.

Five different physical mixtures (M1 to M5) of GTS green glass (**G1** as a representative) with a diameter range of 0.1-0.2 mm were prepared. In each case, the physical mixture contains glass particles from three different pieces of **G1** with a mass ratio of 1:1:1 (Figure 3.8).
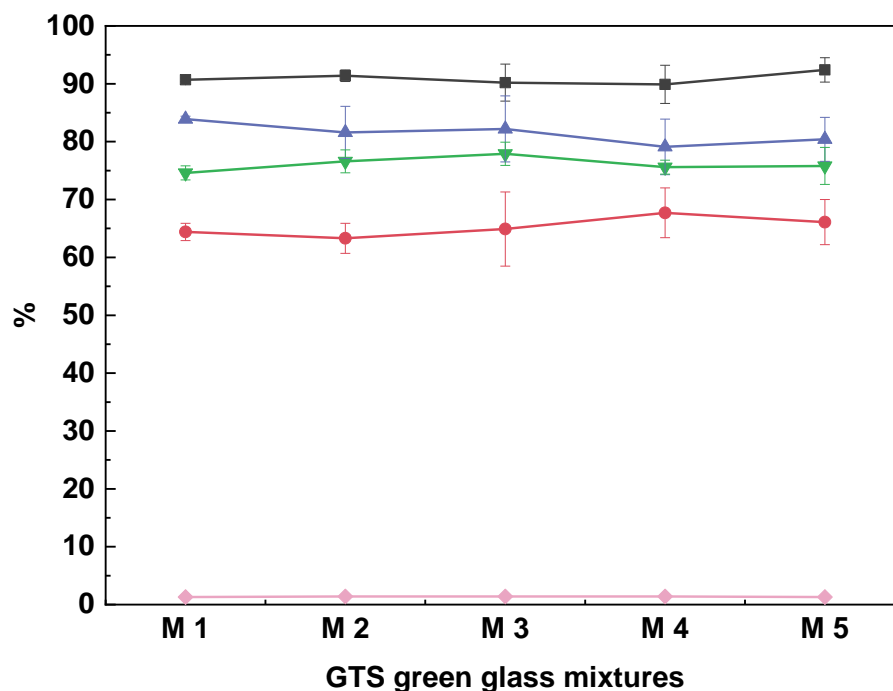
Figure 3.8 Comparison of the phenol conversions (■) observed, carbon mass balance (●), selectivity to CO_2 (▲), H_2O_2 consumption (▼) and selectivity to acids (♦) in reaction solutions for phenol oxidation reactions catalysed by differing physical mixtures of **G1** glass prepared by *ball milling*. For each mixture, the reaction was repeated 4 times. Reaction conditions: 50 mL of phenol (1 g L^{-1}), **G1** recycled glass (Fe: 0.2 wt.%), 0.1-0.2 mm, five physical mixtures M1 to M5, M:S=1:20, $PhOH:H_2O_2$=1:14 (stoichiometric amount towards mineralization), p = endogenous, 80°C, 4 h, 500 rpm.

The negligible impact of varying the physical composition of green GTS glass is evidenced by the constancy of key phenol oxidation parameters across all mixtures tested. Specifically, phenol conversion (90 ± 3%), carbon mass balance (64 ± 5%), H_2O_2 consumption (76 ± 2%), selectivity to CO_2 (82 ± 4%), and selectivity to acids (2 ± 2%) remained statistically unchanged despite the differences in glass component ratios between batches. This compositional robustness was further validated by ANOVA analysis, which indicated no significant variation (at 0.05 level) in phenol conversion between batches of distinct physical mixtures (Appendix A2.1).

The results depict that $Cr(NO_3)_3 \cdot 9H_2O$ exhibited a greater phenol conversion and hydrogen peroxide consumption compared to $Mn(NO_3)_2 \cdot 4H_2O$, despite a similar level of carbon mass balance. This suggests that, while Cr^{3+} can generate more hydroxyl radicals than Mn^{2+}, these radicals only attack phenol to form other aromatic compounds but don't process further. In both cases though the number of hydroxyl radicals produced is insufficient to achieve mineralization.

This demonstrates recycled glass as a robust sustainable catalyst, achieving reliable performance regardless of the precursor glass feedstock. For example, the coefficient of

variance for phenol conversion was just 3% across all recycled glass mixtures tested. This is comparable to the benchmark $Fe(NO_3)_3 \cdot 9H_2O$ and Cu/ZSM-5, which exhibits a conversion variance of 2-3%.[24]

Additionally, the 90% phenol conversion achieved aligns with typical values for industrial acid zeolite catalysts, which range from 80-100%.[62,63] Thus substantiating recycled glass as a viable sustainable alternative and its robustness and reliability provide a promising foundation for practical large-scale implementation in water treatment and other applications.

3.7 Effect of changes of parameters on phenol oxidation via Fenton reaction

To improve and assess the performance of glass, the effect of these parameters on the phenol oxidation activity of glass with different colours and, consequently, different iron content was investigated. The coloured glass included **G1** (Fe wt.%: 0.2 %), **G2** (Fe wt.%: 0.3%), **G3** (Fe wt.%: 0.2%), and **G4** (Fe wt.%: 0.1%).

3.7.1 Effect of glass particle size on the catalytic activity

A difference in particle size of a catalyst, is widely acknowledged to be a parameter often affecting the catalytic activity as it leads to a considerable change in the overall surface area (Figure 3.9), besides possible changes in diffusion next to the catalyst surface. As such, this parameter holds critical implications for the level of activity exhibited by the material, thereby influencing its potential for scale-up and practical applications. When the quantity of catalyst its mass is fixed, a reduction in particle size, per constant total mass leads to a corresponding increase in surface area, resulting in a greater number of active sites available for substrate adsorption and subsequent reaction.

In order to illustrate this important concept, we simplified the glass beads as particles of a specific shape and the substrate to have an accessibility of roughly 10 µm depth into the bulk (Figure 3.9) as the part of the catalyst grain capable of actually leading to a chemical reaction (the internal part would be shielded and not accessible).
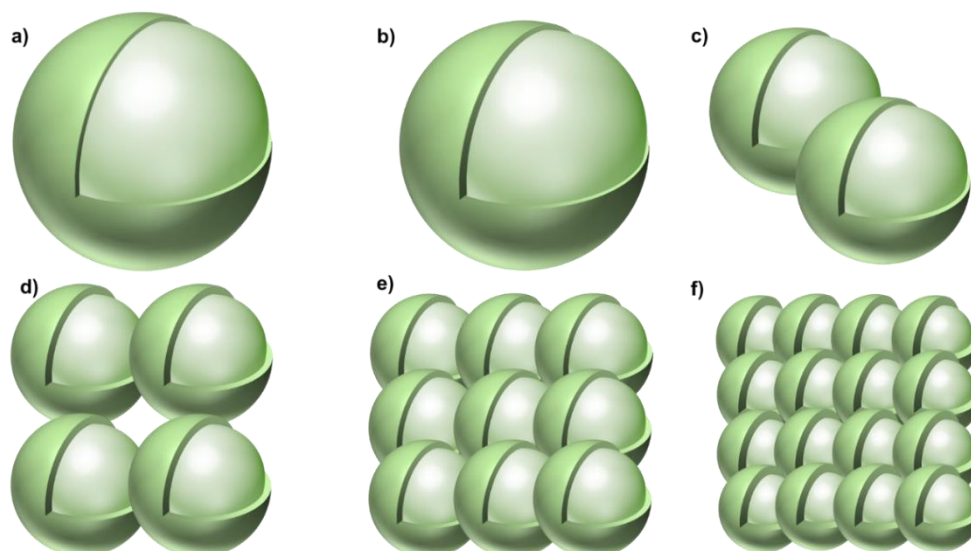
Figure 3.9 Illustration the correlation between the size and surface area of recycled glass (assuming a sphere shape with 10 µm of the surface is active), where a decrease in glass size results in an increase in surface area for the same mass of glass. Diameters are a) 2 mm, b) 1.4 mm, c) 1.0 mm, d) 0.5 mm, e) 0.2 mm, f) 0.1 mm. In this case, and assuming uniform distribution of Fe across the entire beads

Table 3.4 Comparison between the size and surface area of recycled glass (assuming a sphere shape with 10 µm of the surface is active), where a decrease in glass size from 2 mm to 0.1 mm results in an increase in surface area up to 16 times for the same mass of glass.

entry	diameters	external layer V	relative ratio no. of grains at fixed mass	total vol of external layer at fixed mass	relative ratio
	mm	mm^3		mm^3	
a)	2	1.37×10^{-1}	1	0.12	1
b)	1.4	6.51×10^{-2}	3	0.18	1
c)	1	3.08×10^{-2}	8	0.25	2
d)	0.5	7.54×10^{-3}	64	0.48	4
e)	0.2	1.14×10^{-3}	1000	1.14	9
f)	0.1	2.56×10^{-4}	8000	2.04	16

As a means of example, we report a calculation (Table 3.4) about the effect that a reduction in grain size has on the actual surface that is in contact with the external environment.

Assuming a uniform Fe distribution just by reducing the particle size from 2 mm to 0.1 mm increases the actual external contact area by about 16 times. That is more than one order of magnitude. That is why particle size and surface area are such important parameters in catalysis.

In our case, an increased quantity of Fe^{3+} ions are expected to facilitate the decomposition of H_2O_2, leading to the generation of ·OH radicals and to promote the oxidation of phenol. Therefore, an elevated concentration of Fe^{3+} is likely to enhance the efficiency of phenol

oxidation by increasing the availability of these highly reactive radicals. In addition, the shape of the glass beads prepared (spherical or truncated) may also affect the activity level. However, the latter being well in the domain of chemical engineering will not be considered in detail in the current work.

To investigate the effects of particle shape and size on catalytic performance, GTS green glass samples were mechanically processed via ball-milling or hydraulic pressing to produce two sets of size fractions ranging from <0.1 to 2 mm. Ball-milling was expected to yield rounded particle edges, while hydraulic pressing would create sharper edges. Smaller diameters were anticipated to provide higher surface area and active site exposure, potentially improving contact with reactants. Meanwhile, sharp edges were hypothesized to enhance surface interactions versus smooth rounded shapes. The two preparation methods allowed evaluation of how size and shape influence phenol oxidation activity. Phenol oxidation screening was conducted with a nominal M:S ratio of 1:20 and stoichiometric hydrogen peroxide using the different sized glass particles.
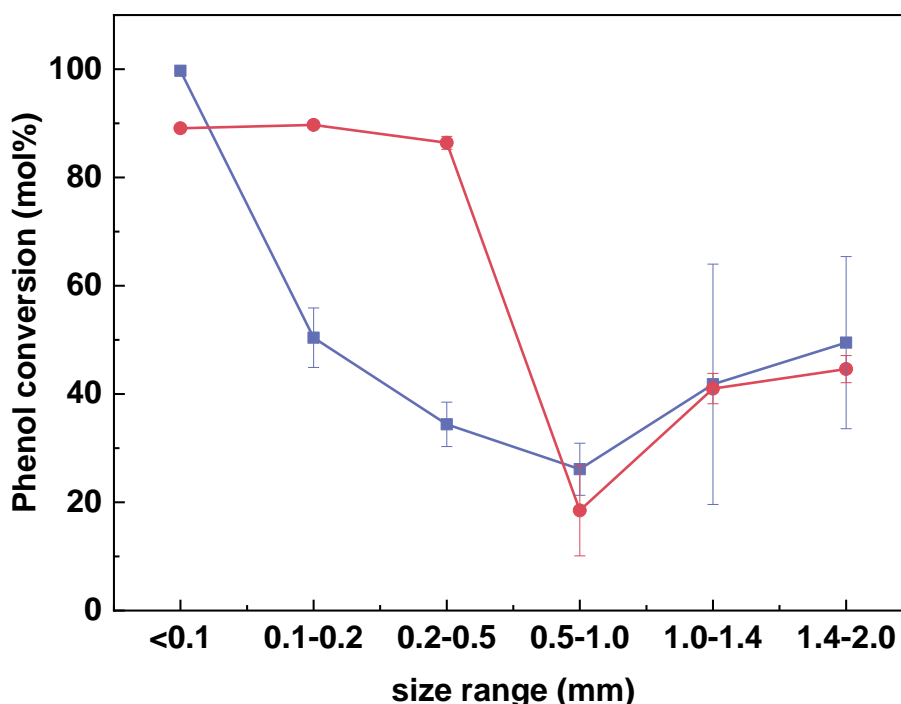
Figure 3.10 Phenol conversion of phenol oxidation with recycled glass prepared by two different methods: ball mill (●) and hydraulic press (■). Reaction conditions: 50 mL of phenol (1 g L^{-1}), **G1** recycled glass (<0.1-2 mm), M:S=1:20, PhOH:H_2O_2 =1:14, p = endogenous, 80°C, 4 h, 500 rpm.

These results revealed an approximate inverse relationship between the size of the glass beads and the overall phenol conversion in both cases with the smallest size of glass (<0.1 mm) showing the highest phenol conversion of 90 ± 3% (Figure 3.10). The results obtained in the current study are consistent with the proposed hypothesis, which confirms that smaller

glass particles possess a greater number of active sites available for the decomposition of H_2O_2 by Fe^{3+} ions (Table 3.4). As a result, a higher degree of phenol conversion is anticipated with decreasing particle size, this in turn provided further evidence that the Fenton reaction is initiated and accelerated by the concentration of iron ions present.

In addition to the size trend, glass beads prepared by ball milling demonstrated consistently high activity up to 0.5 mm, whereas hydraulic pressed samples declined above 0.1 mm. The wider effective size range for ball milled glass simplifies catalyst preparation, as strict size cut-offs are not required. However, from a processing standpoint, hydraulic pressing was considerably easier than ball milling in terms of operation, though fractionation to remove oversized particles was more difficult.

The activity observed with larger recycled glass beads is advantageous, as it enables effective catalysis without stringent size requirements. This simplifies preparation and expands the feasible applications for recycled glass catalysis. However, the discrepancy in conversion between 0.1-0.5 mm glasses prepared via ball-milling versus hydraulic pressing warrants future morphology analysis by SEM to understand the relationships between particle shape and performance.

Overall, this initial data demonstrates several promising attributes of recycled glass as a sustainable catalyst: 1) Phenol conversion reached 90% under mild conditions (80°C, 4 h), rivalling common industrial catalysts; 2) Activity was maintained with larger bead sizes up to 0.5 mm, improving practicality in catalyst recovery. Combined with the abundant supply of waste glass, these results provide a preliminary validation of recycled glass as an active, selective, and environmentally friendly catalyst that warrants further optimization and implementation.

3.7.2 Effect of M:S ratio on the catalytic activity

As previously discussed, in a reaction system with an M:S molar ratio of 1:100, the average conversion of phenol was found to be approximately 65%, while the CMB was 80%. This suggests that only a limited extent of mineralization was achieved, even with the use of the smallest size of glass. Given the toxicity of phenol and its intermediates, it is necessary to maintain a maximum contaminant level of 0.6 mg L^{-1} for phenol in drinking water, as prescribed by the US Environmental Protection Agency.[64] This implies that a phenol conversion of 99.94% is required to meet this standard. Thus, it is necessary to conduct further optimization of the reaction conditions to improve the extent of phenol conversion and achieve a higher degree of mineralization. Furthermore, the scope of the application was expanded to encompass a series of glass colours, namely **G1** (Fe wt.%: 0.2%), **G2** (Fe wt.%: 0.3%), **G3** (Fe wt.%: 0.2%),

and **G4** (Fe wt.%: 0.1%). To compare the performance, comparative reactions were conducted using four different glass types, each with particle sizes smaller than 0.1 mm, employing both a M:S (molar ratio) of 1:50 and 1:100.
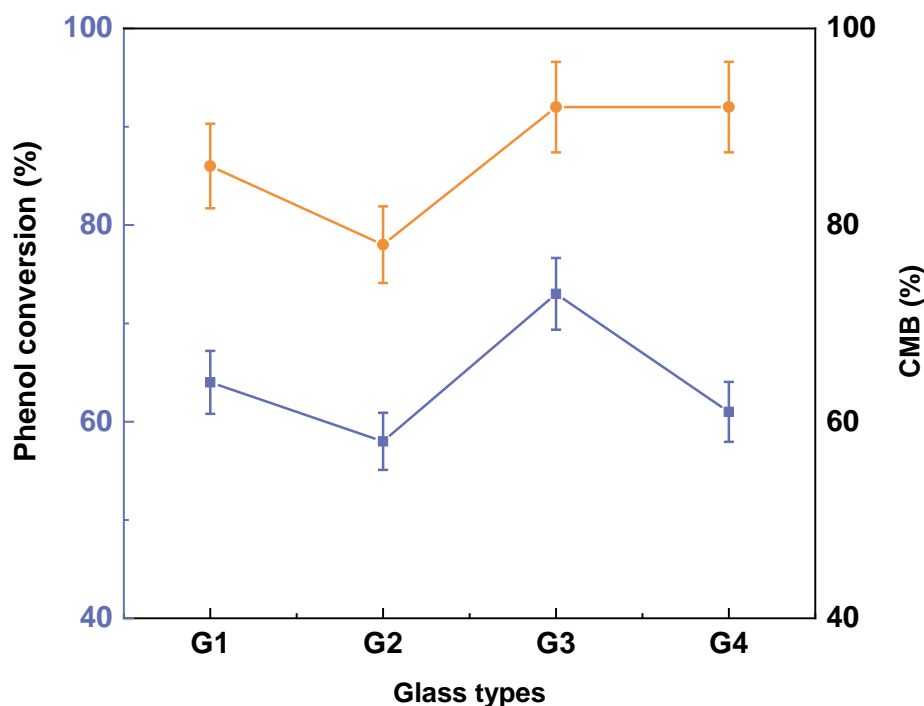
Figure 3.11 Phenol conversion of phenol oxidation with two green glasses, a brown glass and a blue glass as catalyst at two different M:S molar ratio. Reaction conditions: 50 mL of phenol (1 g L^{-1}), **G1** (Fe wt.%: 0.2%), **G2** (Fe wt.%: 0.3%), **G3** (G3 Fe wt.%: 0.2%) and **G4** (Fe wt.%: 0.1%), <0.1 mm, M:S=1:100 (■) and 1:50 (●), PhOH:H$_2$O$_2$=1:14, p = endogenous, 80°C, 4 h, 500 rpm.

The results, as presented in Figure 3.11, indicate that a doubling of the quantity of iron used as a catalyst in the reaction system led to an increase in phenol conversion from 65% to 85%, while also resulting in a decrease in CMB from 80% to 60% (Table 3.5). These observations suggest a direct correlation between the amount of iron content (M:S 1:100, 1:50) employed and the degree of conversion achieved. Furthermore, the consumption of hydrogen peroxide was found to increase from 35% to 55% (Table 3.5) in proportion to the quantity of iron present, consistent with the principle that the presence of iron promotes hydrogen peroxide decomposition. Overall, as expected, these findings demonstrate a significant improvement in both phenol conversion and mineralization when using higher amounts of iron catalyst.

Table 3.5 Phenol conversion, CMB and H_2O_2 conversion of phenol oxidation with two green glasses, a brown glass and a blue glass as catalyst at two different M:S molar ratios. Reaction conditions: 50 mL of phenol (1 g L^{-1}), **G1** (Fe wt.%: 0.2%), **G2** (Fe wt.%: 0.3%), **G3** (G3 Fe wt.%: 0.2%) and **G4** (Fe wt.%: 0.1%), <0.1 mm, M:S=1:100 and 1:50, PhOH:H_2O_2=1:14, p = endogenous, 80°C, 4 h, 500 rpm. Phenol residual and intermediates of the reaction was reported with their HPLC concentration (Phenol was collected at 270 nm, the rest intermediates are collected at 200 nm). Overall phenol conversion and CMB was calculated with an error of 5%.

Glass	M:S Molar ratio	Phenol Conversion %	CMB %	H_2O_2 conversion %
G1		64	95	39
G2	1:100	58	83	33
G3		73	69	37
G4		61	79	36
G1		86	63	53
G2	1:50	78	71	42
G3		92	50	53
G4		92	50	50

3.7.3 Effect of reaction time on the catalytic activity

The use of a higher M:S molar ratio has resulted in a significant increase in phenol conversion to 85%. However, the consistency between the relatively high CMB (60%) and incomplete consumption of H_2O_2 (55%) further indicates that the reaction conditions have not yet reached the optimal point where there is still potential for generating more ·OH species. Therefore, although important, the molar M:S cannot be considered the sole determining factor in this reaction, and other factors must be evaluated. The reaction time of 4 hours appears to be the limiting factor, which means that longer reaction times might help to achieve higher efficiency.

To investigate the impact of reaction time, the reaction was prolonged to 12 hours while maintaining an M:S of 1:100, and all types of glass with diameters less than 0.1 mm were employed as catalysts. Being the most active glass composition, the **G2** (Fe: 0.3 wt.%) results serve as a conservative benchmark, with the trends extending qualitatively to the other glasses (full data in appendix A.2.2).
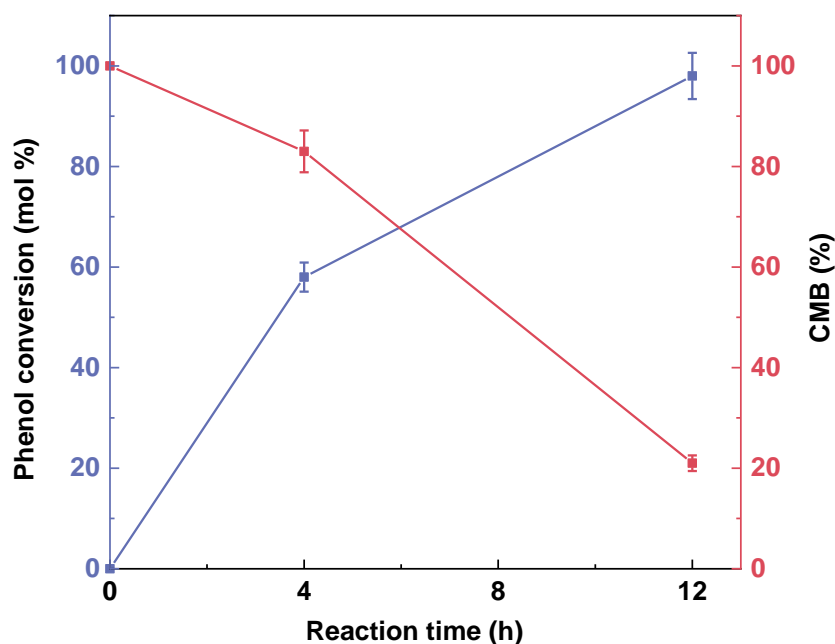
Figure 3.12 Phenol conversion (■) and CMB (■) of phenol oxidation with, **G2** (<0.1 mm) as catalyst at 4 and 12 h. Reaction condition: 50 mL of phenol (1 g L^{-1}), **G2** (Fe: 0.3 wt.%), <0.1 mm, M:S=1:100, PhOH:H_2O_2 molar ratio=1:14, p = endogenous, 80°C, 4 and 12 h, 500 rpm.

As depicted in Figure 3.12, utilizing an M:S ratio of 1:100 and extending the reaction time provides ample opportunity for the efficient reaction between Fe^{3+} and H_2O_2 to take place, and thus decomposition of phenol by ·OH radicals. Furthermore, there was a marked reduction in CMB with longer reaction times, which suggests that the system generates sufficient hydroxyl radicals (·OH) to further degrade its intermediates, and ultimately achieve mineralization. It was shown that extending the reaction time while utilizing an M:S ratio of 1:100 resulted in the same level of hydrogen peroxide (H_2O_2) consumption as that observed when M:S of 1:50 was used, namely 49% and 42% (Table 3.6). At the same time, longer reaction times resulted in a considerable improved mineralization. These findings emphasize the significance of contact time and catalyst regeneration capacity within the system, which enable the continued degradation of phenol and its intermediates. Thus, a potential 16 hours reaction time could be suggested for a full mineralization.

Table 3.6 Phenol conversion, CMB and H_2O_2 conversion of phenol oxidation by **G2** recycled glass (<0.1 mm) as catalyst with two reaction time of 4 and 12 h with two different M:S molar ratios. Reaction conditions: 50 mL of phenol (1 g L^{-1}), **G2** (Fe: 0.3 wt.%), <0.1 mm, M:S=1:100 and 1:50, PhOH:H_2O_2 molar ratio=1:14, p = endogenous, 80°C, 4 and 12 h, 500 rpm. Phenol residual and intermediates of the reaction was reported with their HPLC concentration (Phenol was collected at 270 nm, the rest intermediates are collect at 200 nm). Overall phenol conversion and CMB was calculated with an error of 5%.

M:S molar ratio	Time h	Phenol Conversion %	CMB %	H_2O_2 conversion %
1:100	4	58	83	33
1:100	12	98	21	49
1:50	4	78	71	42

3.8   Activity of recycled glass compared with Fe/ZSM-5 on phenol oxidation

Fe/ZSM-5 is a commonly utilized heterogeneous catalyst for the catalytic wet peroxide oxidation (CWPO) of organic pollutants in wastewater due to its high activity, selectivity, and thermal stability, as well as its environmentally friendly properties. Zeolite ZSM-5, which is used as a support, is known for its high surface area (300-500 m^2 g^{-1}) and pore size (0.54 - 0.56 nm), which enables efficient metal species dispersion and effective adsorption of phenol. Therefore, in this part of the research, Fe/ZSM-5 was selected as a reference material or benchmark of our studies.

Four recycled glass samples (<0.1 mm) and Fe/ZSM-5 (1 wt.% Fe) were evaluated as catalysts at a 1:100 M:S molar ratio. Phenol conversion and carbon mass balance (CMB) were assessed at two reaction times, 4 hours and 12 hours, to compare the temporal evolution of products over Fe/ZSM-5 versus the recycled glasses.
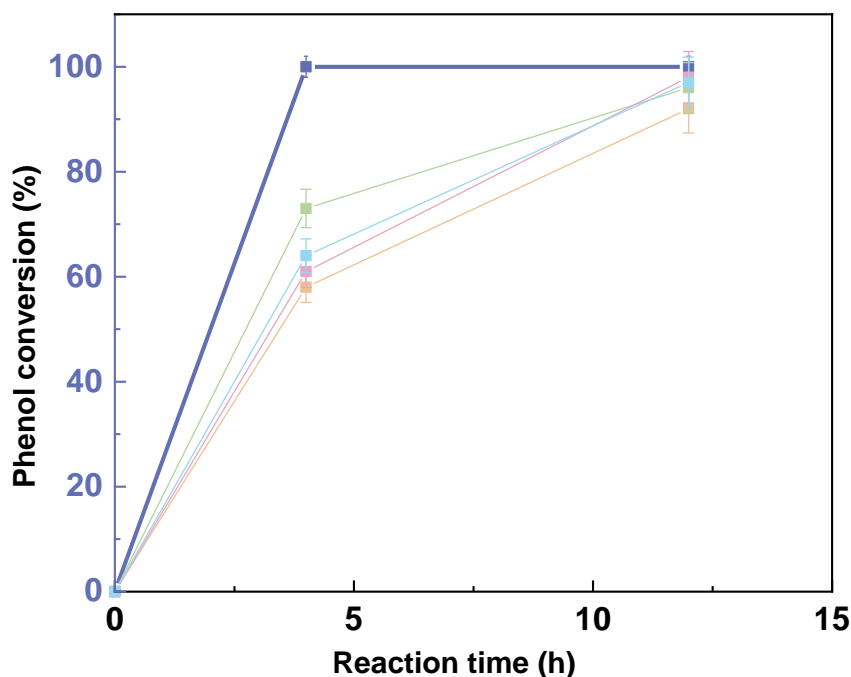
Figure 3.13 Phenol conversion of phenol oxidation with four different recycled glass and Fe/ZSM-5 for 4 and 12 h. Reaction conditions: 50 mL of phenol (1 g L^{-1}), **G1**: (Fe wt.%: 0.2% ■), **G2** (Fe wt.%: 0.3% ■), **G3** (Fe wt.%: 0.2% ■) and **G4** (Fe wt.%: 0.1% ■), and Fe/ZSM-5 (1 wt.% ■), <0.1 mm, M:S=1:100, PhOH:H_2O_2 =1:14, p = endogenous, 80°C, 4 and 12 h, 500 rpm.

The use of Fe/ZSM-5 as a reference catalyst for CWPO of phenol in wastewater has shown that it has a higher initial rate of reaction and reaches complete phenol conversion within 4 hours of reaction, whereas the most active glass catalyst only achieves 80% conversion under the same conditions (Figure 3.13). However, increasing the reaction time narrows the gap in phenol conversion between the two catalysts, and after 12 hours of reaction with M:S of 1:100, complete phenol conversion can be achieved with both catalysts. The 20% CMB, while not full mineralization, represents promising activity given the low cost of the recycled glass precursor. Optimizing the reaction protocol and increasing the M:S ratio could promote further mineralization while remaining economically favourable compared to zeolite catalysts. On the other hand, minimal iron leaching from the recycled glass (0.7-1.2% determined by ICP-OES, section 2.5.5) contrasts sharply with substantial leaching observed for Fe/ZSM-5 (26%) under the same conditions. This enhanced stability results from the glass network strongly retaining iron in the structure, avoiding loss of active sites and associated catalyst degradation. This leaching is believed to be caused by the complexation of Fe with oxalic acid, where it acts as a chelating ligand and thus has a stronger binding affinity than other acid formed, resulted in a limited lifetime of the catalyst.

While recycled glass demonstrated lower activity than Fe/ZSM-5 under the conditions tested, optimization studies revealed phenol conversions over 90% could be attained at longer reaction time (12 h) and with smaller glass sizes (<0.1 mm). However, an advantage of recycled glass is avoidance of the high temperature (>500°C) calcination required to combust coke and regenerate spent zeolite catalysts, apart from its first cleaning step. Furthermore, in the case of a catalyst deactivation, recycled glass can simply be re-melted and enter aggregates for construction.

Considering the comparable performance achieved after optimization along with its operational simplicity and low precursor cost, recycled glass presents a promising sustainable catalyst for catalytic wet peroxide oxidation and water decontamination.

3.9   Conclusion

Phenol, a paradigm for water pollution, has been used as a benchmark to explore the potential of recycled glass as a heterogeneous catalyst in catalytic wet peroxide oxidation.

The effect of thermal decomposition of hydrogen peroxide under the current reaction conditions was found to be negligible. Surface and bulk characterizations of the glass samples have revealed the presence of various metal ions, mostly Fe, Cr, and Mn, which however only Fe has shown potential activity in the oxidation of phenol. Though this is an apparent drawback, it is actually a positive occurrence because it improves the batch-to-batch reproducibility of recycled glass samples of different compositions. This finding underlines the importance of Fe as the key active species in the catalytic oxidation of phenol using the studied glass materials.

The use of a Fe^{3+} aquo species salt in blank tests of phenol oxidation highlighted the crucial role played by both the iron catalyst and hydrogen peroxide in the catalytic wet peroxide oxidation (CWPO) system. The observations suggest that the indirect activation of hydrogen peroxide by Fe^{3+} requires time-wise about the double of the time than Fe^{2+}, at initial reaction rate (ca. 4 h), but the difference is expected to become negligible over a longer reaction period.

The present study successfully demonstrated the concept of using of recycled glass (green and brown) containing Fe^{3+} centres as a heterogeneous catalyst for phenol oxidation by catalytic wet peroxide oxidation (CWPO). The excellent reproducibility of a mixed batch of recycled glass leads to great reduce in the effort of separating during recycling, further reduce the cost of reaction.

In addition, results have indicated that decreasing the size of the glass particles leads to increased phenol conversion and carbon dioxide production with the size range of 0.1-0.5 mm

showing the best catalytic activity. It enables the possibility of a scale-up application in the industry. Additionally, optimization of the glass M:S molar ratio and reaction time can enhance catalyst performance. As a result, the performance of recycled glass can be comparable and promising (i.e., 100% phenol conversion and 20% CMB) to industrial catalyst, namely Fe/ZSM-5 under appropriate reaction conditions (increased mass and longer reaction time) for an overall much lower (about 3000 times) cost.

Based on these promising findings, there is a strong basis for further exploration into using recycled glass as a sustainable catalyst for other water pollutants like ibuprofen.

3.10   References

(1)   Boruah, P. K.; Sharma, B.; Karbhal, I.; Shelke, M. V.; Das, M. R. *Journal of Hazardous Materials*, 2017, **325**, 90-100.

(2)   Vindenes, H. K.; Svanes, C.; Lygre, S. H. L.; Real, F. G.; Ringel-Kulka, T.; Bertelsen, R. J. *Environ Health*, 2021, **20**, 81.

(3)   Antov, P.; Savov, V.; Mantanis, G. I.; Neykov, N. *Wood Material Science & Engineering*, 2021, **16**, 42-48.

(4)   Panzella, L.; Napolitano, A. *Antioxidants (Basel)*, 2017, **6**, 30.

(5)   Panzella, L. *Antioxidants (Basel)*, 2020, **9**, 427.

(6)   Scott, K. A.; Cox, P. B.; Njardarson, J. T. *Journal of Medicinal Chemistry*, 2022, **65**, 7044-7072.

(7)   Grace Pavithra, K.; Sundar Rajan, P.; Arun, J.; Brindhadevi, K.; Hoang Le, Q.; Pugazhendhi, A. *Environmental Research*, 2023, **237**, 117005.

(8)   Mandal, A.; Das, S. K. *Journal of Environmental Chemical Engineering*, 2019, **7**, 103259.

(9)   Almasi, A.; Dargahi, A.; Amrane, A.; Fazlzadeh, M.; Mahmoudi, M.; Hashemian, A. *Fresenius Environmental Bulletin*, 2015, **18**, 690-700.

(10)   Priatna, R.; Syahbandi, E.; Sudewo, B. *SPE Health, Safety and Environment in Oil and Gas Exploration and Production Conference*, 1994, **1**, 25-27.

(11)   Thomas, N.; Dionysiou, D. D.; Pillai, S. C. *Journal of Hazardous Materials*, 2021, **404**, 124082.

(12)   Ziembowicz, S.; Kida, M. *Chemosphere*, 2022, **296**, 134041.

(13)   Kallel, M.; Belaid, C.; Mechichi, T.; Ksibi, M.; Elleuch, B. *Chemical Engineering Journal*, 2009, **150**, 391-395.

(14)   Avetta, P.; Pensato, A.; Minella, M.; Malandrino, M.; Maurino, V.; Minero, C.; Hanna, K.; Vione, D. *Environmental science & technology*, 2015, **49**, 1043-1050.

(15)   Guo, L.; Chen, F.; Fan, X.; Cai, W.; Zhang, J. *Applied Catalysis B: Environmental*, 2010, **96**, 162-168.

(16)   Iboukhoulef, H.; Amrane, A.; Kadi, H. *Desalination and Water Treatment*, 2016, **57**, 1874-1879.

(17)   Perisic, D. J.; Gilja, V.; Stankov, M. N.; Katancic, Z.; Kusic, H.; Stangar, U. L.; Dionysiou, D. D.; Bozic, A. L. *Journal of Photochemistry and Photobiology A: Chemistry*, 2016, **321**, 238-247.

(18)   Fenton, H. J. H. *Journal of the Chemical Society, Transactions*, 1894, **65**, 899-910.

(19)   Pignatello, J. J.; Oliveros, E.; MacKay, A. *Critical Reviews in Environmental Science and Technology*, 2006, **36**, 1-84.

(20)   Skoumal, M.; Rodríguez, R. M.; Cabot, P. L.; Centellas, F.; Garrido, J. A.; Arias, C.; Brillas, E. *Electrochimica Acta*, 2009. **54**, 2077-2085.

(21)   Scheers, T.; Appels, L.; Dirkx, B.; Jacoby, L.; van Vaeck, L.; van der Bruggen, B.; Luyten, J.; Degrèv, J.; van Impe, J.; Dewil, R. *Desalination and Water Treatment*, 2012, **50**, 189-197.

(22)   Rey, A.; Faraldos, M.; Casas, J. A.; Zazo, J. A.; Bahamonde, A.; Rodríguez, J. J. *Applied Catalysis B: Environmental*, 2009, **86**, 69-77.

(23)   Méndez-Arriaga, F.; Esplugas, S.; Giménez, J. *Water Research*, 2008**, 42**, 585-594.

(24)   Zhou, C. Zeolite Catalysts for Water Treatment: Catalytic Wet Peroxide Oxidation (CWPO) of Phenol (Doctoral dissertation, University of Sheffield), 2021.

(25)   Pędziwiatr, P.; Mikołajczyk, F.; Zawadzki, D.; Mikołajczyk, K.; Bedka, A. *Acta Innovations*, 2018, **26**, 45-52.

(26)   Spínola, V.; Mendes, B.; Câmara, J. S.; Castilho, P. C. *LWT - Food Science and Technology*, 2013, **50**, 489-495.

(27)   Styawan, A. A.; Putri, A.; Cholifa, R. R. N. *Urecol Journal. Part D: Applied Sciences*, 2021, **1**, 1-8.

(28)   Cheng, C.; Li, H.; Wang, J.; Wang, H.; Yang, X. *Frontiers of Environmental Science & Engineering*, 2020, **14**, 87.

(29)   Sandri, F.; Danieli, M.; Zecca, M.; Centomo, P. *ChemCatChem*, 2021, **13**, 2653-2663.

(30)   Abe-Matsumoto, L. T.; Sampaio, G. R.; Bastos, D. H. M. *American Journal of Analytical Chemistry*, 2020, **11**, 269-279.

(31)   Cheng, M.; Zeng, G.; Huang, D.; Lai, C.; Xu, P.; Zhang, C.; Liu, Y. *Chemical Engineering Journal*, 2016, **284**, 582-598.

(32)   Oh, H.; Ching, W.-M.; Kim, J.; Lee, W.-Z.; Hong, S. *Inorganic Chemistry*, 2019, **58**, 12964-12974.

(33)   Lin, C. C.; Smith, F. R.; Ichikawa, N.; Baba, T.; Itow, M. *International Journal of Chemical Kinetics*, 1991, **23**, 971-987.

(34)   Zhou, C. Zeolite Catalysts for Water Treatment: Catalytic Wet Peroxide Oxidation (CWPO) of Phenol (Doctoral dissertation, University of Sheffield), 2021.

(35)   Zhu, K.; Liu, C.; Ye, X.; Wu, Y. *Applied Catalysis A: General*, 1998, **168**, 365-372.

(36)   Liotta, L. F.; Gruttadauria, M.; Di Carlo, G.; Perrini, G.; Librando, V. *Journal of Hazardous Materials*, 2009, **162**, 588-606.

(37)   Gerginova, M.; Manasiev, J.; Yemendzhiev, H.; Terziyska, A.; Peneva, N.; Alexieva, Z. *Zeitschrift für Naturforschung C*, 2013, **68**, 0384.

(38)   Santos, A.; Yustos, P.; Quintanilla, A.; García-Ochoa, F.; Casas, J. A.; Rodríguez, J. J. *Environmental science & technology*, 2004, **38**, 133-138.

(39)   Santos, A.; Yustos, P.; Quintanilla, A.; Ruiz, G.; Garcia-Ochoa, F. *Applied Catalysis B: Environmental*, 2005, **61**, 323-333.

(40)   Brussino, P.; Gross, M. S.; Banús, E. D.; Ulla, M. A. *Chemical Engineering and Processing - Process Intensification*, 2019, **146**, 107686.

(41)   Melero, J. A.; Martínez, F.; Botas, J. A.; Molina, R.; Pariente, M. I. *Water Research*, 2009, **43**, 4010-4018.

(42)   Villegas, L. G. C.; Mashhadi, N.; Chen, M.; Mukherjee, D.; Taylor, K. E.; Biswas, N. *Current Pollution Reports*, 2016, **2**, 157-167.

(43)   Aramyan, S. M. *IJESNR*, 2017, **2**.

(44)   Hussain, S.; Aneggi, E.; Maschio, S.; Contin, M.; Goi, D. *Industrial & Engineering Chemistry Research*, 2021, **60**, 11715-11724.

(45)   Javaid, R.; Qazi, U. Y. *International Journal of Environmental Research and Public Health*, 2019, **16**, 2066.

(46)   Posner, A. M. *Transactions of the Faraday Society*, 1953, **49**, 382-388.

(47)   Giannakis, S.; Polo López, M. I.; Spuhler, D.; Sánchez Pérez, J. A.; Fernández Ibáñez, P.; Pulgarin, C. *Applied Catalysis B: Environmental*, 2016, **199**, 199-223.

(48)   Yao, Y.; Cai, Y.; Lu, F.; Qin, J.; Wei, F.; Xu, C.; Wang, S. *Industrial & Engineering Chemistry Research*, 2014, **53**, 17294-17302.

(49)   Wan, Z.; Wang, J. *Journal of Hazardous Materials*, 2017, **324**, 653-664.

(50)   Hu, J.; Zhang, P.; An, W.; Liu, L.; Liang, Y.; Cui, W. *Applied Catalysis B: Environmental*, 2019, **245**, 130-142.

(51)   Pan, K.; Yang, C.; Hu, J.; Yang, W.; Liu, B.; Yang, J.; Liang, S.; Xiao, K.; Hou, H. *Journal of Hazardous Materials*, 2020, **389**, 122072.

(52)   Kakavandi, B.; Takdastan, A.; Pourfadakari, S.; Ahmadmoazzam, M.; Jorfi, S. *Journal of the Taiwan Institute of Chemical Engineers*, 2019, **96**, 329-340.

(53)   Pan, Y.; Su, H.; Zhu, Y.; Vafaei Molamahmood, H.; Long, M. *Water Research*, 2018, **145**, 731-740.

(54)   Kou, S. C.; Poon, C. S. *Cement and Concrete Composites*, 2009, **31**, 107-113.

(55)   Rashad, A. M. *Construction and Building Materials*, 2014, **72**, 340-357.

(56)   Bansal, N. P.; Doremus, R. H. *Handbook of Glass Properties*; Elsevier, 2013.

(57)   Santos, A.; Lewis, R. J.; Morgan, D. J.; Davies, T. E.; Hampton, E.; Gaskin, P.; Hutchings, G. J. *Catalysis Science & Technology*, 2022, **12**, 2943-2953.

(58)   King, H. M. *Elements of Color in Stained and Colored Glass*. https://geology.com/articles/color-in-glass.shtml (accessed 2023-12-11).

(59)   Lu, L.; Wang, G.; Zou, M.; Wang, J.; Li, J. *Applied Surface Science*, 2018, **441**, 1012-1023.

(60)   Mutoro, E.; Crumlin, E. J.; Pöpke, H.; Luerssen, B.; Amati, M.; Abyaneh, M. K.; Biegalski, M. D.; Christen, H. M.; Gregoratti, L.; Janek, J.; Shao-Horn, Y. *The Journal of Physical Chemistry Letters*, 2012, **3**, 40-44.

(61)   Seemala, B., Cai, C. M., Kumar, R., Wyman, C. E., & Christopher, P. *ACS Sustainable Chemistry & Engineering*, 2018, **6**, 2152-2161.

(62)   Zsirka, B.; Vágvölgyi, V.; Győrfi, K.; Horváth, E.; Szilágyi, R. K.; Szabó-Bárdos, E.; Balogh, S.; Kristóf, J. *Applied Clay Science*, 2021, **212**, 106222.

(63)   Bokare, A. D.; Choi, W. *Journal of hazardous materials*, 2014, **275**, 121-135.

(64)   Valkaj, K.; Wittine, O.; Margeta, K.; Granato, T.; Katović, A.; Zrnčević, S. *Polish Journal of Chemical Technology*, 2011, **13**, 28-36.

(65)   Yan, Y.; Jiang, S.; Zhang, H. *Separation and Purification Technology*, 2014, **133**, 365-374.

(66)   US EPA, O. *National Primary Drinking Water Regulations,* 2019.

Chapter 4 Recycled glass as a catalyst for CWPO of ibuprofen

4.1 Overview

Agriculture is the single greatest consumer of clean water resources, using about 70% of fresh water worldwide.[1] To grow crops, substantial water for irrigation is needed - for instance, 1 kg of corn and 1 kg of wheat require about 500 litres and 1000 litres of water to grow respectively. Beef production is even more intensive, needing 43,000 L of water per kilogram of forage crop needed.[2] Currently, there is an increasing concern of "emerging micropollutants" like pharmaceuticals and personal care products (PPCPs).[3] Although the contaminations are in the effluent with apparently low concentrations ($\mu g\ L^{-1}$ or $ng\ L^{-1}$), they are more toxic than one might expect to the environment.[4] For example, PPCPs can have toxic effects on aquatic life, including endocrine disruption in fish, reduced reproductive success, and behavioural changes.[5–7] Attention has recently been paid to groups of non-medical prescribed analgesics and nonsteroidal anti-inflammatory drugs (NSAIDs) due to the very large consumption that leads to their high presence in surface water and ground waters.[8] In England, the annual usage of ibuprofen and diclofenac amounts to approximately 37 tons and 22 tons, respectively.[9,10]

In Germany, around 60-80% of the 16,000 tons of pharmaceuticals prescribed and over-the-counter, originating from human medical care, are discarded annually.[10] Among them, ibuprofen, one of the most popular and widely used drugs for fever and muscle pain, is one of the second most frequently detected pharmaceuticals (carbamazepine, sulfamethoxazole, ibuprofen and naproxen) in the environment after diclofenac that has been detected in 50 countries.[5] For samples taken from aquatic environments, the concentrations are typically measured in $\mu g\ L^{-1}$. Different concentrations of ibuprofen have been detected in wastewater treatment plants in China, Korea, Sweden and the UK ranging from 4×10^{-3} and 600 $\mu g\ L^{-1}$.[11] Concentrations in wastewater samples have been reported as 45 $\mu g\ L^{-1}$ in Canada, 1 $\mu g\ L^{-1}$ in South Africa, 6 $\mu g\ L^{-1}$ in Belgium, and between 700 to 1700 $\mu g\ L^{-1}$ in Pakistan.[12,13,14] However, the concentration of 0.2 $\mu g\ L^{-1}$ of ibuprofen was detected for soil that is irrigated with pharmaceutical containing wastewater.[15] They are persistent pollutants that have adverse effects on plant and aquatic environments. For instance, ibuprofen exposure resulted in decreased shoot and root lengths, fresh and dry weights, and leaf area of cowpea.[16] Exposure to ibuprofen at a concentration of 0.1 $\mu g\ L^{-1}$ in Oryzias latipes led to reproductive impairment, induction of vitellogenin in males, a reduction in the number of broods per pair, and an increase in the number of eggs per brood.[17–19] Since the traditional biological treatment is not able to

fully remove Ibuprofen from sewage, nowadays, in wastewater treatment plants (WWTPs) effluents including emerging and non-biodegradable contaminants are mainly treated with the catalytic wet peroxide oxidation (CWPO) process.[20]

Having an aromatic skeleton like phenol, the decomposition of ibuprofen with recycled glass as a heterogeneous catalyst has also been taken into consideration, and assessing the feasibility of recycled glass for this reaction is one of the main scopes of this thesis work.

However, it is useful to note that organic pollutants in wastewater that are degraded by using the CWPO process are not directly oxidized to CO_2 and water in a single step, but this process involves the formation of various intermediates with higher or indefinite toxicity compared to the parent compound.[21] Several aromatic intermediates have demonstrated higher intrinsic toxicity than ibuprofen itself, including 4-isobutylphenol, hydratropic acid, and 4-isobutylacetophenone.[22] However, the overall risk depends on both the inherent toxicity and the amount present. The final reaction mixtures should contain a minimal amount of more toxic intermediates and maintain safe exposure thresholds to avoid any health concerns. While parent ibuprofen exhibits minimal acidity, oxidation can produce highly acidic intermediates like maleic, fumaric, acetic acids, and other carboxylic acids. The number of acids generated depends on the degradation pathway and mineralization degree. High residual organic acid content creates an acidic effluent unsuitable for irrigation without further processing or neutralization due to adverse impacts on plants.[23] Thus, exploring acid generation and managing the acidity (ideal pH between 6 and 7.5) arising from ibuprofen oxidation intermediates is an integral consideration when evaluating potential water reuse applications, along with toxicity. Therefore, in order to assure a high treatment efficiency of water, the characterization of all the possible more toxic intermediates and acids is necessary.

Typical environmental concentrations of ibuprofen range from 10 ng L^{-1} to 2,400 ng L^{-1}, with direct effluents from drug manufacturing containing higher concentrations.[24] Ibuprofen has a relatively low solubility in water (21 mg L^{-1} at 25 °C), but is highly soluble in organic solvents such as ethanol (660 g L^{-1} at 40 °C for 90% EtOH), methanol (490 g L^{-1} at 27 °C), acetone (610 g L^{-1} at 27 °C), and acetonitrile (420 g L^{-1} at 27 °C).[25] There is, however, a large variation in solubility values reported in the literature ranging from 10[26–28] or 20[29,30] mg L^{-1}, to 50 or even 180 mg L^{-1}.[31,32] In this context, a catalyst demonstrating efficacy at 20 mg L^{-1} model concentrations implies feasible operation at any real-world values below solubility that may actually persist in wastewaters. Considering the large number (thousands) of reaction samples requiring analysis, HPLC protocols were selected as the primary characterization technique given the capability for high throughput measurements and accurate quantification of multiple samples. HPLC also enables convenient comparison with existing ibuprofen degradation

studies with recycled glass across the literature.[33–35] In addition, initial ibuprofen concentrations of 20 mg L^{-1} were chosen for practical detection purposes and to ensure any potential toxic intermediates formed would be present above instrument detection limits for reliable identification and quantification. However, with a wide solubility range spanning nearly an order of magnitude, rather than relying on disparate literature values, that could in turn affect our results, the solubility was estimated in this current work.

Therefore, this research reported in this chapter aims to: 1) confirm the solubility of ibuprofen in water using HPLC, 2) identify intermediates via HPLC analysis and GC-MS method for ibuprofen decomposition via CWPO, 3) conduct a control test on H_2O_2 dosage for ibuprofen mineralization without catalyst via CWPO, and 4) investigate the feasibility of using recycled glass as a heterogeneous catalyst for removing ibuprofen via CWPO.

4.2   Characterization of ibuprofen and intermediates in reaction mixtures

The characterization of ibuprofen and intermediates includes five steps: 1) based on the literature research, prepare a list of potential intermediates of ibuprofen oxidation via CWPO, 2) develop a HPLC protocol for mimicking mixtures using standard solutions of expected intermediates, 3) qualitative analysis for the identification of ibuprofen intermediates in the reaction mixture by HPLC, 4) quantitative analysis of ibuprofen and its intermediates by HPLC external standard methods, 5) attempt to identify any other intermediates by GC-MS and extraction/concentration protocols 6) propose an ibuprofen decomposition pathway based on the identified products and the literature.

4.2.1 Expected intermediates

Due to the nature of CWPO, the radical mechanism of ibuprofen mineralization yields a diversity of products (Table 4.1) depending on different reaction conditions and the effectiveness of different detection techniques. It is fundamentally necessary to predict the reaction pathway and quantify the products that are formed. As mentioned earlier, the presence of some more toxic intermediates may lead to a higher toxicity of the treated sample. However, some studies only reported the degradation of ibuprofen itself without worrying about the more toxic intermediates.[33] It is important to identify the reaction by-products formed during the ibuprofen oxidation. Most of the reaction pathways suggested have hydroxylation of ibuprofen to form 1-hydroxy-ibuprofen and 2-hydroxy ibuprofen as the first step in several parallel reactions, followed by decarboxylation and demethylation to form other by-products such as 1-oxo ibuprofen and 2-(4-Formylphenyl)propanoic acid (Figure 4.1). The hydroxylation, decarboxylation and demethylation repeatedly occurs, resulting in numerous

by-products until they are further decomposed into short-chain acids such as acetic acid, pyruvic acid, formic acid and oxalic acid and finally reach complete mineralization to form water and carbon dioxide. Therefore, by studying the available proposed reaction pathway from the literature, predictions of likely intermediates will be made to act as a basis for quantitative and qualitative analysis in this study.
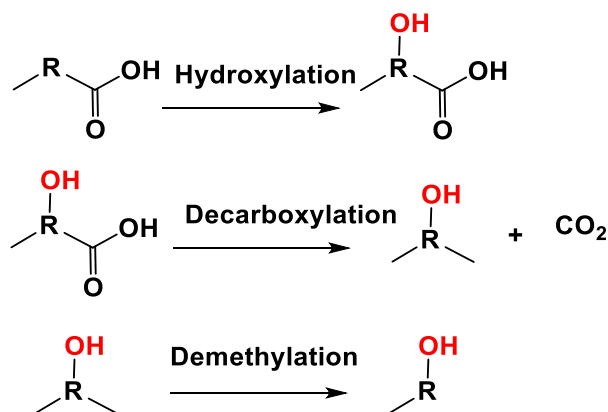
Figure 4.1 General schematics (not balanced) of three general reaction pathways: hydroxylation, decarboxylation and demethylation of ibuprofen degradation via CWPO. Proposed reaction pathway followed these three steps based on literature and experiment results are shown in Figure 4.4.

The most commonly identified intermediates (that is reported with a frequency ≥ 3 times out of 16 papers) from the literature were listed in Table 4.1. Species like **1.** 2-[4-(1-Hydroxy-2-methylpropyl)phenyl]propanoic acid, **3.** 2-hydroxyibuprofen, **8.** 1-(4-isobutylphenyl)-1-ethanol, **9.** 1-oxo-ibu and **10.** 4-isobutyleacetophenone (4-IBAP) were identified in most papers while other intermediates like **2.** 1-ethyl-4-(1-hydroxy)isobutylbenzene, **4.** 2-hydroxy-2-[4-(2methylpropyl)phenyl]propanoic acid, **5.** 4-isobutylphenol, **6.** dihydroxy ibuprofen, **7.** 2-methyl-1-phenylpropane, **11.** 1-(4-acetylphenyl)-2-methyl-1-propanone, **12.** 2-(4-Formylphenyl)propanoic acid, and **13.** 4-isobutylphenol, **14.** 4-isobutylbenzoic acid are less frequently reported. As previously detailed in Chapter 3, it is of fundamental importance to evaluate not only the ibuprofen degradation but also its mineralization to CO_2 and H_2O. Indeed, the reaction could degrade ibuprofen forming secondary compounds and the nature of these compounds is crucial in the evaluation of the process. Therefore, depending on their commercial availability, standards of all the intermediates that are reported were purchased as blank reference to develop an HPLC method and compare them with the reaction mixtures for the identification of intermediates.

Table 4.1 Lists of intermediates identified in reaction mixtures after ibuprofen oxidation over different catalysts reported in the literatures. Fe^{2+} (Fenton reagent) based catalyst Fe_2SO_4 was most effective and commonly used catalyst.

Intermediates	Catalyst	1	2	3	4	5	6	7	8	9	10	11	12	13	14	Ref
	not reported	√						√	√	√	√	√	√	√	√	35
	not reported	√		√		√	√							√		32
	Fe/ZSM-5	√		√			√				√					30
	FeSO$_4$·7H$_2$O	√		√												36
	Fe (II)-acid	√	√	√	√			√			√					22
	not reported	√			√					√	√		√			37
Identified (√) in the literature.	FeSO$_4$								√		√			√		38
	FeSO$_4$·7H$_2$O	√			√				√		√			√		39
	Cu/ZrO$_2$ or Fe/ZrO$_2$						√		√		√					26
	no catalyst	√		√		√										40
	no catalyst			√		√			√		√		√		√	41
	FeSO$_4$		√								√				√	42
	Fe$_3$O$_4$									√	√					34
	Fe (III)					√		√	√	√	√					43
	not reported	√	√		√			√		√	√	√				44
	not reported	√	√	√						√	√	√	√			45
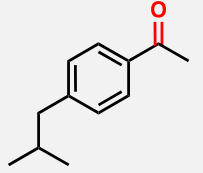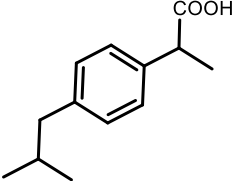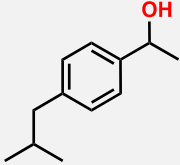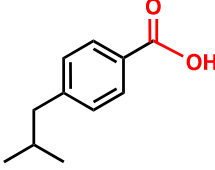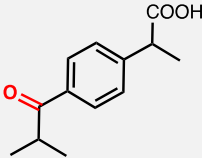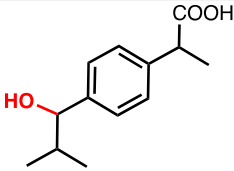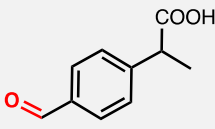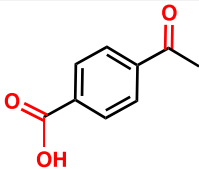
4.2.2 Qualitative analysis of intermediates in reaction mixture by HPLC

A Shimadzu HPLC chromatograph equipped with a UV detector was used to resolve and characterize ibuprofen containing mixtures. Representative HPLC chromatograms of a real reaction mixture of ibuprofen decomposition using the UV detector at fixed wavelengths of 223 nm and 250 nm at the same chromatographic condition are reported below (Figure 4.2). The identification of the intermediates formed in the actual ibuprofen oxidation process was performed by comparison of retention times of the components in standard solution with those of the intermediates in actual reaction mixture. The chromatogram parameters of ibuprofen and intermediates determined from HPLC are resented in Table 4.2.
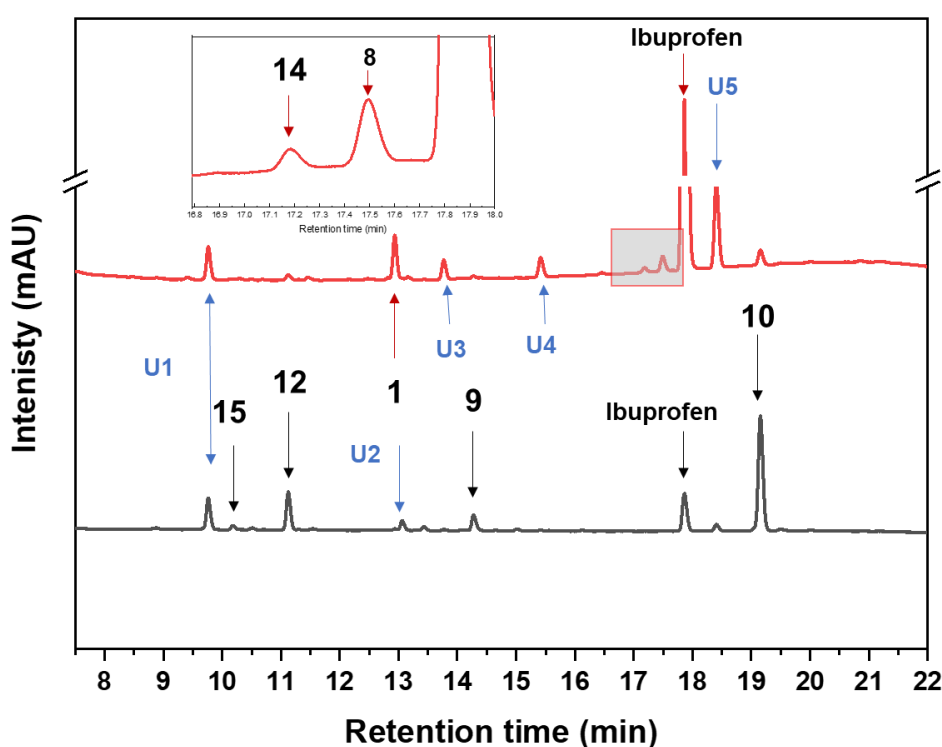
Figure 4.2 HPLC chromatograms of ibuprofen decomposition mixture collected at 223 nm (●) and 250 nm (●).Reaction condition: 50 mL of 40 mg L^{-1} ibuprofen, Fe(NO$_3$)$_3$·9H$_2$O M:S=1:20, ibuprofen:H$_2$O$_2$=1:33, p = endogenous, 80 °C, 4 h, 500 rpm, Three intermediates determined at 223 nm: (**1.** 2-[4-(1-Hydroxy-2-methylpropyl)phenyl]propanoic acid, **14.** 4-Isobutylbenzoic acid, **8.** 1-(4-isobutylphenyl)-1-ethanol) were determined together with **ibuprofen** itself at 17.8 min.Four intermediates determined at 250 nm: **15.** 4-acetylbenzoic acid, **12.** 4-ethylbenzaldehyde, **9.** 1-oxo-ibu, **10.** 4-isobutyleacetophenone. There are 5 unknowns (**U1** to **U5**) which are not yet identified.

Table 4.2 Chromatogram parameters of ibuprofen and intermediates determined from HPLC collected at 223 and 250 nm, products were determined by comparing with literature, sorting in terms of retention times (t_r). Unknown compounds detected as small peaks (response factor dependent) were not discussed. Entry: code of the intermediates.

t_r (min)	Entry	Polarity[46] D	name	Molecular structure
18.9	**10**	0.5	4-isobutyleacetophenone	
17.8	**IBU**	1.0	ibuprofen	
17.4	**8**	1.1	1-(4-isobutylphenyl)-1-ethanol	
16.8	**14**	1.2	4-Isobutylbenzoic acid	
14.2	**9**	3.0	1-oxo-ibu	
12.8	**1**	4.0	2-[4-(1-Hydroxy-2-methylpropyl)phenyl]propanoic acid	
11.1	**12**	5.5	2-(4-Formylphenyl)propanoic acid	
10.1	**15**	6.0	4-acetylbenzoic acid	

Note: t_r means retention time

When the analyte detection was collected at 223 nm, three intermediates **1.** 2-[4-(1-Hydroxy-2-methylpropyl)phenyl]propanoic acid, **14.** 4-Isobutylbenzoic acid, **8.** 1-(4-isobutylphenyl)-1-

ethanol) were determined together with **ibuprofen** itself at 17.8 min.

When the chromatogram was collected at 250 nm, four intermediates were determined at 250 nm: **15.** 4-acetylbenzoic acid, **12.** 4-ethylbenzaldehyde, **9.** 1-oxo-ibu, **10.** 4-isobutyleacetophenone. Some of the small peaks were not considered. Intermediates were identified by comparing retention times with corresponding standard chemicals purchased.

As radical reactions are non-selective, in the sense they are difficult to control as driven purely by statistics, so after attacked by ·OH radical, isomers of **1** might be formed as well, one of the unknowns is at around 13 min which is closed to **1** at 12.8 min, it might be 2-hydroxyibuprofen according to findings from literature.[32]

4.2.3 Qualitative analysis of intermediates in reaction mixture by GC-MS
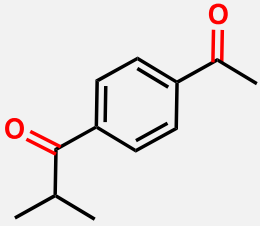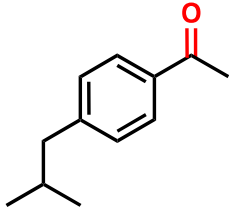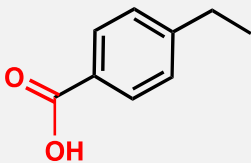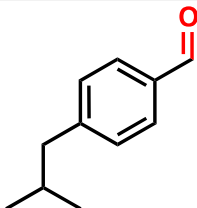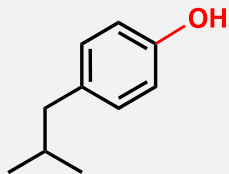
GC-MS analysis was used to identify some of the unknowns from HPLC chromatograms by determining their molecular mass. As mentioned earlier (Section 4.1), ibuprofen and its degradation products are relatively insoluble in water as compared to organic solvents.[47] Ibuprofen decomposition reaction mixtures were extracted with DCM and hexane and concentrated by using a rotary evaporator before analyzing them by GC-MS (Figure 4.3). The chromatographic parameters of ibuprofen and intermediates determined from GC-MS are presented in Table 4.3.
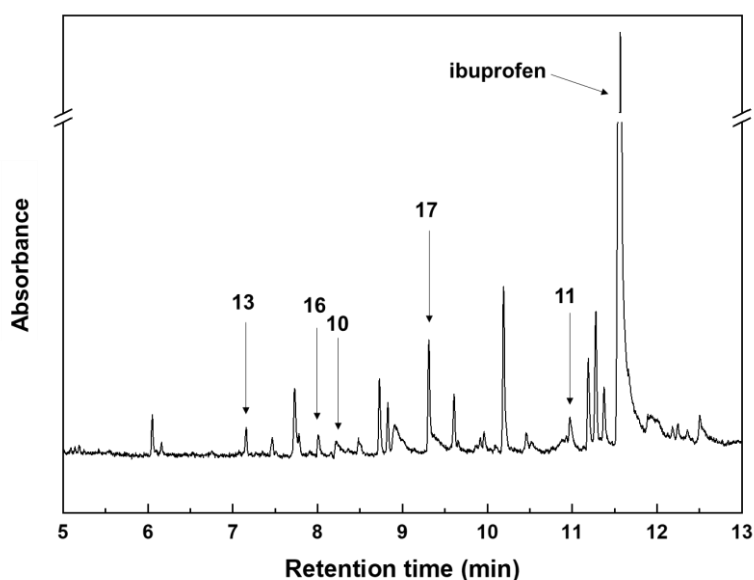
Figure 4.3 Representative GC chromatogram of an ibuprofen decomposition mixture. Reaction conditions: 50 mL of 40 mg L^{-1} ibuprofen, 0.1 wt.% Fe/ZSM-5 M:S=1:2, ibuprofen:H$_2$O$_2$=1:30, p = endogenous, 80 °C, 4 h, 500 rpm. The reaction was repeated four times and mixtures were combined and extracted with DCM and hexane and concentrated by rotary evaporator before analyzing them by GC-MS. Four new intermediates (**13.** 4-Isobutyl phenol, **16.** 4-Isobutylbenzaldehyde, **11.** 1-(4-acetylphenyl)-2-methyl-1-propanone, **17.** 4-Ethylbenzoic acid) were determined, one intermediates detected in HPLC, **10.** 4-isobutylacetophenone.

Table 4.3 Chromatographic parameters of ibuprofen and intermediates determined using GC-MS, products were determined by comparing the mass spectrum with literature, and sorting in terms of retention times (t_r). Some unknown compound peaks detected as small peaks (response factor dependent) were not considered.

Product	t_r(min)	Molecular formula	MW g mol^{-1}	name	Molecular structure
11	11.2	$C_{12}H_{14}O_2$	190	1-(4-acetylphenyl)-2-methyl-1-propanone*	
10	9.3	$C_{12}H_{16}O$	176	4-isobutylacetophenone*	
17	8.3-8.4	$C_9H_{10}O_2$	150	4-Ethylbenzoic acid	
16	8	$C_{11}H_{14}O$	162	4-Isobutylbenzaldehyde	
13	7.7	$C_{10}H_{14}O$	150	4-Isobutyl phenol*	

Note: * are intermediates matching with literatures.[35]

GC-MS analysis of the ibuprofen decomposition mixture detected **13**. 4-isobutyl phenol, **16.** 4-isobutylbenzaldehyde, **11.** 1-(4-acetylphenyl)-2-methyl-1-propanone, **17.** 4-ethylbenzoic acid one intermediates detected in HPLC, **10.** 4-isobutylacetophenone, and some unknown products were also detected but unidentified. Among these four products, **11** and **13** match with literature[35] while **16** and **17** are not found in the literature yet.

In addition, peaks were noticed between 11-13 minutes exhibiting higher molecular weights around 250-500 m/z$^+$. These species potentially indicate condensation products formed through acid-base reactions. For instance, electrophilic addition across the double bond could

yield alcohols and then ether dimers covalently linked at that site (Eq. 4.1 to 4.2):

$$R\text{-}CH=CH\text{-}COOH + H_2O \xrightarrow{H^+} R\text{-}CHOH\text{-}CH_2\text{-}COOH \qquad \text{(Eq. 4.1)}$$

$$2\ R\text{-}CHOH\text{-}CH_2\text{-}COOH \rightarrow R\text{-}CH(CH_2\text{-}COOH)\text{-}O\text{-}CH(CH_2\text{-}COOH)\text{-}R + H_2O \qquad \text{(Eq. 4.2)}$$
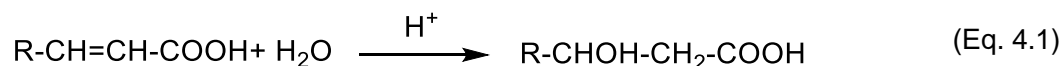
So far, eleven main products were determined from the ibuprofen degradation reaction via Fenton reaction. The use of the HPLC method identified in total seven of the intermediates with three determined at a detection wavelength of 223 nm: **1.** 2-[4-(1-Hydroxy-2-methylpropyl)phenyl]propanoic acid, **14.** 4-isobutylbenzoic acid, **8.** 1-(4-isobutylphenyl)-1-ethanol and four determined at a detection wavelength 250 nm: **15.** 4-acetylbenzoic acid, **12.** 4-ethylbenzaldehyde, **9.** 1-oxo-ibu, **10.** 4-isobutyleacetophenone. GC-MS identified four more: **13**. 4-isobutyl phenol, **16.** 4-Isobutylbenzaldehyde, **11.** 1-(4-acetylphenyl)-2-methyl-1-propanone, **17.** 4-ethylbenzoic acid. Some of the unknowns might be isomers of the detected products due to the nature of radical reaction. By determining eleven intermediates, most of the main products detected can be identified. As compared to the literature, most of the current studies determine around 8-14 intermediates depending on different reaction mechanisms. As such our determinations can be considered acceptable for the experimental work that has been carried out.

4.2.4 Proposed Ibuprofen degradation pathway

By comparing the degradation pathway and products of ibuprofen oxidative treatments suggested in the literature with the identified products in the previous section, a proposed ibuprofen degradation pathway including all the possible intermediates is suggested in Figure 4.4. Out of these products, **1** is the very first product and most common detected intermediate following ·OH attack. Another two important intermediates are **8** and **10** due to their higher toxicity over ibuprofen (Ibuprofen as an emerging organic contaminant in the environment, distribution and remediation).

Nine determined aromatic intermediates from ibuprofen degradation are highlighted in green in Figure 4.4. Out of these products, compounds **10**, **13**, and **23** (circled in red) require particular focus as they were previously identified as more toxic intermediates.[22] Due to exceeding the toxicity of the original ibuprofen target, these three compounds necessitate further breakdown. Additionally, product **22** (highlighted in orange), another aromatic intermediate, likely undergoes ring opening after its formation. This ring cleavage enables the subsequent production of aliphatic acids prior to their ultimate mineralization into carbon dioxide and water.
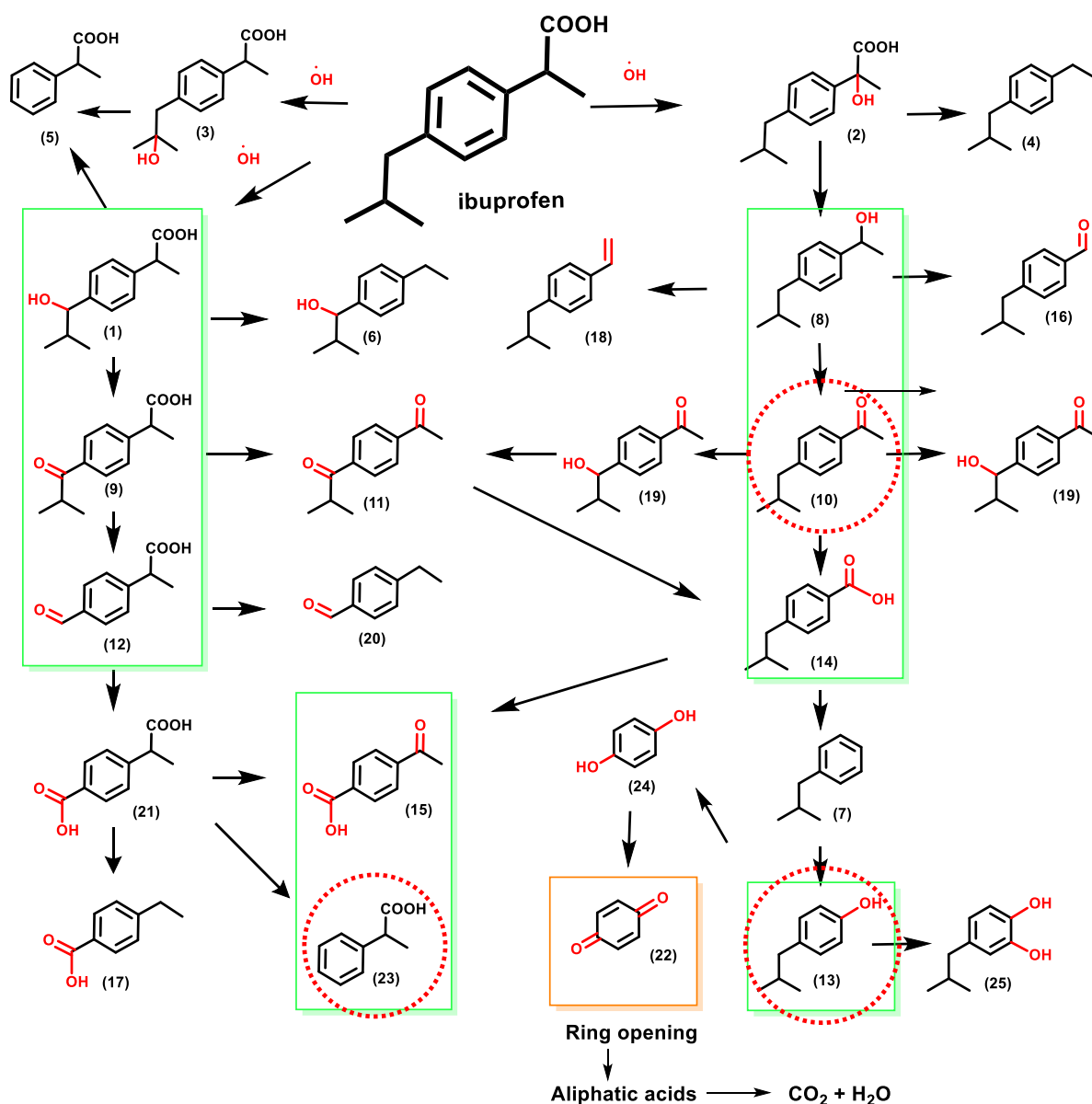
Figure 4.4 Possible degradation pathways and products of ibuprofen from oxidative and thermal treatments are suggested. Only aromatic intermediates are listed, carboxylic acids are not shown. The IUPAC name of the possible products are as follows: (**1**) 2-[4-(1-hydroxy-2-methylpropyl)phenyl]propanoic acid; (**2**) 2-(4-isobutylphenyl)propanoic acid; (**3**) 2-[4-(2-hydroxy-2-methylpropyl)-phenyl]propanoic acid; (**4**)1-ethyl-4-(1-hydroxy)isobutylbenzene; (**5**) 1,2-hydroxyibuprofen; (**6**) 4-ethyl-α-(1-methylethyl)benzenemethanol; (**7**) 2-methyl-1-phenylpropane; (**8**) 1-(4-isobutylphenyl)-1-ethanol; (**9**) 1-oxo Ibuprofen; (**10**) 4'-isobutylacetophenone; (**11**) 1-(4-acetylphenyl)-2-methyl-1-propanone; (**12**) 2-(4-formylphenyl)propionic acid; (**13**) 4-isobutylphenol; (**14**) 4-isobutylbenzoic acid; (**15**) 4-acetylbenzoic acid; (**16**) 4-isobutylbenzaldehyde; (**17**) 4-ethylbenzoic acid; (**18**) 4-isobutylstyrene; (**19**) 1-[4-(1-hydroxy-2-methylpropyl)phenyl]ethenone; (**20**) 4-ethylbenzaldehyde; (**21**) 4-carboxy-α-methylbenzene acetic acid; (**22**) benzosemiquinone; (**23**) 2-phenylpropionic acid; (**24**) hydroquinone; (**25**) 4-(2-methylpropyl)-1,2-benzenediol. Determined products (●): **1, 8, 9, 10, 12, 13, 14, 15** and **23**; toxic than ibuprofen (●):**10, 13,** and **23.** Intermediates before ring opening and mineralization (●): **22**.

4.2.5 Quantitative analysis of intermediates in reaction mixture by HPLC

After identifying all the potential degradation products, quantification of products **1, 8, 9, 10, 12, 14, 15** as determined from HPLC are therefore carried out by external standard methods. Standard solutions of these products mimicking the expected concentration reaction range were prepared and analysed by HPLC for calibration curves for quantitative purposes (that will be afterwards used for catalytic tests).

Before any calibration curve is made, it is important to first determine a suitable wavelength to be used for the UV detector, as different compounds may have their highest absorbance at different wavelengths depending on their own structure, which will severely affect the response factor of the calibration curve.

First, a UV spectrum was used to identify the best absorbance wavelength for each of the interested intermediates including ibuprofen itself. Three representative UV-spectra of ibuprofen and its intermediates are shown in Figure 4.5, demonstrating different absorbance maxima at wavelengths of 196, 223 and 250 nm (UV-spectra of other intermediates in Appendix A3.1).
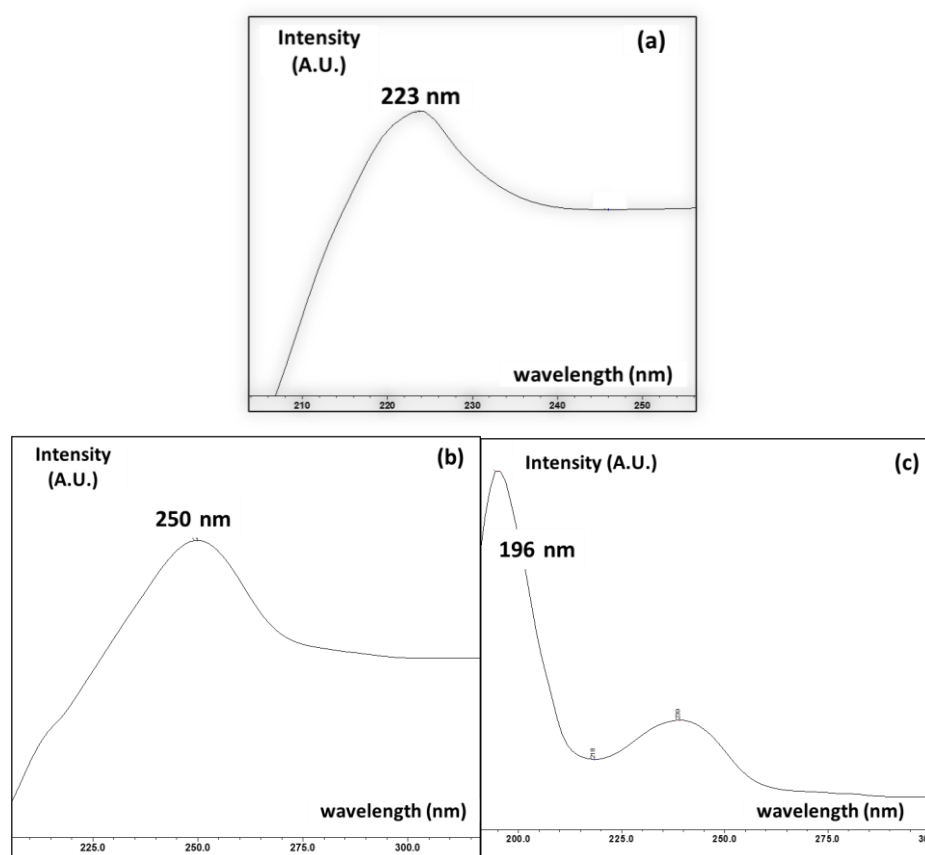
Figure 4.5 UV spectrum of (a) ibuprofen, (b) **9.** 1-oxo-ibuprofen and (c) **14.** 4-isobutylbenzoic acid solutions showing the highest absorbance wavelength at 223, 250 and 196 nm respectively.

Calibration curves were built, and RFs were calculated based on three best absorbance wavelengths 196, 223 and 250 nm (Table 4.4). By looking at these RF of each compound, although it would be more convenient if the chromatographs were collected under the same wavelength, it was undeniable that the best RF was generated by using wavelengths of 196, 223 and 250 nm respectively (Table 4.4 green values). It follows that to choose a different wavelength could severely affect the determination of the remaining compounds, as the difference in the response factor is at least one order of magnitude (Table 4.4). Therefore, by considering each RF, 223 was selected as a compromise wavelength (Figure 4.6) for calibration curves building for ibuprofen, intermediates **1, 8** and **14** while calibration curves for intermediates **9, 10, 12 and 15** were built based on chromatograms collected at 250 nm.

Table 4.4 Response factor for ibuprofen and its potential intermediates at λ =196, 233 and 250 nm.

Product Entry	Response factors at different detection wavelength λ (mUA×min)/(mg L^{-1})		
	196 nm	223 nm	250 nm
Ibuprofen	-	1×10^5	3×10^4
1	-	2×10^{10}	5×10^8
8	$4 \cdot 10^{10}$	2×10^{10}	4×10^8
9	-	5×10^4	3×10^5
10	-	2×10^4	2×10^5
12	-	3×10^4	3×10^5
14	$5 \cdot 10^{10}$	2×10^{10}	3×10^4
15	-	4×10^4	3×10^5
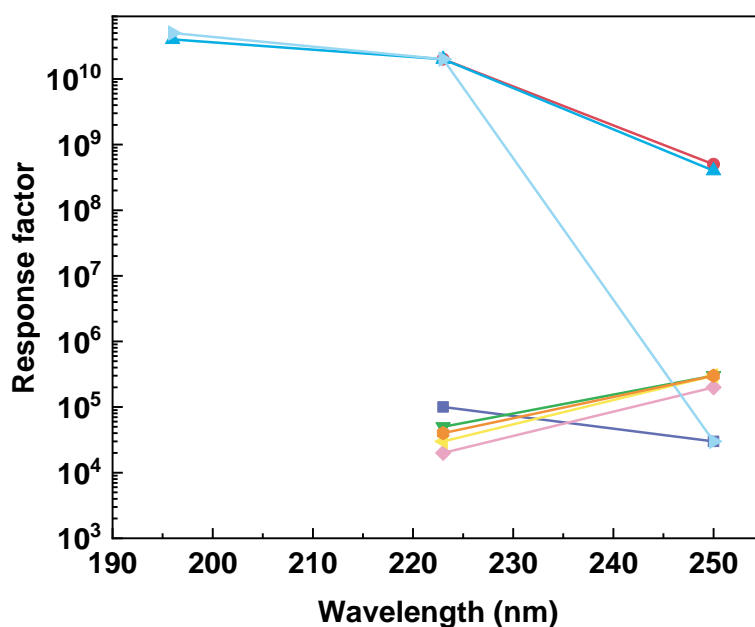
Figure 4.6 Response factors calculated for ibuprofen (●) and its intermediates (**1**:●; **8**:●; **9**:●; **10**:●; **12**:●; **14**:● and **15**:●) at 196, 223 and 250 nm.
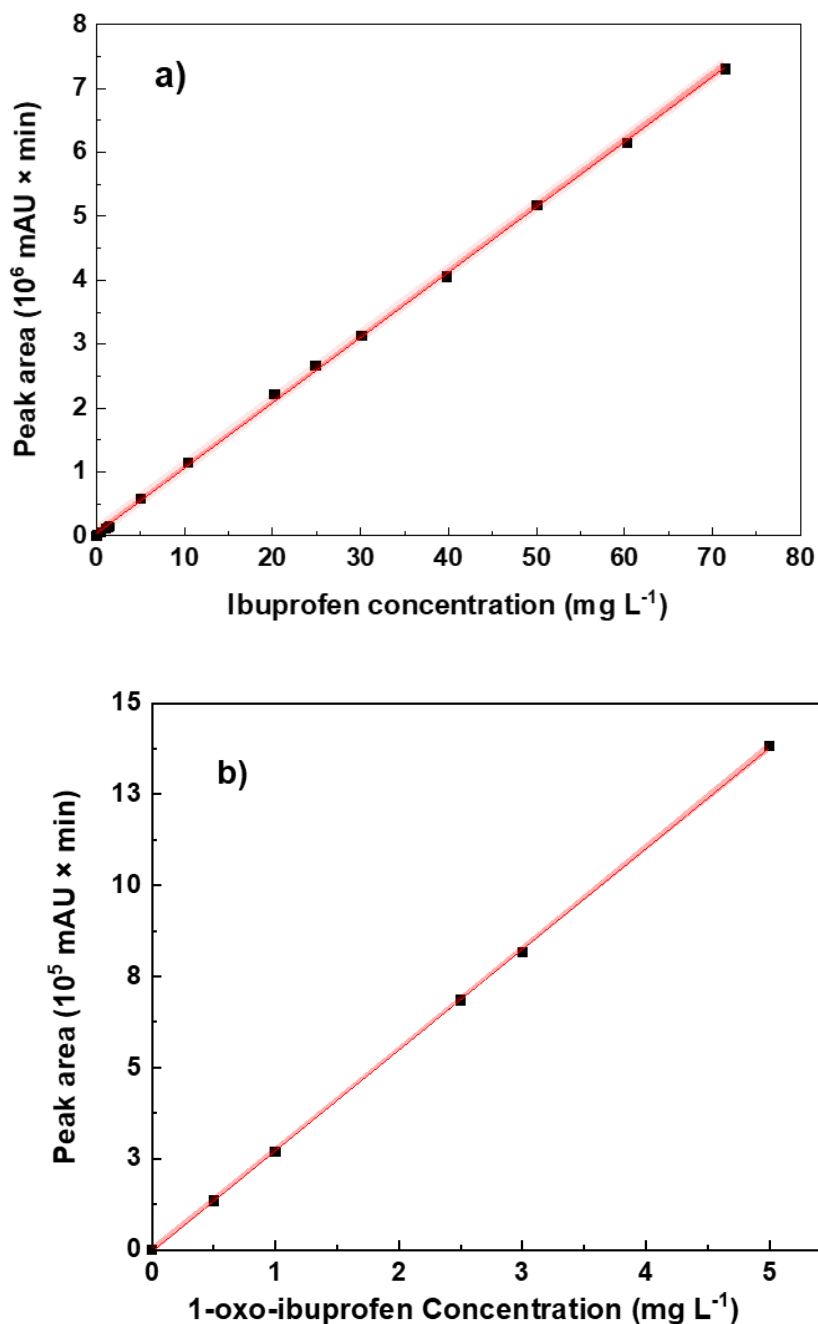
Figure 4.7 Calibration curve of (a) ibuprofen collected at **223** nm with an intercept of $4{\times}10^4 \pm 2{\times}10^4$, a sensitivity slope of $1{\times}10^5 \pm 5{\times}10^2$ and a R^2 of 0.9996, (b) 1-oxo IBU collected at **250** nm with signal intercept of $-5{\times}10^3 \pm 4{\times}10^3$, a slope of $3{\times}10^5 \pm 1{\times}10^3$ and a R^2 of 0.9999.

Calibration curves were built at 223 and 250 nm for ibuprofen and intermediates (Figure 4.7). A representative calibration curve of 1-oxo-ibuprofen was shown (other calibration curves at Appendix A3.2). A linear regression analysis showed that, the R^2 value of the lines are nearly 1. The correlation coefficient, R, is a measure of the strength of the degree of correlation, between the dependent (signal) and independent (concentration) values. It should be noted that this is a measure of correlation not a measure of linearity, but the more it closes to 1, the better the correlation by using a linear regression model. It is worth noting though, that a good

R value (>0.95) could lead to statistical significance which only indicates some evidence for correlation, the uncertainty associated to it may be prohibitively large. Hence it does not necessarily mean that the data would be appropriate for calibration. On the other hand, R^2 is often used to describe the fraction of the total variance in the data that is contributed by the line that has been fitted. Ideally, if there is a good linear correlation, most of the variability can be accounted for by the fitted line, R^2 should therefore be close to 1. In this case, the calibration lines all had a good linear correlation.

Furthermore, ideally, the calibration line should be expected to go through the origin of the axis as when no chemical was added, no signal should appear, and the intercept should not be significantly different from zero. As shown in Figure 4.7, considering the errors (standard deviations,σ), the intercept for calibration curves is compatible with zero within 1 or 2σ, this could be further confirmed by the confidence interval for the interception shown in Figure 4.7. It was believed the confidence interval included origin, which meant the intercept is not statistically different from zero. The *p*-value represents the probability of obtaining the observed data or more extreme values, assuming the null hypothesis is true. Here the null hypothesis is no difference from a flat calibration curve with zero slope and intercept. Therefore, higher p-values indicate decreasing evidence to reject this ineffective calibration scenario due to lower statistical significance. Typically, $p > 0.05$ is considered inadequate to reject the null case with enough confidence.

In addition to p-values, t-values quantify how many estimated standard deviations each coefficient falls from zero. For the small sample sizes here, $t < 2.6$ aligns with $p > 0.05$ indicating insignificant difference from a horizontal line, affirming properly proportional calibrations.

Consequently, the five calibration curves were considered accurate for quantitative determination for our catalyst tests. It will then be important that the concentrations that will be detected for the intermediates and ibuprofen fall within the range of the calibration curves. Hence, the appropriate range for ibuprofen calibration curve in terms of linearity so far to determine ibuprofen conversion and CMB was from 0.5 mg L^{-1} to 72 mg L^{-1} where the usual concentration for the reaction mixtures fall between 0 and 21 mg L^{-1}.

4.3   Ibuprofen solubility estimate

From literature, by using different preparation methods and analytical tools, ibuprofen solubility values in water vary within a wide range from 10 to 180 mg L^{-1} (Table 4.5). Our solubility study considered an initial concentration of 20 mg L^{-1} at lab temperature (25°C) with constant stirring. Ibuprofen was not soluble for the range from 0.5 to 21 mg L^{-1} after 48 hours of stirring under

room temperature even with the aid of sonication. The samples were then heated at 80°C with stirring to promote dissolution, and then centrifuged at 5000 rpm for 15 minutes to separate any remaining undissolved solids. The ibuprofen concentration in the supernatant was then quantified by HPLC to determine the dissolved amount.

An appropriate amount of ibuprofen (0.03 to 50 mg) was weighed and dissolved in deionized water to obtain aqueous solutions with concentrations from 0.05 to 103 mg L^{-1}. In order to verify the correctness of these concentrations, analysis via HPLC was conducted.

Table 4.5 Literature data for ibuprofen solubility in pure water and their respective determination methods. Ibuprofen solubility values vary within a wide range from 10 to 180 mg L^{-1}, the solubility determined in this report (72 mg L^{-1}) is within the literature range.

T °C	ibuprofen amount mg L^{-1}	Ref	Time h	Separation method	Analytical method
25	10	26–28	-*	-	-
25	20	29,30	-	-	-
25	56	48	48	Filtration 0.2 µm	HPLC-UV-vis
25	83	49	>98	Centrifugation	UV-vis
27	49	50	24	Centrifugation	UV-vis
27	80	51	48	Filtration 0.2 µm	HPLC-UV-vis
-	180	18	-	-	-
21	72	This report	48	Centrifugation	HPLC-UV-vis

*"-"not known
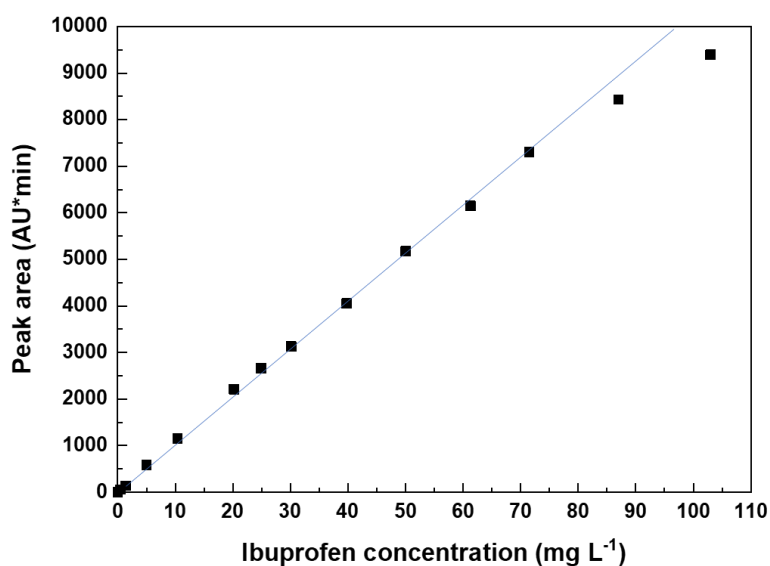
Figure 4.8 Calibration curves of ibuprofen solutions collected at λ=223 nm with concentrations from 0.05 to 103 mg L^{-1}. Figure of peak areas (AU*min) against respective concentrations (mg L^{-1}) ranged from 0 mg L^{-1} to 72 mg L^{-1}, R^2 = 0.9993. Beyond this range, signals deviate towards lower values.

A linear interpolation of the data points shows linearity up to 72 mg L^{-1} (Figure 4.8). Above this limit, the HPLC signal deviates to values lower than expected. This bending effect occurs when the ibuprofen solution becomes saturated. In fact, if the solution is saturated, the HPLC signal will only detect the ibuprofen present in soluble form, leaving the remainder as a solid and non-detectable residue. This, in turn, will result in a signal and concentration in the solution that are lower than expected.

This estimate is compatible with literature data reporting a solubility of around 60 mg L^{-1}. As such, our solutions were prepared at a maximum concentration of 60 mg L^{-1}.

4.4   Effect of the H_2O_2: IBU molar ratio (H_2O_2 dosage) on oxidation efficiency

Having estimated the solubility of ibuprofen, it is important to investigate how different doses of H_2O_2 affect the oxidation efficiency of ibuprofen, as it plays a crucial role in the Fenton reaction. As explained in the previous Chapter 3, while increasing the initial concentration of H_2O_2 enhances the organic contaminant degradation rate, it may also increase the rate of undesired H_2O_2 scavenging. That is, beyond a certain point, increasing the initial H_2O_2 concentration does not improve the conversion efficiency and can even result in a detrimental effect, which has been reported in various studies.[52–54]

Although with respect to mineralization, the stoichiometric ratio H_2O_2 to ibuprofen is 33 (Eq. 4.3), the literature reports a wide range of H_2O_2 dosages from 0.4 to 505 (Table 4.6) and varying effects on the reaction under different conditions.

$$C_{13}H_{18}O_2 + 33\ H_2O_2 \rightarrow 13\ CO_2 + 42\ H_2O \qquad \text{(Eq. 4.3)}$$
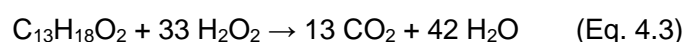
In previous research on Fenton oxidation of ibuprofen, complete conversion has been achieved by using elevated amounts of hydrogen peroxide beyond stoichiometric levels. Multiple studies (Table 4.6) have demonstrated nearly 100% ibuprofen decomposition with H_2O_2: ibuprofen molar ratios up to 505:1, while adjusting reaction conditions such as temperature and catalyst selection. However, this does not necessarily imply a 100% selectivity to CO_2 and H_2O due to radical termination processes, which may actually result in lower mineralization levels when there is a large excess of oxidant.

This ability to drive full conversion even with different conditions implies excess peroxide likely continuously generates hydroxyl radicals that overwhelm losses from radical recombination side reactions. However, reducing the H_2O_2 amount required would be economically and environmentally beneficial. Further optimization of reaction parameters would enable the maintenance of high ibuprofen conversion at significantly lower and more sustainable

hydrogen peroxide levels.

Therefore, it is critical to determine the optimal H_2O_2 dosage under the specific reaction conditions employed in our study to ensure optimal ibuprofen conversion and minimize the impact of H_2O_2 scavenging.

Table 4.6 H_2O_2 dosage used in other studies for ibuprofen (IBU) degradation in different reaction conditions.

IBU amount mg L^{-1}	H_2O_2 : IBU*	Catalyst mg L^{-1}	M:S **	Catalyst	T °C	IBU conversion %	Mineralization %***	Ref
10	505	12.5	4	Cu/ZrO$_2$	70	100	53	26
20	66	7.5	1	FeSO$_4$	25	100	40	55
20	66	7.5	1	FeSO$_4$	25	100	10	55
10	206	50	16	γ-Cu-Al$_2$O$_3$	r.t.	98	63	27
10	505	12.5	5	Fe/ZrO$_2$	70	97	40	26
50	14	430	32	FeSO$_4$	r.t.	93	90	56
20	66	163	30	Fe-MFI zeolite	25	88	27	57
10		5	2	FeSO$_4$	r.t.	85	3	28
10		5	2	Fe(OH)O goethite	r.t.	80	30	28
180	0.4	67	1	FeSO$_4$	30	80	40	22
60	31	25.2	2	FeSO$_4$	20	80	15	36
10		5	2	Zervo valent iron	r.t.	79	41	28
180	0.4	67	1	FeSO$_4$	30	60	10	22

* H_2O_2 to ibuprofen molar ratio
**M:S molar metal to substrate ratio
*** as determined by total organic carbon

To cover the range of H_2O_2 to ibuprofen molar ratios reported in the literature, control experiments were conducted on a 50 mL aqueous solution of ibuprofen (20 mg L^{-1}) with a molar ratio up to 800, including the stoichiometric value of 33. This was initially done in the absence of a catalyst, and as such, the only way to form ·OH radicals would be through thermal decomposition.
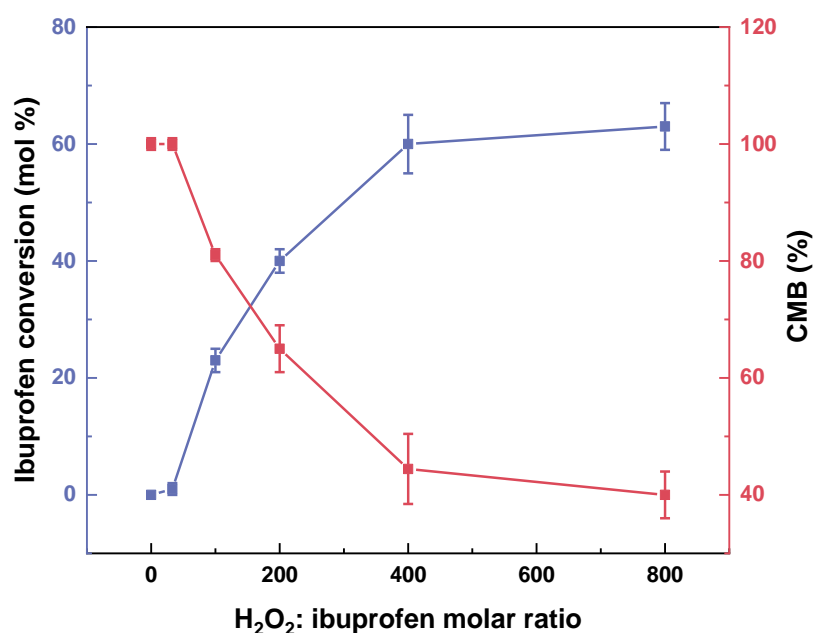
Figure 4.9 Trends of Ibuprofen conversion (■) and carbon mass balance (■) for ibuprofen oxidation with different hydrogen peroxide addition. Reaction conditions: 50 mL of ibuprofen (20 mg L^{-1}), ibuprofen:H$_2$O$_2$ molar ratio=1:0, 33, 80, 100, 400 and 800, p = endogenous, 80 °C, 4 h, 500 rpm. The slope of the curve became less and less steep until a plateau at a ratio of 400, the conversion reached a limit at about 62%, the carbon mass balance matched the trend of the conversion, and it decreased up to about 40%.

As discussed, increased initial concentration of H$_2$O$_2$ increases the degradation rate or organic pollutants, this matched the trend in ibuprofen conversion and a positive correlation between the ibuprofen conversion and the initial amount of H$_2$O$_2$ was observed. It was also noticed that the slope of the curve (Figure 4.9) became less and less steep until a plateau at a ratio of 400, the conversion reached a limit at about 62%, the carbon mass balance matched the trend observed the conversion, in the sense that the higher the conversion the higher the mineralization and in turn the lower the mass balance, up to a value of ca. 40%. Our data are consistent with the fact that a high initial concentration of H$_2$O$_2$ also leads to undesired ·OH scavenger effects.[58]

Therefore, by the addition of H$_2$O$_2$ alone, the larger the initial concentration does not lead to a higher conversion and mineralization. To circumvent this detrimental effect, a multiple addition method instead of single addition of H$_2$O$_2$ can be considered. This is to control the interaction between ·OH and H$_2$O$_2$, preventing the formation of the less reactive ·OOH and ensuring that the reaction is primarily between ·OH and the pollutant. According to a study by Prasad,[58] approximately 23% more of mineralization of stripped sour water was observed. More ·OH are available for oxidation and less portion of H$_2$O$_2$ will participate to form non-active species.

In any case though, either single or multiple additions, catalysts are necessary to be added to increase the H_2O_2 decomposition rate to $\cdot OH$ and at the same time reduce the unnecessary dosage of H_2O_2.

4.5 Activity of Fe^{3+} and Fe^{2+} in the CWPO of ibuprofen

It should be recalled that (Chapter 3, Section 3.4.1) from a comparison of two metal precursors Fe^{3+} and Fe^{2+} as active species for the Fenton reaction has shown a difference for phenol decomposition activity only at the beginning of the reaction (24 h with respect to a total 72 h reaction) and different M:S molar ratio. In view of these results, and that the sole thermal decomposition of H_2O_2 is not able to achieve full ibuprofen mineralization, we carried out the same type of control test prior to the statistical study of recycled glass containing Fe^{3+} in the CWPO of ibuprofen as a necessary benchmark.

As well as by considering the effects of both Fe^{2+} or Fe^{3+} which can both theoretically initiate the reaction (Eq. 3.3 and 3.4).

4.5.1 Control tests of using Fe^{3+} and Fe^{2+}

As discussed in section 4.2, seven ibuprofen decomposition intermediates: 4-acetylbenzoic acid, 2-(4-Formylphenyl)propanoic acid, 1-oxo-ibu, 4-isobutyleacetophenone), 2-[4-(1-Hydroxy-2-methylpropyl)phenyl]propanoic acid, 4-Isobutylbenzoic acid and 1-(4-isobutylphenyl)-1-ethanol) are determined by HPLC together with some unknown peaks. Furthermore due to the complexities of the chromatograms from ibuprofen decompositionfive different H_2O_2 to ibuprofen molar ratio were selected, in order to gradually lead to a larger amount of products and so facilitate the identification of the compounds in the reaction mixture. Ibuprofen decomposition with IBU:H_2O_2 molar ratio of 0, 10, 30 (less than), 33 (stoichiometry value with respect to mineralization) and 40 (more than) of with and without $Fe(NO_3)_3 \cdot 9H_2O$ and $FeSO_4 \cdot 7H_2O$ to as catalyst were conducted to study the activity on ibuprofen decomposition (Figure 4.10) in terms of: ibuprofen conversion (mol%), CMB% and H_2O_2 consumption.
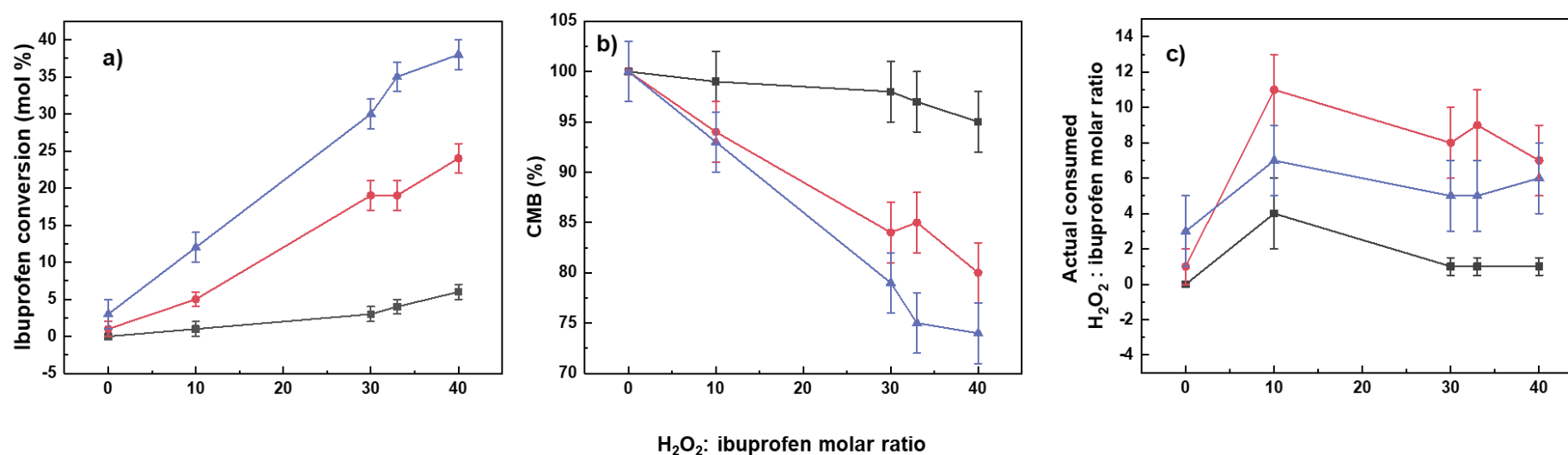
Figure 4.10 Control tests for the comparison between the use of $Fe(NO_3)_3 \cdot 9H_2O$ and $FeSO_4 \cdot 7H_2O$ as starting catalyst on ibuprofen decomposition via Fenton reaction. Catalyst activity is evaluated in terms of: a) ibuprofen conversion (mol %), b) CMB (mol%) and c) actual consumed H_2O_2: ibuprofen (molar ratio). In the presence of different amount of H_2O_2 only (■); in presence of different amount of H_2O_2 and $Fe(NO_3)_3 \cdot 9H_2O$ (●) and in presence of different amount of H_2O_2 and $FeSO_4 \cdot 7H_2O$ (▲). Reaction conditions: 50 mL of ibuprofen (20 mg L^{-1}), M:S=1:20, ibuprofen:H_2O_2=1: 0, 10, 30, 33, 40, p = endogenous, 80 °C, 4 h, 500 rpm. The addition of $FeSO_4 \cdot 7H_2O$ as starting catalyst showed a significant higher activity on ibuprofen decomposition as compared to the addition of no catalyst and $Fe(NO_3)_3 \cdot 9H_2O$ at all different amount of H_2O_2.

Control tests in the absence of catalyst and H_2O_2 showed a 1 ± 1 mol% of ibuprofen conversion, that is compatible with zero, after 4 h of reaction, showing the resistance of ibuprofen being decomposed by heating only in the absence of catalyst or conversely the stability of ibuprofen at such conditions. From the stability tests of H_2O_2 reported in Chapter 3 (Section 3.2), only 3% of H_2O_2 was decomposed after 4 h without the presence of substrate and catalyst at 80°C, indicating only a negligible degradation under the reaction conditions. This is consistent with literature data; for example, studies have noted substantial variability in hydrogen peroxide half-life spanning 6 mins to 6 days depending on temperature, pH, and solution components.[59,60–65] Nonetheless, the stability tests and literature comparisons give evidence that negligible H_2O_2 decomposition should occur within the 4-hour CWPO reaction time frame used in this work. In addition, the ibuprofen conversion increased to only 5% over 4 h (a short reaction time) even in the presence of H_2O_2 (stoichiometric ratio 1:33), suggesting that though slightly improved the ibuprofen removal efficiency, the addition of H_2O_2 formed a few ·OH radicals via hydrothermal decomposition when no effective catalyst involved, hence, it had a negligible effect on the contaminant abatement.

A control test in the absence of H_2O_2 but in the presence of $Fe(NO_3)_3 \cdot 9H_2O$ and $FeSO_4 \cdot 7H_2O$ showed a limited ibuprofen conversion (3% practically comparable with 0%), indicating that both H_2O_2 and Fe species are required to degrade ibuprofen . The addition of $Fe(NO_3)_3 \cdot 9H_2O$ and $FeSO_4 \cdot 7H_2O$ significantly increased the ibuprofen conversion (24% and 38% respectively) when $IBU:H_2O_2$ molar ratio of 40 was added. This result was better than the reaction performance (23%) when $IBU:H_2O_2$ molar ratio of 100 was added without catalyst.

Similar to the decomposition of phenol, the conversion of ibuprofen after 4 hours using Fe^{2+} ($FeSO_4 \cdot 7H_2O$) as catalyst is higher than that using Fe^{3+} ($Fe(NO_3)_3 \cdot 9H_2O$). This is further evidenced by the greater amount of products detected by HPLC for $FeSO_4 \cdot 7H_2O$ (7 products) than $FeSO_4 \cdot 7H_2O$ (6 products). This difference might be due that unlike the classical Fenton process, Fe^{3+} ion required an additional step to react with H_2O_2 to generate Fe^{2+} ion and ·OOH at the beginning of the reaction, for every centre of Fe^{3+} a molecule of H_2O_2 reacts to form Fe^{2+}. Less active ·OOH will be formed instead of ·OH during this essential step which largely decreases the oxidation activity in ibuprofen decomposition. As a result, some more H_2O_2 (though small) was always consumed by every converted ibuprofen while a smaller conversion was observed for each different dosage of H_2O_2. This result further confirmed the theory and highly matched with phenol decomposition observation. However, it was suggested when the reaction time is prolonged, after all the initial Fe^{3+} ions are converted to Fe^{2+} this difference will be minimised and eventually, no significant difference will be noticed. This assumption can be further confirmed by increasing the reaction time to 72 h.

4.5.2 Kinetic study on Fe^{3+} and Fe^{2+} as catalyst in the CWPO of ibuprofen
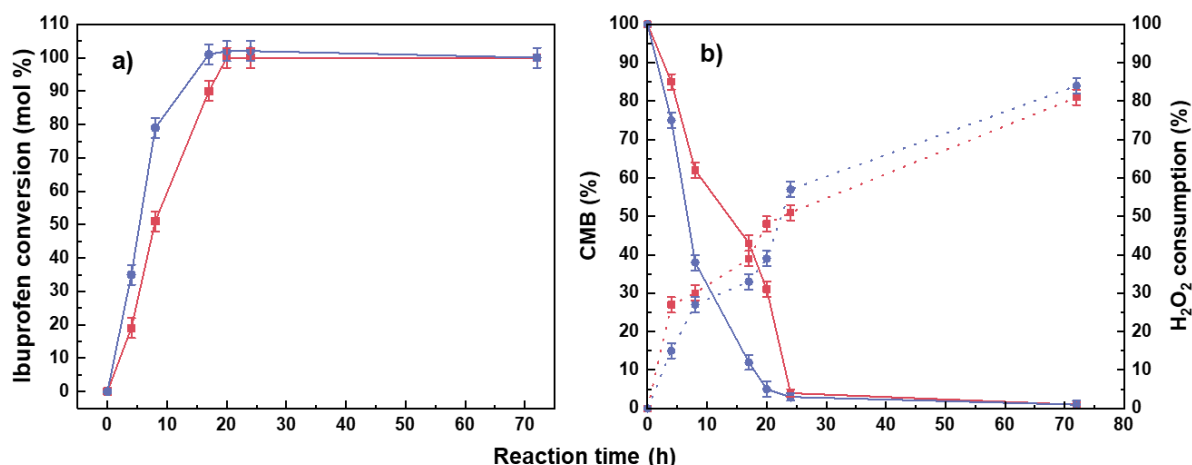
Figure 4.11 Kinetic study for the comparison between the use of $Fe(NO_3)_3 \cdot 9H_2O$ (■) and $FeSO_4 \cdot 7H_2O$ (●) as starting catalyst on ibuprofen decomposition via Fenton reaction. Catalyst activity is evaluated in terms of: a) ibuprofen conversion (mol %) and b) CMB (mol%) (solid) and H_2O_2 consumption (%) (dotted). Reaction conditions: 50 mL of ibuprofen (20 mg L^{-1}), M:S=1:20, ibuprofen:H_2O_2=1:33, p = endogenous, 80 °C, reaction time: 0, 4, 8, 17, 20, 24 and 72 h, 500 rpm. The initial rate of ibuprofen decomposition by $FeSO_4 \cdot 7H_2O$ as starting catalyst is twice as fast as $Fe(NO_3)_3 \cdot 9H_2O$.

A longer reaction time allowed to detect an increased the activity of $Fe(NO_3)_3 \cdot 9H_2O$ and $FeSO_4 \cdot 7H_2O$ towards H_2O_2 decomposition and in turn on ibuprofen degradation leading to a complete ibuprofen molar conversion within 24 and 16.5 h respectively (Figure 4.11). The rate of reaction by using $FeSO_4 \cdot 7H_2O$ is nearly twice as fast as $Fe(NO_3)_3 \cdot 9H_2O$ at early stage of the reaction (5-10 h), after 24 h of reaction, the reaction reached completion in both cases Thus, showing that indeed Fe^{2+}/Fe^{3+} act as a catalyst cycle.

Furthermore, the CMB% reveals a clear trend of both Fe^{3+} and Fe^{2+} (Figure 4.11b solid line), the gradually decreasing CMB showed an increasing CO_2 formation with increasing in reaction time. When Fe^{2+} was used a much faster ibuprofen mineralisation occurred. The H_2O_2 consumption data also revealed the same trend (Figure 4.11b dotted line), the amount of H_2O_2 consumed per unit ibuprofen converted were higher for Fe^{3+} due to extra step up to 20 h where the consumption values were statistically similar. However, for both catalysts, even after 72 h reaction, fully mineralization was not achieved proved by a 93 % H_2O_2 consumption and potential scavenging effect discussed previously (Section 4.4). Even though, the most toxic ibuprofen intermediates were not detected at this stage, showing a success in pollutant abatement so far. From Figure 4.11b (solid line), the steep decrease of CMB is detected, suggesting a fast production of CO_2. This further proved the hypothesis that extra step by $Fe(NO_3)_3 \cdot 9H_2O$ is needed than $FeSO_4 \cdot 7H_2O$ in order to trigger the redox cycle in classical Fenton process, and this difference in H_2O_2 decomposition activity between this two ions cannot be denied.

This result supports the working hypothesis of Fe^{3+} centre, like that presence in a glassy matrix can be active for the catalytic decomposition of ibuprofen by using a Fenton system. In the next section, GTS green glass of different diameters will be used as a benchmark to investigate the effect of different parameters on heterogeneous reaction via the Fenton reaction.

4.6 Use of recycled glass for the abatement of ibuprofen via Fenton reaction

In order to make sure our catalytic tests were carried out under the kinetic regime and to assess the feasibility of this material for this reaction, a set of different reaction conditions were taken into account by changing reaction time, stirring rate, M:S molar ratio, H_2O_2 amount and catalyst size.

4.6.1 Effect of reaction time and grain size on the activity of GTS green glass

Reaction time is a crucial parameter for evaluating catalyst performance, as both conversion and selectivity are time-dependent. If equilibrium or completion are reached, neither conversion nor selectivity will change in an observable manner.

Furthermore, as the size and, to some extent, the shape of a catalyst can also affect both conversion and selectivity, a range of reaction times and particle sizes were considered to investigate the feasibility of recycled glass as a catalyst for the absorption of ibuprofen.

These included reactions between 0 and 24 h for the oxidation of ibuprofen with three different sizes of **G1** recycled glass: <0.1 mm, 0.1-0.2 mm and 0.2-0.5 mm. Extending the reaction time from 4 hours to 24 hours resulted in improved ibuprofen conversion for all sizes of recycled glass tested, increasing from approximately 30% to 100%. This aligns with the timescale expected for efficient contaminant decomposition via hydroxyl radical oxidation from the data gathered in Chapter 3. The longer catalytic test duration enabled improved mineralization as well, evidenced by increasing CO_2 selectivity and decreasing carbon balances (Figure 4.12 b, c).

Glass particles <0.1 mm demonstrated a remarkable enhancement, enhancing ibuprofen conversion from 35% to 100% after just 3 hours, along with notable improvements in H_2O_2 consumption (Figure 4.12 c). This indicated that the ·OH radicals generated from H_2O_2 readily converted ibuprofen to intermediates and the formation CO_2 that matched the CMB% value. Whereas glass with diameters of 0.1-0.2 mm and 0.2-0.5 mm, had approximately half the rate and only achieved a complete ibuprofen conversion and a good CO_2 after 24 h reaction. The

smaller sizes probably provide more exposed catalytic sites interacting with hydrogen peroxide to support hydroxyl radical generation. Approximately 4 times larger in terms of outer layer at fixed mass assuming 10 µm catalyst depth accessible to the surroundings.

At 6 h reaction time, grains of <0.1 mm, led to 100% ibuprofen conversion, while 75% of the H_2O_2 was consumed, as the added H_2O_2 was calculated after complete mineralisation of ibuprofen. Therefore, at this stage, the reaction mixture contains only intermediates, as evidenced by a largely positive CMB% (Figure 4.12b). The resident toxic intermediates were fully converted with <0.1 mm diameter after 6 h, so the 6 h reaction can be considered a good starting point for optimization.
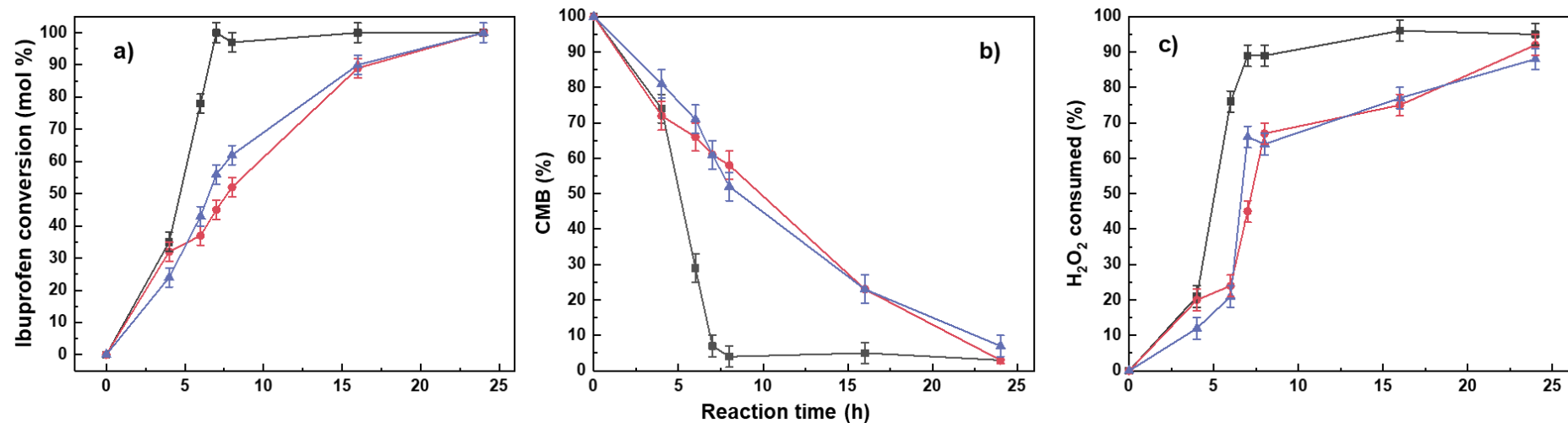
Figure 4.12 Effect of reaction time (up to 24 h) and grain sizes (<0.1 mm (■), 0.1-0.2 mm (●) and 0.2-0.5 mm (●)) on ibuprofen decomposition with GTS green glass as catalyst via Fenton reaction. Catalyst activity is evaluated in terms of: a) Ibuprofen conversion (mol %), b) CMB (%) and (c) H_2O_2 consumption (%). Reaction conditions: 50 mL of ibuprofen (20 mg L^{-1}), **G1** recycled glass (Fe: 0.2 wt.%), <0.1 mm, 0.1-0.2 mm and 0.2-0.5 mm, M:S=1:5, ibuprofen:H_2O_2=1:33, p = endogenous, 80 °C, reaction time: 0, 4, 6, 7, 8, 16, 20 and 24 h, 500 rpm. The rate of ibuprofen decomposition by **G1** recycled glass (<0.1 mm) as starting catalyst is the fastest due to the higher surface area as compared to the other diameters.

4.6.2 Effect of stirring rate on the activity of GTS green glass (G1)

The external diffusion is the phenomenon of mass transfer of a reagent from a fluid phase to the surface of the catalyst. It is an ever-present phenomenon for any heterogeneous catalyst and especially when the fluid phase is a liquid rather than a gas, and when the reaction is carried out in a batch reactor rather than a fluid catalytic bed. The stirring rate can significantly affect external diffusion and, therefore, affect reaction efficiency in a batch-to-batch reaction.[66,67] A low stirring rate can lead to reduced mixing of the reacting species, including the catalyst surface. Additionally, glass beads may settle at the bottom of the reaction flask, further reducing mass transfer. The combined result of these effects could be a decrease in the reaction rate. Vice versa, if an increase in stirring rate increases the conversion, and hence reduces the diffusion, the external diffusion may contribute (or even to be, as in an ideal case) the rate determining step in ibuprofen decomposition process. If, instead, no changes in the reaction-defining parameters (as in our case conversion and CMB) are detected by changing the stirring rate, this means that the reaction is not affected by mass transfer limiting phenomena, and therefore the reaction is in a kinetic regime.[66,67] To determine whether our tests operate in a kinetic or diffusion regime, the activity of the **G1** recycled glass catalyst was studied at different stirring rates (300 to 800 rpm). A particle size of less than 0.1 mm was chosen because of their larger surface area, also for the same M:S ratio, a larger number of glass beads are required, making the effect of varying the stirring rate more observable.
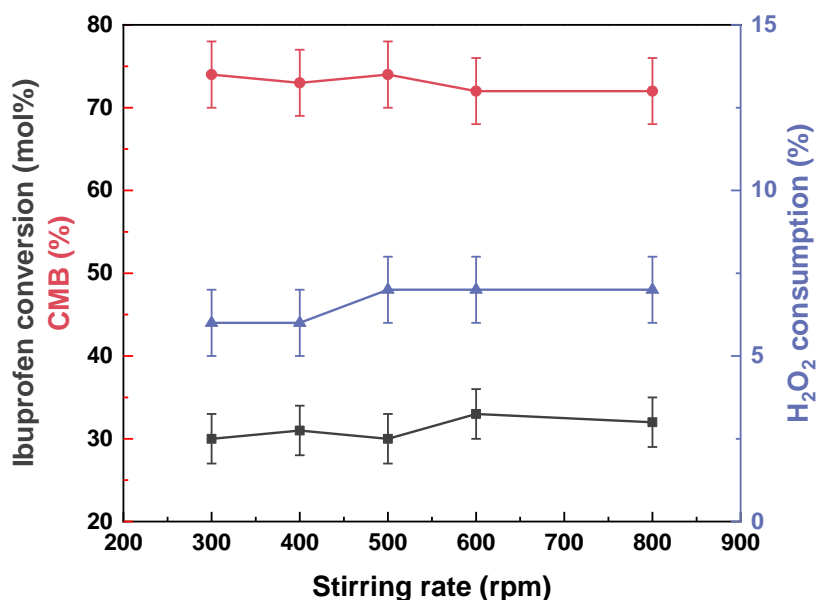
Figure 4.13 Effect of different stirring rates on activity of **G1** recycled glass (<0.1 mm) as catalyst in ibuprofen decomposition via the Fenton reaction. Catalyst activity is evaluated in terms of: ibuprofen conversion (mol % ■), CMB (% ●) and H_2O_2 consumption (% ▲) was recorded and presented. Reaction conditions: 50 mL ibuprofen (20 mg L^{-1}), **G1** recycled glass (Fe: 0.2 wt.%), <0.1 mm, M:S=1:5, ibuprofen:H_2O_2=1:33, p = endogenous, 80 °C, 4 h, 300-800 rpm.

The ibuprofen conversion and CMB% with changing in stirring rate (300 to 800 rpm) were statistically identical within the experimental error (Figure 4.12). H_2O_2 consumption also showed a constant value under different stirring rate. This implies the effects of the external diffusion limitation can be neglected when stirring speeds ranging from 300 rpm to 500 rpm are applied, and the reaction is under kinetic regime, thus reflecting the acceleration rate operated by Fe centres for our reaction.

4.6.3 Effect of initial H_2O_2 Concentration

Given the results reported in Section 4.6.2, a grain size of <0.1 mm and a stirring rate of 500 rpm, were selected for the investigation of the optimal amount of H_2O_2 to achieve high ibuprofen conversion.

The use of H_2O_2 is essential during CWPO, the theoretical minimum and stoichiometric amount of H_2O_2 required for compete ibuprofen mineralization is 33 times of ibuprofen added. However, stoichiometric amount did not normally lead to a full mineralization due to undesired scavenging effects of H_2O_2,[58] therefore, more H_2O_2 for the mineralization of this substrate is always in need. However, it was explained previously that, higher amount of H_2O_2 may lead to an opposite result where too much free radicals are present.[68] Hence, the identification of an appropriate range for H_2O_2 to be used without being affected by the undesired side-reactions is important when designing this kind of experiments and tests.

With catalyst diameter less than 0.1 mm, the increase for H_2O_2 from 1:33 to 1:40 resulted in a sharp increase of the ibuprofen conversion from approximately 35% to around 85%, with the CO_2 selectivity increased accordingly shown by the decreasing trend of CMB%. Whereas further increase in H_2O_2 amount to 1:160 only resulted in a slightly increase of ibuprofen conversion to 95 % (Figure 4.14 a). Thus, it will not be worth to increase the amount of H_2O_2 beyond 1:40, as this will just lead to a slight improvement only in the ibuprofen conversion. The consumed H_2O_2:IBU ratio gradually increased to 28 (Figure 4.14 c) after the total H_2O_2 was added into the reaction, this matched with the ibuprofen conversion and CMB% as a complete mineralization was not observed. It re-enforced the result from section 4.4 whereby changing only the H_2O_2 dosage is hard to achieved mineralisation due to potential scavenging effects.
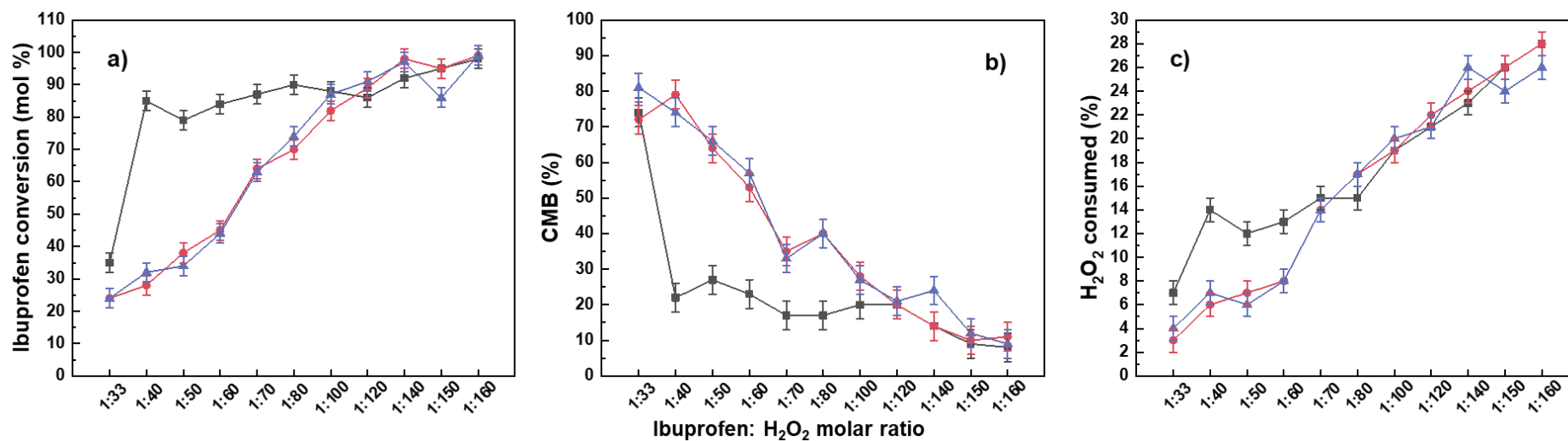
Figure 4.14 Effect of initial ibuprofen to H_2O_2 ratio (1:33-1:160) in ibuprofen decomposition with **G1** recycled glass as catalyst (<0.1 (■), 0.1-0.2 (●) and 0.2-0.5 (▲)) mm via Fenton reaction. Catalyst activity is evaluated in terms of: a) Ibuprofen conversion (mol %), b) CMB (%) and (c) H_2O_2 consumption (%). Reaction conditions: 50 mL of ibuprofen (20 mg L^{-1}), **G1** recycled glass (Fe: 0.2 wt.%), <0.1, 0.1-0.2 and 0.2-0.5 mm, M:S=1:5, p = endogenous, 80 °C, 4 h, 500 rpm. Activity of glass with diameter <0.1 mm is a higher than the other two diameters before ibuprofen to H_2O_2 ratio of 1:100, after this ratio, the difference between three diameters is negligible.

For catalyst with diameters 0.1-0.2 and 0.2-0.5 mm, a plateau of ibuprofen conversion (98 ± 4%) was only observed after further increasing of the H_2O_2 dosage to 1:100 (Figure 4.16 a). The difference in conversion across glass bead diameters can be attributed to the change in surface area for a fixed catalyst mass. Assuming (Section 3.7.1) an interaction of the catalyst surface with the surroundings equal to a penetration depth of 10 μm and spherical shape, the relative surface areas for 0.1 mm, 0.2 mm and 0.5 mm beads are estimated to be 16:9:4. Thus, the smaller 0.1mm size presents the greatest surface area and associated iron content, enabling a faster activation of H_2O_2 into hydroxyl radicals to drive ibuprofen decomposition. However, with increasing H_2O_2 dosage, the slower reaction rates for larger diameters can be observed. This suggests that by tuning conditions like oxidant amounts, the different sizes can eventually achieve similar mineralization, albeit with slower kinetics for larger beads.

In conclusion, an ibuprofen:H_2O_2 ratio of 1:40 appears a good compromise amount for **G1** recycled glass diameter less than 0.1 mm for further reaction condition. Whereas with diameter 0.1-0.2 and 0.2-0.5 mm, an ibuprofen:H_2O_2 ratio of 1:100 (accounting for the experimental error) showed a promising performance in ibuprofen.

4.6.4 Effect of metal to substrate molar ratio (M:S)

In addition to stirring rate, the amount of catalyst used also affects reaction efficiency. In a batch reactor system, increasing the amount of catalyst while keeping other parameters constant should result in an increase in conversion if there are no mass transfer limitations. This however as long as the reaction has not reached completion or its equilibrium value yet. This is because there would be more catalytic active sites available to facilitate the reaction with the reactants. However, if the addition of more catalyst does not lead to an increase in rate this means the rate determining step is the diffusion control.

These tests may help to determine the minimum optimum catalyst (M:S molar ratio) required to ensure that the system achieves kinetic rather than diffusion control, while avoiding waste from excess catalyst. As a result, effect of catalyst amount was then studied with M:S from 1:40 to 10:1 (Figure 4.15).
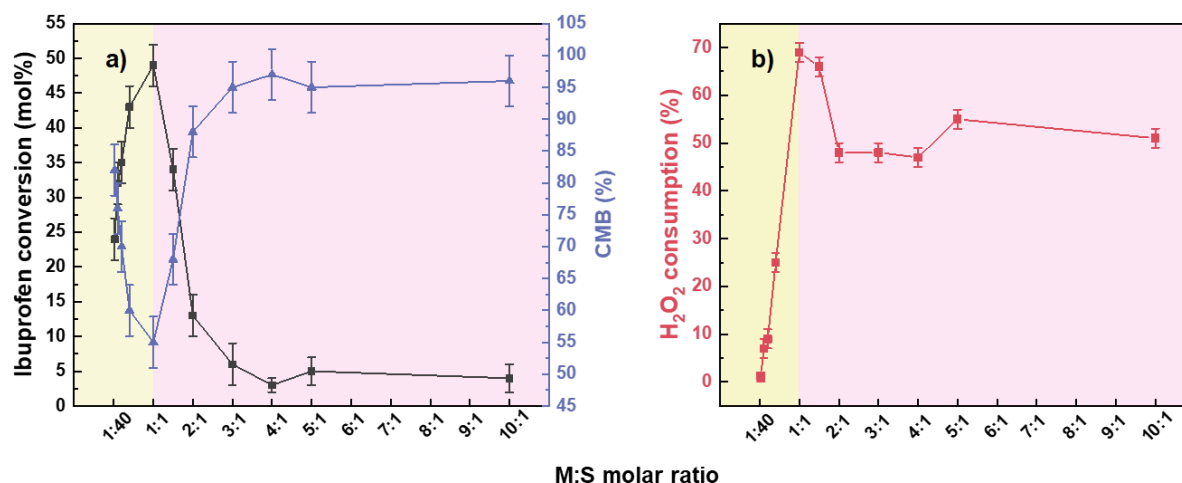
Figure 4.15 Effect of M:S ratio (1:40 – 10:1) on ibuprofen decomposition with **G1** recycled glass (<0.1 mm) as a catalyst via the Fenton reaction. Catalyst activity is evaluated in terms of: a) ibuprofen conversion (mol %■) and CMB (%▲) and (b) H_2O_2 consumption (%■). Reaction conditions: 50 mL of ibuprofen (20 mg L^{-1}), **G1** recycled glass (Fe: 0.2 wt.%), <0.1 mm, M:S=1:40-10:1, ibuprofen:H_2O_2=1:33, p = endogenous, 80 °C, 4 h, 500 rpm. Ibuprofen conversion reached a peak value at M:S=1:1 where inefficient mixing start to affect the reaction. The normal M:S ratio is 1:5, which lies well in the kinetic regime, where diffusion is negligible. Yellow area: kinetic regime, pink area: diffusion regime.

As shown previously, the diffusion effect is negligible when we use M:S ratio of 1:5 by changing the stirring rate. When the M:S ratio was lower than 1:1 (Figure 4.15: yellow area), an increasing amount of catalyst led to an increase in ibuprofen conversion to about 50%, implying that the reaction is under kinetic regimes and diffusion limitation effects can be neglected. However, when the catalyst amount was increased above 1:1 (Figure 4.15: pink area), an opposite trend was observed. Ibuprofen conversion decreased sharply and reached a plateau about 5%. It is expected to reach a plateau instead, but due to the practicality on how the experiments were done, this sudden drop in conversion could be due to the lack of physical mixing. The amount of catalyst added is too much (Table 4.7) and preclude the mixing, making the oxidation in a batch-to batch reaction much inefficient. Although this is a challenge for a preliminary study using a batch-to batch reactor, this will not be an issue with a fixed-bed reactor and will be considered for future studies. Moreover, these results show that it is not always the more the catalyst, the better.

Furthermore, despite the M:S ratio exceeding 3:1, the consumption of H_2O_2 was observed to be as high as 50%, while the conversion of ibuprofen was only 5%. This suggests that although ·OH radicals were generated; they were not utilized to react with the organic substrates and may have terminated each other during the process.

Table 4.7 Actual mass of catalyst added according to different M:S ratio from 1:40 to 10:1 to study the effect of M:S ratio of **G1** recycled glass (<0.1 mm) on ibuprofen decomposition via Fenton reaction. Reaction conditions: 50 mL ibuprofen (20 mg L^{-1}), **G1** recycled glass (Fe: 0.2 wt.%), <0.1 mm, M:S=1:40-10:1, ibuprofen:H_2O_2 =1:33, p = endogenous, 80 °C, 4 h, 500 rpm. The normal M:S ratio is 1:5, which lies well in the kinetic regime, where diffusion is negligible.

Reaction regime	M:S Molar ratio	Catalyst amount g
Negligible diffusion /Kinetic regime	1:40	0.005
	1:10	0.02
	1:5	0.04
	1:2.5	0.07
Turning point	1:1	0.2
Non-negligible diffusion /Diffusion regime	1.5:1	0.3
	2:1	0.4
	3:1	0.6
	4:1	0.7
	5:1	0.9
	10:1	1.9

To summarize, without changing the stirring rate, the diffusion effect is negligible for reactions with M:S ratios less than 1:1, when the catalyst amount is over this threshold, diffusion limitation will dominate and be the rate determining step, causing an opposite effect on overall conversion and a waste of resources. Therefore, the chosen M:S ratio of 1:5 or even 1:2.5 can be an ideal amount in terms of catalyst activity and experimental preparation for our set up.

Overall, complete ibuprofen conversion, high H_2O_2 consumption and CO_2 formation, thorough oxidation of toxic intermediates was obtained. Thus, indicating it is possible to achieve a water purification efficiently from the aspect of low toxicity and high biodegradability with the recycled GTS green catalyst under the experimental conditions. Therefore, with appropriate choice of reaction parameters, full mineralization within a reaction time of 4 h can be achieved. As a reference, this time is comparable with using zeolite of the decomposition of aromatic compounds.[69]

With different reaction condition and decreased cost, high water purification can be achieved. Decomposition of ibuprofen with other colour of recycled glass that contain Fe^{3+} was then conducted to investigate the possibilities Fenton-like reactions in ibuprofen purification with the above reaction condition as a start.

4.7 Activity of various types of glass as heterogeneous catalyst in the CWPO of ibuprofen

Based on the results from **G1** recycled glass, other recycled glasses with various colours like

other green (**G2**), brown (**G3**) and transparent (**G4**) that contain iron (0.3, 0.2 and 0.07% respectively) were considered to have the ability to trigger the Fenton reaction of ibuprofen. Considering potential post-treatment operations to the catalyst, sizes larger than 0.1 mm are preferred for ease of recovery. Therefore, in this section, the investigation of various types of recycled glasses with diameters of 0.1 to 1 mm toward their catalytic activity in the decomposition of ibuprofen was conducted based on the optimum conditions derived from 0.1 mm GTS green glass. The goal was to assess the trade-off between increased surface area and ease of recovery, and in turn reuse, for the different glass bead sizes.

For each type of glass -although with different iron content - an increased ibuprofen conversion was observed while decreasing in diameter. That said, within the ranges that have been explored (<0.1 to 0.5 mm), particle size is more important than the Fe content. This is expected as a fixed M:S molar ratio resulted in the same amount of catalyst required for each diameter. Therefore, the smaller the diameter, the higher the surface area, indicating a higher amount of iron available for ·OH generation. In contrast, at different diameters, different iron content associated with the glass demonstrated no clear effect in ibuprofen conversion, implying that if the M:S ratio and diameter were determined, the type of recycled glass for desired ibuprofen conversion only varied by the mass required due to different iron amount possessed. Moreover, although different recycled glass demonstrated different activity, diameters larger than 0.1 mm showed relatively better activity through all type of glasses and showing a promising ibuprofen conversion, low CMB%, relatively high H_2O_2 consumption (17%) (Figure 4.16 b, c) and low metal leaching (less than 0.2 wt.% measure by ICP-OES), therefore, can be the second better choice. This highlights that possibility that recycled glasses can be collected and cleaned without proper separation in terms of colour; a simplified pre-treatment of the glassed can be achieved by controlling a diameter range of 0.1-0.5 mm for brown and green of any brand with reasonable iron content. This idea can be tested in the future experiments. The post-treatment of filtering out the catalyst is easier with this range of diameter as compared to those with less than 0.1 mm. This further reduced the cost of using recycled glass and at the same time contributing to circular economy.
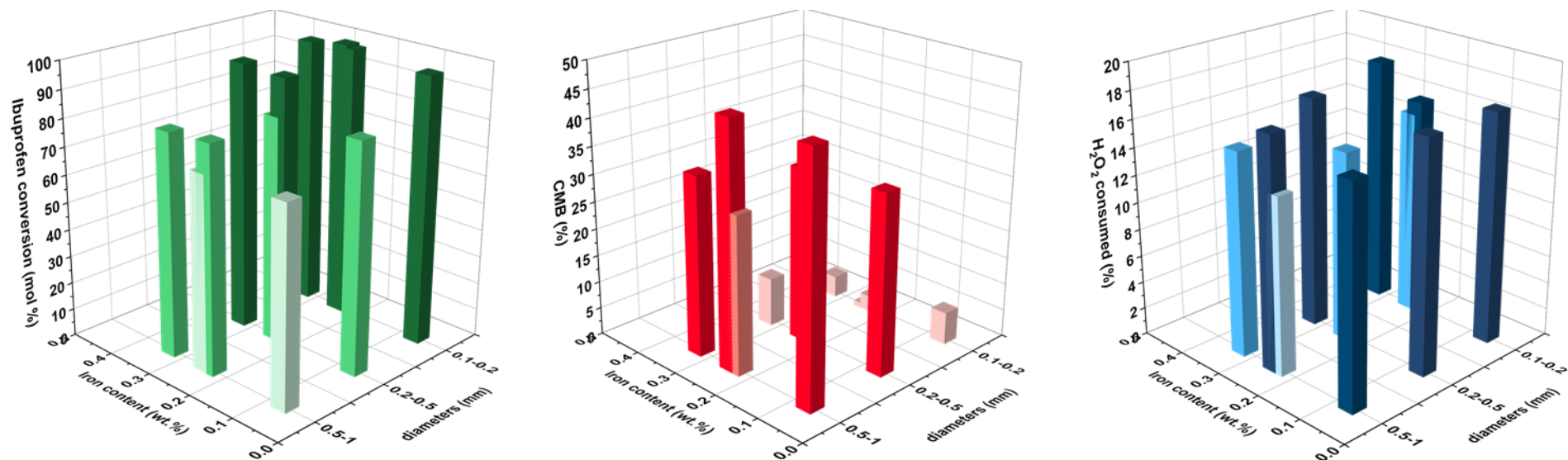
Figure 4.16 Activity of four different types of recycled glass, **G1**, **G2**, **G3**, **G4** (Fe content 0.2, 0.3, 0.2 and 0.07 wt.% respectively) in ibuprofen decomposition with three catalyst sizes:<0.1, 0.1-0.2 and 0.2-0.5 mm via the Fenton reaction. Catalyst activity is evaluated in terms of: a) Ibuprofen conversion (mol %), >95% (●), 80-95% (●) and 71-80% (●). b) CMB (%) >30% (●), 15-30 % (●) and 0-15 % (○) and (c) H_2O_2 consumption (%, max consumption 23%): >15 % (●), 13-15% (●) and 12-13 % (○). Reaction conditions: 50 mL of ibuprofen (20 mg L^{-1}), ibuprofen:H_2O_2=1:140, p = endogenous, 80 °C, 4 h, 500 rpm.

4.8   Conclusion

Agriculture is the largest large scale consumer of fresh water globally, with particularly high usage in European nations.[70] However, the presence of recalcitrant micro pollutants such as pharmaceutical residues poses threats to both crop cultivation and connected ecosystems.[71,72] Ibuprofen, a frequently detected anti-inflammatory drug, has shown phytotoxic impacts that inhibit plant growth at concentrations as low as 40 µg L^{-1} [73,74] Conventional wastewater treatment methods can be insufficient in fully removing ibuprofen as explained in Chapter 1. Catalytic Wet Peroxide Oxidation (CWPO) has recently shown promise as an alternative advanced technology for ibuprofen mitigation.[75] Drawing inspiration from glass-catalysed phenol degradation (Chapter 3), this work investigates recycled glass for ibuprofen removal. The use of waste glass embodies the concept of the circular economy, where materials are reused to reduce the overall cost of wastewater treatment, which in turn benefits the irrigation of the plant. The benefits generated may affect other sectors, thus resulting in a net saving of resources.

The solubility of ibuprofen in water is relatively low, with an estimated value of 72 mg L^{-1} determined by High-Performance Liquid Chromatography (HPLC). This value sets an upper limit for use in investigating the degradation of ibuprofen. Additionally, the presence of potentially more toxic intermediates, such as 4-ethylbenzaldehyde, necessitated the characterization of the eleven detected intermediates during the Catalytic CWPO process using both HPLC and GCMS methods. This step was taken to ensure the complete removal of both ibuprofen and any more toxic intermediates generated during the CWPO process.

In CWPO processes, hydroxyl radicals play a crucial role in oxidation. However, it has been observed that, in the absence of any catalyst, an excessive dosage of H_2O_2 (H_2O_2 to ibuprofen molar ratio of 400) can lead to severe scavenging effects, resulting in a waste of resources. Moreover, it has been found that achieving complete ibuprofen conversion is difficult without the presence of a suitable catalyst. In this regard, a comparison between the use of Fe^{2+} and Fe^{3+} as catalysts was investigated. The study revealed that the rate of reaction with of Fe^{3+} was as twice slower than Fe^{2+} at the early stage of the reaction (5-10 h out of 24 h), but due to the redox cycle, the difference in reaction rate becomes negligible over time (over 24 h). This finding provides a basis for exploring the use of other heterogeneous catalysts containing Fe^{3+}, which is the most stable oxidation state of iron.

To ensure that our catalytic tests were carried out under the kinetic regime using **G1** recycled glass as a representative, a range of different reaction parameters were studied. These parameters included reaction time (4-24 h), stirring rate (300-800 rpm), M:S (1:40 to 10:1),

ibuprofen to H_2O_2 ratio (1:33-1:160), and catalyst size (<0.1 mm, 0.1-0.2 mm and 0.2-0.5 mm). The findings suggested that, with an appropriate choice of reaction parameters, full mineralization of ibuprofen within 4 hours could be achieved. Building on these promising results, other types of recycled glass **G2**, **G3**, **G4** with iron content ranging from 0.3, 0.2 and 0.07 wt.% respectively and three different glass diameters (0.1-0.2, 0.2-0.5, and 0.5-1 mm) were investigated. Irrespective of the iron content, it was found that the smaller the diameter of the recycled glass catalyst, the higher the ibuprofen conversion due to the higher surface area, and in turn the supposed fraction of Fe in contact with the surroundings and the solution. In addition, a low metal leaching (less than 0.2 wt.%) of all types of recycled glass ensures that the catalyst can be reused.

In summary, the application of recycled glass as a catalyst in the removal of ibuprofen has been extensively studied, and promising results have been obtained. The use of recycled glass as a catalyst not only provides a greener approach to ibuprofen removal but also enables the application of circular economy principles such as waste valorisation. For example, recycled glass materials are used in construction applications as a substitute for sand in concrete, allowing diversion from landfills and reducing raw material needs.[76] Other efforts have investigated converting waste glass into supplemental cementitious materials, again displacing traditional concrete formulations.[77] This work mirrors these concepts by utilizing recycled glass waste as a catalyst instead of conventional manufactured catalysts, allowing demonstration of circular principles where materials are recovered at their highest value to reduce the need for new resource inputs. Additional future circular applications could investigate reusing any post-process glass material as construction fillers, embodying the reducing, reusing, and recycling system mind-set. The success of this study provides a strong basis for exploring other potential applications of recycled glass catalysts, including the synthesis of fine chemicals.

4.9   References

(1)   FAO. *Water for Sustainable Food and Agriculture Water for Sustainable Food and Agriculture*; 2017.

(2)   Pimentel, D.; Berger, B.; Filiberto, D.; Newton, M.; Wolfe, B.; Karabinakis, E.; Clark, S.; Poon, E.; Abbett, E.; Nandagopal, S. Water Resources: Agricultural and Environmental Issues. In *Food, Energy, and Society, Third Edition* 2007, **54**, 183-200.

(3)   Priya, A. K.; Gnanasekaran, L.; Rajendran, S.; Qin, J.; Vasseghian, Y. *Environmental Research*, 2022, **204**, 112298.

(4)   Scaria, J.; Gopinath, A.; *Journal of Cleaner Production*, 2021, **278**, 124014.

(5)   Weber, F.-A.; Aus Der Beek, T.; Carius, A.; Grüttner, G.; Hickmann, S.; Ebert, I.; Hein, A.; Küster, A.; Rose, J.; Koch-Jugl, J.; Stolzenberg, H.-C. *Environmental Toxicology and Chemistry*, 2014, **35**, 823-835.

(6)   Ebele, A. J.; Abdallah, M. A.; Harrad, S. *Emerging Contaminants,* 2017, **3**, 1-16.

(7)   Patel, M.; Kumar, R.; Kishor, K.; Mlsna, T.; Pittman Jr, C. U.; Mohan, D. *Chemical reviews*, 2019, **119**, 3510-3673.

(8)   Raitano, G.; Goi, D.; Pieri, V.; Passoni, A.; Mattiussi, M.; Lutman, A.; Romeo, I.; Manganaro, A.; Marzo, M.; Porta, N.; Baderna, D.; Colombo, A.; Aneggi, E.; Natolino, F.; Lodi, M.; Bagnati, R.; Benfenati, E. *Environment International*, 2018, **119**, 275-286.

(9)   Nikolaou, A.; Meric, S.; Fatta, D. *Analytical and bioanalytical chemistry*, 2007, **387**, 1225–1234.

(10)   Mussa, Z. H.; Al-Qaim, F. F.; Jawad, A. H.; Scholz, M.; Yaseen, Z. M. *Toxics*, 2022, **10**, 598.

(11)   Luo, Y.; Guo, W.; Ngo, H. H.; Nghiem, L. D.; Hai, F. I.; Zhang, J.; Liang, S.; Wang, X. C. *Science of The Total Environment*, 2014, **473-474**, 619-641.

(12)   Guerra, P.; Kim, M.; Shah, A.; Alaee, M.; Smyth, S. A. *Science of the Total Environment*, 2014, **473-474**, 235-243.

(13)   Vergeynst, L.; Haeck, A.; De Wispelaere, P.; Van Langenhove, H.; Demeestere, K. *Chemosphere*, 2015, **119**, S2-8.

(14)   Matongo, S.; Birungi, G.; Moodley, B.; Ndungu, P. *Chemosphere*, 2015, **134**, 133-140.

(15)   Vazquez-Roig, P.; Andreu, V.; Blasco, C.; Picó, Y. *Science of The Total Environment*, 2012, **440**, 24-32.

(16)   Wijaya, L.; Alyemeni, M.; Ahmad, P.; Alfarhan, A.; Barcelo, D.; El-Sheikh, M. A.; Pico, Y. *Plants (Basel)*, 2020, **9**, 1473.

(17)   Gonzalez-Rey, M.; Bebianno, M. J. *Environmental Toxicology and Pharmacology*, 2012, **33**, 361-371.

(18)   Han, S.; Choi, K.; Kim, J.; Ji, K.; Kim, S.; Ahn, B.; Yun, J.; Choi, K.; Khim, J. S.; Zhang, X.; Giesy, J. P. *Aquatic Toxicology*, 2010, **98**, 256-264.

(19)   Wang, L.; Peng, Y.; Nie, X.; Pan, B.; Ku, P.; Bao, S. *Comparative Biochemistry and Physiology Part C: Toxicology & Pharmacology*, 2016, **179**, 49-56.

(20)   Yan, Y.; Jiang, S.; Zhang, H. *Separation and Purification Technology*, 2014, **133**, 365-374.

(21)   Feng, L.; Song, W.; Oturan, N.; Karbasi, M.; van Hullebusch, E. D.; Esposito, G.; Giannakis, S.; Oturan, M. A. *Chemical Engineering Journal*, 2023, **451**, 138483.

(22)   Zheng, B. G.; Zheng, Z.; Zhang, J. B.; Luo, X. Z.; Wang, J. Q.; Liu, Q.; Wang, L. H. *Desalination*, 2011, **276**, 379-385.

(23)   Ali, S.; Akhtar, T.; Alam, M. *International Journal of Research in Engineering and Social Sciences*, 2015, **5**, 14-26.

(24)   Santos, J. L.; Aparicio, I.; Alonso, E. *Environment International*, 2007, **33**, 596-601.

(25)   Wang, S.; Song, Z.; Wang, J.; Dong, Y.; Wu, M. *Journal of Chemical & Engineering Data*, 2010, **55**, 5283-5285.

(26)   Hussain, S.; Aneggi, E.; Briguglio, S.; Mattiussi, M.; Gelao, V.; Cabras, I.; Zorzenon, L.; Trovarelli, A.; Goi, D. *Journal of Environmental Chemical Engineering*, 2020, **8**, 103586.

(27)   Lyu, L.; Zhang, L.; Wang, Q.; Nie, Y.; Hu, C. *Environmental Science & Technology*, 2015, **49**, 8639-8647.

(28)   Ziylan, A.; Ince, N. H. *Catalysis Today*, 2015, **240**, 2-8.

(29)   Adityosulindro, S.; Barthe, L.; González-Labrada, K.; Jáuregui Haza, U. J.; Delmas, H.; Julcour, C. *Ultrasonics Sonochemistry*, 2017, **39**, 889-896.

(30)   Adityosulindro, S.; Julcour, C.; Barthe, L. *Journal of Environmental Chemical Engineering*, 2018, **6**, 5920-5928.

(31)   Monteiro, R. T.; Santana, R. M. da R.; Silva, A. M. R. B. da; Lucena, A. L. A. de; Zaidan, L. E. M. C.; Silva, V. L. da; Napoleão, D. C. *Revista Eletrônica em Gestão, Educação e Tecnologia Ambiental*, 2018, **22**, 3.

(32)   Méndez-Arriaga, F.; Esplugas, S.; Giménez, J. *Water Research*, 2010, **44**, 589-595.

(33)   Hirami, Y.; Hunge, Y. M.; Suzuki, N.; Rodríguez-González, V.; Kondo, T.; Yuasa, M.; Fujishima, A.; Teshima, K.; Terashima, C. *Journal of Colloid and Interface Science*, 2023, **642**, 829-836.

(34)   Sabri, N.; Hanna, K.; Yargeau, V. *Science of The Total Environment*, 2012, **427-428**, 382-389.

(35)   Caviglioli, G.; Valeria, P.; Brunella, P.; Sergio, C.; Attilia, A.; Gaetano, B. *Journal of Pharmaceutical and Biomedical Analysis*, 2002, **30**, 499-509.

(36)   Marković, M.; Jović, M.; Stanković, D.; Kovačević, V.; Roglić, G.; Gojgić-Cvijović, G.; Manojlović, D. *Science of the Total Environment*, 2015, **505**, 1148-1155.

(37)   Han, Z.; Lu, L.; Wang, L.; Yan, Z.; Wang, X. *Chromatographia*, 2017, **80**, 1353-1360.

(38)   Loaiza-Ambuludi, S.; Panizza, M.; Oturan, N.; Özcan, A.; Oturan, M. A. *Journal of Electroanalytical Chemistry*, 2013, **702**, 31-36.

(39)   Skoumal, M.; Rodríguez, R. M.; Cabot, P. L.; Centellas, F.; Garrido, J. A.; Arias, C.; Brillas, E. *Electrochimica Acta*, 2009, **54**, 2077-2085.

(40)   Marco-Urrea, E.; Pérez-Trujillo, M.; Vicent, T.; Caminal, G. *Chemosphere*, 2009, **74**,

(41)   Illés, E.; Takács, E.; Dombi, A.; Gajda-Schrantz, K.; Rácz, G.; Gonter, K.; Wojnárovits, L. *Science of The Total Environment*, 2013, **447**, 286-292.

(42)   Scheers, T.; Appels, L.; Dirkx, B.; Jacoby, L.; Van Vaeck, L.; Van der Bruggen, B.; Dewil, R. *Desalination and water treatment*, 2012, **50**, 189-197.

(43)   Rao, Y.; Xue, D.; Pan, H.; Feng, J.; Li, Y. *Chemical Engineering Journal*, 2016, **283**, 65-75.

(44)   Zeng, J.; Yang, B.; Wang, X.; Li, Z.; Zhang, X.; Lei, L. *Chemical Engineering Journal*, 2015, **267**, 282-288.

(45)   Reza, D.; Behzad, S.; Farid, F.; Rezvan, B. *Environmental Technology & Innovation*, 2018, **11**, 308-320.

(46)   Raab, M. T., Prýmek, A. K., & Giordano, A. N. *Journal of Undergraduate Chemistry Research*, 2021, **20**, 68.

(47)   Janus, E.; Ossowicz, P.; Klebeko, J.; Nowak, A.; Duchnik, W.; Kucharski, Ł.; Klimowicz, A. *RSC advances*, 2020, **10**, 7570-7584.

(48)   Kocbek, P.; Baumgartner, S.; Kristl, J. *International Journal of Pharmaceutics*, 2006, **312**, 179-186.

(49)   Jouyban, A.; Soltanpour, S.; Acree, W. E. *Journal of Chemical & Engineering Data*, 2010, **55**, 5252-5257.

(50)   Bhattamishra, S. D.; Padhy, R. K. *Indian Journal of Chemical Technology*, 2009, **16**, 426-430.

(51)   Bolten, D.; Lietzow, R.; Türk, M. *Chemical Engineering and Technology*, 2013, **36**, 426-434.

(52)   Li, Z.; Tan, X.; Wu, J.; Jiang, Y.; Gai, H. *Chinese Journal of Environmental Engineering*, 2018, **12**, 760-767.

(53)   Cihanoğlu, A.; Gündüz, G.; Dükkancı, M. *Applied Catalysis B: Environmental*, 2015, **165**, 687-699.

(54)   Queirós, S.; Morais, V.; Rodrigues, C. S. D.; Maldonado-Hódar, F. J.; Madeira, L. M. *Separation and Purification Technology*, 2015, **141**, 235-245.

(55)   Adityosulindro, S.; Barthe, L.; González-Labrada, K.; Jáuregui Haza, U. J.; Delmas, H.; Julcour, C. *Ultrasonics Sonochemistry*, 2017, **39**, 889-896

(56)   Monteiro, R. T.; Santana, R. M. da R.; Silva, A. M. R. B. da; Lucena, A. L. A. de; Zaidan, L. E. M. C.; Silva, V. L. da; Napoleão, D. C. *Revista Eletrônica em Gestão, Educação e Tecnologia Ambiental*, 2018, **22**, 3.

(57)   Adityosulindro, S.; Julcour, C.; Barthe, L. *Journal of Environmental Chemical Engineering*, 2018, **6**, 5920-5928.

(58)   Prasad, J.; Tardio, J.; Jani, H.; Bhargava, S. K.; Akolekar, D. B.; Grocott, S. C. *Journal of Hazardous Materials*, 2007, **146**, 589-594.

(59)   De Laat, J.; Gallard, H. *Environmental science & technology*, 1999, **33**, 2726-2732.

(60)   Abbot, J.; Brown, D. G. *Canadian Journal of Chemistry*, 1990, **68**, 1537-1543.

(61)   Hiatt, R. R.; Strachan, W. M. J. *The Journal of Organic Chemistry*, 1963, **28**, 1893-1894.

(62)   Lin, C. C.; Smith, F. R.; Ichikawa, N.; Baba, T.; Itow, M. *International Journal of Chemical Kinetics*, 1991, **23**, 971-987.

(63)   Mok, J. S.; Helms, W. J.; Sisco, J. C.; Anderson, W. E. *Journal of Propulsion and Power*, 2005, **21**, 942-953.

(64)   Tse, K. M. The Kinetics and Induced Decomposition on the Thermal Decomposition of Hydroperoxides (Master Thesis, University of Brock), 1976.

(65)   Williams, B. H. *Transactions of the Faraday Society*, 1928, **24**, 245.

(66)   Bankupalli, S.; Kotra, V.; Cheedipudi, V. L. *International Journal of Chemical Reactor Engineering*, 2008, **6**, 1.

(67)   Taran, O. P.; Zagoruiko, A. N.; Yashnik, S. A.; Ayusheev, A. B.; Pestunov, A. V.; Prosvirin, I. P.; Parmon, V. N. *Journal of Environmental Chemical Engineering*, 2018, **6**, 2551-2560.

(68)   Sandri, F.; Danieli, M.; Zecca, M.; Centomo, P. *ChemCatChem*, 2021, **13**, 2653-2663.

(69)   Kanakaraju, D.; Glass, B. D.; Oelgemöller, M. Advanced Oxidation Process-Mediated Removal of Pharmaceuticals from Water: A Review. *Journal of Environmental Management*, 2018, **219**, 189–207.

(70)   United Nations, The United Nations World Water Development Report 2023: Partnerships and Cooperation for Water. UNESCO, Paris.

(71)   Pinto, I.; Simões, M.; Gomes, I. B. *Antibiotics (Basel)*, 2022, **11**, 1700.

(72)   Moghadam, A. A.; Shuai, W.; Hartmann, E. M. *Current Opinion in Biotechnology*, 2023, **80**, 102902.

(73)   Pietrini, F.; Di Baccio, D.; Aceña, J.; Pérez, S.; Barceló, D.; Zacchini, M. *Journal of hazardous materials*, 2015, **300**, 189-193.

(74)   Abbasi, N. A.; Shahid, S. U.; Majid, M.; Tahir, A. Chapter 17 - Ecotoxicological Risk Assessment of Environmental Micropollutants. In *Environmental Micropollutants*; Hashmi, M. Z., Wang, S., Ahmed, Z., Eds.; Advances in Pollution Research; Elsevier, 2022; 331–337.

(75)   Huaccallo-Aguilar, Y.; Diaz de Tuesta, J. L.; Álvarez-Torrellas, S.; Gomes, H. T.; Larriba, M.; Ovejero, G.; García, J. *Journal of Environmental Management*, 2021, **281**, 111913.

(76)   Nassar, R.-U.-D.; Soroushian, P. *Construction and Building Materials*, 2012, **29**, 368-377.

(77)   Li, B.; Ling, T. C.; Yu, J. G.; Wu, J.; Chen, W. *Journal of Cleaner Production*, 2019, **241**, 118155.

Chapter 5 Benzyl alcohol selective oxidation using recycled glass

5.1   Introduction

Benzyl alcohol (BnOH) is an important aromatic alcohol used as a solvent in inks, paints, glues, and resins,[1] in household cleaners and detergents,[2] and as a food additive like almond products.[3] Because of its organoleptic properties, it is a member of the fragrance structural group aryl alkyl alcohols, being frequently used as a fragrance ingredient in several consumer products such as shampoos, soaps, and cosmetic products.[2] Noteworthy, it has bacteriostatic and antiseptic properties with however a modest toxicity, which increases its versatility.[2] The oxidation of benzyl alcohol to benzaldehyde – together with the oxidation of benzyl alcohol homologues - is also an important process, both in industry and academia.[4,5] In industry it is used as the raw material for a large number of products, including perfume, beverage, pharmaceutical intermediates.[6–9] They are also of interest as a replacement source of fine chemicals due to the future limited supply of petroleum remaining, as this decreasing supply is leading to a continual rise in petroleum price. Therefore, it made benzyl alcohol an important chemical that has been produced extensively. In the industrial production process, its wastewater contains a significant amount of benzyl alcohol, with concentrations ranged from 0.5 to 21 g L^{-1}.[10,11] From the promising results described Chapters 3 and 4 concerning the degradation of phenol and ibuprofen, this prompted us to investigate the possibility to apply recycled glass via Fenton reaction for the removal or the selective oxidation of benzyl alcohol.

In fact, in academia, BnOH can be considered as a model compound for the investigation and development of novel catalysts.[12,13] This is because the oxidation of benzyl alcohol is expected to lead to one product only, benzaldehyde (unless additional oxidation of the aldehyde to the benzoic acid: Figure 5.1) and, as such, it is possible to probe acid properties by reaction with the OH group of the molecule or by activating the C-H bond in alpha to the hydroxyl one. Furthermore, this partial oxidation may be carried out at a relatively mild conditions which is a further advantage for our study and to assess the capability of iron centres in recycle glass to carry out such an oxidation reaction.
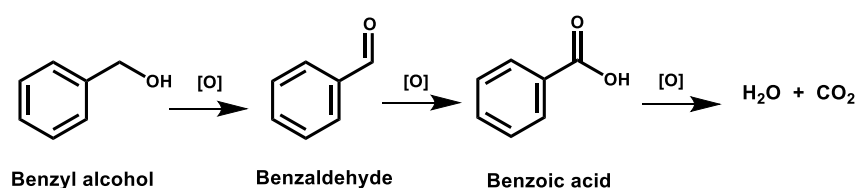
Figure 5.1 General schematics for the oxidation of benzyl alcohol to benzaldehyde, benzoic acid, and ultimately water and carbon dioxide. [O] is an arbitrary oxidant containing oxygen.

Traditionally, benzaldehyde is synthesized by hydrolysis of benzyl chloride or vapor/liquid-phase oxidation of toluene. In the former method, the chlorinated by-products and corresponding toxic acidic would be generated, which is undesirable for scale-up and industrial application,[14,15] while the vapor/liquid oxidation of toluene was also limited because of the harsh reaction conditions (120–150 °C and at 10 atm)[16] and low selectivity (5%).[17,18] Benzaldehyde production from benzyl alcohol oxidation is widely adopted in industry.[4,5] As explained above, this has resulted in benzyl alcohol being chosen as a model compound for catalytic oxidation reactions, allowing the screening of new catalysts and helping benchmark the catalyst's activity.

However, this is achieved by using oxidants with a strong oxidizing property such as potassium permanganate ($KMnO_4$)[19] and dichromate ($K_2Cr_2O_7$).[20] However, a series of environmental issues are present, like heavy metal residues that also need to be disposed of, which besides a high environmental impact also needs a higher treatment cost, making them non-ideal for industry aimed for cleaner production. Therefore, the use of green oxidants such as H_2O_2[21] and O_2[9,22–26] has attracted extensive attention for many years.

It is noted that, in the absence of a catalyst neither O_2 nor H_2O_2 have appreciable activity. Therefore, the choice of catalyst is important to exploit these green oxidants. In the past decade, heterogeneous precious metals catalysts, like Au,[27,28] Pt,[29] Ru,[30] and Pd[31] were employed for the selective oxidation of benzyl alcohol to benzaldehyde, based on their excellent performances. However, the high cost and limited resource of noble metals hindered their practical application on a large scale (unless very small amount <0.3 wt.% of precious metal is used). Therefore, non-toxic, Earth abundant, and low environmental impact Fe-based catalysts as among the most environmentally friendly have been a focus of attentions.[32–36]

Based on this and the properties of recycled glass described so far, the use of recycled glass as a catalyst for the oxidation of benzyl alcohol is considered. Although the potential for complete mineralisation of benzyl alcohol via the Fenton reaction will be investigated on the basis of previous results, the primary objective of this chapter is to explore the applicability of using recycled glass as a catalyst for the selective oxidation of benzyl alcohol to benzaldehyde, a valuable intermediate in fine chemical synthesis.

Therefore, in this chapter the following aspects will be investigated: 1) development of a ^{1}H-NMR method with a suitable internal standard for benzyl alcohol and its oxidation products, particularly benzaldehyde; 2) evaluation of recycled glass catalysis for selective oxidation of benzyl alcohol to the valuable benzaldehyde intermediate; 3) exploration of the potential for

complete mineralization of the pollutant benzyl alcohol using recycled glass catalysis and H_2O_2 as the oxidant.

5.2   Development of an ^{1}H-NMR benzyl alcohol quantification method

In the case of phenol and ibuprofen mineralization a large number of intermediates could be detected (Sections 3.5 and 4.2), and for those compounds HPLC coupled with UV-Vis was used to separate and identify the compounds. Benzyl alcohol oxidation, on the other hand, is expected to lead to two main oxidation products only, benzaldehyde and benzoic acid before being further degraded to acids from ring opening and ultimately water and carbon dioxide. (Figure 5.1) In this case, NMR, which allows rapid and cheap analysis of samples, is preferred, as this allows the screening of a large number of samples in a relatively short time if compared to chromatographic methods.

A flow chart (Figure 5.2) clearly explains the steps required to validate the NMR method. In order to accurately quantify the reaction components, it is essential that the ^{1}H-NMR spectra and characteristic peaks of each individual compound (benzyl alcohol, benzaldehyde, and other potential intermediates/products) are fully characterised and identified before the method is applied to actual reaction mixtures. Next, an appropriate internal standard need to be chosen (Section 5.2.2). Once the determination of the carbon mass balance calculation is compatible with 100% (and it must be because the mixture for quantification is prepared, so no decarboxylation can occur), the method is then validated for further use.

Criteria:
1. Chemical shift: well-defined and distinct.
2. Minimal interference from other components.
3. Stability.
4. Non-reactivity during experiment and NMR analysis.
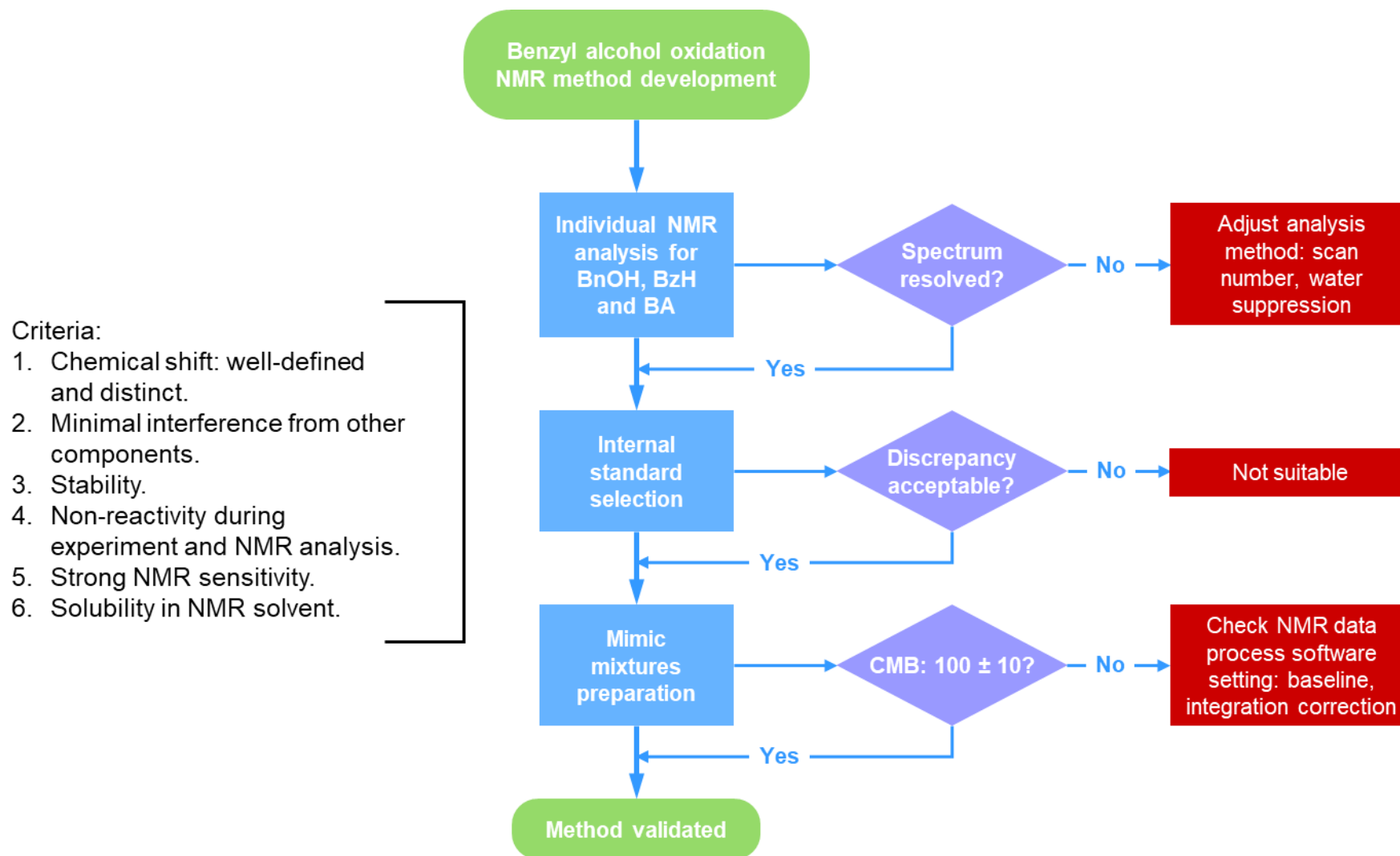5. Strong NMR sensitivity.
6. Solubility in NMR solvent.

Figure 5.2 Schematic of Benzyl alcohol oxidation ^{1}H-NMR development.[37]

5.2.1 ¹H-NMR analysis of standards

Standards of benzyl alcohol (99 wt.% purity), benzaldehyde (99.5 wt.% purity) and benzoic acid (99 wt.% purity) were used for developing quantification and qualification methods. The known purity levels were accounted for in the calculations to accurately identify and quantify our reaction mixture compounds via direct ¹H-NMR measurements, in addition to literature data available for these compounds. Due to the low solubility of these three chemicals in water (ca. 40, 2.9 and 3.4 g L^{-1} respectively[38,39]), standard solutions of three chemicals with concentration in the range of 1 g L^{-1} were prepared separately using co-solvent (volume ratio of water and methanol 95 : 5) to ensure all of the chemicals were fully dissolved. Hence, this guaranteed an accurate theoretical value for discrepancy calculation, which is crucial to apply as correction factor in later section. ¹H-NMR analysis of benzyl alcohol (Figure 5.3), benzaldehyde (Figure 5.4) and benzoic acid (Figure 5.5) were performed with DMSO-d6 as solvent as well as using a water suppression algorithm[40,41] to minimize the interference of water peak (δ 4.76 - 4.66 ppm), as water is the solvent for our abatement reactions.

Generally speaking, to assess if a chosen NMR method is suitable for the simultaneous analysis of multiple chemicals, it is important to ensure that high-quality spectra can be obtained in the first instance. This implies: 1) a clear resolution of peaks without significant overlap for precise chemical shift measurement and accurate compound identification, 2) a high signal-to-noise ratio (SNR) to enhance the detection limit detection enabling a resolved peak integration and quantitative analysis, 3) a stable baseline that is free of artifacts, drift effects or impurities that could compromise the area integration process, 4) accurate and reproducible positioning of peaks on the chemical shift scale ensures the spectrum's precision, 5) well-defined peak shapes and appropriate intensities reflect sample purity and concentration relationships, 6) during the analysis of the spectra, proper phase adjustment further enhancing peak intensity and symmetry.[42]

The obtained spectra (Figure 5.3 to Figure 5.5) of three chemicals satisfy these comprehensive criteria. Therefore, the current method is acceptable for further method development for a dependable results, informed analysis, and insightful interpretation.
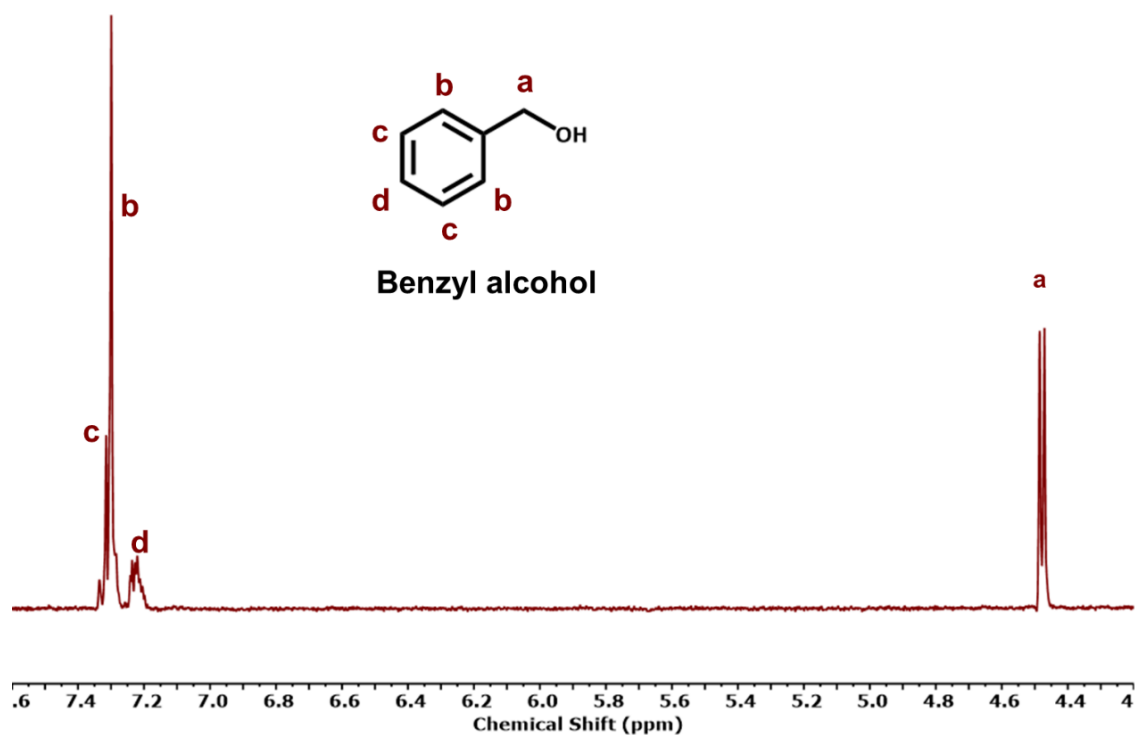
Figure 5.3 Benzyl alcohol: ¹H-NMR (400 MHz, DMSO-d6), c: δ ppm 7.35 (d, 2H), b: 7.30 (m, 2H), d: 7.23 (dd, H), a: 4.50 (d, 2H).
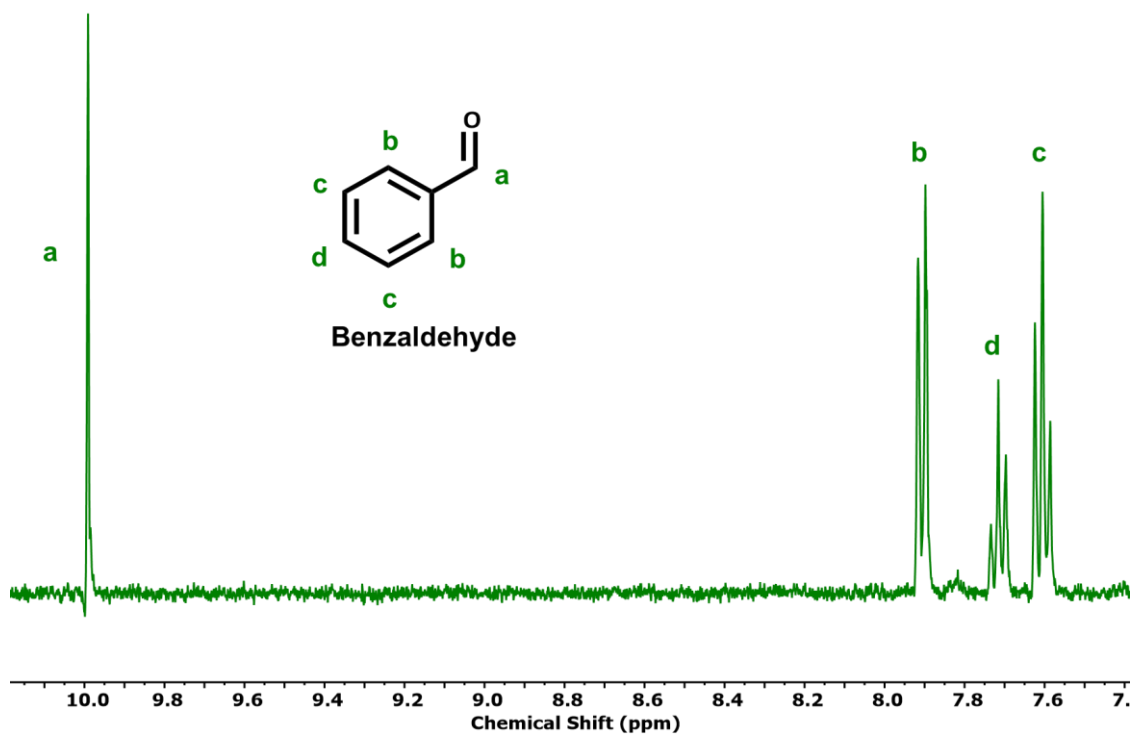
Figure 5.4 Benzaldehyde: ¹H-NMR (400 MHz, DMSO-d6), a: δ ppm 9.99 (s, 1H), b: 7.90 (d, 2H), d: 7.70 (t, 1H), c: 7.60 (t, 2H)
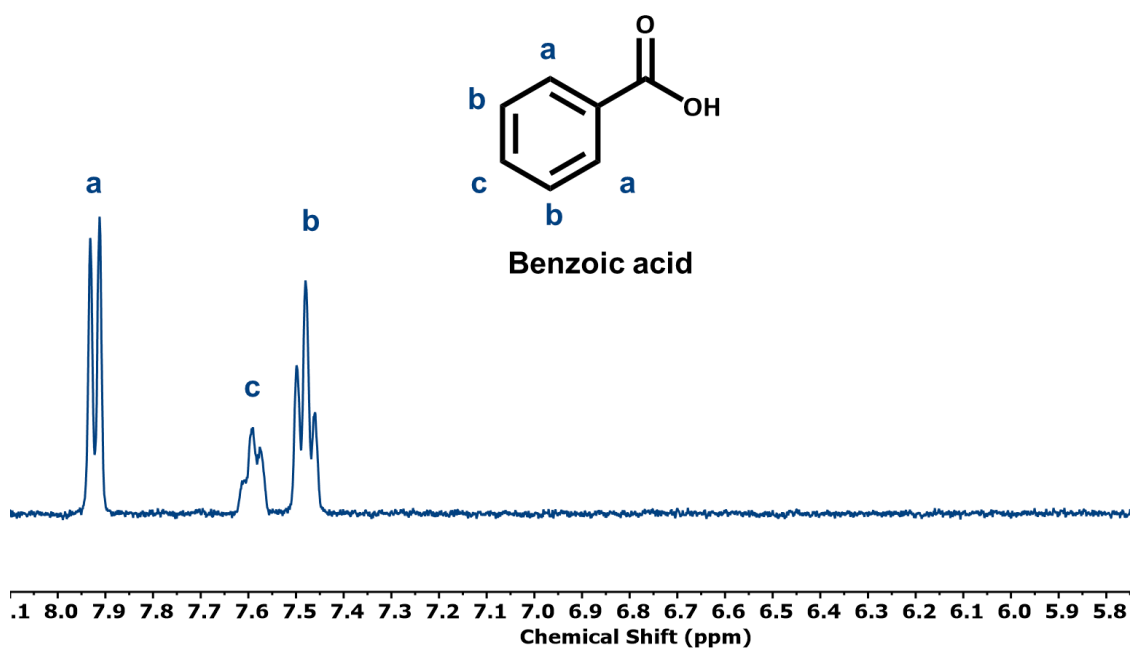
Benzoic acid

Figure 5.5 Benzoic acid ¹H-NMR (400 MHz, DMSO-d6): a: δ ppm 7.92 (d, 2H), c: 7.58 (t, 1H), b: 7.47 (t, 2H). H on OH is not visible due to rapid proton exchange effect with water or other H in benzoic acid, leading to broad or weak signals that are often not detected in the NMR spectrum
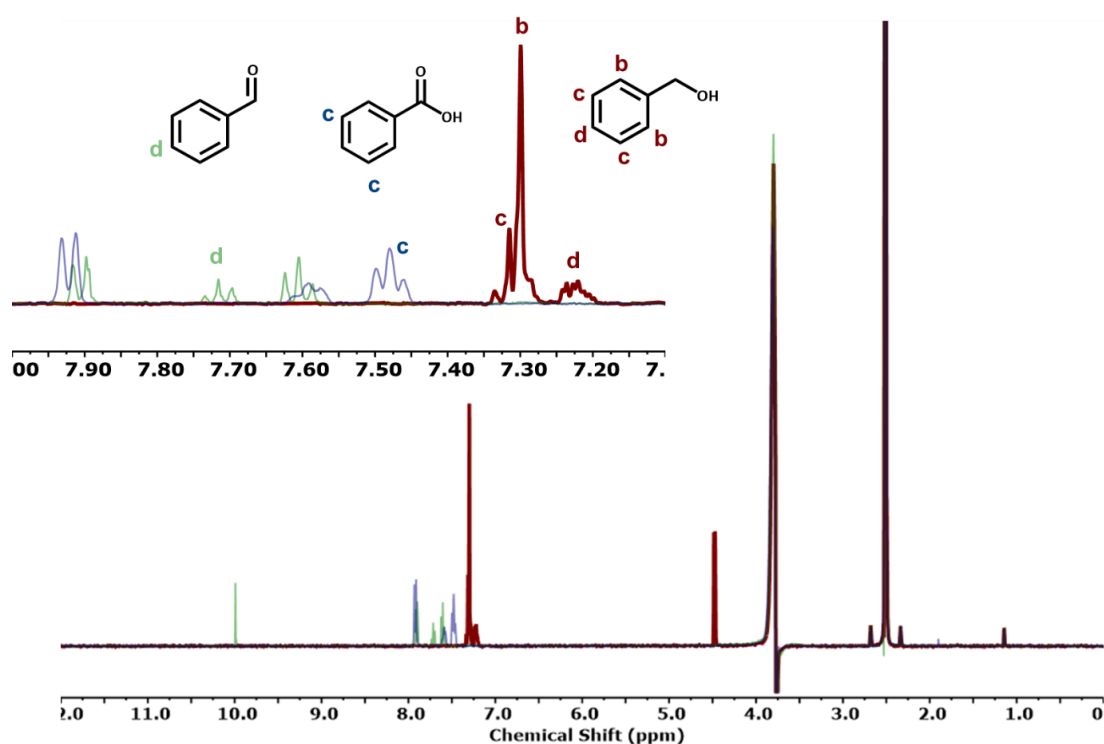
Figure 5.6 Stacked ¹H-NMR spectra of benzyl alcohol (●) and two oxidation products benzaldehyde (●) and benzoic acid (●). The main figure highlights the full spectral ranges, while the inset focuses on the regions containing the diagnostic, characteristic peaks for each compound. Using this stacked spectrum with highlighted regions allows straightforward identification and quantification of the reaction components.
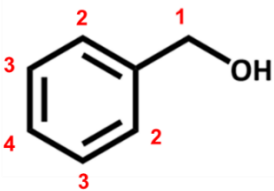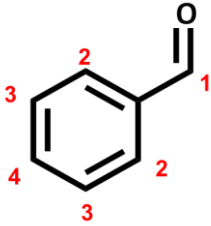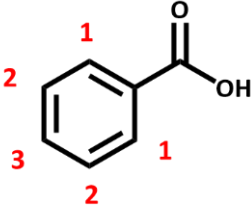
After accurately characterizing individual spectra of these standards, it was essential to find the characterization peaks used in the reaction mixture that are not overlapping with each other, thus ensuring an accurate quantitative result. A stacking of the three individual spectra of the three chemicals (Figure 5.6), shows that although some of the peaks of benzaldehyde and benzoic acid are overlapped, peak a, b and c, from benzyl alcohol, peak c and d from benzoic acid and benzaldehyde respectively are well resolved and distinct from other peaks, and can be used as characteristic peaks for qualification purposes.

However, and in practice, NMR signals can be influenced by various factors, such as: sample concentration, temperature, and magnetic field homogeneity of the spectrometer. Hence, qNMR (quantitative NMR) analysis is widely performed by adding a known amount of an internal standard (IS) to the sample solution to normalize these variations for more accurate quantification of the components. In a ^{1}H-NMR spectrum, the integral area of a resonance due to the analyte protons (nuclei) is directly proportional to its molar concentration and to the number of nuclei that give rise to that resonance.[42] Therefore, analyte concentration (C_a) can be determined by comparing peak areas between IS (A_{IS}) and analyte (A_a) (Eq. 5.1).

$$C_a = \frac{A_a}{A_{IS}} \times C_{IS} \qquad \text{(Eq. 5.1)}$$

As a result, the choice of an appropriate internal standard is a critical step for the overall accuracy of the method. The selection of an appropriate internal standard for benzyl alcohol oxidation reaction will be discussed in next section.

Table 5.1 A summary of ^{1}H-NMR data of benzyl alcohol and its corresponding potential oxidation products benzaldehyde and benzoic acid with the characteristic chosen for the calculation of conversion and CMB%.

Compound	Characteristic peak δ (ppm)
Benzyl alcohol 	7.23 (t$_4$, H), 7.30 (t$_2$, 2H), 7.35 (t$_3$, 2H)
Benzaldehyde 	7.70 (t$_4$, 1H)
Benzoic acid 	7.47 (t$_3$, 2H)

5.2.2 Choice of internal standard

As shown in Figure 5.2 in Section 5.2, there are a few requirements that a suitable internal standard should meet: 1) The chosen internal standard should have a well-defined and distinct chemical shift in the NMR spectrum that is easily distinguishable from other signals in the sample. For example, it should be located in a region of the spectrum where there is minimal interference that is in our case overlap, with signals of interest (characteristic peaks of other chemicals) in the sample, as this could lead to inaccurate quantification or interpretation of the NMR data. 2) The internal standard should be highly soluble in the NMR solvent used for the sample, ensuring it is evenly distributed throughout the sample solution. 3) The selected internal standard should be stable and not react with the sample components (analyte or solvent) under the NMR instrument's operating conditions. 4) The internal standard should have a strong NMR signal or at least comparable with the analyte, which aids in accurate concentration determination and reduces the measurement's overall uncertainty. 5) Of particular importance for this work, an appropriate internal standard should be soluble in both reaction solvent and the chosen NMR solvent.

By considering the above criteria as a whole, six potential internal standards were identified and selected for further tests: 1,1,2,2-tetrachloroethane (1,1,2,2-TCE), 1,2-dichloroethane (1,2-DCE), dichloromethane (DCM), heptane, triethanolamine (TEA) and 2-propanol. Their physical properties and discrepancy on three chemicals are listed in Table 5.2 Based on the selected internal standard and reaction solvent (water), DMSO-d6 that is able to dissolve all of the standards and at the same time miscible with water was chosen as NMR solvent.

When internal standards were used to quantify the concentrations of benzyl alcohol, benzaldehyde and benzoic acid, the relative deviation between the measured and expected values was calculated using the formula ((measured value-expected value)/expected value) ×100%. A deviation value greater than 0 indicates a positive deviation, i.e. the detected amount of the compound exceeds its actual presence. Conversely, a deviation value less than 0 indicates a negative deviation, i.e. the compound was detected in lower amounts than expected. A deviation within ± 5% is considered acceptable from error propagation from the measurement integration peaks of both the compound and the internal standard. It may be worth noting that 1,1,2,2-TCE exhibits a high viscosity of 1.77 cPs at 20°C. In comparison, water has a viscosity of 1.002 cPs at the same temperature and 1.79 cPs at 0.01°C. This characteristic of high viscosity may result in a loss of chemical during transfer, causing less internal standard to be used and ultimately leading to a positive deviation in the analytical results. Similarly, 1,2-DCE and DCM possess low boiling points of 83.5°C and 39.6°C, respectively. The low boiling points can contribute to a loss of chemical during transfer, leading to a positive deviation in the final analytical outcomes. Heptane, on the other hand, exhibits low solubility in water at 3.4 mg L^{-1} at 20°C. Consequently, when 15 μL of heptane is mixed with 200 μL of water in DMSO-d6 (with an expected concentration of 51 g L^{-1}), less standard is dissolved than anticipated, resulting in a positive deviation. TEA, due to its structure having a low dipole moment of 0.68 D at 25°C (in contrast to water with a dipole moment of 1.85 D), is unlikely to be miscible with water. This characteristic may lead to a high positive deviation in the analytical results when TEA is used as a solvent or internal standard. While 2-propanol shows a deviation within an acceptable range of 10%, although it is worth noting that it has a relatively lower boiling point of 82.5°C, which may need to be considered in certain analytical applications.

Table 5.2 Physical-chemical properties of six selected internal standards for benzyl alcohol oxidation NMR analysis with DMSO-d6 as solvent. ^{1}H-NMR were performed under water suppression method. Each analysis was repeated 3 times. Deviation of each chemical is listed based on various characteristic peaks.

	Solubility in water at 20 ºC mg L^{-1}	Dipole moment D at 25 ºC	Boiling point ºC	Viscosity cPs at 20 ºC	Deviation for BnOH %	Deviation for BzH %	Deviation for BA %
water	-	1.85	100	1.002	-	-	-
Internal standard							
1,1,2,2-TCE	2.86	1.31	146.7	1.77	87	-9	122
1,2-DCE	8.7	1.83	83.5	0.84	207	45	340
DCM	20	1.14	39.6	0.44	2	-40	17
Heptane	0.0034	0	98.4	0.376	848-781	267-1200	970-2470
TEA	112.4	0.68	89.3	0.363	80	27	27
2-propanol	miscible	1.66	82.5	2.05 (25 ˚C)	2	-21	0-9

Among all the six potential internal standards, 2-propanol showed an acceptable deviation for all three compounds. Accordingly, to verify the reproducibility of NMR instrument when using 2-propanol as internal standard and water suppression method, at least seven separate NMR samples for all three compounds were prepared without changing other parameters in our protocol.

Table 5.3 Relative deviation % and standard deviation (SD) of NMR quantitative result for benzyl alcohol, benzaldehyde and benzoic acid when using 2-propanol as internal standard. Each NMR sample includes 500 μL of DMSO-d6, 200 μL of analyte and 15 μL of 2-propanol solution.

Chemical	Expected mol	Measured mol	RSD %	Deviation %
Benzyl alcohol	2.05×10^{-6}	2.14×10^{-6}	2	4
Benzaldehyde	1.95×10^{-6}	1.60×10^{-6}	1	-18
Benzoic acid	1.64×10^{-6}	1.84×10^{-6}	3	12

2-propanol produced consistent and reproducible results (RSD less than 3%), allowing for reliable calibration and comparison between different NMR experiments (Table 5.3). the results of repeated analysis on the same sample showed the overall reproducibility of NMR technique on the selected chemicals thus providing vital information for method development decision making. Moreover, in the investigation of repeated analysis for BnOH, a commendable deviation of 4% was achieved, falling within an acceptable range (± 5%). In the case of benzaldehyde, however, a notable negative discrepancy of -18% was observed. However, as this appeared to be systematic, it could be treated as a systematic error, and as such to can be taken into account as a correction factor for our calculations. In principle, the

detection of any by-product (benzoic acid) would indicate the preliminary presence and then conversion of benzaldehyde, while the absence of evident by-products may be attributed to the trace amount of the product, making it challenging to be observed in the NMR spectrum. For benzoic acid, although the % accuracy is 12%, surpassing the 5% threshold previously reported. This is also considered acceptable if accounting for multiple repetitions on different times for succeeding application.

As a result, 2-propanol was proved an appropriate internal standard in the quantitative analysis of benzyl alcohol, benzaldehyde and benzoic acid when they are prepared separately. Afterwards, mimic mixtures of different stages of benzyl alcohol oxidation would be prepared to verify if 2-propanol is suitable when multiple chemicals are present.

5.2.3 Application of 2-propanol as internal standard on mimic mixtures

As 2-propanol as internal standard showed an accurate and consistent results on individual chemical, it is also important to validate if the use of 2-propanol is applicable on mixtures containing all three compounds at different stages of the oxidation process. To this scope, five different mixtures of standard solution of benzyl alcohol, benzaldehyde and benzoic acid were prepared by using different molar ratio to mimic different stages of the reaction (Table 5.4). Calculation of CMB% for each mixture was done with correction factor to validate the method where all the products are known.

Table 5.4 Five mimic mixtures of benzyl alcohol, benzaldehyde and benzoic acid were prepared in terms of different molar ratio between benzyl alcohol, benzaldehyde and benzoic acid. The accuracy in terms of the ratios are calculated, and the CMB% is calculated with correction factor from previous section. Each NMR sample includes 500 µL of DMSO-d6, 200 µL of analyte and 15 µL of 2-propanol solution.

Mixture	BnOH: BzH:BA Molar ratio	*Deviation on BzH %	Deviation on BA %	CMB %
#1	6:1:2	-40	-5	94
#2	3:2:1	-30	0	95
#3	1:1:1	-30	-1	95
#4	1:5:2	-31	3	97
#5	1:3:4	-26	3	97

*relative deviation= ((measured value-expected value)/expected value) ×100%, with the value of BnOH as a standard.

When analysing the molar ratios of benzyl alcohol, benzoic acid and benzaldehyde in five different mimic mixtures, a consistent pattern of deviation emerged despite the compounds having different initial molar ratios. To facilitate comparison, the molar ratio of benzyl alcohol was taken as the standard reference, as it had the smallest individual deviation among the

three compounds. The analysis showed that for benzyl alcohol and benzoic acid the measured molar ratios were within an acceptable range of 3% accuracy compared to the expected values for all five mixtures. However, a systematic underestimation of about 30% was observed for the measured molar ratio of benzaldehyde in all five mixtures. This 30% underestimation for benzaldehyde is consistent with the individual deviations observed when benzaldehyde (18% lower than expected) and benzoic acid (12% higher than expected) were analysed separately, further supporting the presence of a systematic error in the benzaldehyde measurements. The consistency of this deviation for benzaldehyde across different mimic mixture compositions allowed to use this error as systematic and therefore used as a correction factor.

By applying correction factors of 4%, -18% and 12% (deviation for individual chemical in Table 5.3) for benzyl alcohol, benzaldehyde and benzoic acid, respectively, the CMB% for the five mimic mixtures is approximately 95%, which is compatible with 100% when considering the random experimental error of the sample of data. Therefore, this sufficiently validate our methodology for the quantification of our compounds in this reaction mixture. However, this as long as we use a co-solvent during standard solution preparation to ensure accuracy, we select appropriate standards based on different physical properties, dilute the internal standard to match the sample magnitude in NMR analysis, correct for phase and baseline changes when interpreting NMR spectra, and the considering the error propagation when analysing discrepancies.

5.3   Benzyl alcohol mineralization tests via Fenton reaction

As detailed in Chapters 3 and 4, recycled glass as a heterogeneous catalyst showed promising performance for the degradation of phenol and ibuprofen via the Fenton reaction, offering a more environmentally friendly and cost-effective alternative to conventional wastewater treatment. Building on the successful ^{1}H-NMR analysis protocol developed, we investigate the potential of recycled glass catalysts for the mineralisation of benzyl alcohol, another common aromatic industrial pollutant.

5.3.1 Catalytic Control tests

Similar to previous chapter, an important step is to perform control tests to investigate the role of catalyst and oxidant in a new reaction system. Hence, benzyl alcohol (1 g L^{-1}) degradation reaction with both homogeneous iron catalyst ($Fe(NO_3)_3 \cdot 9H_2O$) and green recycled glass (**G2**, Fe content 0.3 wt.%) were conducted. To fully mineralise a mole of benzyl alcohol via Fenton reaction, a stoichiometric amount of H_2O_2 was initially used (BnOH:H_2O_2 1:17 Equation 5.2).

Reactions were conducted with iron catalyst (M:S molar ratio of 1:100) at 80 °C for 24 hours under endogenous pressure.

$$C_7H_8O + 17\ H_2O_2 \rightarrow 7\ CO_2 + 21\ H_2O \qquad \text{(Eq. 5.2)}$$
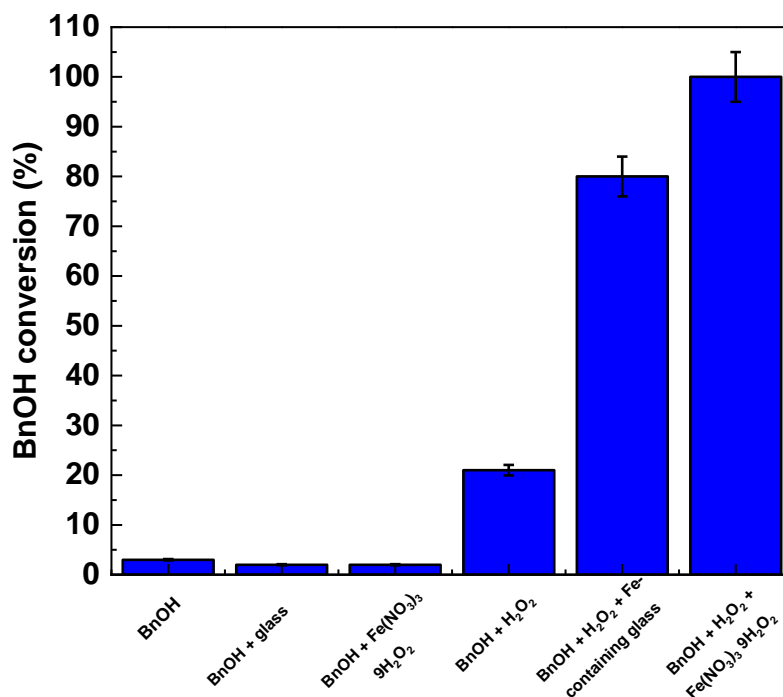
Figure 5.7 Control tests of BnOH conversion in the presence and absence of catalysts and in the presence and absence of oxidizing agent. Reactions conditions: 50 mL of BnOH (1g L^{-1}), $Fe(NO_3)_3 \cdot 9H_2O$, **G2** recycled glass (Fe: 0.3 wt.%) M:S=1:100, <0.1 mm, $BnOH:H_2O_2$=1:17 (stoichiometric amount towards mineralization), p = endogenous, 80 °C, 24 h, 500 rpm. Both catalyst and H_2O_2 are important in triggering Fenton reaction.

The negligible benzyl alcohol conversion (2 ± 2%) observed after 24 hours in the absence of H_2O_2 (Figure 5.7) can be attributed to the absence of hydroxyl radicals (·OH), which are central to the Fenton reaction mechanism. This observation emphasises that the catalyst alone does not directly oxidise the organic compound. Consequently, sole thermal oxidation without H_2O_2 is insufficient for the decomposition of benzyl alcohol under current conditions, highlighting the importance of the Fenton mechanism facilitated by H_2O_2. Upon the introduction of a stoichiometric quantity of H_2O_2, a marked enhancement in BnOH conversion was observed, reaching 80 ± 3% and 100 ± 3% when utilizing recycled glass and various iron salts, respectively (Figure 5.7). Fe centres proved their important role in facilitating the generation of ·OH radicals, thereby yielding enhanced conversion rates. Additionally, in the catalyst's absence, the thermal decomposition of H_2O_2 (ca. 3%, as studied in Section 3.2.1, Section 3.3.1) yielded a limited extent of BnOH conversion. Benzyl alcohol conversion can certainly be improved with the addition of catalyst. This observation correlated well with the

Fenton reaction of phenol and ibuprofen, demonstrating the underlying hypothesis that organic pollutants, particularly aromatics, can be effectively degraded by an analogous reaction mechanism using recycled glass. This provides another green and environmentally friendly alternative to conventional wastewater treatment methods or catalytic systems, which may involve the use of hazardous chemicals, toxic materials or energy-intensive processes.

5.3.2 Effect of H_2O_2 dosage

At a dosage of stoichiometric amount of H_2O_2, control tests using recycled glass showed a promising benzyl alcohol conversion of $80 \pm 3\%$ after 24 hours. As previously investigated, a stoichiometric amount of H_2O_2 is unlikely to lead to complete mineralization to CO_2 and H_2O due to some undesired side reactions (Eq. 5.3 and 5.4) which will affect the overall degradation efficiency of H_2O_2. To achieve a more complete mineralization, benzyl alcohol oxidation with double the amount of H_2O_2 was doubled using green recycled glass (Fe: 0.3 wt.%) of four different sizes (<0.1, 0.1-0.2, 0.2-0.5 and 0.5-1 mm).

$$H_2O_2 + \cdot OH \rightarrow H_2O + \cdot OOH \qquad (Eq. 5.3)$$
$$\cdot OOH + \cdot OH \rightarrow H_2O + O_2 \qquad (Eq. 5.4)$$
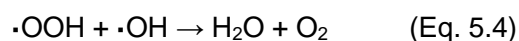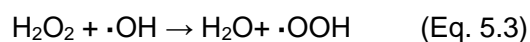
Upon the introduction of twice the stoichiometric equivalent of H_2O_2 (towards H_2O and CO_2), an unfavourable observation emerges wherein the conversion of BnOH experiences a diminishment (Figure 5.8). This showed that the excess of hydroxyl radical ($\cdot OH$) inhibited BnOH oxidation process, attributing to the pronounced scavenging effect exerted by extra H_2O_2. In addition, it is worth to note that the scavenging effect gets smaller when the glass sizes get larger, probably because less Fe centres available in total on the surface of the glass beads. This emphasizes the importance of the iron species in generating hydroxyl radical in Fenton reaction, thus implying the reaction is indeed undergoing a radical pathway via Fenton reaction, as observed for ibuprofen oxidation.
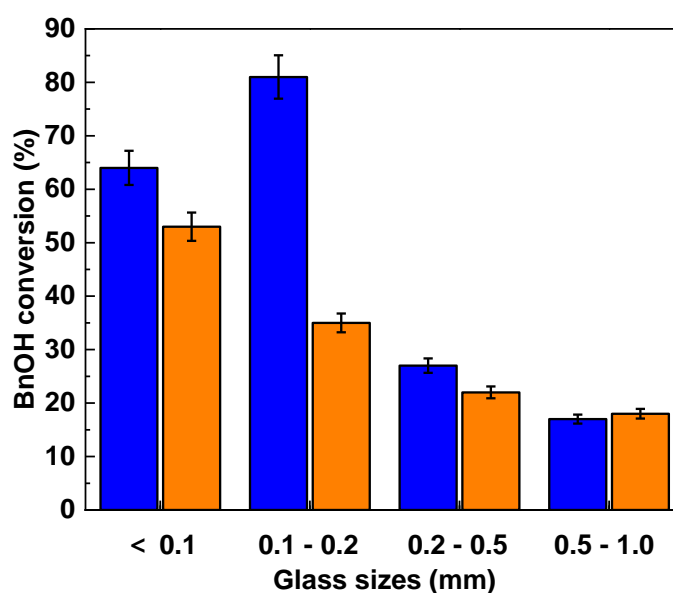
Figure 5.8 Effect of H_2O_2 dosage on BnOH conversion using four different average diameters of glass beads. Reaction conditions: 10 mL of BnOH (1g L^{-1}), **G2** recycled glass (Fe: 0.3 wt.%) M:S=1:100, <0.1, 0.1-0.2, 0.2-0.5 and 0.5-1 mm, BnOH:H_2O_2=1:17 (stoichiometric amount towards mineralization●) and 1:34 (●), p = endogenous, 80 °C, 24 h, 500 rpm. H_2O_2 scavenging effect were observed when extra H_2O_2 were added.

An increase in glass beads size should correspondingly reduce the exposed fraction of Fe^{3+} centres to H_2O_2, thereby leading to a decline in reactivity. This expected trend is matched in all cases but one when the glass used changed from below 0.1 mm to 0.1-0.2 mm with a stoichiometric amount of H_2O_2 used (Figure 5.8). This unexpected deviation might be attributed to an uncontrollable alteration in the shape of the glass grains upon milling. A sharply fractured surface, as opposed to a smooth one, demonstrates augmented reactivity, consequently resulting in an elevated BnOH conversion.[43,44]

5.3.3 Effect of initial concentration of BnOH

However, as in the kinetics study, alterations in the quantity of reactants may exert a direct influence on the rate of a chemical reaction based on the order of the reaction with respect to each.[45,46] Besides changes in H_2O_2 concentration, changes in BnOH amount were also considered. The doubling the amount of H_2O_2 did not result in a desired result, thus, the initial BnOH concentration was then increased from 1 g L^{-1} to 12 g L^{-1}. Reaction was conducted with **G2** recycled glass (Fe 0.3 wt.%) as catalyst (M:S 1:100, less than 0.1 mm) and BnOH:H_2O_2 of 1:17 (stoichiometric amount w/t mineralization) and 1:34 for 24 hours at 80 °C.
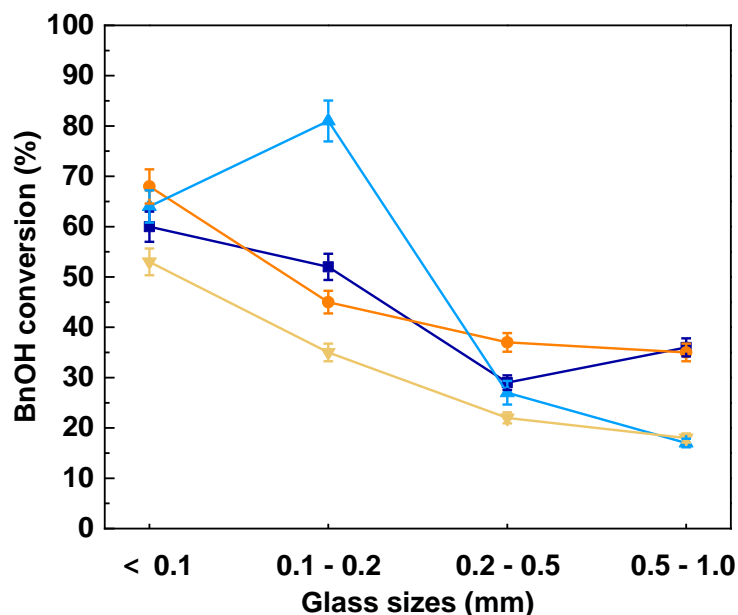
Figure 5.9 Effect of changes of initial concentration on conversion were studied with two different H_2O_2 dosage. Reaction conditions: 10 mL of BnOH (1 g L^{-1}), **G2** recycled glass, M:S=1:100, <0.1, 0.1-0.2, 0.2-0.5 and 0.5-1 mm, BnOH:H_2O_2=1:17 (●) and 1:34 (●); 10 mL of BnOH (12 g L^{-1}), BnOH:H_2O_2=1:17 (●) and 1:34 (●), p = endogenous, 80 ˚C, 24 h, 500 rpm. No notable disparity emerges between the two initial concentrations, suggesting that the reaction tends towards a zero-order kinetic profile with respect to BnOH concentration, H_2O_2 decomposition rate dictate the rate of the process.
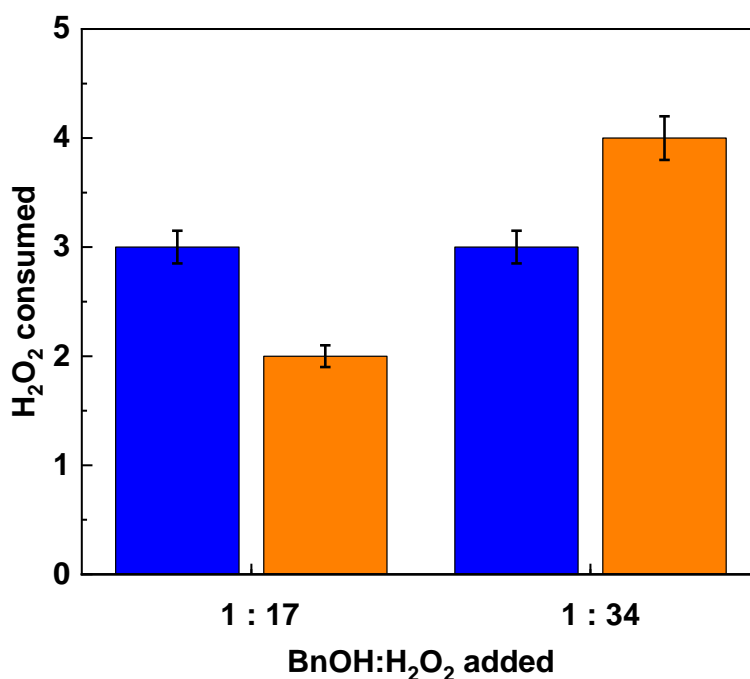
Figure 5.10 H_2O_2 consumption for two initial BnOH concentrations. Reaction conditions: 10 mL of BnOH (1 g L^{-1} (●) and 12 g L^{-1} (●)), **G2** recycled glass, M:S=1:100, <0.1mm as representative, BnOH:H_2O_2=1:17 and 1:34, p = endogenous, 80 °C, 24 h, 500 rpm. While maintaining similar BnOH conversion, the increased initial concentration (in both H_2O_2 dosage) led to no notable alterations in H_2O_2 consumption.

Regardless of whether a concentration of 1 g L^{-1} or 12 g L^{-1} is employed, a twofold increase of H$_2$O$_2$ content did not yield substantial alterations in BnOH conversion (Figure 5.9). Moreover, no notable disparity emerges between the two initial concentrations, suggesting that the reaction tends towards a zero-order kinetic profile with respect to BnOH concentration. This would imply that any of the BnOH decomposition step are not taking part in the rate determining step of the reaction, or the attack of ·OH spices to the alcohol, and as such it is the H$_2$O$_2$ decomposition rate that will eventually dictate the rate of the process. Consequently, the changing of BnOH concentration is evidently unnecessary to achieve complete conversion.

Moreover, while maintaining similar BnOH conversion, the increased initial concentration (in both H$_2$O$_2$ dosage) led to no notable alterations in H$_2$O$_2$ consumption (Figure 5.10). Therefore, the decreasing CMB and benzaldehyde selectivity (Table 5.5 and Table 5.6) implies an increase in rate of reaction towards the formation of CO$_2$, thus a greater extent of mineralization. Furthermore, the emergence of benzaldehyde signals the occurrence of oxidation reaction.

Therefore, the change in initial concentration of BnOH will not lead to a significant increase in BnOH conversion, but a notable change in selectivity change from benzaldehyde towards CO$_2$ can be observed, a better mineralization is resulted. This is probably due to the formation of reactive acyl radicals that can also take part in the decomposition process towards a current benzyl alcohol species, for example, abstraction of hydrogens from benzyl alcohol to generate oxidizable benzyloxy radicals (C$_6$H$_5$CH$_2$O·), undergo decarboxylation to produce phenyl ethyl radicals (C$_6$H$_5$CH(·)OH) that re-initiate alcohol oxidation, and directly oxidize benzyl alcohol via H-atom transfer and, in turn, promote mineralization.

Table 5.5 BnOH (12 g L^{-1}) conversion, CMB%, benzaldehyde (BzH), benzoic acid (BA) and formic acid selectivity. Reaction condition: **G2** recycled glass (Fe: 0.3 wt.%), M:S = 1:100, <0.1, 0.1-0.2, 0.2-0.5 and 0.5-1 mm, BnOH:H$_2$O$_2$ molar ratio of 1:17 and 1:34, p = endogenous, 80 °C, 24 h, 500 rpm.

Catalyst size	BnOH : H$_2$O$_2$	Selectivity %			conversion %	CMB %
		BzH	BA	formic acid		
<0.1 mm	1:17	8	13	12	60	51
0.1-0.2 mm	1:17	8	16	14	52	59
0.2-0.5mm	1:17	7	13	10	29	77
0.5-1 mm	1:17	8	16	14	36	72
<0.1 mm	1:34	3	18	8	68	44
0.1-0.2 mm	1:34	4	21	9	45	65
0.2-0.5mm	1:34	3	17	7	37	70
0.5-1 mm	1:34	3	15	7	35	71

Table 5.6 BnOH (1 g L^{-1}) conversion, CMB%, benzaldehyde (BzH), benzoic acid (BA) and formic acid selectivity. Reaction conditions: **G2** recycled glass (Fe: 0.3 wt.%), M:S=1:100, <0.1, 0.1-0.2, 0.2-0.5 and 0.5-1 mm, BnOH:H$_2$O$_2$ molar ratio of 1:17 and 1:34, p = endogenous, 80 ˚C, 24 h, 500 rpm.

Catalyst size	BnOH : H$_2$O$_2$	Selectivity %			Conversion %	CMB %
		BzH	BA	formic acid		
<0.1 mm	1:17	19	2	47	64	51
0.1-0.2 mm	1:17	19	4	36	81	39
0.2-0.5mm	1:17	18	0	40	27	78
0.5-1 mm	1:17	15	4	33	17	87
<0.1 mm	1:34	18	2	30	53	58
0.1-0.2 mm	1:34	17	1	24	35	72
0.2-0.5mm	1:34	16	3	22	22	82
0.5-1 mm	1:34	12	3	19	18	85

5.4   Benzyl alcohol oxidation towards benzaldehyde using H$_2$O$_2$ as oxidant

From the data reported in the section above, full mineralization of BnOH towards water and carbon dioxide is not achieved under the current reaction conditions. However, the presence of benzaldehyde as a product suggested that the synthesis of fine chemicals by changing the H$_2$O$_2$ dose might be possible. Moreover, as studied in previous chapters, thermal decomposition of H$_2$O$_2$ will lead to the formation of O$_2$ and H$_2$O (Eq. 5.5). This was considered as an undesired side reaction for wastewater decomposition reaction via Fenton reaction. However, H$_2$O$_2$ could be used as an in situ source of molecular oxygen to mimic the oxidation of benzyl alcohol catalysed by molecular O$_2$ (Figure 5.11).

$$H_2O_2 \rightarrow 0.5\ O_2 + H_2O \qquad (Eq.\ 5.5)$$
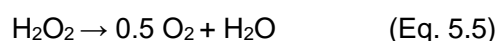
The molecular oxygen formed can then be activated and abstract hydrogen atom from benzyl alcohol molecule, mimicking the key steps of the molecular O$_2$ oxidation pathway. This allows the selective oxidation to benzaldehyde to be studied in a manner analogous to molecular O$_2$ activation, while avoiding the direct use of gaseous O$_2$. As a result, mimic oxidation of BnOH towards benzaldehyde production was designed to investigate the possibility of BnOH selective oxidation using H$_2$O$_2$ as oxidant. Therefore, benzyl alcohol oxidation with a small BnOH:H$_2$O$_2$ molar ratio of 1:1 and 1:2 was conducted to study the possible oxidation reaction mechanism towards benzaldehyde. Effect of H$_2$O$_2$ dosage, initial BnOH concentration towards benzaldehyde selectivity and effect of time was studied in this section.
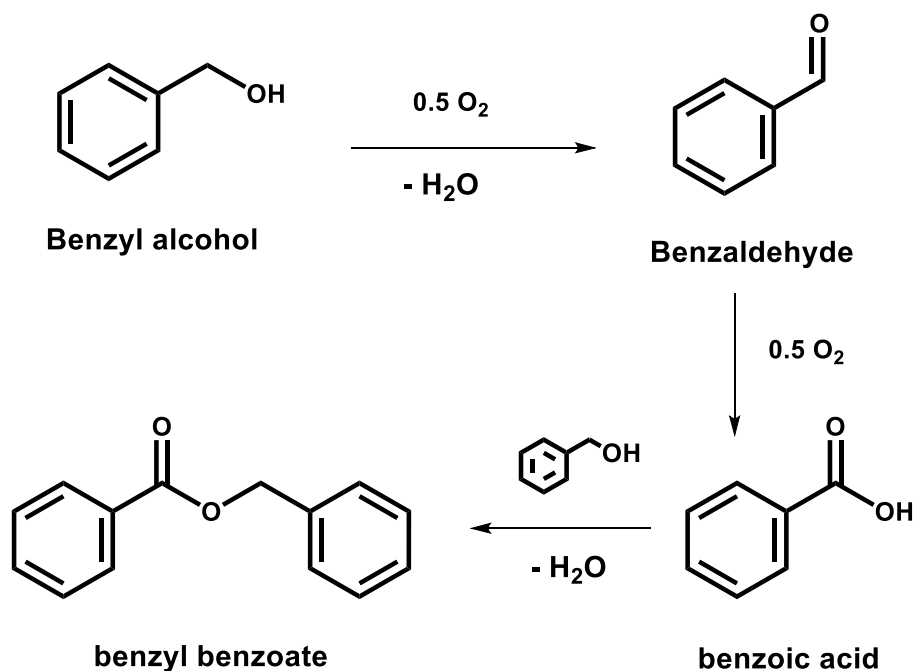
Figure 5.11 Formal reaction scheme of benzyl alcohol to form benzaldehyde, benzoic acid and benzyl benzoate.

5.4.1 Effect of H_2O_2 dosage and initial concentration on selective oxidation of BnOH towards benzaldehyde

In previous section, zero order with respect to BnOH concentration was concluded. That said, although a change in the initial concertation of BnOH is not expected per se to change the rate of the reaction, intermediates from the decomposition of BnOH, like benzyl radicals, could interfere with or trap the generation of ·OH radicals from H_2O_2. So that changes in concentration of BnOH could eventually affect the reaction via termination processes. Furthermore, as we were also interested to estimate the productivity of our materials, we therefore increased the amount of BnOH to 12 g L^{-1}. Therefore, selective oxidation of 10 mL BnOH (1 g L^{-1} and 12 g L^{-1}) towards the formation of benzaldehyde with a BnOH:H_2O_2 ratio of 1:1 and 1:2 was conducted with four different sizes of **G2** recycled glass (Fe: 0.3 wt.% M:S 1:100) for 24 hours at 80°C under endogenous pressure.
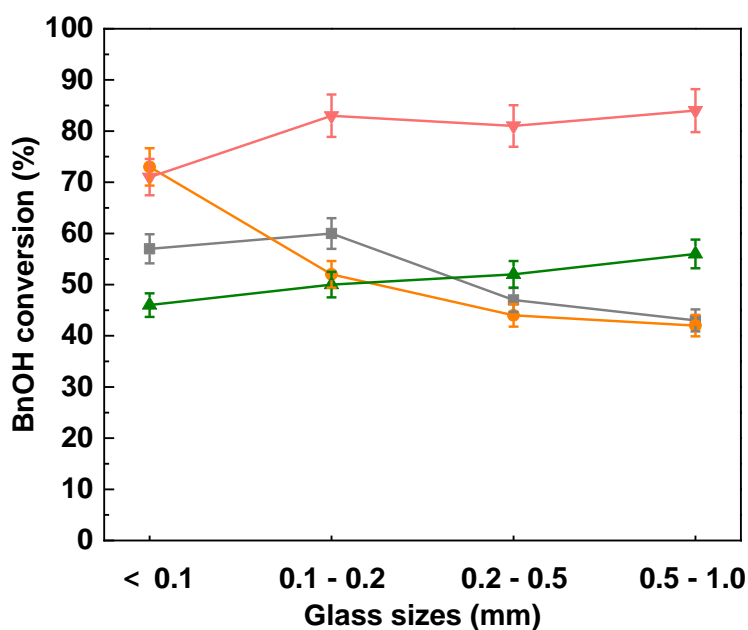
Figure 5.12 Effect of initial concentration on conversion were studied with two different H_2O_2 dosage. Reaction conditions: 10 mL of BnOH (1 g L^{-1}), **G2** recycled glass (Fe: 0.3 wt.%), M:S=1:100, <0.1, 0.1-0.2, 0.2-0.5 and 0.5-1 mm, BnOH:H_2O_2=1:1 (●) and 1:2 (●); 10 mL of BnOH (12 g L^{-1}), BnOH:H_2O_2=1:1 (●) and 1:2 (●), p = endogenous, 80 °C, 24 h, 500 rpm.

With an initial BnOH concentration of 1 g L^{-1}, a twofold increase of hydrogen peroxide content (from 1:1 to 1:2) yielded a noteworthy enhancement in BnOH conversion, enhancing it from 50% to 80% Figure 5.12). Moreover, the BnOH conversion for the four different sizes remain constant after the 24-hour reaction. This trend suggests that, within this timeframe, the reaction may have attained its maximum conversion. Therefore, to identify potential variations in conversion attributable to different glass sizes, shorter reaction durations, such as 4 hours, can be employed as a further work.

On the other hand, with an initial BnOH concentration of 12 g L^{-1}, the doubling of hydrogen peroxide content yielded marginal alterations in BnOH conversion. This effect could potentially be attributed to the diffusion constraints arising when employing a substantial quantity of glass, wherein solely the surface-adjacent glass particles are exposed to BnOH. Consequently, an anticipated decrease in conversion was observed with the augmentation of glass particle sizes.

When a BnOH to H_2O_2 ratio of 1:1 was used, changing different initial BnOH concentration showed no different between 1 g L^{-1} and 12 g L^{-1} for all 4 sizes at a 24-hour reaction. Hence under this reaction condition, zero order of BnOH concentration with respect to overall conversion was confirmed, thus, it is not necessary to change the initial concentration to get

a higher conversion. This unchanged BnOH matched with the observation where BnOH to H_2O_2 ratio of 1:17 and 1:34 were used.

In contrast, when a BnOH to H_2O_2 ratio of 1:2 was used, significant decrease in BnOH conversion was observed when initial BnOH concentration was increased 10 times. This might be due to the trapping of ·OH radical from acyl or acyl-like species thus inducing a termination reaction pathway (Eq. 5.6) and in turn a lower conversion. A further decreasing trend of BnOH conversion was observed when the size of glass is increasing. Both phenomena indicate a radical pathway where the extent of BnOH conversion is related to the amount of catalyst available. On the other hand, by considering the selectivity of benzaldehyde, initial concentration of 12 g L^{-1} with 1:2 ratio of hydrogen peroxide will be relatively high: 25-35% (Figure 5.7), however, it was still not ideal, but provides us an indication that the synthesis of benzaldehyde is possible. Further pressurized system could be an option worth to try.

$$\cdot OH + PhC(\cdot)O \rightarrow PhCOOH \quad (Eq. 5.6)$$

An increased H_2O_2 consumption data (for 1:1 and 1:2 ratios) was observed with increasing H_2O_2 concentration (Figure 5.12). This observation suggested the presence of non-radical pathway (Figure 5.13 ab), with radical reactions playing a subsidiary role (Eq.5.7- 5.12). This aligns well with the notable increase in BnOH conversion. This phenomenon is further corroborated by the product selectivity favouring benzaldehyde over those associated with the 1:17 and 1:34 ratios.

Propagation:
$$PhCH_2OH + \cdot OH \rightarrow PhCH_2O\cdot + H_2O \quad (Eq. 5.7)$$
$$PhCH_2O\cdot + PhCH_2OH \rightarrow PhCH_2OH + PhC(\cdot)HOH \quad (Eq. 5.8)$$
$$PhC(\cdot)HOH + H_2O_2 \rightarrow PhCHO + H_2O + \cdot OH \quad (Eq. 5.9)$$

Termination:
$$2 \cdot OH \rightarrow H_2O_2 \quad (Eq. 5.10)$$
$$\cdot OH + PhCH_2O\cdot \rightarrow PhCHO + H_2O \quad (Eq. 5.11)$$
$$2 PhCH_2O\cdot \rightarrow PhCHO + PhCH_2OH \quad (Eq. 5.12)$$
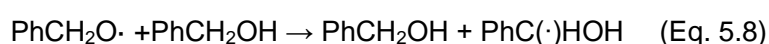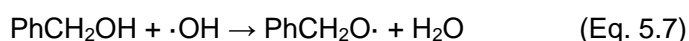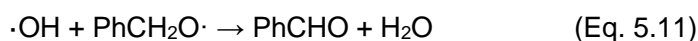
Or: a) "Pure acid base" pathway
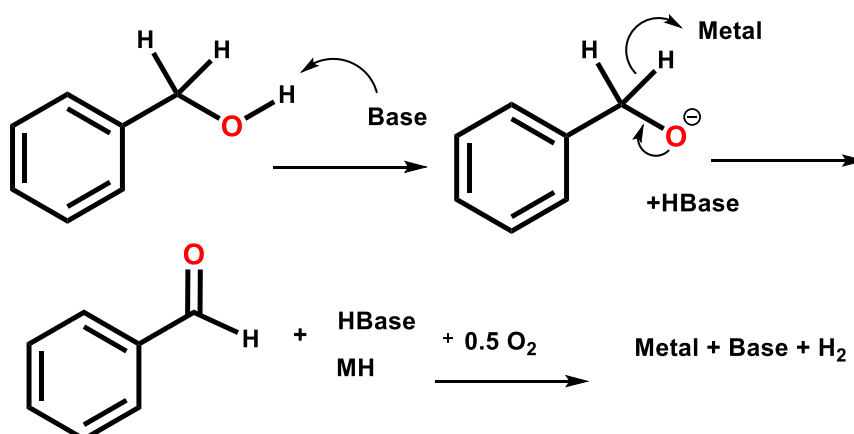
Or: b) Radical H abstraction assisted by an O or metal centre
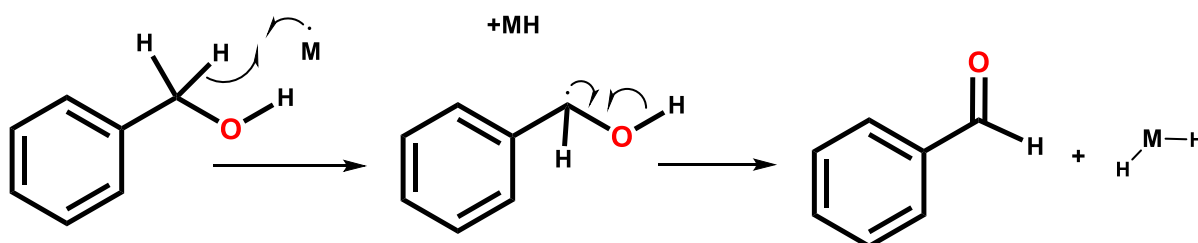
Figure 5.13 Suggested possible benzyl alcohol H-abstraction pathway: a) acid-base pathway, b) radical H-abstraction pathway to form benzaldehyde and water if M is an oxygen species or anhydride if M is a metal.

In conclusion, when limited amount of H_2O_2 was used, H_2O_2 scavenging was not presence, and a direct correlation between H_2O_2 dosage and BnOH conversion was observed (Figure 5.14), suggesting a dominant non-radical pathway: H-abstraction pathway. Only slight increase benzaldehyde selectivity (25-35%) was resulted when increasing initial BnOH concentration (Table 5.7 and Table 5.8), hence, systems using additional pressure might be worth to be considered.
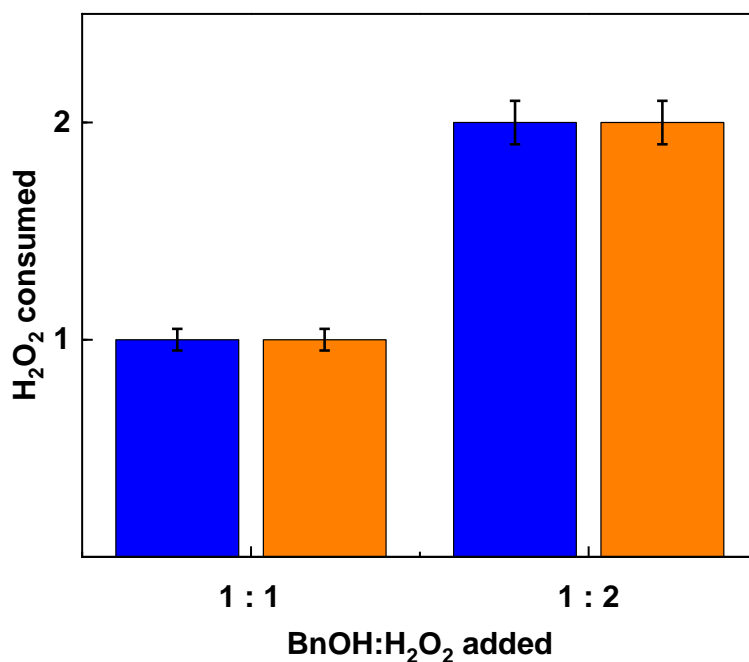
Figure 5.14 H_2O_2 consumption for two initial BnOH concentrations. Reaction conditions: 10 mL of BnOH of 1 g L^{-1} (•) and 12 g L^{-1} (•), **G2** recycled glass, M:S=1:100, <0.1mm as representative, BnOH:H_2O_2=1:1 and 1:2, p = endogenous, 80 °C, 24 h, 500 rpm.

Table 5.7 BnOH (12 g L^{-1}) conversion (Con%), CMB%, benzaldehyde (BzH), benzoic acid (BA) and formic acid selectivity with four different sizes of catalyst. Reaction conditions: **G2** recycled glass (Fe: 0.3 wt.%), M:S=1:100, <0.1, 0.1-0.2, 0.2-0.5 and 0.5-1 mm, BnOH:H_2O_2 ratio of 1:1 and 1:2, p = endogenous, 80 °C, 24 h, 500 rpm.

Catalyst size	BnOH : H_2O_2	Selectivity %			Con %	CMB %
		BzH	BA	formic acid		
<0.1 mm	1:1	25	8	21	57	60
0.1-0.2 mm	1:1	39	7	40	60	67
0.2-0.5 mm	1:1	33	6	38	47	71
0.5-1 mm	1:1	21	4	33	43	68
<0.1 mm	1:2	31	8	27	73	54
0.1-0.2 mm	1:2	29	3	32	52	64
0.2-0.5mm	1:2	25	5	30	44	69
0.5-1 mm	1:2	22	7	32	42	70

Table 5.8 BnOH (1 g L^{-1}) conversion (Con%), CMB%, benzaldehyde (BzH), benzoic acid (BA) and formic acid selectivity with four different sizes of catalyst. Reaction conditions: **G2** recycled glass (Fe: 0.3 wt.%), M:S=1:100, <0.1, 0.1-0.2, 0.2-0.5 and 0.5-1 mm, BnOH:H$_2$O$_2$ ratio of 1:1 and 1:2, p = endogenous, 80 °C, 24 h, 500 rpm.

catalyst size	BnOH : H$_2$O$_2$	Selectivity %			Con %	CMB %
		BzH	BA	formic acid		
<0.1 mm	1:1	16	1	39	46	63
0.1-0.2 mm	1:1	17	1	35	50	60
0.2-0.5 mm	1:1	16	1	36	52	58
0.5-1 mm	1:1	14	2	33	56	54
<0.1 mm	1:2	18	3	45	71	46
0.1-0.2 mm	1:2	16	3	41	83	35
0.2-0.5mm	1:2	19	3	40	81	39
0.5-1 mm	1:2	19	3	38	84	37

5.4.2 Kinetic studies

In order to better understand the trend in the effect of reaction time on BnOH conversion and benzaldehyde selectivity, experiments were carried out using reactions with three different BnOH:H$_2$O$_2$ molar ratios (1:1, 1:2 and 1:4). In these reactions, four different types of recycled glass (particle size less than 0.1 mm) were used for different reaction times (4, 12, 16, 20 and 24 h) at a temperature of 80 °C.
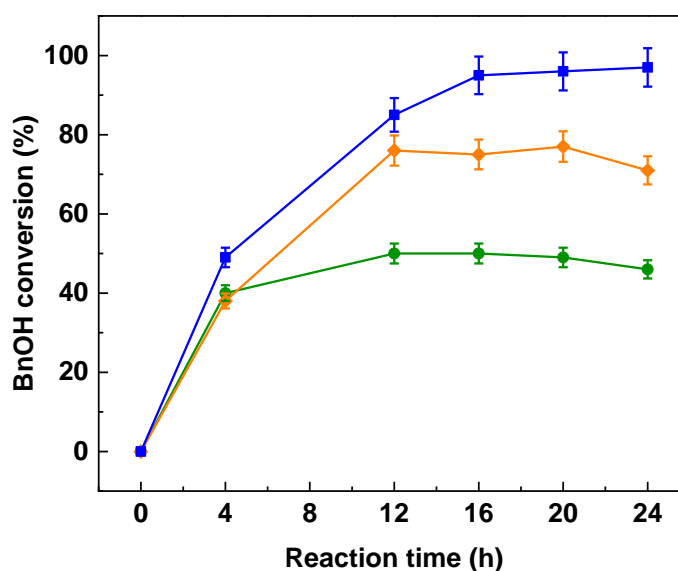
Figure 5.15 Kinetic study of BnOH (1 g L^{-1}) oxidation after 4, 12, 16, 20 and 24 hours reaction. Reaction conditions: **G2** recycled glass (Fe: 0.3 wt.%), M:S=1:100, <0.1 mm as a representative, BnOH:H$_2$O$_2$ molar ratio of 1:1 (●), 1:2 (●) and 1:4 (●), p = endogenous, 80 °C, 24 h, 500 rpm.

The conversion of BnOH reaches a plateau (95 ± 3%) after 16 hours when BnOH:H_2O_2 ratio of 1:4 was used. while for the other two H_2O_2 dosages (1:1 and 1:2), it was achieved 4 hours earlier and kept as 70 ± 3% and 40% respectively. Notably, the increase in the H_2O_2 has led to a greater initial rate of reaction and a higher BnOH conversion within the same reaction time (Figure 5.15). These results showed a direct proportion between H_2O_2 dosages and the BnOH conversion. Unlike the cases where scavenging effect observed when extra H_2O_2 were added, the plateau in this case was likely due to the finishing consumption of the H_2O_2. Moreover, as compared to previous scenario where H_2O_2 dosages of 1:17 was used, BnOH conversion is higher (95 ± 2%) than before (60 ± 2%), this showed the negative effect of scavenging effect and thus implies an existence of radical pathway in the reaction dominating where higher H_2O_2 was utilised.

Moreover, with a smaller amount of H_2O_2 (1:1), the size (amount of iron present) of the glass beads did not make a significant difference on BnOH conversion considering the experimental error. When the amount of hydrogen peroxide increased (1:2 and 1:4), the difference in conversion appears evident (Appendix A4.1). The initiation of this variation was facilitated by the presence of iron on the catalyst, thus emphasizing the radical pathway as the predominant mechanism for the conversion. This is evidenced by the direct proportionality observed between the conversion rate and the concentration of radicals. The kinetic study further confirmed that the conversion results are time dependent relative data, as given enough time, no matter what sizes of glass is used, the conversion will be stable at certain level. Though for catalytic purposes and abatement of pollutants it is important this time to be the shortest possible. In addition, the benzaldehyde yield, remained low as 10% at different stage and condition of our reaction (Table 5.9), thus showing an intermediate like behaviour.

In conclusion, this kinetic study clearly showed the existence of both non-radical and radical pathways in the reaction up to a BnOH:H_2O_2 ratio of 1:4.

Table 5.9 Benzyl alcohol (BnOH: 1g L^{-1}) conversion% (Con%), CMB%, and selectivity% of benzaldehyde (BzH), benzoic acid (BA) and formic acid of BnOH oxidation. Reaction conditions: **G2** recycled glass (Fe: 0.3 wt.%), M:S=1:100, <0.1 mm, as a representative, BnOH:H$_2$O$_2$ molar ratio of 1:1, 1:2 and 1:4, p = endogenous, 80 °C, 24 h, 500 rpm.

Reaction time h	BnOH: H$_2$O$_2$	Selectivity %			Con %	CMB %	Yield %		
		BzH	BA	formic acid			BzH	BA	formic acid
4	1:1	33	0	27	40	72	10	0	8
	1:2	38	0	31	38	75	11	0	9
	1:4	36	2	38	49	69	12	1	13
12	1:1	22	0	41	50	53	6	0	11
	1:2	25	4	43	76	47	9	1	15
	1:4	23	4	48	85	41	8	1	17
16	1:1	31	0	38	41	72	9	0	11
	1:2	19	3	44	75	44	6	1	14
	1:4	12	5	56	95	27	3	1	14
20	1:1	19	1	36	49	62	6	0	11
	1:2	20	3	45	77	43	7	1	15
	1:4	11	5	56	96	25	3	1	13
24	1:1	16	0	39	46	63	5	0	11
	1:2	18	3	45	71	46	6	1	15
	1:4	8	0	55	97	17	1	0	9

5.5   Benzyl alcohol oxidation and degradation pathways determination tests of using H$_2$O$_2$ as oxidant

From the previous experimental results, other than the expected oxidation products such as benzaldehyde, benzoic acid and formic acid, it was noticed that yellow-brownish product was formed where none of the expected products are coloured. This product did not seem to be a result of neither H-abstraction pathway nor a radical pathway. In an acidic reaction condition containing alcohol, an ester and a conjugated product (Figure 5.16 and Figure 5.17) can be resulted from esterification and dehydration respectively. In addition, formic acid is always the first product and comprises the highest selectivity, also indicating a radical dominating reaction. Therefore, in order to figure out what are the possible reaction pathways of BnOH reaction with H$_2$O$_2$, radical termination tests using TEMPO were designed to have a clear observation.
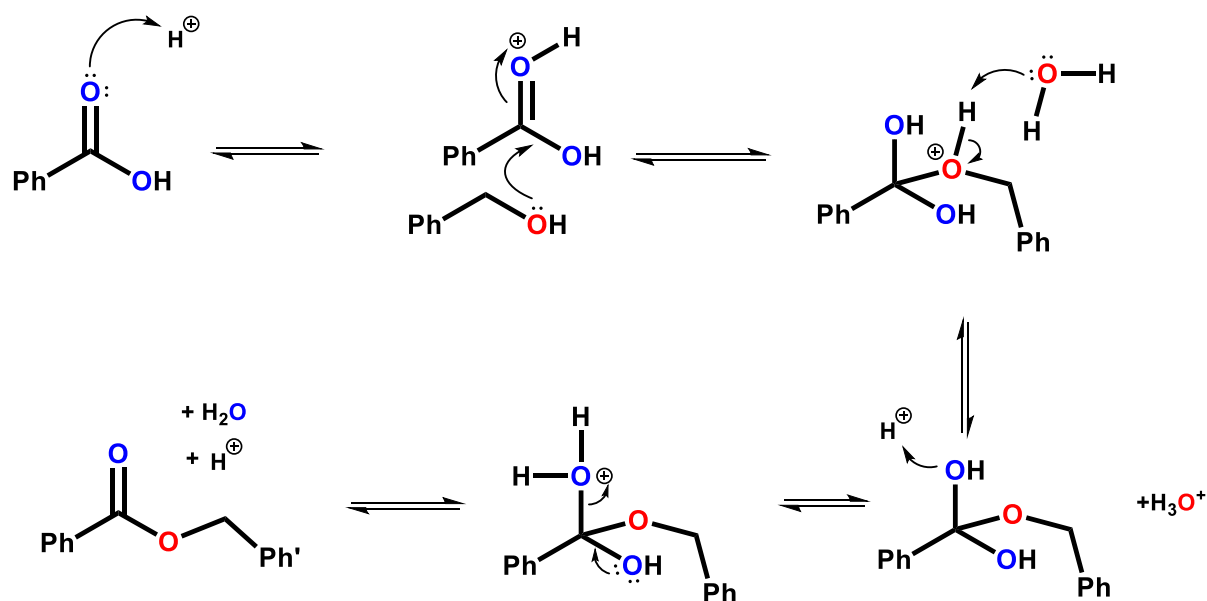
Figure 5.16 Esterification in acidic condition of benzyl alcohol and benzoic acid to form benzyl benzoate.
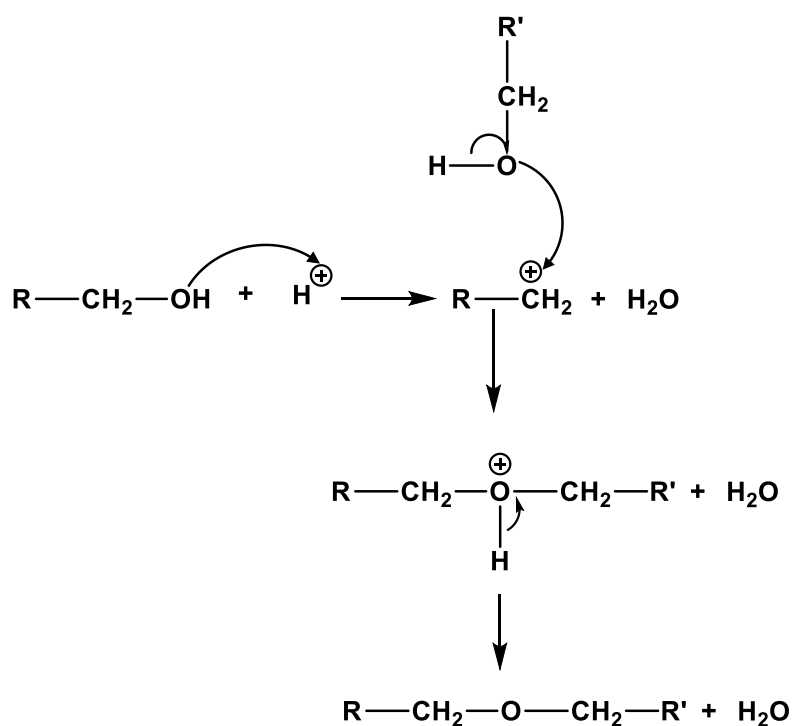
Figure 5.17 Condensation product formation from benzyl alcohol in acidic condition.

5.5.1   Use of TEMPO as inhibitor

In order to directly illustrate the hydroxyl radical produced by iron catalyst and estimate the proportion between the two pathways, a well-known radical, 2,2,6,6-tetramethylpiperidine-1-oxyl (TEMPO) shown in the Figure (Figure 5.18 left), that can serve as a radical scavenger or oxidant was added to interfere the reaction. If oxidation reaction with alcohol using H_2O_2

contains radical pathway, TEMPO may terminate the active ·OH species (Figure 5.18). Moreover, it may also undergo redox reaction to form RNO^+ which can oxidise benzyl alcohol to benzaldehyde (Figure 5.19).[47] The switch between the two is usually amount-dependent. By studying how reaction would be affected upon adding different amount of TEMPO (BnOH: TEMPO of 1:100, 1:10 and 1:4) will provide valuable indication about reaction pathway.
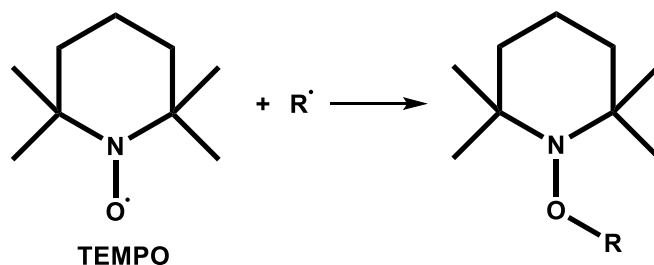
Figure 5.18 Reaction of 2,2,6,6-tetramethylpiperidine-1-oxyl (TEMPO) radical, a strong oxidant (left) with neutral radical, R· is a radical.
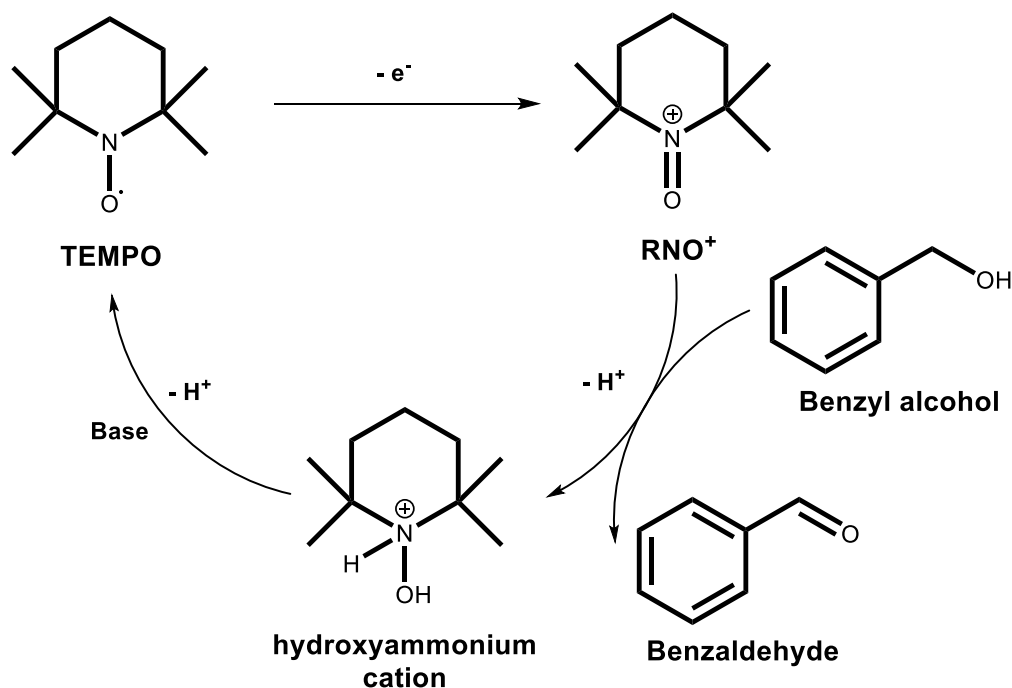
Figure 5.19 Tempo (RNO·) can undergo one-electron oxidation to give the oxoammonium salt (RNO^+) which can oxidise benzyl alcohol to benzaldehyde and itself being reduced to hydroxyammonium cation. In a basic medium, a comproportionation reaction occurs when a mixture of hydroxyammonium cation and oxoammonium salt is converted back to TEMPO.[47,48]

Therefore, BnOH oxidation were conducted with and without TEMPO addition (TEMPO to BnOH 1:100, 1:10 and 1:4). Reactions were carried out with recycled glass **G2** (Fe: 0.3 wt.%, <0.1, 0.1-0.2, 0.2-0.5 and 0.5-1 mm) as catalyst (M: S ratio of 1:100) with $BnOH:H_2O_2$ molar ratio of 1:2. All reactions last for 24 hours at 80 °C, p = endogenous.
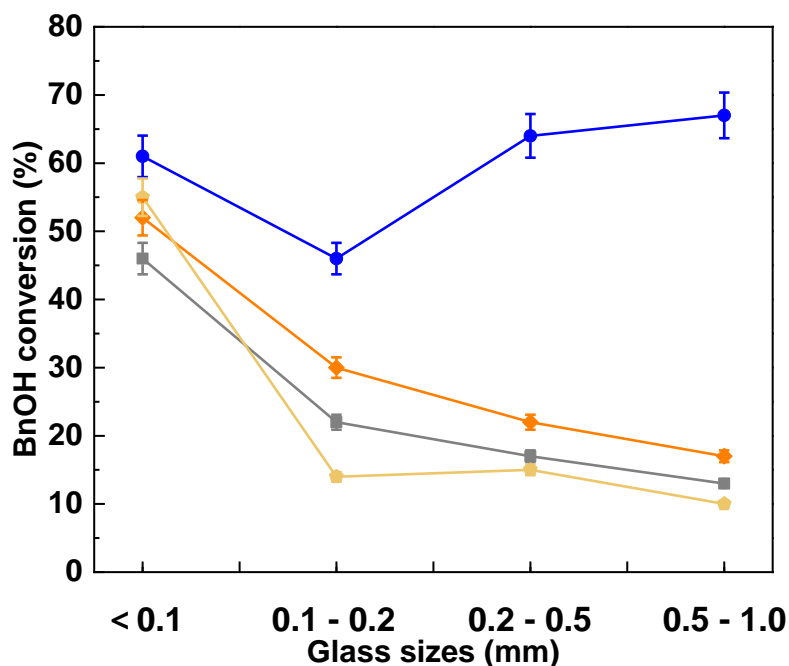
Figure 5.20 BnOH oxidation were conducted with and without TEMPO (•) addition (TEMPO to BnOH 1:100(•), 1:10(•) and 1:4(•)). Reaction conditions: **G2** recycled glass (Fe: 0.3 wt.%), M:S=1:100, <0.1, 0.1-0.2, 0.2-0.5 and 0.5-1 mm, BnOH:H_2O_2 molar ratio of 1:2, p = endogenous, 80 °C, 24 h, 500 rpm.

Without the addition of TEMPO, BnOH conversion has an average value of ca. 60%, with 100% H_2O_2 conversion for all different glass sizes (Figure 5.20). As discussed earlier in Section 5.4.1, this plateau region indicates that the reaction has reached the maximum achievable conversion due to a finished consumption of the available H_2O_2 provided after 24 hours.

In contrast, a positive correlation was observed between the amount of TEMPO added and its effect on BnOH conversion at all three TEMPO dosages. As the TEMPO to BnOH molar ratio increased from 1:100 to 1:4, there was an average decrease of 5% in BnOH conversion (Figure 5.23). The decrease in BnOH conversion may be due to two possible factors. Firstly, since both TEMPO and hydroxyl radicals are free radicals, they may undergo termination reactions with each other, thereby reducing the availability of ·OH radicals required for the Fenton reaction. Secondly, it might also due to the redox reaction (+ 0.61 V) between TEMPO and Fe^{2+} produced from Fe^{2+}/Fe^{3+} interconversion (Eq. 5.13), thus limiting the availability of Fenton agent in the reaction, and in turn inhibiting the production of hydroxyl radical. Therefore, this lacking of hydroxyl radical will in turn led to a reducing in overall BnOH conversion.[47]

$$RNO· + Fe^{2+} + H^+ \rightarrow RNOH + Fe^{3+} \qquad (Eq. 5.13)$$
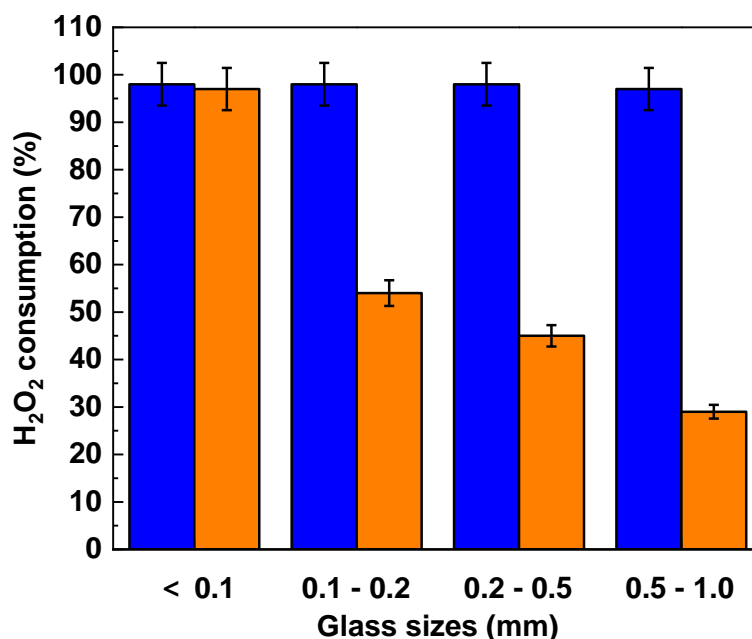
Figure 5.21 H_2O_2 consumption with 1:2 of H_2O_2 addition for BnOH oxidation (1 g L^{-1}) with (●) and without (●) TEMPO addition. Reaction condition: **G2** recycled glass (Fe: 0.3 wt.%), M:S=1:100, <0.1mm, BnOH:H_2O_2 molar ratio of 1:2, TEMPO to BnOH molar ratio 1:100, p = endogenous, 80 °C, 24 h, 500 rpm.

In order to corroborate the results reported above, H_2O_2 consumption was measured after the reaction (Figure 5.21). As compared to reactions free from TEMPO radicals, all of the H_2O_2 was consumed to either hydroxyl radicals or oxygen and water. With the addition of TEMPO, the consumption of H_2O_2 was inhibited. The observation indicates that the Fe catalyst is deficient in generating hydroxyl radicals under the current reaction conditions, as hydrogen peroxide is not being effectively decomposed. Consequently, the first hypothesis seems unlikely. If it were true, the restriction on BnOH conversion would not affect H_2O_2 consumption, as the inhibition should occur after the production of ·OH. Therefore, as proposed in the second hypothesis, by impeding the Fe^{2+}/Fe^{3+} interconversion, both the consumption of H_2O_2 and the conversion of BnOH are likely to be affected. This phenomenon was also observed by Fengqiang Shi where EPR and fluorescence spectroscopies were used to show direct evidence that TEMPO inhibited hydroxyl radical production from the Fenton-like reaction of iron(II)-citrate with hydrogen peroxide by up to 90%.[47] Therefore, the fact that TEMPO inhibits ·OH production from Fenton-like reaction with Fe^{3+} as catalyst was proved, and thus emphasizing a radical dominating pathway.

In addition, the inhibition effect of TEMPO gradually increased when glass size increased, this because of less iron ion was exposed to H_2O_2 to form hydroxyl radicals (Figure 5.20). Besides, larger decrease in formic acid selectivity and thus yield can also be observed (Table 5.10). Thus implying that not only TEMPO is quenching ·OH radicals, but it is also scavenging acyl

carbon-centred radicals, and thus suggesting that the oxidation process from the aldehyde to the acid is also radical, as would be expected by McElroy et al.[49]

However, despite being a quencher, TEMPO can also act with a nearly opposite nature; that is, it can be an oxidiser and, as such, accelerate reaction pathways instead. For the latter, this occurs when TEMPO interconverts to a salt known as oxoammonium salt (Figure 5.19[48]). For this latter role, TEMPO can be used to selectively oxidize primary alcohols to aldehydes and secondary alcohols to ketones.[48] However, similarity to activity/concentration dependency observed for H_2O_2 (Section 4.4) with the larger amount of TEMPO added, it doesn't necessarily trigger further radical/oxidation reaction (hydrogen-abstraction). Therefore, the TEMPO radical concentration may still be insufficient to undergo both redox reaction with iron, and alcohol to have a notable increase in benzaldehyde yield (Table 5.10).

Very importantly though, no matter the amount of TEMPO that was added in the reaction media, the conversion of alcohol always ended up between 10 and 20%. This can be explained by the existence of a non-radical pathway involving molecular oxygen activation and probably an acid-base reaction to take away an H in alpha to the COH group of the alcoholic group and then an H-abstraction from the alcoholic group (Figure 5.13).[50–53] Therefore, a realistic estimate of ratio between radical and non-radical pathway could be 9:1.

In conclusion, dehydration test of 1-phenylethanol confirmed the absence of cationic pathway. Together with the TEMPO test of, the termination of BnOH oxidation reaction largely implied a radical reaction pathway that is dominating the Fenton reaction pathway and a small extent of H-abstraction pathway by molecular oxygen were observed. This result shows demonstrated that by applying BnOH oxidation via the Fenton reaction is unlikely to achieve fine chemical synthesis. As such, in order to increase the selectivity of benzaldehyde, aerobic oxidation with air or molecular oxygen is necessary. Thus, in the next section, investigation on aerobic oxidation of BnOH with both static and dynamic systems is discussed.

Table 5.10 BnOH conversion, CMB, selectivity and yield of benzaldehyde (BzH), benzoic acid (BA) and formic acid of BnOH oxidation. Reaction conditions: **G2** recycled glass (Fe: 0.3 wt.%), M:S=1:100, <0.1, 0.1-0.2, 0.2-0.5 and 0.5-1 mm, BnOH:H_2O_2 molar ratio of 1:2, TEMPO to BnOH molar ratio of 1:100, 1:10 and 1:4, p = endogenous, 80 °C, 24 h, 500 rpm.

TEMPO: BnOH	Catalyst sizes	Selectivity %			Conversion %	CMB %	yield %		
		BzH	BA	formic acid			BzH	BA	formic acid
no TEMPO	less than 0.1 mm	12	1	39	61	48	4	0	11
	0.1-0.2 mm	3	0	10	46	64	1	0	3
	0.2-0.5mm	10	0	34	64	43	3	0	9
	0.5-1 mm	10	0	31	67	49	3	0	10
1:100	less than 0.1 mm	16	0	39	52	58	5	0	12
	0.1-0.2 mm	10	2	30	30	74	2	0	7
	0.2-0.5mm	8	2	21	22	81	1	0	4
	0.5-1 mm	4	3	2	17	84	1	0	0
1:10	less than 0.1 mm	7	0	26	26	77	1	0	5
	0.1-0.2 mm	8	2	23	22	80	1	0	4
	0.2-0.5mm	12	0	22	49	58	3	0	6
	0.5-1 mm	5	3	9	13	88	1	0	1
1:4	less than 0.1 mm	7	0	18	65	41	2	0	5
	0.1-0.2 mm	17	1	16	14	89	2	0	2
	0.2-0.5mm	11	0	15	53	53	3	0	4
	0.5-1 mm	9	5	1	10	92	1	0	0

5.6 Selective benzyl alcohol oxidation using different gas-liquid catalytic reactor

The investigation of the reaction pathway for benzyl alcohol oxidation with H_2O_2 illustrated the concurrent existence of both radical and the likely presence of an oxygen activation pathways. Although the formation of oxygen activated products was confirmed, the reaction was predominantly radical-dominated, with only approximately 10% of the total conversion attributable to the non-radical molecular oxygen activation. Consequently, the selectivity and yield of benzaldehyde remained low (less than 10%) when using H_2O_2 as the oxygen source. As such to improve benzaldehyde selectivity, aerobic oxidation of BnOH (Eq. 5.14) utilizing air or pure O_2 as the oxygen source was examined. Three different systems were investigated: open air, static pressurized, and dynamic bubbling, insufflating air or molecular oxygen. This was done to evaluate the potential for achieving selective benzaldehyde synthesis from BnOH over recycled glass catalysts under these conditions.

$$PhCH_2OH + 0.5\ O_2 \rightarrow PhCOH + H_2O \quad \text{(Eq. 5.14)}$$

5.6.1 Aerobic oxidation with open air

It is important to consider whether externally provided molecular oxygen might be a limiting reagent due to its poor solubility in the reaction medium (Figure 5.22), unlike the in situ formed oxygen from the thermal decomposition of H_2O_2. The in situ oxygen generated within the system is likely more accessible and reactive compared to the externally supplied O_2 gas. Molecular oxygen has a very low solubility in pure or fresh water (about 4 to 24 mg L^{-1}, 1.0 atm at room temperature).[54–56]
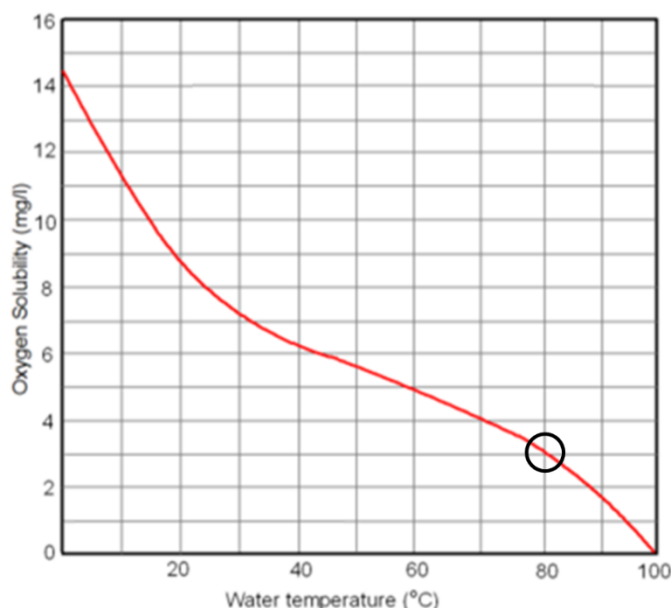
Figure 5.22 Solubility of oxygen from air in water with increasing in temperature. At our reaction conditions (80°C), this (black circle) is roughly 3 time lower than that at room temperature.[55]

For a reaction with 10 mL of BnOH water solution (1 g L^{-1}) at 80 °C and 1 atm, the stoichiometric amount of oxygen needed for complete conversion from benzyl alcohol to benzaldehyde is 4.6×10^{-5} mol where only 9.4×10^{-7} mol (Table 5.12) of O_2 can be dissolved.

To increase the contact between BnOH and O_2, external support such as pressurized systems and continuous oxygen bubbling system were considered. Pressurized systems can increase the solubility of O_2 and reduce the mass transfer limitation effect, while bubbling system that continuously provides a supply of O_2, which is vented at the same time after mixing can provide a better mixing with a higher local O_2 concentration (Table 5.11).

Table 5.11 Pros and cons of using static pressurized system and open flow system for aerobic benzaldehyde synthesis from benzyl alcohol.[57–59]

	Static Pressurized System	**Open flow System**
Pros	- Higher reaction rates due to increased oxygen solubility.	- Simple setup and equipment requirements.
	- Enhanced mass transfer of oxygen leads to improved product yields.	- Better mixing of reactants and oxygen through bubbling.
	- Suitable for reactions requiring higher oxygen concentrations.	- Generally safer due to lower pressure.
Cons	- Requires specialized equipment and safety precautions.	- Reaction rates may be limited by oxygen transfer rate.
	- Higher energy consumption.	- Longer reaction times compared to pressurized systems.
	- Potential for side reactions due to high pressure and temperature.	- Lower oxygen concentration in the reaction mixture.

5.6.2 Aerobic oxidation with pressurized systems

To increase the solubility of oxygen, a Radley set-up with a 50 mL ACE round bottom flask was used. A gauge pressure, which is the pressure relative to ambient atmospheric pressure, was set from 1 to 3 bar (1 to 3 bar above the ambient atmospheric pressure) with air as the source of oxygen.

The amount of oxygen and nitrogen dissolved in water can be calculated with Henry's law (Eq. 5.15). The concentration is proportional to the partial pressure of the gas. Therefore, the solubility of oxygen at 1, 2 and 3 bar at 80°C are 1.9×10^{-4}, 2.8×10^{-4} and 3.7×10^{-4} mol L^{-1} respectively (Table 5.12).

$$c = p_g/k_H \quad \text{(Eq. 5.15)}$$

Where:

c= solubility of dissolved gas

k_H= proportionality constant depending on the nature of the gas and the solvent

p_g= partial pressure of gas

Table 5.12 Solubility of oxygen at 80 °C and the no. of mole of oxygen required and actual dissolved at difference pressure (1 atm, P_g 1, 2 and 3 bar).

Gauge pressure	Solubility of oxygen in water at 80 °C mg L^{-1}	Solubility of oxygen in water at 80 °C mol L^{-1}	O₂ dissolved from air mol	O₂ required mol
0*	3	9.4×10^{-5}	9.4×10^{-7}	4.62×10^{-5}
1	6	1.9×10^{-4}	1.9×10^{-6}	4.62×10^{-5}
2	9	2.8×10^{-4}	2.8×10^{-6}	4.62×10^{-5}
3	12	3.7×10^{-4}	3.7×10^{-6}	4.62×10^{-5}

*P_g=0 correspond to an atmosphere pressure of 1 atm.

Control experiments were conducted with benzyl alcohol alone and with added $Fe(NO_3)_3 \cdot 9H_2O$ at M:S molar ratios of 1:100, 1:10, 1:5, and 1:3 at 80°C and 100°C. No conversion of BnOH was observed under these conditions (Table 5.13). Although the calculated number of moles of oxygen dissolved in the initial 10 mL of reaction solution was less than the stoichiometric amount required (4.62×10^{-5} mol, as shown in Table 5.12), the continuous 24-hour supply of air should have provided a total of approximately 4.0×10^{-2} mol of oxygen, which is sufficient to meet the reaction requirements. Furthermore, even when using an oxygen cylinder setup, ensuring a constant supply of oxygen from the open cylinder would prevent oxygen from becoming a limiting reagent during the 24-hour reaction period.

In addition, although the 10 mL reaction volume and continuous stirring can reduce mass transfer limitations, the externally supplied molecular oxygen still needs to displace the solvent molecules from the catalyst surface to participate in the reaction. This process requires energy and could create an additional diffusional barrier, even in the small-volume, well-mixed system. Therefore, assuming negligible diffusional effects may not be accurate, as oxygen must overcome the solvation shell around the catalyst to reach the active sites.

The reaction temperature of 100°C approached the upper limit employed in other aerobic BnOH oxidation studies.[12] A commonly used upper temperature limit of around 100°C aims to prevent undesirable side reactions (over-oxidation, decarboxylation), or degradation of reactants and products that may occur at higher temperatures. Moreover, as demonstrated in other reports,[60] directly supplying molecular oxygen improves benzaldehyde yields compared to using air due to higher partial pressure. It is implied that one of the elementary steps in the reaction mechanism is bimolecular with respect to oxygen. This is because the rate of a bimolecular reaction depends on the partial pressure or concentration of the reactants. Hence, applying molecular oxygen should increase dissolved O_2 concentrations and enhance benzaldehyde synthesis.

Table 5.13 BnOH conversion (con%) and CMB% results for of BnOH oxidation. Reaction conditions: 10 mL BnOH (1 g L^{-1}), Fe(NO$_3$)$_3$·9H$_2$O, M:S=1:100, 1:10, 1:5 and 1:3, molecular oxygen provided by pressurized system, p = 1, 2 and 3 bar, 80 and 100 °C, 24 h, 500 rpm. There is no reaction observed after 24 hours.

Pg bar	Catalyst M:S 1:100	M:S	Temperature °C	con%	CMB%
1 to 3	-	-	80	0	100
1 to 3	Fe(NO$_3$)$_3$·9H$_2$O	1:100	80	1	99
1 to 3	Fe(NO$_3$)$_3$·9H$_2$O	1:10	80	1	99
1 to 2	Fe(NO$_3$)$_3$·9H$_2$O	1:10	100	1	99
2	Fe(NO$_3$)$_3$·9H$_2$O	1:5	100	1	99
2	Fe(NO$_3$)$_3$·9H$_2$O	1:3	100	0	100

The oxygen source was replaced with molecular oxygen, with a reaction temperature 100 °C, at a M: S molar ratio of 1:5 and gauge pressure of 2 bar, no conversion was observed with Fe(NO$_3$)$_3$·9H$_2$O as catalyst. The use of recycled glass with Fe^{3+} showed no conversion (Table 5.13). On the other hand, formation of benzaldehyde was observed with FeSO$_4$·7H$_2$O at an M:S molar ratio of 1:10 and 1:5 (Table 5.14). This result implied that at the reaction condition of M:S of 1:10 at 100 °C, Fe^{2+} can successfully activate molecular O_2.[61]

Moreover, the interconversion between Fe^{2+} and Fe^{3+} plays a crucial role in the aerobic oxidation mechanism. It involves Fe^{2+} donating an electron to O_2, thereby converting Fe^{2+} to Fe^{3+} (Eq. 5.16 to 5.17). However, this Fe^{2+}/Fe^{3+} interconversion does not propagate as a full

redox cycle, unlike the case with H_2O_2 where Fe^{3+} needs to be reduced back to Fe^{2+}. As a result, once all Fe^{2+} is converted to Fe^{3+}, the reaction may be quenched due to insufficient activated oxygen supply.[61]

$$Fe^{2+} + O_2 \rightarrow Fe^{3+} + O_2 \cdot^- \qquad \text{(Eq. 5.16)}$$
$$2H^+ + Fe^{2+} + O_2 \cdot^- \rightarrow Fe^{3+} + H_2O_2 \qquad \text{(Eq. 5.17)}$$
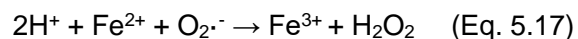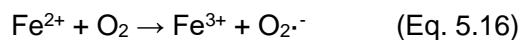
Literature reports a dynamic flow of molecular oxygen which has successfully achieved a benzaldehyde yield of 36% at 80°C with Fe^{3+} as the catalyst (M:S 1:33) after 24 hours of reaction.[60] For further investigation, a set-up with a mass flow controller supplying molecular oxygen was used.

Table 5.14 BnOH conversion (con), CMB, selectivity and yield towards benzaldehyde (BA) synthesis. Reaction conditions: 10 mL BnOH (1 g L^{-1}), Fe(NO$_3$)$_3$·9H$_2$O, FeSO$_4$·7H$_2$O and **G2** recycled glass (Fe: 0.3 wt.%), M:S=1:100, 1:10 and 1:5 <0.1, 0.1-0.2, 0.2-0.5 and 0.5-1 mm, molecular oxygen provided by pressurized system, p = 2 bar, 100 °C, 24 h, 500 rpm.

Catalyst	M:S	Con %	CMB %	Selectivity %		Yield %	
				BA	formic acid	BA	formic acid
-	-	0	100	0	0	0	0
Fe(NO$_3$)$_3$·9H$_2$O	1:10	0	100	0	0	0	0
Fe(NO$_3$)$_3$·9H$_2$O	1:5	0	100	0	0	0	0
G2	1:5	-2	102	0	0	0	0
FeSO$_4$·7H$_2$O	1:100	0	100	0	0	0	0
FeSO$_4$·7H$_2$O	1:10	9	92	11	0	9	0
FeSO$_4$·7H$_2$O	1:5	19	85	24	2	40	3

5.6.3 Aerobic oxidation with flow of O_2 by mass flow controller

Aerobic oxidation of BnOH was conducted with molecular oxygen provided at a flow rate of 5 mL min^{-1}. $Fe(NO_3)_3 \cdot 9H_2O$ and $FeSO_4 \cdot 7H_2O$ catalyst were used as control tests before recycled glass (Fe: 0.3 wt.%) was used. Control tests were carried out and showed that O_2 was not the limiting reagent (Appendix A4.2).

At 100°C, both Fe^{3+} ($Fe(NO_3)_3 \cdot 9H_2O$) and Fe^{2+} ($FeSO_4 \cdot 7H_2O$) led to approximately 20% conversion of benzyl alcohol at M:S molar ratios of 1:100 and 1:10 (Table 5.15). However, selectivity favoured carbon dioxide formation over benzaldehyde. Recycled glass was used at an M:S molar ratio of 1:5, with successive oxidation reactions conducted using freshly prepared glass. After 5 reaction cycles, 52% BnOH conversion to mostly formic acid was attained. Gas chromatography-mass spectrometry could be suggested to identify any reaction intermediates based on mass fragmentation patterns if further investigation is interested.

Nevertheless, these results demonstrate the ability of both Fe^{3+} and Fe^{2+} ions to activate molecular oxygen and catalyse benzyl alcohol oxidation. This study can be viewed as a preliminary investigation, laying the groundwork for further exploration into glass modification to enhance selectivity towards benzaldehyde. With additional development, this approach could enable a greener and more environmentally friendly method for selective benzaldehyde synthesis.

Table 5.15 BnOH conversion, CMB results for BnOH oxidation by molecular oxygen. Reaction conditions: 8 mL BnOH (1 g L^{-1}), $Fe(NO_3)_3 \cdot 9H_2O$, $FeSO_4 \cdot 7H_2O$ and **G2** recycled glass (Fe: 0.3 wt.%), M:S=1:100, 1:10 and 1:5, <0.1 mm, molecular oxygen provided by a mass flow controller, flow rate of 5 mL min^{-1}, $p = 2$ bar ,100 °C, 4 h, 500 rpm. Reaction mixture with recycled glass was recycled and repeated with same reaction condition using fresh prepared glass beads for another four runs. Only reaction with reactivity towards formic acid was observed for all reaction.

Catalyst	M:S	Conversion %	CMB %
-	-	4	96
$Fe(NO_3)_3 \cdot 9H_2O$	1:100	18	82
$Fe(NO_3)_3 \cdot 9H_2O$	1:10	16	84
$FeSO_4 \cdot 7H_2O$	1:100	9	94
$FeSO_4 \cdot 7H_2O$	1:10	16	84
G2	1:5	30	70
2nd run	1:5	36	64
3rd run	1:5	40	60
4th run	1:5	44	56
5th run	1:5	52	48

5.7   Conclusion

Benzaldehyde is an important aromatic aldehyde used as additives in perfumes, beverages, and a as a platform chemical for the synthesis of pharmaceuticals. Traditionally synthesized from benzyl chloride and toluene, these methods generate toxic chlorinated by-products under harsh conditions. Thus, benzaldehyde production via benzyl alcohol oxidation has become prevalent in industry due to facile control and high yields. The resulting growth in benzyl alcohol demand and in turn its manufacturing has led to contaminated wastewater, motivating the use of a greener oxidant. Recently, benzyl alcohol mineralization was explored via Fenton reactions along with aerobic oxidations using air or O_2 after elucidating the reaction pathways. This work examined recycled glass as a catalyst for more environmentally friendly benzaldehyde synthesis from benzyl alcohol oxidation with molecular oxygen.

The ^{1}H-NMR method for analysing benzyl alcohol oxidation was validated using 2-propanol as an internal standard and DMSO-d6 as the NMR solvent, and extensively utilized for quantitative analysis in this work.

Hydrogen peroxide scavenging effects observed during benzyl alcohol mineralization indicated the presence of a radical pathway. Varying the initial benzyl alcohol concentration did not increase mineralization but improved benzaldehyde selectivity, suggesting the concurrent existence of a radical and non-radical pathway. The H-abstraction pathway was more pronounced under mimicked benzaldehyde synthesis conditions using H_2O_2.

Pathway determination experiments using O_2 deficiency or inhibitors like TEMPO demonstrated the reaction with H_2O_2 proceeded via a Fenton-like mechanism, which was predominantly radical-mediated with approximately 10% attributable to a molecular oxygen activation pathway.

Due to the low aqueous solubility of oxygen, different experimental set-ups were employed to increase dissolved or local O_2 concentrations for aerobic benzaldehyde synthesis based on the findings. However, Fe^{3+} and thus recycled glass did not exhibit significant selectivity towards benzaldehyde formation under the conditions tested.

5.8　　References

(1)　Freitag, W.; Stoye, D. *Paints,* Coatings and Solvents; John Wiley & Sons, 2008.

(2)　Scognamiglio, J.; Jones, L.; Vitale, D.; Letizia, C. S.; Api, A. M. *Food and Chemical Toxicology*, 2012, **50**, S140-S160.

(3)　Younes, M.; Aquilina, G.; Castle, L.; Engel, K. H.; Fowler, P.; Fürst, P.; Gürtler, R.; Gundert-Remy, U.; Husøy, T.; Mennes, W.; Moldeus, P.; Oskarsson, A.; Shah, R.; Waalkens-Berendsen, I.; Wölfle, D.; Boon, P.; Crebelli, R.; Di Domenico, A.; Filipič, M.; Mortensen, A.; Van Loveren, H.; Woutersen, R.; Gergelova, P.; Giarola, A.; Lodi, F.; Frutos Fernandez, M. J. *EFSA Journal*, 2019, **17**, 05876.

(4)　Lv, L. B.; Yang, S. Z.; Ke, W. Y.; Wang, H. H.; Zhang, B.; Zhang, P.; Li, X. H.; Chisholm, M. F.; Chen, J. S. *ChemCatChem*, 2018, **10**, 3539-3545.

(5)　Thao, N. T.; Nhu, N. T.; Lin, K. S. *Journal of the Taiwan Institute of Chemical Engineers*, 2018, **83**, 10-22.

(6)　J. Jachuck, R. J.; K. Selvaraj, D.; S. Varma, R. *Green Chemistry*, 2006, **8**, 29-33.

(7)　Ragupathi, C.; Judith Vijaya, J.; Narayanan, S.; Jesudoss, S. K.; John Kennedy, L. *Ceramics International*, 2015, **41**, 2069–2080.

(8)　Ndolomingo, M. J.; Meijboom, R. *Applied Surface Science*, 2017, **398**, 19-32.

(9)　Zhu, S.; Cen, Y.; Yang, M.; Guo, J.; Chen, C.; Wang, J.; Fan, W. *Applied Catalysis B: Environmental*, 2017, **211**, 89-97.

(10)　Christoskova, S. T.; Stoyanova, M. *Water Research*, 2002, **36**, 2297-2303.

(11)　Sadiq, M.; Ilyas, M.; Alam, S. *Tenside Surfactants Detergents*, 2012, **49**, 37-42.

(12)　Marotta, R.; Di Somma, I.; Spasiano, D.; Andreozzi, R.; Caprio, V. *Chemical Engineering Journal*, 2011, **172**, 243-249.

(13)　Huang, K.; Fu, H.; Shi, W.; Wang, H.; Cao, Y.; Yang, G.; Peng, F.; Wang, Q.; Liu, Z.; Zhang, B.; Yu, H. *Journal of Catalysis*, 2019, **377**, 283-292.

(14)　Datta Mal, D.; Khilari, S.; Pradhan, D. *Green Chemistry*, 2018, **20**, 2279-2289.

(15)　Lu, C.; Hu, J.; Meng, Y.; Zhou, A.; Zhang, F.; Zhang, Z. *Chemical Engineering Research and Design*, 2019, **141**, 181-186.

(16)　Gizli, A.; Aytimur, G.; Alpay, E.; Atalay, S. *Chemical Engineering & Technology*, 2008, **31**, 409-416.

(17)　Miao, C.; Zhao, H.; Zhao, Q.; Xia, C.; Sun, W. *Catalysis Science & Technology*, 2016, **6**, 1378-1383.

(18)　Guo, C. C.; Liu, Q.; Wang, X. T.; Hu, H. Y. *Applied Catalysis A: General*, 2005, **282**, 55-59.

(19)　Mahmood, A.; Robinson, G. E.; Powell, L. *Organic Process Research & Development*, 1999, **3**, 363-364.

(20)　Thottathil, J. K.; Moniot, J. L.; Mueller, R. H.; Wong, M. K. Y.; Kissick, T. P. *The Journal of Organic Chemistry*, 1986, **51**, 3140-3143.

(21) Cánepa, A. L.; Elías, V. R.; Vaschetti, V. M.; Sabre, E. V.; Eimer, G. A.; Casuscelli, S. G. *Applied Catalysis A: General*, 2017, **545**, 72-78.

(22) Cao, Y.; Luo, X.; Yu, H.; Peng, F.; Wang, H.; Ning, G. *Catalysis Science & Technology*, 2013, **3**, 2654-2660.

(23) Cao, Y.; Li, Y.; Yu, H.; Peng, F.; Wang, H. *Catalysis Science & Technology*, 2015, **5**, 3935-3944.

(24) Chen, C. T.; Nguyen, C. V.; Wang, Z. Y.; Bando, Y.; Yamauchi, Y.; Bazziz, M. T. S.; Fatehmulla, A.; Farooq, W. A.; Yoshikawa, T.; Masuda, T.; Wu, K. C. W. *ChemCatChem*, 2018, **10**, 361-365.

(25) Chen, H.; Shen, J.; Chen, K.; Qin, Y.; Lu, X.; Ouyang, P.; Fu, J. *Applied Catalysis A: General*, 2018, **555**, 98-107.

(26) Yuan, Z.; Liu, B.; Zhou, P.; Zhang, Z.; Chi, Q. *Catalysis Science & Technology*, 2018, **8**, 4430-4439.

(27) Zhan, G.; Huang, J.; Du, M.; Sun, D.; Abdul-Rauf, I.; Lin, W.; Hong, Y.; Li, Q. *Chemical Engineering Journal*, 2012, **187**, 232-238.

(28) Albadi, J.; Alihoseinzadeh, A.; Razeghi, *Catalysis Communications*, 2014, **49**, 1-5.

(29) Liu, J.; Zou, S.; Lu, L.; Zhao, H.; Xiao, L.; Fan, J. *Catalysis Communications*, 2017, **99**, 6-9.

(30) Ganesamoorthy, S.; Muthu Tamizh, M.; Shanmugasundaram, K.; Karvembu, R. *Tetrahedron Letters*, 2013, **54**, 7035-7039.

(31) Villa, A.; Wang, D.; Dimitratos, N.; Su, D.; Trevisan, V.; Prati, L. *Catalysis Today*, 2010, **150**, 8-15.

(32) Hu, Y.; Chen, L.; Li, B. *Catalysis Communications* 2018, **103**, 42-46.

(33) Martín, S. E.; Suárez, D. F. *Tetrahedron Letters*, 2002, **43**, 4475-4479.

(34) Wang, N.; Liu, R.; Chen, J.; Liang, X. *Chemical Communications*, 2005, **37**, 5322-5324.

(35) Zhang, E.; Tian, H.; Xu, S.; Yu, X.; Xu, Q. *Organic Letters*, 2013, **15**, 2704-2707.

(36) Hu, Y.; Chen, L.; Li, B. *RSC Advances*, 2016, **6**, 65196-65204.

(37) Gathungu, R. M.; Kautz, R.; Kristal, B. S.; Bird, S. S.; Vouros, P. T. *Mass Spectrometry Reviews*, 2018, **39**, 35-54.

(38) *Benzyl alcohol.* https://go.drugbank.com/drugs/DB06770 (accessed 2024-03-18).

(39) *Benzoic acid.* https://go.drugbank.com/drugs/DB03793 (accessed 2024-03-18).

(40) Sokolenko, S.; McKay, R.; Blondeel, E. J. M.; Lewis, M. J.; Chang, D.; George, B.; Aucoin, M. G. *Metabolomics*, 2013, **9**, 887-903.

(41) Giraudeau, P.; Silvestre, V.; Akoka, S. *Metabolomics*, 2015, **11**, 1041-1055.

(42) Liu, S.; Yao, S.; Zhang, H.; Hu, C. *AAPS PharmSciTech*, 2017, **18**, 1895-1900.

(43) Li, H.; Shang, J.; Yang, Z.; Shen, W.; Ai, Z.; Zhang, L. *Environmental science & technology*, 2017, **51**, 5685-5694.

(44) Li, X.; Huang, X.; Xi, S.; Miao, S.; Ding, J.; Cai, W.; Liu, S.; Yang, X.; Yang, H.; Gao, J.; Wang, J.; Huang, Y.; Zhang, T.; Liu, B. *Journal of the American Chemical Society*, 2018, **140**, 12469-12475.

(45) Arnaut, L.; Formosinho, S.; Burrows, H. *Chemical Kinetics*, 2021, **133**, 77-113.

(46) Singh, R. *Computer Applications in Food Technology*, 1996, **217**, 91–107.

(47) Shi, F.; Zhang, P.; Mao, Y.; Wang, C.; Zheng, M.; Zhao, Z. *Biochemical and Biophysical Research Communications*, 2017, **483**, 159-164.

(48) Bobbitt, J. M. *ChemInform*, 2011, **42**.

(49) McElroy, W. J.; Waygood, S. J. *Journal of the Chemical Society, Faraday Transactions*, 1991, **87**, 1513-1521.

(50) Dess, D. B.; Martin, J. C. *Journal of the American Chemical Society*, 1991, **113**, 7277-7287.

(51) Brown, H. C.; Rao, C. G.; Kulkarni, S. U. *The Journal of Organic Chemistry*, 1979, **44**, 2809-2810.

(52) Banerji, K. K. *Bulletin of the Chemical Society of Japan*, 1978, **51**, 2732-2734.

(53) Ashenhurst, J. *Master Organic Chemistry.* 2015 https://www.masterorganicchemistry.com/2015/05/21/demystifying-alcohol-oxidations.

(54) *Oxygen and water*. https://water.lsbu.ac.uk/water/o2water.html (accessed 2024-04-16).

(55) *Oxygen - Solubility in Fresh and Sea Water vs. Temperature*. https://www.engineeringtoolbox.com/oxygen-solubility-water-d_841.html (accessed 2024-04-16).

(56) Chwastowski, J.; Ciesielski, W.; Khachatryan, K.; Kołoczek, H.; Kulawik, D.; Oszczęda, Z.; Soroka, J. A.; Tomasik, P.; Witczak, M. *Water*, 2020, **12**, 2488.

(57) Caravati, M.; Grunwaldt, J.-D.; Baiker, *Catalysis Today*, 2004, **91-92**, 1-5.

(58) Obermayer, D.; Balu, A. M.; Romero, A. A.; Goessler, W.; Luque, R.; Kappe, C. O. *Green chemistry*, 2013, **15**, 1530-1537.

(59) Hommes, A.; Disselhorst, B.; Yue, J. *AIChE Journal*, 2020, **66**, 17005.

(60) Sahu, D.; Silva, A. R.; Das, P. *RSC advances*, 2015, **5**, 78553-78560.

(61) Mundra, S.; Tits, J.; Wieland, E.; Angst, U. M. *Chemosphere*, 2023, **335**, 138955.

Chapter 6 1-phenylethanol selective oxidation using recycled glass

6.1   Introduction

1-Phenylethanol (1-PEA) is a simple aromatic secondary alcohol which is an important raw material for spices, aromatic agents, and chemical intermediates such as the nonsteroidal anti-inflammatory drug Ibuprofen, and possesses versatility across chemical syntheses.[1] Optically active phenyl ethanol derivatives, which per se is also chiral, serve as chiral synthetic building blocks and intermediates within various industries including pharmaceuticals, agrochemicals, flavours, and fine chemicals.[2,3] In particular, (R)-1-phenylethanol finds specialized use as a fragrance, solvatochromic dye, ophthalmic preservative, and inhibitor of cholesterol intestinal adsorption in pharmaceutical, cosmetic, and chemical applications.[2] Additionally, the esterified derivatives of racemic 1-phenylethanol hold roles in perfumeries, soaps, detergents, cosmetics, room sprays, deodorants, and flavours.[3] Consequently, demand of 1-PEA continues to rise and is expected to reach 100 metric tons annually, primarily driven by its use as a fragrance additive.[4]

In addition to its use in the pharma sector, 1-PEA serves as an intermediate by-product in the petrochemical industry during the coproduction of propylene oxide and styrene monomer (POSM). However, 1-PEA was (and still is) mostly discharged into aquatic systems mainly through industrial emissions.[5,6] POSM production processes generate 1-PEA in wastewater effluents at concentrations ranging from 114-240 mg L^{-1}, it accounts for 12 wt.% of the styrene and propylene oxide (SPO) wastewater[7–9] and is considered to be hazardous to human health and may cause many acute effects such as skin irritation and transient corneal injury.[10]

Toxicity studies on freshwater organisms show a 96-hour median lethal concentrations (LC50) of 100 mg L^{-1} in zebrafish,[11] 48-hour LC50 values of 345 mg L^{-1} in golden orfe,[12] 48-hour median effective concentrations (EC50) of 45.32 mg L^{-1} in invertebrates, and 72-hour EC50 of 200 mg L^{-1} in aquatic algae and cyanobacteria.[11] In recent decades, POSM plants have proliferated globally,[13] substantially escalating the likelihood of 1-PEA release into nearby

waterways and marine environments. The extensive utilization of 1-PEA coupled with the rise in POSM facilities warrants concern regarding potential ecological impact, which the current work aims to address within a circular economy framework.

The removal of 1-PEA from petrochemical wastewaters is a significant challenge. Research has shown that conventional wastewater treatment methods, such as activated sludge processes or aerobic biological treatment, are ineffective due to the compound's recalcitrant nature and resistance to biodegradation.[14] In addition, existing advanced oxidation processes wastewater treatment technologies are costly, require high-energy consumption and are not environmentally friendly due to the use of oxidants like Cl_2, ClO_2, which will lead to production of by-products that need further treatment.[15,16] With recycled glass to replace conventional catalyst, the cost are highly reduced, since the used glass beads can be further reused. Consequently, selecting the most appropriate advanced treatment method with H_2O_2 as oxidant is more environmentally friendly and has become an urgent task in the field of environmental protection.

Moreover, as mentioned in Chapter 5, the conversion of alcohols to carbonyls via oxidation has been extensively studied due to the importance of ketones and aldehydes in biomass conversion[17] and fine chemical synthesis.[18,19] So the current work could potentially open up new routes to these important applications.

In fact, stoichiometric oxidants typically, $KMnO_4$ and $K_2Cr_2O_7$ for benzyl alcohol have been widely used in the fine chemicals industry.[20,21] However, as explained in Chapter 5, using these oxidants has its limitations due to the toxicity of the produced waste or the spent transition metal left[18,22,23]. The main oxidation product of 1-PEA, acetophenone (AP), is also an important compound used in spices, flavours and pharmaceutical industries.[19,24,25] As a result, the primary scope for this chapter will include investigating the possibility of AP synthesis by aerobic oxidation using recycled glass.

By using the same scheme used and described in Chapter 5, in this chapter, we will describe 1) the identification of a ^{1}H-NMR method for the quantification of 1-phenylethanol oxidation

products; 2) the feasibility and effectiveness of acetophenone synthesis from 1-phenylethanol oxidation with recycled glass using air or molecular oxygen; 3) the feasibility and effectiveness of using the Fenton reaction with recycled glass in removing 1-phenylethanol from wastewater in place of a partial oxidation.

6.2 Identification of an ^{1}H-NMR 1-phenylethanol oxidation quantification method

As previously discussed in Chapter 5, unlike phenol and ibuprofen decomposition via the Fenton reaction where a very large number of intermediates were normally detected (Chapter 3 and 4), oxidation process of 1-phenylethanol is expected to lead to acetophenone (Figure 6.1). Therefore, ^{1}H-NMR quantification method was then developed based on the validated method of benzyl alcohol where 2-propanol was applied as internal standard and DMSO-d6 as NMR solvent.
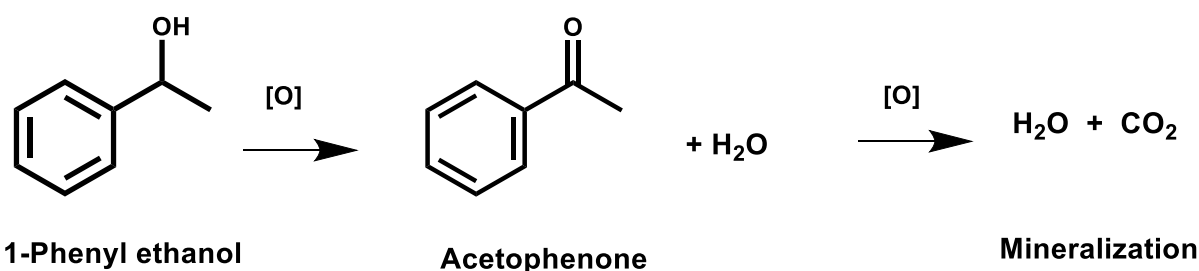
Figure 6.1 Oxidation of 1-phenylethanol to acetophenone and ultimately water and carbon dioxide. [O] is an arbitrary oxidant containing oxygen.

6.2.1 ^{1}H-NMR analysis of standards

Firstly, standard solutions of 1-phenylethanol and acetophenone were used to have an appropriate starting point to develop quantification and qualification via ^{1}H-NMR. Although 1-phenylethanol and acetophenone have a relatively high solubility in water (17.5 g L^{-1} and 6 g L^{-1} respectively), to maintain a consistency with previous experiments, co-solvent was still used for standards making. 1 g L^{-1} of 1-phenylethanol was prepared by dissolving ca. 0.1 g of 1-phenylethanol and 1 g L^{-1} of acetophenone were prepared by dissolving ca. 0.1 g of acetophenone using co-solvent (volume ratio of water and methanol 95:5) to ensure all the

chemicals were fully dissolved. ^{1}H-NMR analysis of 1-phenyl alcohol (Figure 6.2) and acetophenone (Figure 6.3) were performed with deuterated DMSO-d6 as solvent under water suppression to avoid the interference of water peak (δ ppm 4.76-4.66).

As discussed in Chapter 5, several criteria must be met to ensure a reliable and informative characterization via spectroscopy. These include clear peak resolution, a high signal-to-noise ratio, and a stable baseline, precise and consistent peak positioning, well-defined peak shapes, and appropriate signal intensity. The NMR spectra obtained for the two chemicals under study (Figures 6.2 and 6.3) fulfil these requirements. The spectra exhibit sharp, narrow peaks with high signal intensity relative to the baseline noise. The baseline is in phase without distortions. Peak positions are consistent between samples with ± 0.05 ppm. Therefore, the NMR methodology employed here satisfies the essential prerequisites for robust method development.
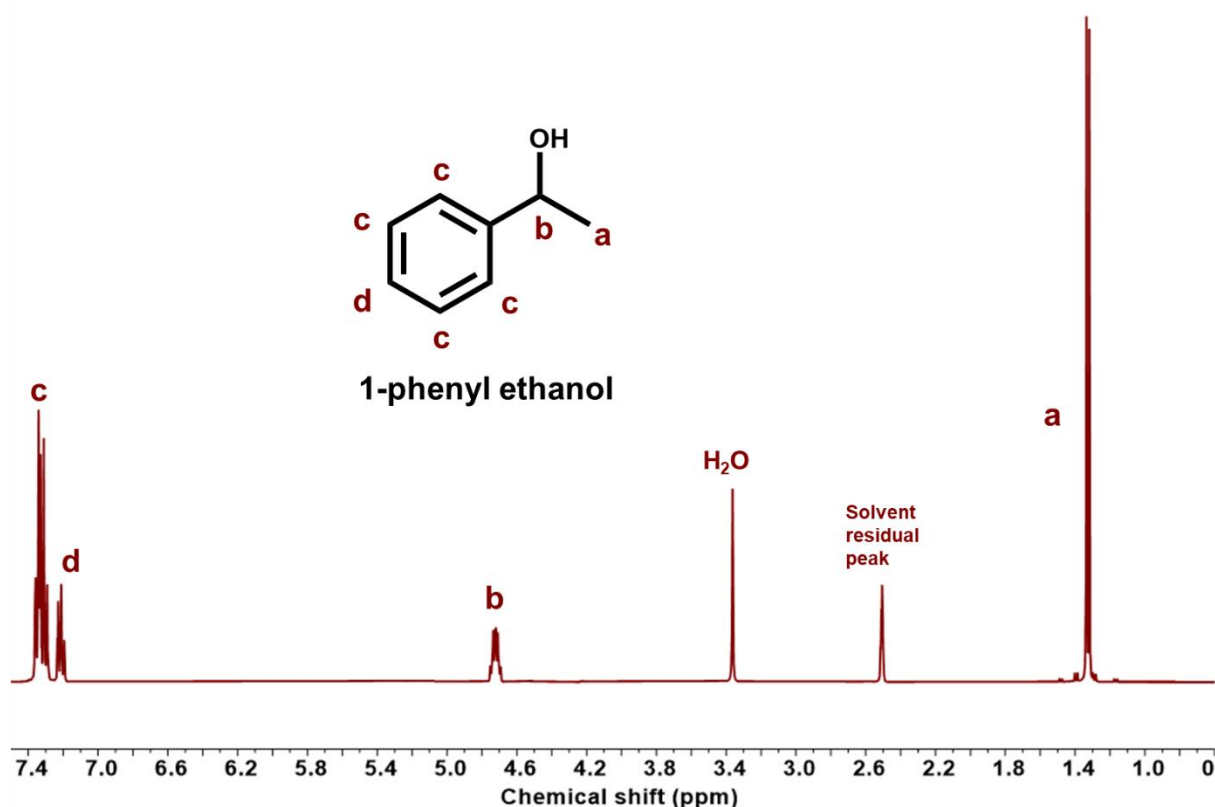
Figure 6.2 1-phenylethanol: ^{1}H-NMR (400 MHz, DMSO-d6), c: δ ppm 7.33 (m, 4H), d: 7.30 (m, 1H), b: 4.72 (q, 1H), a: 1.32 (d, 3H).
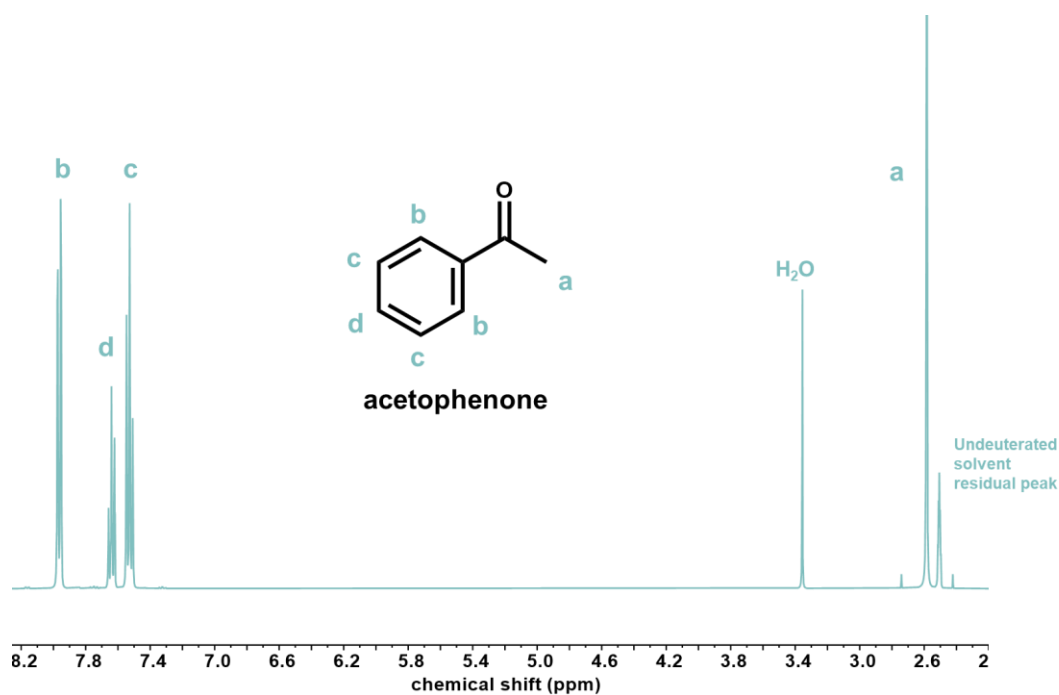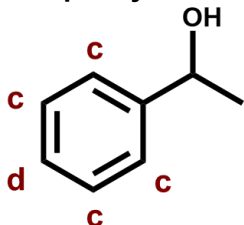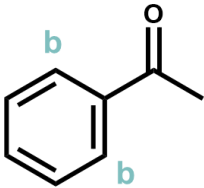
Figure 6.3 Acetophenone: ^{1}H-NMR (400 MHz, deuterated DMSO-d6), b: δ ppm 7.92 (dt, 2H), d: 7.58 (tt, 1H), c: 7.47 (tt, 2H), a: 2.58 (s, 3H).
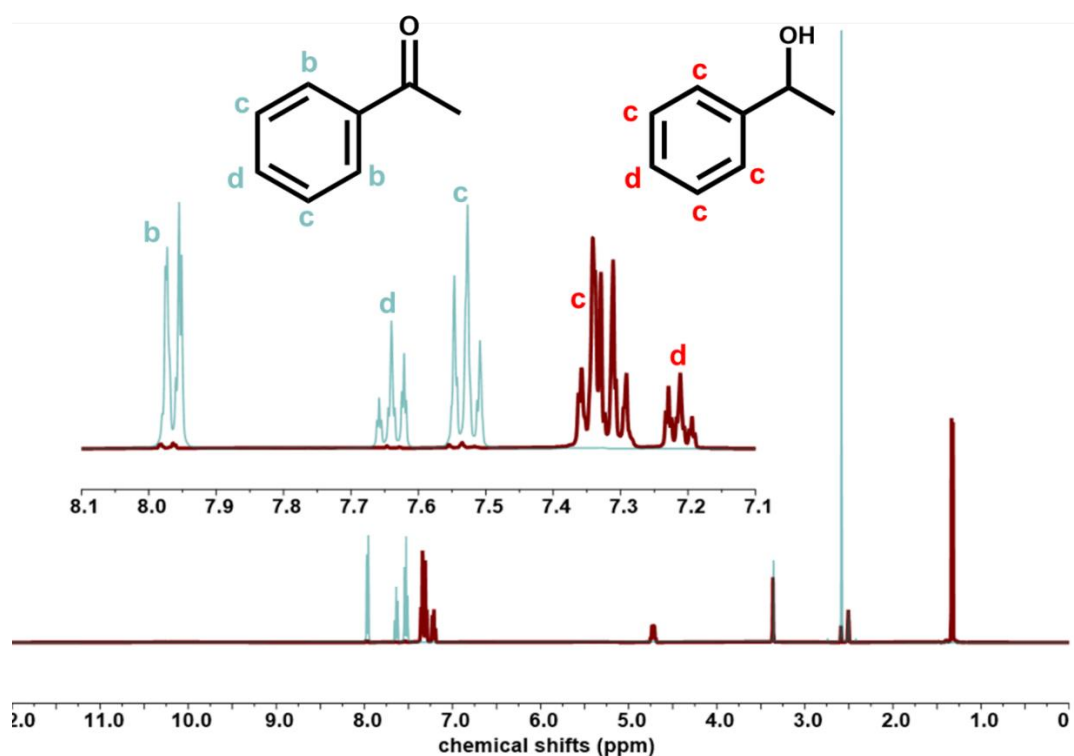
Figure 6.4 Stacked ^{1}H-NMR spectra of 1-phenylethanol (●) and its oxidation product acetophenon (●). The main figure highlights the full spectral ranges, while the inset focuses on the regions containing the diagnostic, characteristic peaks for each compound. Using this stacked spectrum with highlighted regions allows straightforward identification and quantification of the reaction components.

After properly characterizing the individual NMR spectra of the chemicals, it is crucial to identify non-overlapping characteristic peaks for each compound when present in a reaction mixture. This ensures accurate quantification of each analyte. By overlaying the spectra of 1-phenylethanol and acetophenone (Figure 6.4), suitable distinct peaks were determined for each as follows: 1-phenylethanol: δ ppm 7.3 (m, 5H) and acetophenone: δ ppm 7.95 (d, 2H) (Table 6.1). Using these isolated peaks, a quantitative NMR calculation was used to determine the molar concentration of each component in a mixture.

Table 6.1 A summary of NMR data of 1-phenylethanol and its corresponding potential dehydration products acetophenone with the characteristic chosen for the conversion and CMB%.

Compound	Characteristic peak δ (ppm)
1-phenylethanol	c and d: 7.33-7.30 (m, 5H)
Acetophenone	b: 7.92 (dt, 2H)

Given the similar chemical shift regions for 1-phenylethanol, acetophenone, benzyl alcohol, and its products, 2-propanol, previously validated as a suitable internal standard for benzyl alcohol oxidation, is also a good choice for the current system. To verify instrumental reproducibility using 2-propanol as the internal standard and water suppression, a minimum of five distinct NMR samples were prepared for each compound according to a fixed protocol.

For 1-phenylethanol, the deviation was determined to be -3% for sample preparation and 1% for the NMR instrument, which fall within acceptable ranges (± 5%) using the co-solvent

method. For acetophenone, a slightly larger deviation of -8% was observed for sample preparation. However, given that quantification relies on two distinct peaks only, this discrepancy is deemed acceptable, and was subsequently incorporated as a correction factor in subsequent CMB% calculations given the standard deviation was in a range of 1% or less.

6.2.2 Application of 2-propanol as internal standard on the mimic mixture

While 2-propanol demonstrated accurate and consistent results as an internal standard for the individual chemicals, it is useful to further validate its applicability for mixtures containing all three compounds at varying stages of oxidation. As such, five distinct model mixtures of 1-phenylethanol and acetophenone standard solutions were prepared, encompassing different molar ratios to mimic progressive reaction stages (Table 6.2). CMB% calculations for each mixture were performed incorporating the previously determined correction factor, thereby validating the quantitative methodology for systems where all product concentrations are known.

Table 6.2 Five mimic mixtures of 1-phenylethanol (1-PEA) and acetophenone (AcP) were prepared in terms of different molar ratio. The discrepancy between expected and measured ratios is calculated as relative deviation, and the CMB% is calculated with correction factor from previous section. Each NMR sample includes 500 µL of DMSO-d6, 200 µL of analyte and 15 µL of 2-propanol solution.

Mixture	1-PEA: AcP molar ratio	*Deviation on Acp %	CMB %
#1	7.4:1	9	101
#2	1.9:1	-2	102
#3	1.2:1	-5	102
#4	1:1.4	-3	99
#5	1:3.8	0	98

*relative deviation= ((measured value-expected value)/expected value) ×100%, with the value of 1-PEA as a standard.

Except for mixture #1, where a limited acetophenone was added, (in relative terms) both compounds exhibited similar deviation patterns across the four model mixtures. For simplified comparison, the molar ratio of 1-phenylethanol was set as the standard due to its lower inherent variance. Analysis of the four mimic mixtures revealed the % deviation of the

measured versus expected molar ratios for 1-phenylethanol and acetophenone fell within an acceptable range (-3%). This aligned with the previously observed discrepancy between the two compounds (-5%). Given acetophenone's larger intrinsic quantification inaccuracy (-8%), the greater divergence noted when smaller amounts were added is acceptable, if taking into account that a small integration error will have larger effect on a small peak rather than a large one. The consistency within this comprehensive data set demonstrates reliable, coherent results.

Incorporation of the correction factor resulted in CMB% values of approximately 101% for the five model mixtures, compatible with 100% when accounting for experimental error. Thus validating also the use of a co-solvent during standard solution preparation to ensure accuracy. Noteworthy the internal standard concentration was diluted to match sample magnitude for NMR analysis.

Consequently, the NMR method for 1-phenylethanol oxidation has been successfully validated, providing a robust and reliable approach for future analyses in this chapter.

6.3   1-Phenylethanol mineralization via the Fenton reaction

Based on the attempted mineralization of benzyl alcohol to carbon dioxide and water via the Fenton reaction, although full mineralization was not achieved (50%), an analogous study was still worth to be applied to explore the capabilities of recycled glass to oxidize, either partially or in full 1-phenylethanol.

6.3.1 Control tests

A critical initial step is the performance of control experiments to elucidate the roles of the catalyst and oxidant within the novel reaction system. Accordingly, 1-phenylethanol (1 g L^{-1}) abatement reactions were carried out, like in the case of benzyl alcohol utilizing two different unsupported iron salt catalysts, $Fe(NO_3)_3 \cdot 9H_2O$ and $FeSO_4 \cdot 7H_2O$. In the first instance, based on the stoichiometric reaction (Eq. 6.1), the complete mineralization of one mole of 1-phenylethanol via the Fenton reaction requires 20 moles of H_2O_2. To investigate the effect of

198

H_2O_2 concentration, gradually increasing dosages from a 1-phenylethanol:H_2O_2 molar ratio of 1:1 up to 1:400 was applied. The reactions proceeded with an iron catalyst at a M:S molar ratio of 1:100, at 80°C for 4 hours under endogenous pressure.

$$C_8H_{10}O + 20\ H_2O \rightarrow 8\ CO_2 + 25\ H_2O \quad \text{(Eq. 6.1)}$$
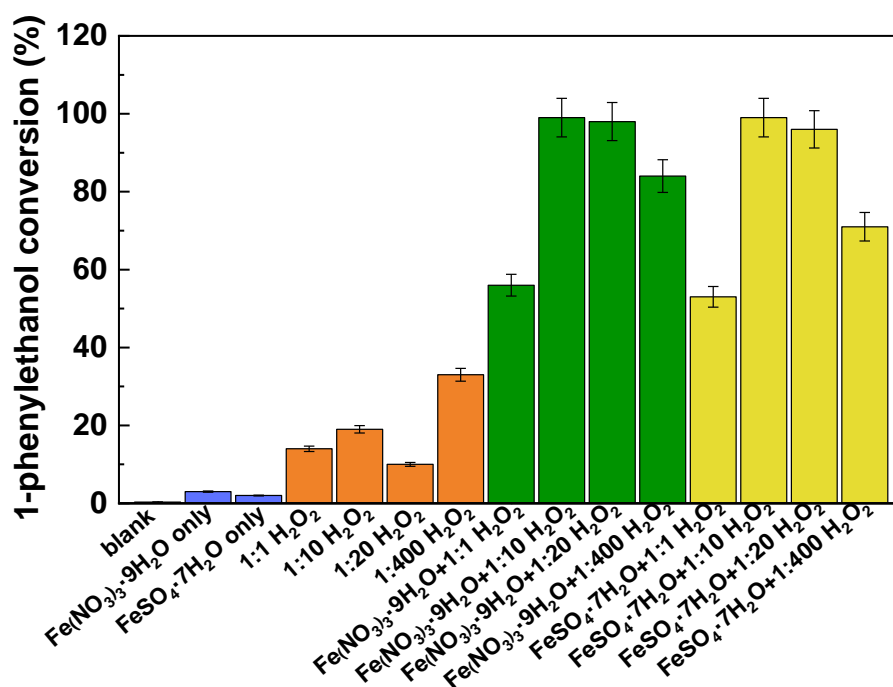
Figure 6.5 1-phenylethanol oxidation conversion of different control tests: blank, $Fe(NO_3)_3\cdot9H_2O$ and $FeSO_4\cdot7H_2O$ only (●), different amount of hydrogen peroxide only(●), and $Fe(NO_3)_3\cdot9H_2O$ (●) and $FeSO_4\cdot7H_2O$ (●) with four different amount of hydrogen peroxide. Reaction conditions: 10 mL of 1-PEA (1 g L^{-1}), $Fe(NO_3)_3\cdot9H_2O$ and $FeSO_4\cdot7H_2O$, M:S=1:100, 1-PEA:H_2O_2=1:1, 1:10, 1:20 and 1:400, p = endogenous, at 80°C, 4 h, 500 rpm.

As expected, negligible 1-phenylethanol conversion (2 ± 1%) was observed after 4 hours in the absence of H_2O_2 (Figure 6.5). The lack of hydroxyl radical (·OH) generation effectively prevent oxidation of 1-phenylethanol under these conditions. Upon introduction of up to stoichiometric quantities of H_2O_2 without catalyst, 1-phenylethanol conversions remained below 20%, with only a more than 30% increase to 33% observed with excess H_2O_2 due to the limited amount of hydroxyl radical generated from thermal decomposition of H_2O_2 (ca. 3%, as studied in Section 3.2.1). However, with the addition of two different iron salts, $Fe(NO_3)_3\cdot9H_2O$ and $FeSO_4\cdot7H_2O$, a significant enhancement in conversion from 10% to 100% at the

stoichiometric level was achieved. This highlights, also for this substrate, the vital role of iron salts in catalysing hydroxyl radical formation and thereby promoting the Fenton reaction.

It is also notable that the addition of excess H_2O_2 led to an unfavourable 20% decrease in 1-phenylethanol conversion (Figure 6.5). This observation suggests that the generation of surplus hydroxyl radicals inadvertently inhibited the 1-phenylethanol oxidation process. The decreased conversion can be attributed to radical scavenging by the excess H_2O_2, lowering the overall ·OH availability (Eq. 3.6 and 3.7).

The inhibitory effect of excess hydrogen peroxide is consistent with previous observations in Fenton reactions involving other aromatic pollutants such as phenol, ibuprofen, and benzyl alcohol, and suggests that the quenching is probably due to the excess of H_2O_2 rather than a specific substrate. In view of these data, we then move on to the investigation on the application of recycled glass in this reaction mechanism.

6.3.2 Effect of different recycled glasses

Four different coloured recycled glass samples (Fe wt.%: 0.07 to 0.3) with varying particle diameters were chosen for catalytic testing. It was evident that the catalytic efficiency of recycled glass was lower compared to pure iron salts though by using a same molar M:S ratio of 1:100. Hence, an initial reaction time of 24 hours was selected for the recycled glass experiments. Reactions were conducted using a stoichiometric amount of hydrogen peroxide (1-PEA:H_2O_2 1:20) at 80°C under endogenous pressure.
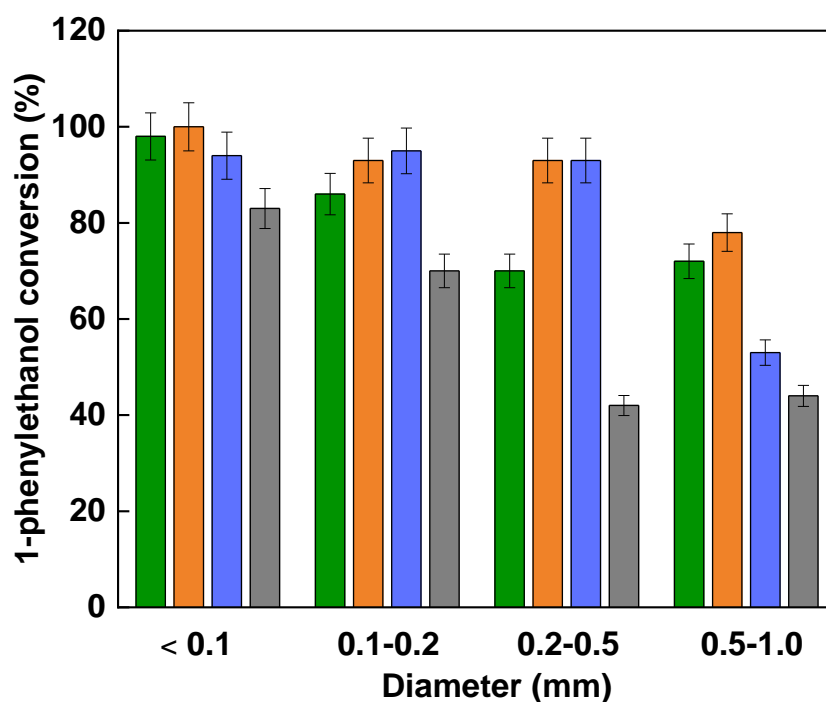
Figure 6.6 1-phenylethanol oxidation conversion with 4 different types of recycled glass beads. Reaction condition: 10 mL of 1-PEA (1 g L^{-1}), $Fe(NO_3)_3 \cdot 9H_2O$ and $FeSO_4 \cdot 7H_2O$, **G2** recycle glass (Fe: 0.3 wt.% ●), **G3** recycle glass (Fe: 0.2 wt.% ●), **G4** recycled glass (Fe: 0.2 wt.% ●), and **G5** recycled glass (Fe: 0.07 wt.% ●). (<0.1, 0.1-0.2, 0.2-0.5 and 0.5-1 mm, M:S=1:100, 1-PEA:H_2O_2=1:20 (stoichiometric amount), p = endogenous, at 80°C, 24 h, 500 rpm.

Given the free-radical mechanism we elucidated in the case of benzyl alcohol (see sections 5.3.2 and 5.3.3), the reactivity trend observed for 1-phenylethanol degradation using recycled glass catalysts of varying sizes is anticipated to follow the principles previously outlined. Specifically, increasing the glass particle size is expected to decrease the exposure of Fe^{3+} sites to H_2O_2, thereby reducing hydroxyl radical generation and resulting in lower overall reactivity (Figure 6.6). This confirms the possibility of application of recycled glass in removing 1-phenylethanol from wastewater, if an appropriate bead size is selected.

Table 6.3 1-phenylethanol (1 g L^{-1}) conversion, CMB%, acetophenone (AcP) and formic acid selectivity with 4 different types of recycled glass beads. Reaction conditions: 10 mL of 1-PEA (1 g L^{-1}), **G2** recycle glass (Fe: 0.3 wt.%), **G3** recycle glass (Fe: 0.2 wt.%), **G4** recycled glass (Fe: 0.2 wt.%), and **G5** recycled glass (Fe: 0.07 wt.%), <0.1, 0.1-0.2, 0.2-0.5 and 0.5-1 mm, M:S=1:100, 1-PEA:H$_2$O$_2$=1:20 (stoichiometric amount), p = endogenous, at 80°C, 24 h, 500 rpm.

Catalyst (Fe. wt.%)	Diameter mm	Conversion %	CMB %	Selectivity %	
				AcP	formic acid
G2 (0.3)	<0.1	98	16	9	44
	0.1-0.2	86	36	22	28
	0.2-0.5	70	51	27	25
	0.5-1	72	50	22	23
G3 (0.2)	<0.1	100	19	0	48
	0.1-0.2	93	20	9	36
	0.2-0.5	93	23	12	44
	0.5-1	78	38	17	30
G4 (0.2)	<0.1	94	21	12	35
	0.1-0.2	95	20	13	19
	0.2-0.5	93	23	17	2
	0.5-1	53	64	29	23
G5 (0.07)	<0.1	83	33	15	33
	0.1-0.2	70	46	21	8
	0.2-0.5	42	68	21	29
	0.5-1	44	68	23	27

It is notable that after a 24-hour reaction, high mineralization of 1-phenylethanol was achieved with the smallest glass size (M:S 1:100 at 80 °C), as evidenced by the low carbon mass balance (Table 6.3, CMB < 20%). In contrast, reactions with the other glass sizes typically resulted in ca. 40% CMB. This is a surprising result since previous substrates like phenol and benzyl alcohol, with simpler structures, struggled to reach full mineralization under identical conditions. On the other hand, the H in alpha position with respect to the carbon of the hydroxyl group can easily be abstracted by free radical species[26,27] that is the ionization step for this substrate would be much more favourable than for benzyl alcohol and much more favourable than phenol. This could explain the lower CMB we detect. Nevertheless, a rigorous interpretation of the data indicates that the lower CMB may involve non-chemical or non-entirely chemical factors. 1) The inability of NMR to detect all intermediates, for example if decarboxylation occurs, this could lead to methanol, which due to its high volatility by the time

an NMR sample is collected. 2) The formation of precipitates. 3) Potential reactor leakage.

As a consequence, some control experiments were undertaken: 1) Reduction the reaction time and temperature to minimize evaporation of volatile by-products although this may also inhibit catalyst efficacy. 2) Use of closed systems, like pressurized reaction vessels.

6.3.3 Control tests on intermediates formation

To investigate potential volatile intermediates formed during the 24-hour 1-phenylethanol degradation reaction, two modifications were made to the original conditions. First, the temperature was lowered from 80°C to 60°C (Table 6.4), despite the possibility of reduced catalyst efficacy. Second, the reaction time was shortened to 6 hours, in an effort to detect intermediates before further decomposition. **G1** recycled glass beads (Fe: 0.23 wt.%) with four particle size ranges (<0.1, 0.1-0.2, 0.2-0.5, and 0.5-1 mm) was chosen as a representative catalyst. Reactions were performed at an M:S ratio of 1:100, with the stoichiometric quantity of hydrogen peroxide (1-PEA:H_2O_2 1:20) under endogenous pressure.

Table 6.4 1-phenylethanol (1 g L^{-1}) conversion (con), selectivity and yield of acetophenone (AcP) and formic acid. Reaction conditions: 10 mL of 1-PEA (1 g L^{-1}), **G1** recycled glass (Fe: 0.23 wt.%), <0.1, 0.1-0.2, 0.2-0.5 and 0.5-1 mm, M:S=1:100, 1-PEA:H_2O_2 =1:20 (stoichiometric amount), p = endogenous, at 80°C, 24 h; 60°C, 24h; 80°C, 6 h, 500 rpm. Despite the reduction on either reaction temperature or time, no clear intermediate peak other than acetophenone was observed, any minor losses would be under the detection limit of NMR and can be considered insignificant.

T °C	Time h	Diameter mm	Con %	CMB %	Selectivity %		Yield %	
					AcP	formic acid	AcP	formic acid
60	24	<0.1	64	47	12	46	4	14
		0.1-0.2	46	63	14	35	4	10
		0.2-0.5	33	73	15	34	4	8
		0.5-1	30	76	16	37	4	8
80	6	<0.1	73	52	17	29	6	11
		0.1-0.2	39	70	21	20	6	5
		0.2-0.5	33	72	10	49	2	12
		0.5-1	33	75	30	21	7	5
80	24	<0.1	98	16	9	44	1	7
		0.1-0.2	86	36	22	28	7	9
		0.2-0.5	70	51	27	25	10	9
		0.5-1	72	50	22	23	8	8

The ^{1}H-NMR spectra of the reaction mixtures under milder conditions revealed no clear

intermediate peak other than acetophenone in any sample. As a result, under the current reaction conditions (80°C, 24 h), any minor losses would be under the detection limit of NMR and can be considered insignificant.

Furthermore, under the milder reaction conditions, two sets of reactions (Figure 6.7, grey, orange lines) exhibited an overall 40% decrease in 1-phenylethanol conversion compared to the standard conditions (Figure 6.7, blue), as anticipated. Despite the lower conversions, the decreasing reactivity trend with increasing catalyst particle size from <0.1 to 1 mm persisted. As for all these substrates smaller particles expose more Fe^{3+} sites to interact with H_2O_2 to generate the hydroxyl radicals required for 1-phenylethanol decomposition. The consistency of this reactivity trend demonstrates that, for a fixed H_2O_2 dosage, the availability of hydroxyl radicals depends on the accessible Fe^{3+} sites, which in turn governs the ultimate 1-phenylethanol conversion.
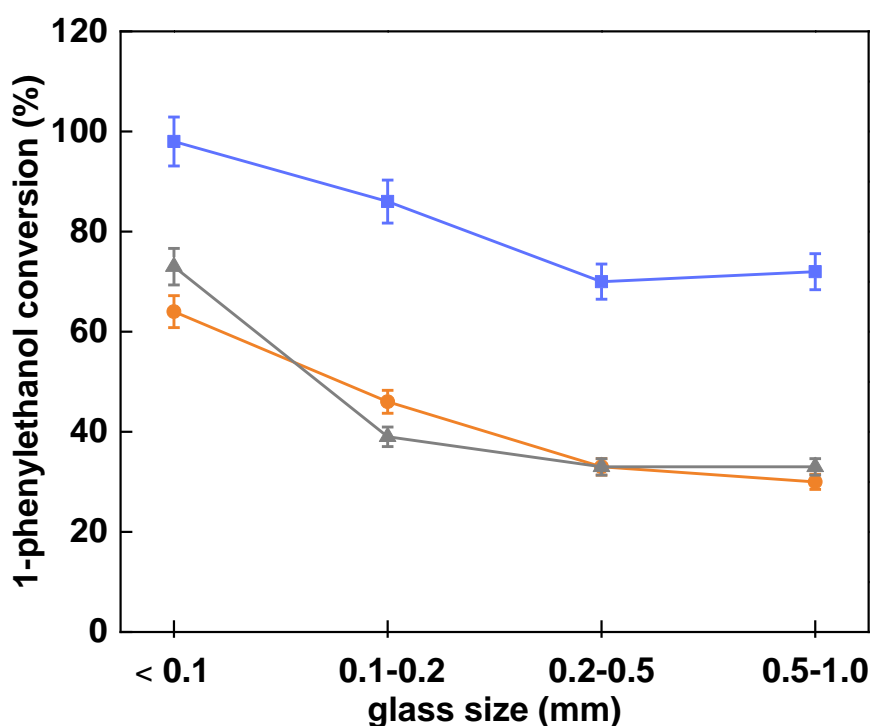
Figure 6.7 1-phenylethanol (1 g L^{-1}) conversion (con). Reaction conditions: 10 mL of 1-PEA (1 g L^{-1}), **G1** recycled glass (Fe: 0.23 wt.%), <0.1, 0.1-0.2, 0.2-0.5 and 0.5-1 mm, M:S=1:100, 1-PEA:H_2O_2=1:20 (stoichiometric amount), p = endogenous, at 80°C, 24 h (●); 60°C, 24h (●); 80°C, 6 h (●), 500 rpm.

In conclusion, no obvious intermediate was detected within the limits of ^{1}H-NMR, indicating negligible carbon loss through volatilization. However, conjugated products may also form under acidic conditions (Figure 6.8), which may contribute to the loss of carbon. Further work with more sensitive analytical techniques such as HPLC can be applied to comprehensively close the carbon balance and fully account for reaction intermediates and products like ethanol.
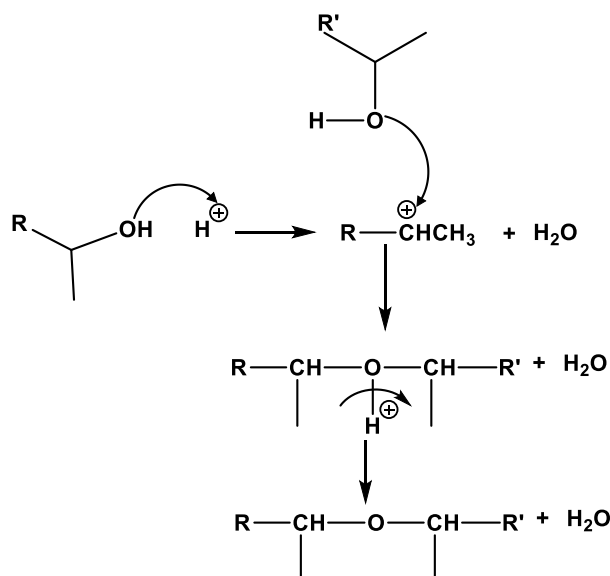
Figure 6.8 Acid catalysed condensation product formation from 1-phenylethanol to diethyl phenyl ether.

6.4   1-phenylethanol partial oxidation with H_2O_2

Although the promising result of a high mineralisation (>75%) of 1-phenylethanol by H_2O_2 was achieved, a high selectivity to formic acid is undesirable as it results in acidic water. Therefore, an increased selectivity to acetophenone via oxidation of 1-phenylethanol was then investigated.

As the previous reaction conditions have led to a high selectivity towards formic acid, water and carbon dioxide, to study if a shorter reaction will increase the selectivity of acetophenone, a kinetic study was undertaken using 1-phenylethanol (1 g L^{-1}) aqueous solutions. **G2** recycled glass containing (Fe: 0.3 wt.%) and four particle size ranges.

Table 6.5 Selectivity, yield of acetophenone (AcP) and formic acid, conversion (con) and CMB% of 1-phenylethanol oxidation with of kinetic study of 1-phenylethanol oxidation with **G2** recycled glass as catalyst (Fe: wt.0.3%). Reaction conditions: 10 mL of 1-PEA (1 g L^{-1}), **G2** recycled glass (Fe: 0.3 wt.%), <0.1, 0.1-0.2, 0.2-0.5 and 0.5-1 mm, M:S=1:100, 1-PEA:H$_2$O$_2$=1:20 (stoichiometric amount), p = endogenous, at 80°C, 4, 8, 24 h, 500 rpm.

| Time h	diameter mm	Selectivity %		Yield %		Con %	CMB %
		AcP	formic acid	AcP	formic acid		
4	<0.1	18	9	5	3	49	60
	0.1-0.2	19	6	3	1	21	83
	0.2-0.5	27	8	4	1	15	90
	0.5-1	20	6	4	1	21	83
18	<0.1	16	10	4	2	86	29
	0.1-0.2	22	8	7	2	71	45
	0.2-0.5	25	8	8	3	50	63
	0.5-1	23	6	6	2	38	71
24	<0.1	15	31	4	8	89	28
	0.1-0.2	20	29	6	9	86	35
	0.2-0.5	19	29	6	8	88	33
	0.5-1	21	25	7	8	78	41

Selectivity trends over reaction time provide insight into opportunities to improve the acetophenone yield. With shorter reaction times (Table 6.5, less than 18 h), acetophenone selectivity exceeded that of formic acid, however yields remained low. This trend supports acetophenone as a likely intermediate toward the production of formic acid, which can then undergo mineralization to carbon dioxide and water (Figure 6.9). The kinetic profiles indicate that smaller glass particles catalyse faster reaction rates initially, yet ultimately achieve similar 1-phenylethanol conversion. This aligns with previous results emphasizing the role of accessible iron ions in governing Fenton reaction kinetics. Thus, for optimized 1-phenylethanol mineralization, the particle size, dosage, and specific type of recycled glass catalyst are not critical factors, provided sufficient reaction time is allowed, given appropriate reaction conditions. However, at present achieving selective acetophenone synthesis requires milder conditions, which simultaneously limits achievable yields.
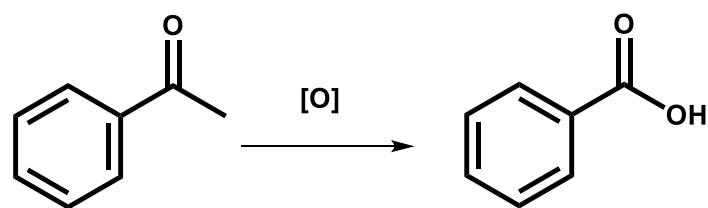
Oxidative cleavage of the methyl group
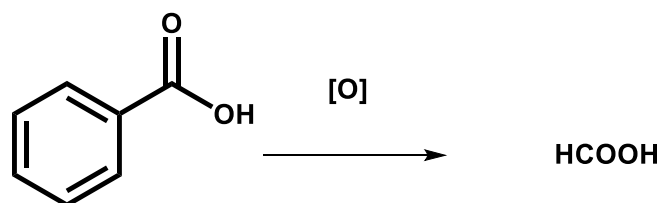
Oxidative Decarboxylation

Figure 6.9 General schemetics of acetophenone as an intermediate of 1-phenylethanol towards formic acid and then water and carbon dioxide. [O] is an arbitrary oxidant containing oxygen.

As discussed in Chapter 5, the investigation of benzyl alcohol oxidation pathways in the presence of H_2O_2 demonstrated the concurrent occurrence of both radical and H-abstraction mechanisms. The overall transformation was predominantly radical-mediated (Eq. 6.2-6.3), with only approximately 10% of benzyl alcohol conversion proceeding through the H-abstraction pathway (Figure 6.10). This aligns with the observations for 1-phenylethanol oxidation, wherein limited yields of the oxidation product acetophenone were attained from both radical and non-radical routes:

Propagation:

$$\cdot OH + PhCH(OH)CH_3 \rightarrow PhCH=CH_2 + H_2O + \cdot OH \qquad (Eq. 6.2)$$

Termination:

$$2\,PhCH(CH_3)O\cdot \rightarrow PhCH=CH_2 + PhCH(CH_3)OH + H_2O_2 \quad (Eq. 6.3)$$
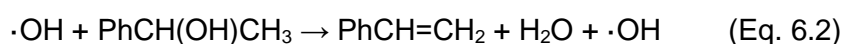
1-Phenylethanol   **acetophenone**
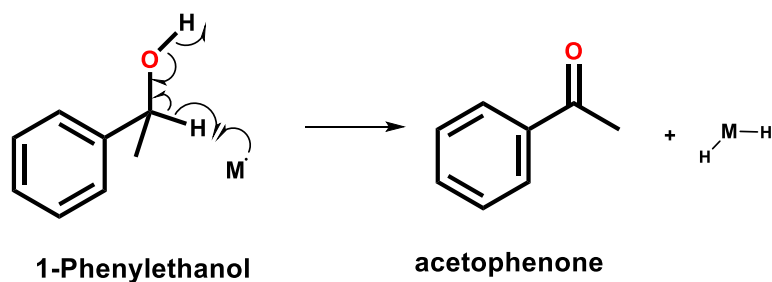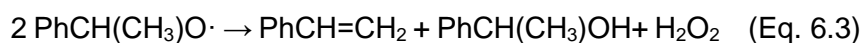
Figure 6.10 Possible H-abstraction pathway of 1-phenylethanol to form acetophenone and water if M is an oxygen species or anhydride if M is a metal.

6.5 Aerobic selective 1-phenylethanol oxidation using molecular oxygen

6.5.1 Aerobic oxidation using air at atmospheric pressure

To improve acetophenone selectivity, aerobic oxidation of 1-phenylethanol (Eq. 6.4) was explored utilizing atmospheric air or pure molecular oxygen as the oxidant. In contrast to the possible in situ generated oxygen from H_2O_2 thermal decomposition, it is critical to ascertain whether the externally supplied molecular oxygen acts as a limiting reagent owing to its poor water solubility (about 4 to 24 mg L^{-1}, 1.0 atm at room temperature).[28–30] For a reaction containing 10 mL of 1 L^{-1} 1-PEA aqueous solution at 80°C and 1 atm, the stoichiometric quantity of oxygen required for complete conversion from 1-phenylethanol to acetophenone is 4.1×10^{-5} mol. However, only 9.4×10^{-7} mol of O_2 can be dissolved in 10 mL of 1 L^{-1} 1-PEA aqueous solution under these conditions. Apparently, no detectable conversion was observed in this case. However, considering the continuous stirring provided, the open system, with enough time provided, mass transport limitations are unlikely in effect. Consequently, oxygen should not act as a limiting reagent. However, the lack of effective interaction precludes definitive evaluation of the selectivity towards acetophenone production through aerobic oxidation in this system.

$$PhCH(OH)CH_3 + 0.5\ O_2 \rightarrow PhCOCH_3 + H_2O \quad \text{(Eq. 6.4)}$$

One of our potential goals for this chapter is to test if aerobic oxidation can produce acetophenone in a selective manner. As a result, in order to enhance the contact between 1-phenylethanol and molecular oxygen, techniques including the use of pressurized system and continuous stirring by bubbling molecular O_2 were explored.

6.5.2 Aerobic oxidation with pressurized system

Similar to benzyl alcohol oxidation, the solubility of oxygen was increased using a pressurised reactor of the Radley setup and a 50 mL ACE round bottom flask. Air was used as the supply of oxygen, and the gauge pressure was set at 1, 2 and 3 bar.

The amount of air dissolved in water was calculated in Chapter 5 according to Henry's law

(Eq. 5.15). The concentration is proportional to the partial pressure of the gas. Therefore, the solubility of oxygen at 1, 2 and 3 bar at 80°C are 1.9×10^{-4}, 2.8×10^{-4} and 3.7×10^{-4} mol L^{-1} respectively (Table 5.12).

It is crucial to emphasise, however, that the studies were conducted in such a way that an oxygen source (either air or molecular oxygen) was always accessible. In other words, cylinders delivered oxygen by keeping regulators open when connected to reaction flaks. This eliminates any quantity constraints and allows O_2 to continually supply the catalyst as the reaction uses it. Previously, pressurized reactors with air were explored for selective benzaldehyde synthesis but did not achieve benzyl alcohol conversion even at higher M:S ratios (1:5) or temperatures (100 °C). Given the similarities between benzyl alcohol and 1-phenylethanol, negligible 1-phenylethanol conversion under pressurized air is expected. Thus, only preliminary tests were conducted to verify this result. Blank tests were then conducted with 1-PEA alone and with $Fe(NO_3)_3 \cdot 9H_2O$ and $FeSO_4 \cdot 7H_2O$ (M:S 1:100), at 80°C.

As anticipated, no 1-PEA conversion was observed under pressurized air (Table 6.6), despite oxygen availability not being limited. While the calculated amount of dissolved O_2 was below stoichiometric needs (4.62×10^{-5} mol), the continuous 24-hour air feed should have provided sufficient oxidant. Additionally, the small 10 mL reaction volume, continuous stirring, and extended reaction time were expected to minimize mass transport effects. This lack of reactivity under oxygen-rich conditions further implies that oxygen quantity is likely not to be the reason for the lack of conversion. Instead, higher temperatures may be essential to activate the oxidation reaction and enable aerobic pathways.

This requirement for higher temperatures aligns with the findings of Chen et al., wherein negligible 1-PEA conversion was attained below 100 °C. The catalytic activity was minimal at low temperatures but exhibited a sharp increase above 100 °C.[31] probably due to the relatively high activation energy barrier of 72 kJ mol^{-1}.[32] Although they enhanced O_2 solubility, the alcohol oxidative dehydrogenation (towards acetophenone) rate still declines remarkably at lower temperatures due to kinetic limitations. Hence, using both molecular oxygen and higher

temperatures (up to 160 °C) will be essential to further optimise the reaction as future work.

Table 6.6 Conversion and CMB% results for 1-phenylethanol oxidation under pressurized system. Reaction condition: 10 mL of 1-PEA (1 g L^{-1}), Fe(NO$_3$)$_3$·9H$_2$O, FeSO$_4$·7H$_2$O, **G2** recycled glass (Fe: 0.3 wt.%), <0.1 mm, M:S=1:5, p = 1, 2 and 3 bar, air and molecular oxygen, at 80 and 100 °C, 24 h, 500 rpm. The increase in temperature from 80 to 100°C successfully activate molecular oxygen to convert 1-phenylethanol. Therefore, temperature has a larger effect than pressure.

Gauge Pressure bar	Catalyst	Temperature °C	Oxygen source	conversion %	CMB %
1,2,3	-	80	air	0	100
1,2,3	Fe(NO$_3$)$_3$·9H$_2$O	80	air	-2	102
1,2,3	FeSO$_4$·7H$_2$O	80	air	0	100
2	-	100	Molecular oxygen	-2	102
2	Fe(NO$_3$)$_3$·9H$_2$O	100	Molecular oxygen	18	82
2	FeSO$_4$·7H$_2$O	100	Molecular oxygen	29	71
2	G2 (Fe: 0.3 wt.%)	100	Molecular oxygen	13	87

Replacing the oxygen source with pure molecular O$_2$ and increasing the temperature to 100°C at a M:S molar ratio of 1:5 and 2 bar gauge pressure still showed negligible 1-PEA conversion without a catalyst present. Comparative testing revealed higher reactivity with Fe^{2+} than Fe^{3+}, consistent with prior observations for benzyl alcohol oxidation. Recycled glass with surface Fe^{3+} demonstrated slightly lower but comparable conversion trends versus Fe(NO$_3$)$_3$·9H$_2$O under identical conditions (Table 6.6). This marginal difference is reasonable considering the total iron content was used for the recycled glass amount, while only surface sites contribute to catalysis.

However, acetophenone was not detected in any reactions. Since no volatile intermediates were discovered (as discussed earlier), the incomplete carbon balances suggest undetected intermediates like conjugated products that may precipitated out of the system or most likely carbon dioxide formation accounting for the missing carbon which are all what was desired (Table 6.6). While modifying the temperature enabled oxygen activation with iron catalysts in the pressurized system, selective aerobic oxidation to acetophenone was not realized under these conditions. Consequently, a mass flow controller set-up for controlled molecular oxygen

delivery was employed for further study into the potential for selective acetophenone synthesis.

6.5.3 Aerobic oxidation by insufflating O_2

Aerobic oxidation of 1-PEA was investigated by supplying molecular oxygen at a flow rate of 5 mL min^{-1} by insufflating it into the reaction mixture. $Fe(NO_3)_3 \cdot 9H_2O$ and $FeSO_4 \cdot 7H_2O$ (M:S 1:100) were initially employed as control catalysts, followed by **G2** recycled glass (0.3 wt.% Fe, <0.1 mm) with higher M:S ratio (M:S 1:5) Control tests were carried out that O_2 was not the limiting reagent (Appendix A4.2).

Notably, 40% 1-PEA conversion was observed (Table 6.7) with molecular oxygen at 100°C without a catalyst present. This conversion exceeds that achieved with catalysts in the pressurized system (30%), confirming insufficient oxygen activation below 100°C, consistent with the pressurized reactor findings. While pressurized systems generally improve oxygen solubility and mass transfer kinetics, enabling faster oxidation rates and higher alcohol conversions, the performance here surprisingly exceeded expectations. Although both systems were stirred, the constant replenishment of the gas-liquid interface and enhanced mixing from insufflation may provide additional mass transfer benefits beyond relying solely on dissolved oxygen diffusion. Ultimately, the simplicity and absence of solubility constraints make bubbling systems could suit for lab-scale set-ups, potentially outweighing the mass transfer advantages of pressurization.

Adding iron salt catalysts (M:S 1:100) increased conversion by 20% beyond the 40% baseline, while recycled glass (M:S 1:5) enhanced conversion by an additional 15%. Comparable 57% 1-PEA conversion was achieved using recycled glass samples with varying iron contents, highlighting the promise of this approach. However, selectivity remained directed unfavourably toward carbon dioxide over the desired acetophenone product, thus showing similarities with previous observations for benzaldehyde synthesis.

Table 6.7 Conversion and CMB% results for 1-phenylethanol oxidation by stirring-bubbling system. Reaction condition: 10 mL of 1-PEA (1 g L^{-1}), Fe(NO$_3$)$_3$·9H$_2$O, FeSO$_4$·7H$_2$O, **G1** (Fe: 0.2 wt.%), **G2** (Fe: 0.3 wt.%), **G3** (Fe: 0.2 wt.%), **G4** (Fe: 0.07 wt.%) recycled glass, <0.1 mm, M:S=1:5, 1:100, p = 2 bar, molecular oxygen supplied rate 5 mL min^{-1}, introduced by mass flow controller, at 80 and 100 °C, 4 h, 500 rpm. The increase in temperature from 80 to 100°C successfully activate molecular oxygen to convert 1-phenylethanol.

Catalyst	M:S	Temperature °C	conversion %	CMB %
-	-	80	0	100
-	-	100	41	59
Fe(NO$_3$)$_3$·9H$_2$O	1:100	100	65	35
FeSO$_4$·7H$_2$O	1:100	100	57	44
G1	1:5	100	53	47
G2	1:5	100	60	40
G3	1:5	100	57	43
G4	1:5	100	38	62

Repeated reuse of freshly prepared recycled glass (0.3 wt.% Fe) yielded 90% 1-PEA conversion after 4 cycles without notable by-product formation. Although sufficient oxygen was supplied theoretically for complete mineralization to carbon dioxide, direct single-step conversion of 1-PEA to CO$_2$ seems unlikely based on prior selectivity results. Gas chromatography-mass spectrometry could enable product identification by characteristic fragmentation patterns as a future work.

The reaction rate decreased with each successive cycle (Figure 6.11) as starting 1-PEA concentration decreased. After four repetitions, conversion reached 90 ± 5% with a 9 ± 3% CMB. Given the slowing kinetics, additional cycling provided diminishing returns. However, considering the low cost of recycled glass, attaining 95% conversion in just 4 cycles represents a very promising result. Overall, these findings demonstrate the efficacy of both Fe^{3+} and Fe^{2+} in activating molecular oxygen and catalysing 1-phenylethanol oxidation, despite unselective behaviour. While the desired acetophenone product was not obtained, this study provides groundwork for future explorations into glass modifications to enhance selectivity. With further development, this approach may enable a greener, sustainable process for selective acetophenone synthesis.
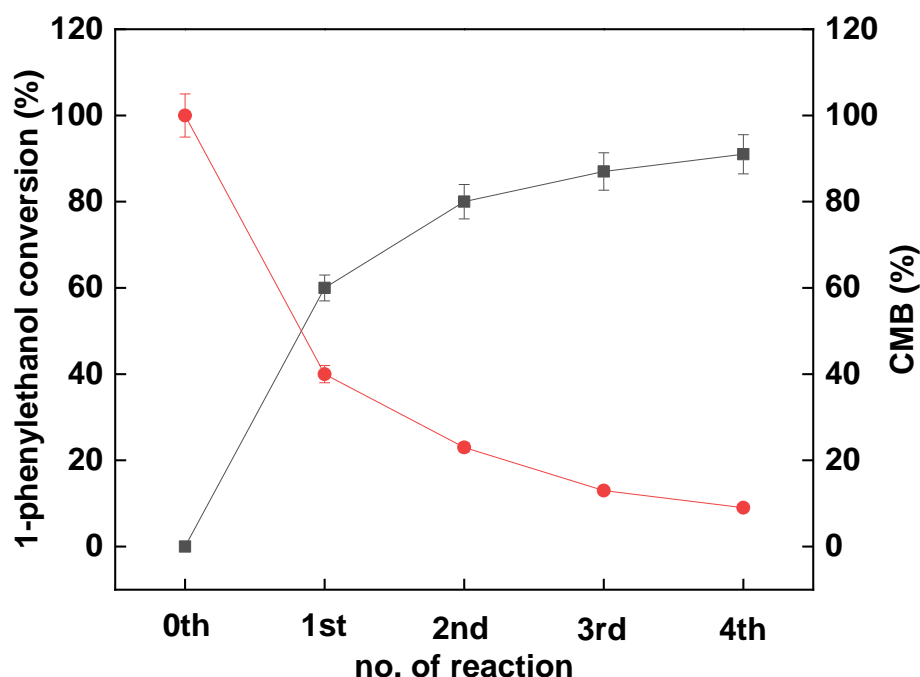
Figure 6.11 Conversion (●) and CMB% (●) results for 1-phenylethanol oxidation by stirring-bubbling system. Reaction condition: 8 mL BnOH (1 g L^{-1}), Fe(NO$_3$)$_3$·9H$_2$O, FeSO$_4$·7H$_2$O and **G2** recycled glass (Fe: 0.3 wt.%), M:S = 1:5, <0.1 mm, molecular oxygen provided by mass flow controller, flow rate of 5 mL min^{-1}, p = 2 bar ,100 °C, 4 h, 500 rpm. Reaction mixture with recycled glass was recycled and repeated with same reaction conditions using fresh prepared glass beads for another four runs. Only reaction with reactivity towards formic acid was observed for all reaction.

6.6   Conclusion

1-Phenylethanol (1-PEA) is extensively utilized as a fragrance additive in cosmetics and flavoring agent in foods and beverages. It is also generated as an intermediate by-product during the coproduction of propylene oxide and styrene monomers (POSM) in the petrochemical industry. The widespread use of 1-PEA in consumer products combined with proliferation of POSM facilities has substantially increased the likelihood of 1-PEA release into aquatic environments via industrial wastewater effluents. Removal of these aromatic compounds from petrochemical wastewaters is an important environmental issue, as conventional treatment methods have proven ineffective. Fenton oxidation using recycled glass catalysts represents a promising green, sustainable approach for 1-PEA remediation, as demonstrated in this work.

In addition, the transformation of 1-PEA to acetophenone is a useful reaction in organic synthesis, given acetophenone's role in perfumes, pharmaceuticals, and as a chemical intermediate. To avoid toxic waste generation, greener alternatives to traditional potassium permanganate and potassium dichromate oxidants have been suggested, including aerobic oxidation mediated by hydrogen peroxide or molecular oxygen.

A robust and reliable ^{1}H-NMR quantification method was successfully validated for 1-phenylethanol oxidation, providing a sound analytical foundation for this work based on prior findings with benzyl alcohol.

In summary, the oxidation of 1-phenylethanol occurred predominantly through the hydroxyl radical pathway, as evidenced by declining reactivity with increasing recycled glass particle size. Recycled glass was demonstrated to be an effective sustainable catalyst for complete 1-phenylethanol degradation, providing an alternative green approach for 1-PEA removal from wastewater.

However, incomplete carbon balances indicate additional undetected intermediates or most likely carbon dioxide may have formed. Further analysis using more sensitive techniques like HPLC should be explored to fully close the mass balance and elucidate all products. While an oxygen activation pathway was active, only negligible acetophenone yields were obtained.

Aerobic oxidation was investigated using three systems - open to air, pressurized, and gas-insufflating - with air or oxygen as the oxidant. Despite achieving 0, 15 and 60% 1-PEA conversion respectively, acetophenone was not generated even after repeated cycling to 95% conversion.

Although selective synthesis of fine chemicals was not entirely achieved, these results represent a valuable foundational investigation, providing key insights to guide future optimization of reaction conditions and improvements in acetophenone selectivity.

6.7   References

(1)   A. Chaudhari, S.; R. Kar, J.; S. Singhal, R. *Current Organic Chemistry*, 2015, **19**, 1732-1754.

(2)   Li, X.; Xu, L.; Wang, G.; Zhang, H.; Yan, Y. *Process Biochemistry*, 2013, **48**, 1905-1913.

(3)   Kamble, M. P.; Chaudhari, S. A.; Singhal, R. S.; Yadav, G. D. *Biochemical Engineering Journal*, 2017, **117**, 121-128.

(4)   Bozan, A.; Songur, R.; Mehmetoglu, Ü. *Turkish Journal of Chemistry*, 2020, **44**, 1352-1365.

(5)   Petty, J. D.; Huckins, J. N.; Alvarez, D. A.; Brumbaugh, W. G.; Cranor, W. L.; Gale, R. W.; Rastall, A. C.; Jones-Lepp, T. L.; Leiker, T. J.; Rostad, C. E.; Furlong, E. T. *Chemosphere*, 2004, **54**, 695-705.

(6)   Bedient, P. B.; Rifai, H. S. Newell, C. J. *Prentice Hall PTR.* 1999.

(7)   Dou, X.; Meng, F.; Duan, W.; Liu, Q.; Li, H.; Du, S.; Peng, X. *Journal of Oceanology and Limnology*, 2019, **37**, 1342-1352.

(8)   Ngo, Q.; Dao, L.; Grigoriev, E.; Petukhov, A. *Journal of Biodiversity and Environmental Sciences*, 2015, **6**, 587-598.

(9)   Dao, L.; Grigoryeva, T.; Laikov, A.; Devjatijarov, R.; Ilinskaya, O. *Ecotoxicology and Environmental Safety*, 2014, **108**, 195-202.

(10)   Pohanish, R. P., Sittig, M., Eds.; Elsevier ; William Andrew: Amsterdam ; Boston : Waltham, MA, 7th Ed, Copyright © 2017 Elsevier Inc. All rights reserved 2017.

(11)   1-phenylethanol, *Brief Profile - ECHA*. https://echa.europa.eu/brief-profile/-/briefprofile/100.002.461 (accessed 2023-10-30).

(12)   *1-Phenylethanol 98 98-85-1*. http://www.sigmaaldrich.com (accessed 2023-10-30).

(13)   Lemmer, S.; Klomp, R.; Ruemekorf, R.; Scholz, R. *Chemical Engineering & Technology*, 2001, **24**, 485-488.

(14)   Gallego, J. P.; Quimica, R.; López, S. R.; Maugans, C. *Chemistry Environmental Science*, 2002, **61**, 1829-1836.

(15)   Battaglin, W. A.; Furlong, E. T.; Burkhardt, M. R. *U.S. Geological Survey*, 2001.

(16)   Hellström, T. *The Swedish Water and Wastewater Association*, 2000, **113**, 31.

(17)   Arts, S. J. H. F. F.; Mombarg, E. J. M.; Bekkum, H. van; Sheldon, R. A. *Synthesis*, 1997, **1997**, 597-613.

(18)   Sheldon, R. A.; Arends, I. W. C. E.; Dijksman, *Catalysis Today*, 2000, **57**, 157-166.

(19)   Shi, R.; Wang, F.; Tana; Li, Y.; Huang, X.; Shen, W. *Green Chemistry*, 2010, **12**, 108-113.

(20)   Cainelli, G.; Cardillo, G. Oxidation of Alcohols. In *Chromium Oxidations in Organic Chemistry*; Cainelli, G., Cardillo, G., Eds.; Reactivity and Structure Concepts in Organic Chemistry; Springer-Verlag Berlin, Heidelberg, 1984, 118-216.

(21)   Hayashi, M.; Yamada, K.; Nakayama, S.; Hayashi, H.; Yamazaki, S. *Green Chemistry*, 2000, **2**, 257-260.

(22)   Zhan, B. Z.; Thompson, *Tetrahedron*, 2004, **60**, 2917-2935.

(23)   Sheldon, R. A. *Journal of Chemical Technology & Biotechnology*, 1997, **68**, 381-388.

(24)   Mallat, T.; Baiker, A. *Chemical Reviews*, 2004, **104**, 3037-3058.

(25)   Zaccheria, F.; Ravasio, N.; Psaro, R.; Fusi, A. *Chemical Communications*, 2005, **14**, 253-255.

(26)   Beebe, T. R.; Howard, F. M. *Journal of the American Chemical Society*, 1969, **91**, 3379-3380.

(27)   Brandi, P.; Galli, C.; Gentili, P. *The Journal of Organic Chemistry*, 2005, **70**, 9521-9528.

(28)   *Oxygen and water*. https://water.lsbu.ac.uk/water/o2water.html (accessed 2024-04-16).

(29)   *Oxygen - Solubility in Fresh and Sea Water vs. Temperature*. https://www.engineeringtoolbox.com/oxygen-solubility-water-d_841.html (accessed 2024-04-16).

(30)   Chwastowski, J.; Ciesielski, W.; Khachatryan, K.; Kołoczek, H.; Kulawik, D.; Oszczęda, Z.; Soroka, J. A.; Tomasik, P.; Witczak, M. *Water*, 2020, **12**, 2488.

(31)   Chen, Y.; Bai, L.; Zhou, C.; Lee, J.-M.; Yang, Y. *Chemical Communications*, 2011, **47**, 6452-6454.

(32)   Chen, Y.; Guo, Z.; Chen, T.; Yang, Y. *Journal of Catalysis*, 2010, **275**, 11-24.

Chapter 7 Conclusions and Future Work

7.1   Conclusions

Water pollution from organic wastewater has become a significant global problem. Treatment of organic wastewater containing persistent and toxic pollutants, such as phenolic compounds and pharmaceuticals, is essential for sustainable development as traditional methods including physical, biological and chemical approaches are often ineffective. Advanced Oxidation Processes (AOPs) such as photochemical, wet catalytic, sonochemical, O_3, electrochemical and Fenton oxidation offer effective solutions for mineralising pollutants or improving biodegradability. Among those, catalytic wet hydrogen peroxide oxidation (CWPO) stands out due to its mild reaction conditions (20-80°C, atmosphere pressure), which lowers the operational costs by using a green oxidant like H_2O_2 and at least in principle leading to H_2O and CO_2 as byproducts. The Fenton process that uses iron species (Fe^{2+} or Fe^{3+}) to break down H_2O_2 to generate ·OH radicals as oxidant stands out for its versatility, robustness, simplicity and rapidity in degrading pollutants. However, despite being a promising technique for wastewater treatment, post-treatment of Fe contamination became a concern, as a result, heterogeneous catalysts with active metal species (e.g., Fe, Cu) on different supports (e.g., zeolites, activated carbons) are used to overcome the drawbacks. Supports can stabilize metal active species at the surface, thus promoting performance and recovery. Although iron-containing zeolite has been shown to be efficient as a catalyst in the Fenton reaction, it is rather expensive to scale up. Recycled soda-lime glass (green beer glass bottles), with similar elemental composition as zeolite, with ferric oxide (more than 0.1 wt.% loading) could potentially be used as a heterogeneous catalyst due to the availability in large quantities, and it is cheaper (£20 per metric tonne for recycled green glass[1]) than zeolite (£700 per kg). To the best of our knowledge, the use of ferrous glass, especially in the range of 4 mm to 0.1 mm, for water treatment applications has not been explored. Therefore, with the abundance in the waste sector, recycled ferrous glass could become a precious resource to be introduced and used as a sustainable heterogeneous catalyst.

As such, using recycled glass as a catalyst in water treatment fully encapsulates circular economy principles, when a product reaches the end of its life, its materials are recycled and reused, generating additional value within the economy. The recovered glass can also be reused after the purification process in construction or packaging. By integrating these principles, water purification is transformed from a process of removing contaminants to a platform for resource recovery. This aligns with the circular economy's goal of closing loops, reducing environmental impact and benefiting agricultural irrigation. The result is a more sustainable, efficient, and resilient water management system that conserves precious water resources.

As a result, this thesis contributed to the advancement of abatement reaction by integrating the principles of the circular economy through the innovative reuse of abundant waste materials - specifically recycled glass - for water purification, targeting contaminants such as phenol and ibuprofen. This method not only facilitates the reuse of treated water, particularly for irrigation purposes, but also creates a closed-loop material cycle that adds value and extends the life of these materials. In addition, the research is exploring the utility of recycled glass in the field of fine chemical synthesis, investigating its efficacy in the oxidation processes of benzyl alcohol and 1-phenylethanol, thereby broadening the potential applications of recycled materials in environmental sustainability and chemical manufacturing processes.

7.1.1 Water purification by CWPO using recycled glass as catalyst.

Phenol, a paradigm for water pollution, has been used as a benchmark to explore the potential of recycled glass as a heterogeneous catalyst in catalytic wet peroxide oxidation.

Hydrogen peroxide can provide $\cdot OH$ radicals during the Fenton reaction, which in turn decompose the organic substrate.

Theoretically, in the Fenton process, both Fe^{2+} and Fe^{3+} can initiate the reaction, as a catalytic cycle will be formed between them. To get some insights into activity of Fe^{3+} which will be present in recycled glass, comparisons between Fe^{2+} and Fe^{3+} as catalyst in phenol mineralization were conducted (M:S 1:100, $PhOH:H_2O_2$ 1:14 (stoichiometric towards

mineralization), 4 h, 80 °C, p = endogenous, 500 rpm). The observation that the Fenton-like reaction involving indirect activation of hydrogen peroxide by Fe^{3+} requires time-wise about double the time of Fe^{2+} at the early stage of the reaction (5-10 h), suggests a relatively comparable performance between the two iron oxidation states, and due to the redox cycle, the difference in reaction rate becomes negligible over time in CWPO. Consequently, this provides a solid basis for further exploration of the use of glass materials embedded with Fe^{3+} centres, offering promising avenues for environmental applications, particularly in pollutant degradation processes where the Fenton-like reaction plays a crucial role.

Characterization of recycled glass was done to study the composition, as it can influence the catalytic outcomes. ICP-OES and XPS were done to determine the bulk and surface composition respectively. Elemental analysis (ICP-OES) on 12 samples showed a consistent composition: silicon (30 wt.%), sodium (8 wt.%) and calcium (7 wt.%), negligible fluctuations between samples made it a robust catalyst system, and the glass colour and feedstock variability will not influence the catalyst performance. Thus, this result indicates recycled soda-lime is a reliable and sustainable catalyst in terms of composition. XPS results revealed that more Fe is distributed at the surface (0.5 at.%) rather than the bulk (0.1 at.%), this reflects the iron propensity to readily oxidize facilitates migration of Fe from the bulk to the surface as Fe_2O_3 over time.

In addition, minor amounts of transition metals in the form of MnO and Cr_2O_3 were detected, and they are known to possess catalytic activity in the Fenton reaction. Therefore, metal activity control tests using $FeSO_4 \cdot 7H_2O$, $Cr(NO_3)_3 \cdot 9H_2O$ and $Mn(NO_3)_2 \cdot 4H_2O$ was conducted. Phenol conversion, CMB and H_2O_2 consumption results indicate that the recycled glass catalyst activity is primarily dictated by the iron content, with other metals playing a minimal role. The reliability despite variability in glass feedstock enhances the viability of recycled glass as a sustainable catalyst for scaled-up water treatment processes.

As non-uniform chemical composition for glass recycled from recycling facility, glass performance may not be consistent. Activity control tests for mixed green recycled glasses

from diverse batches and manufacturers were conducted. Results on conversion, CMB, H_2O_2 consumption, selectivity to CO_2, and selectivity to acids all showed a variance of 3% which is an excellent result in terms of reproducibility, especially considering the source of the raw material This demonstrates recycled glass as a robust sustainable catalyst, achieving reliable performance regardless of the precursor glass feedstock, thus providing a promising foundation for practical large-scale implementation in water treatment and other applications.

The present study successfully demonstrated the concept of using of recycled glass (green and brown) containing Fe^{3+} centres as a heterogeneous catalyst for phenol oxidation by catalytic wet peroxide oxidation (CWPO). The excellent reproducibility of a mixed batch of recycled glass leads to a great reduction in the effort of separating during recycling, further reduce the cost of reaction. In addition, results have indicated that decreasing the size of the glass particles leads to increased phenol conversion and carbon dioxide production with the size range of 0.1-0.5 mm showing the best catalytic activity. It enables the possibility of scale-up application in industry. Additionally, optimization of the glass M:S molar ratio and reaction time can enhance catalyst performance. As a result, the performance of recycled glass can be comparable and promising (i.e., 100% phenol conversion and 20% CMB) to industrial catalyst, namely Fe/ZSM-5 under appropriate reaction conditions (increased mass and longer reaction time) for an overall much lower (about 3000 times) cost.

Based on these very promising findings, the application of recycled glass as a sustainable catalyst for ibuprofen was studied.

To ensure the complete removal of both ibuprofen and any more toxic intermediates generated during the CWPO process, characterization of the eleven detected intermediates during the catalytic CWPO process was conducted using both HPLC and GCMS methods. The presence of potentially more toxic intermediates such as **1.** 2-[4-(1-hydroxy-2-methylpropyl)phenyl]propanoic acid, **14.** 4-isobutylbenzoic acid, **8.** 1-(4-isobutylphenyl)-1-ethanol and four determined at a detection wavelength 250 nm: **15.** 4-acetylbenzoic acid, **12.** 4-ethylbenzaldehyde, **9.** 1-oxo-ibu, **10.** 4-isobutyleacetophenone were identified by HPLC and

13. 4-Isobutyl phenol, **16.** 4-Isobutylbenzaldehyde, **11.** 1-(4-acetylphenyl)-2-methyl-1-propanone, **17.** 4-Ethylbenzoic acid were identified by GCMS which enables the calculation of carbon mass balance and CO_2 formation. The number of identified products is well above the average compared to the current literature, and so for better calculations, more work is needed for unidentified products awaiting further identification.

The complete decomposition of ibuprofen could be achieved under mild reaction conditions (ibuprofen:H_2O_2 1:140, 80 °C, p = endogenous, 4 h, 500 rpm) with recycled glass (Fe: 0.07 to 0.3 wt.%) as catalyst. Especially recycled glass (Fe: 0.3 wt.%, M:S 1:1) with diameters 0.1-0.5 mm, which showed 100% ibuprofen conversion, 90% CO_2 formation, low metal leaching (less than 0.2 wt.%) under the experimental conditions, demonstrating the capability of reusing the catalyst.

The work was extended to the mineralization of alcohols. Mineralization of benzyl alcohol with recycled glass (Fe: 0.3 wt.%, M:S 1:100) was also conducted (BnOH:H_2O_2 = 1:17, 80 °C, p = endogenous, 24 h, 500 rpm). Despite an increase in H_2O_2, benzyl alcohol concentration, at a relative long reaction time (24 h), BnOH conversion was limited to at 60%, and varying the initial benzyl alcohol concentration did not increase mineralization but improved benzaldehyde selectivity, suggesting the concurrent existence of a radical and non-radical pathway and a zero-order kinetic profile with respect to BnOH concentration.

The mineralization of 1-phenylethanol occurred predominantly via the hydroxyl radical pathway, as evidenced by the decreasing reactivity with increasing recycled glass particle size. High mineralization of 1-phenylethanol was achieved with the smallest glass size (M:S 1:100, 24 h 80 °C), as evidenced by the low carbon mass balance (CMB < 20%). However, further analysis using more sensitive techniques such as HPLC should be explored to complete the mass balance and elucidate all products.

7.1.2 Potential application of glass in fine chemical synthesis

The selective oxidation of benzyl alcohol to benzaldehyde and of 1-phenyl ethyl alcohol to acetophenone were investigated.

Due to the low aqueous solubility of oxygen, different experimental set-ups - open air, pressurised and gas insufflating - with air or oxygen as the oxidant were employed to increase dissolved or local O_2 concentrations for aerobic benzaldehyde and acetophenone synthesis based on the findings. A maximum of 52% conversion of BnOH was achieved at 100 °C with recycled glass (Fe: 0.3 wt.%, M:S 1:5) after 4 more repeated cycling and no benzaldehyde was formed. Similarly, despite achieving 60% conversion of 1-PEA, acetophenone was unexpectedly not produced even after repeated cycling with recycled glass up to 95% conversion. Fe^{3+} and thus recycled glass did not exhibit significant activity towards benzaldehyde formation under the conditions tested.

To explain these results catalytic tests in the presence of radical inhibitors like TEMPO were carried out. The results demonstrated that the reaction with H_2O_2 primarily follows a Fenton-like mechanism. This pathway is mainly radical mediated, with approximately 10% of the reaction activity attributable to the activation of molecular oxygen. This finding highlights the predominance of radical mechanisms in the process, while also indicating a notable contribution from a molecular oxygen activation pathway, underscoring the complexity and efficiency of the catalytic reaction under study.

Although the selective synthesis of fine chemicals was not fully achieved, these results represent a valuable fundamental investigation, providing key insights to guide future optimisation of reaction conditions and improvements in acetophenone selectivity.

7.2 Future work

The future work of this project will focus on:

1) **Characterization of glass:** To understand the discrepancies in phenol conversion observed with glass beads of different morphologies (sharp edges from hydraulic pressing and rounded edges from ball milling), a detailed morphological analysis is essential. Comprehensive studies using scanning electron microscopy (SEM) can elucidate the correlation between particle morphology and catalytic performance. SEM can reveal detailed surface structures, including shape, roughness, texture, and particle distribution.

Additionally, SEM equipped with energy-dispersive X-ray spectroscopy (EDS) can produce elemental maps to show the spatial distribution of iron (Fe) on the glass surface. This will provide valuable insights into the uniformity and localization of iron centers and quantitative data on Fe concentration. Such analysis will enable us to better understand the impact of different preparation methods and select the most appropriate technique based on specific needs.[2,3]

2) **Surface modification:** In order to increase the surface area of non-porous glass beads beyond that achievable through mere alteration of their size, surface roughening can be employed. Chemical etching using strong bases, such as sodium hydroxide (NaOH) and hydrofluoric acid (HF), has been demonstrated to effectively enhance the surface properties of non-porous glass beads.[4,5] These bases react with the silica network, forming Na_2SiO_3 and SiF_4, respectively. This results in a textured surface with an increased surface area. Furthermore, the application of coatings through techniques such as sol-gel can facilitate the enhancement of the surface concentration of metals, including iron and copper. The sol-gel method is a versatile technique for the creation of transition metal oxide coatings (e.g., Cu, Zn) on glass substrates. This technique results in the formation of a porous structure, which increases the surface area and the accessibility of catalytic sites. Subsequent treatments, including calcination, enhance the adhesion and stability of metal oxides on the glass surface, thereby ensuring their efficacy during catalytic processes. These coating methods ensure a uniform distribution of metal oxides, thereby providing a greater number of active sites for catalytic reactions. Consequently, such surface modifications could significantly enhance the efficiency of glass beads in catalytic wet peroxide oxidation (CWPO) processes.

3) **Scale-up:** To effectively integrate into the circular economy, scaling up the reactor is essential for industrialization. Preliminary studies with batch reactors have highlighted challenges with inefficient mixing at higher catalyst levels. To address these issues and support potential scale-up efforts, future investigations should consider using fixed bed reactors or plug flow reactor configurations. These reactor types are more advantageous in non-laboratory water treatment contexts due to their ability to maintain high catalyst concentrations and deliver efficient catalytic performance. They offer efficient catalyst utilization, scalability, and effective heat and mass transfer management, making them suitable for continuous and large-scale operations.

4) **Circular economy practice:** Previous results showed negligible variance in catalytic performance when mixing green recycled glass from diverse batches and manufacturers, simplifying the glass pre-treatment process in CWPO. To further streamline the separation of green and brown glass, it is recommended to evaluate the catalytic capabilities of mixed-colour glass (specifically brown and green) within the 0.1-0.5 mm diameter range and containing significant amounts of iron. This research could lead to the development of a cost-effective glass pre-treatment process, increasing the feasibility of using recycled glass in various catalytic applications. If promising results are obtained, outreach activities can be organized to promote the recycling of green and brown glass bottles within the community. This would not only reduce the overall cost of this green project but also engage the community in the circular economy, fostering a collaborative effort towards sustainable practices.

5) To confirm the efficiency of the CWPO technique and the universal applicability of the prepared catalysts, it is important to study other common organic compounds found in wastewater, beyond phenol and ibuprofen. Potential targets include diclofenac,[6,7] bisphenol A,[8] and chlorophenols,[9] either individually or in combination. Additionally, testing with real wastewater samples is recommended to identify any practical issues that may arise before scaling up. This comprehensive approach will validate the effectiveness of the CWPO technique and the prepared catalysts across a broader range of pollutants, ensuring their suitability for diverse water treatment applications.
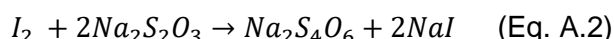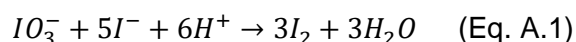
7.3   Reference

(1)   Tomić, T.; Schneider, D. R. *Journal of Environmental Management*, 2020, **267**, 110564.

(2)   Ogbezode, J. E.; Ezealigo, U. S.; Bello, A.; Anye, V. C.; Onwualu, A. P. *Discover Nano* 2023, **18**, 125.

(3)   Predoi, G.; Ciobanu, C. S.; Iconaru, S. L.; Predoi, D.; Dreghici, D. B.; Groza, A.; Barbuceanu, F.; Cimpeanu, C.; Badea, M.-L.; Barbuceanu, S.-F.; Furnaris, C. F.; Belu, C.; Ghegoiu, L.; Raita, M. S. *Polymers*, 2021, **13**, 2351.

(4)   Blass, J.; Köhler, O.; Fingerle, M.; Müller, C.; Ziegler, C. *physica status solidi (a)*, 2013, **210**, 988-993.

(5)   Ono, Y.; Hayashi, Y.; Urashima, S.; Yui, H. *International Journal of Applied Glass Science*, 2022, **13**, 676-683.

(6)   Zhu, J.; Zhang, G.; Xian, G.; Zhang, N.; Li, J. *Frontiers in Chemistry*, 2019, **7**, 796.

(7)   Han, F.; Ye, X.; Chen, Q.; Long, H.; Rao, Y. *Separation and Purification Technology*, 2020, **232**, 115967.

(8)   Hu, Z.; Leung, C.-F.; Tsang, Y.-K.; Du, H.; Liang, H.; Qiu, Y.; Lau, T.-C. *New Journal of Chemistry*, 2011, **35**, 149-155.

(9)   Villegas, L. G. C.; Mashhadi, N.; Chen, M.; Mukherjee, D.; Taylor, K. E.; Biswas, N. *Current Pollution Reports*, 2016, **2**, 157-167.

APPENDIX

A1.1 Na₂S₂O₃ standardization

KIO_3 standard solution was used for $Na_2S_2O_3$ concentration standardisation:

Fundamental principle:

$$IO_3^- + 5I^- + 6H^+ \rightarrow 3I_2 + 3H_2O \quad \text{(Eq. A.1)}$$

$$I_2 + 2Na_2S_2O_3 \rightarrow Na_2S_4O_6 + 2NaI \quad \text{(Eq. A.2)}$$

Therefore, the molar ratio of IO_3^- and $Na_2S_2O_3$ is as follows:

$$\frac{n_{(IO_3^-)}}{n_{(Na_2S_2O_3)}} = \frac{1}{6} \quad \text{(Eq. A.3)}$$

A1.2 Method standardization procedure:

1) Known concentration of H_2O_2 solution was added into glass stopped flask, 1 mL of H_2SO_4 solution and 1 mL of KIO_3 were added into the flask, and the mixture was mixed thoroughly, sealed with the glass stopper.

2) The mixture was titrated with $Na_2S_2O_3$ immediately after step 1. The flask was gently stirred for sufficient reaction between iodine and sodium thiosulfate and prevent iodine loss. About 0.5 mL of starch indicator was added in the final stages of the titration (after the solution has reached a pale yellow colour) as an indicator to turn the solution into blue. A few more drops of $Na_2S_2O_3$ was added until the mixture turned transparent and stayed for about 30 second. The $Na_2S_2O_3$ volume ($V_{(Na_2S_2O_3)}$) used was recorded.

3) The concentration of $Na_2S_2O_3$ can be calculated using the following formula:

$$X_{(Na_2S_2O_3)} = \frac{\frac{C_{(IO_3^-)}}{Mw_{(IO_3^-)}} \times V_{(IO_3^-)} \times 6}{V_{(Na_2S_2O_3)}} M \quad \text{(Eq. A.4)}$$

$X_{(Na_2S_2O_3)}$ is the molar concentration of $Na_2S_2O_3$ in the reaction mixture.

$C_{(IO_3^-)}$ is the concentration of standard KIO_3 used for titration

$Mw_{(IO_3^-)}$ is the molecular weight of KIO_3

$V_{(IO_3^-)}$ is the volume of KIO_3 used in reaction

$V_{(Na_2S_2O_3)}$ is the volume of Na₂S₂O₃ used for titration

Determination of H₂O₂

1) Solution of Na₂S₂O₃ with a concentration of 0.001 M was diluted from the 0.1 M Na₂S₂O₃ standard solution using 100 mL volumetric flask for H₂O₂ titration.

2) H₂O₂ solution (1 or 2 mL depending on concentration) was added into glass stopped flask, 1 mL of H₂SO₄ solution and 1 mL of KI were added into the flask, the mixture was mixed thoroughly, sealed with the glass stopper and placed in a dark place for 10 min.

3) The mixture after reaction under darkness was titrated with Na₂S₂O₃. The flask was gently stirred for sufficient reaction between iodine and sodium thiosulfate and prevent iodine loss. About 0.5 mL of starch indicator was added in the final stages of the titration (after the solution has reached a pale yellow colour) as an indicator to turn the solution into blue. A few more drops of Na₂S₂O₃ was added until the mixture turned transparent and stayed for about 30 second. The Na₂S₂O₃ volume used was recorded.

4) For each sample, the measurement was repeated three times for accuracy and an average volume of Na₂S₂O₃ consumed was used for calculation of H₂O₂ concentration using the formula above.

5) A blank test without any sample using step 2 to 4 should be done, the Na₂S₂O₃ column (V$_{blank}$) was reduced from the titration results.

Appendix

A2.1 ANOVA tests in Origin:

A one-way ANOVA test was performed in Origin for the phenol conversions obtained for the reactions catalysed by different physical mixtures of green GTS glass (0.1-0.2 mm), the details of which are shown below:

Table A.1 Descriptive statistics.

	N analysis	N missing	Mean	Standard deviation	Standard error of mean
Mix 1	4	0	80.68	0.296	0.148
Mix 2	4	0	81.39	0.971	0.485
Mix 3	4	0	80.24	3.189	1.595
Mix 4	4	0	79.92877	3.29299	1.64649
Mix 5	4	0	82.37431	2.13849	1.06925

Table A.2: Overall ANOVA.

	DF	Sum of squares	Mean square	F value	Prob>F
Model	4	15.35067	3.83767	0.72086	0.59095
Error	15	79.85573	5.32372		
Total	19	95.2064			

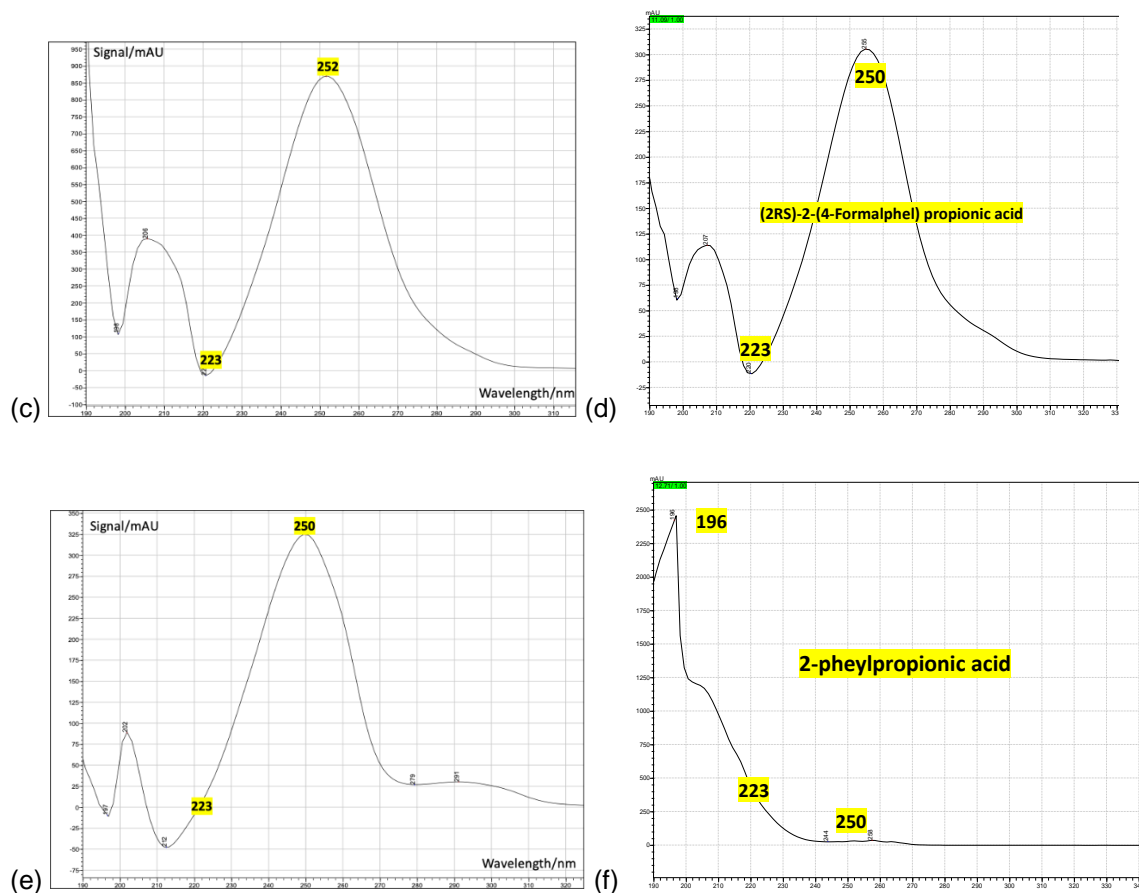At the 0.05 level, the population means are not significantly different.

A2.2 Kinetic study of phenol oxidation

Table A.3 Phenol oxidation by different recycled glasses (**G1 to G4**, Fe: 0.07- 0.3 wt.%) with M:S 1:100 and 1:50, at 80°C for 4 and 12 hours. A stoichiometric amount of hydrogen peroxide was added as source of radicals. Phenol residual and intermediates of the reaction were reported with their concentration. Overall phenol conversion and CMB and hydrogen peroxide consumption was calculated with an error of 5%.

Glass	M:S	Time h	Conversion %	CMB %	H_2O_2 conversion %	H_2O_2/PhOH Molar ratio
G1			64	95	39	9
G2	1:100	4	58	83	33	8
G3			73	69	37	7
G4			61	79	36	8
G1			97	17	58	8
G2	1:100	12	92	31	49	7
G3			96	21	55	8
G4			98	15	58	8
G1			86	63	53	9
G2	1:50	4	78	71	42	8
G3			92	50	53	8
G4			92	50	50	8

A3.1 UV-vis spectrum of ibuprofen oxidation intermediates

(a) 1-hydroxyibuprofen (b) 1-(4-iso-butylphynel)ethanol

Appendix

(c)

(d) (2RS)-2-(4-Formalphel) propionic acid
223 250

(e) 250 223

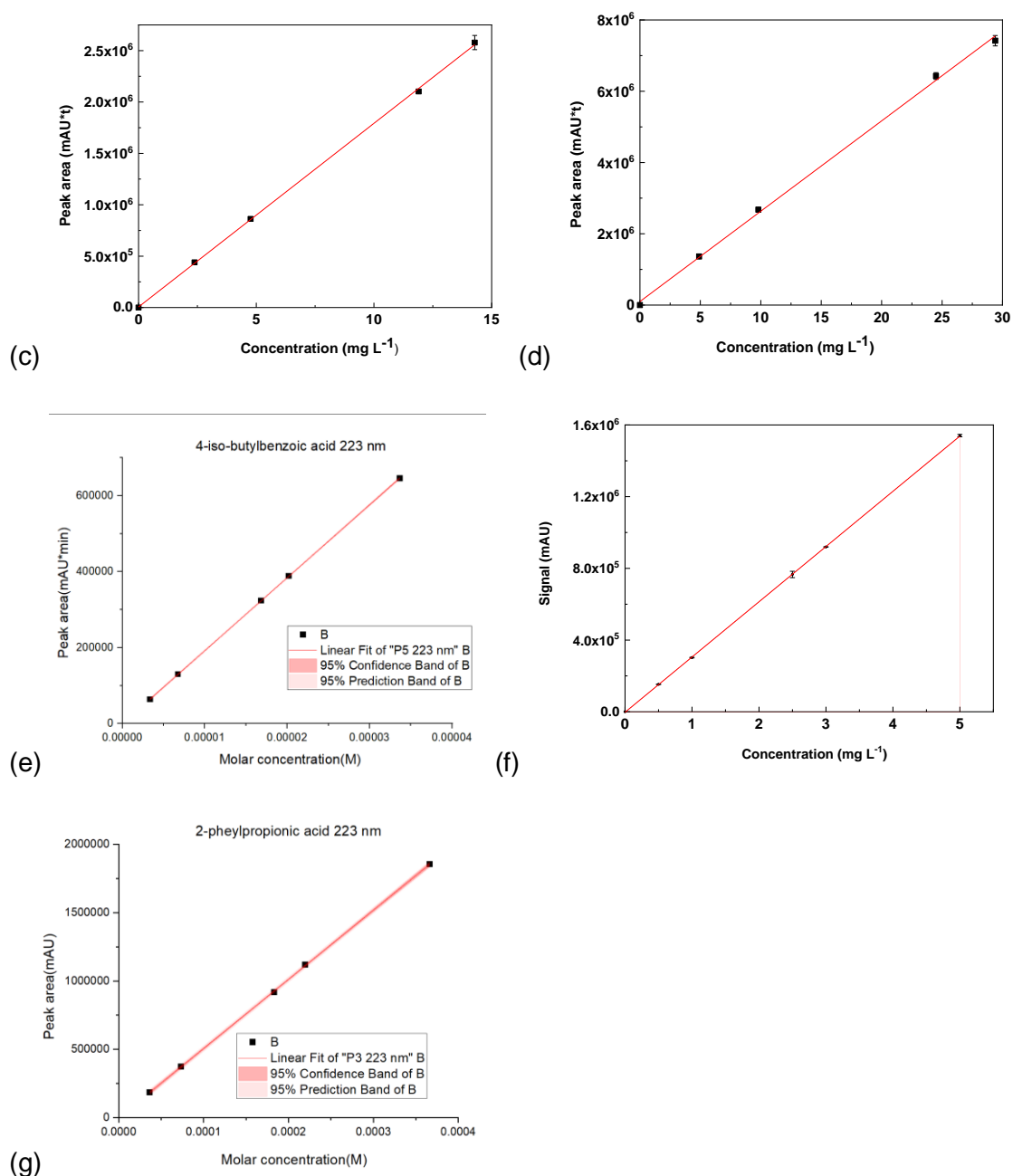(f) 196 2-pheylpropionic acid 223 250
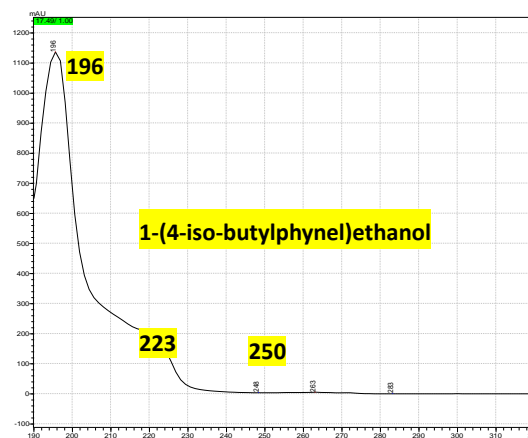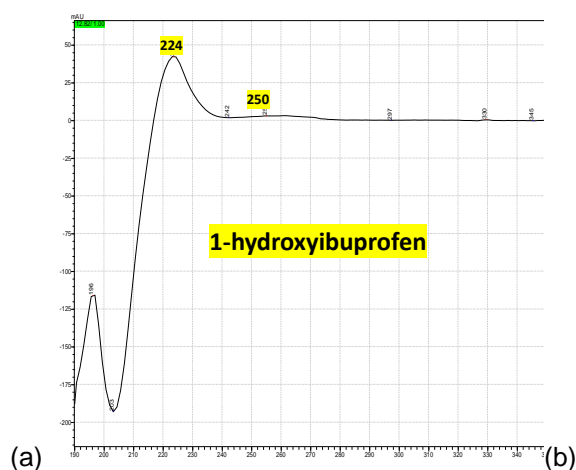
Figure A.1 UV spectrum of ibuprofen oxidation intermediates standard solutions obtained for (a) **1**, 1-hydroxyibuprofen/2-[4-(1-hydroxy-2-methylpropyl)phenyl]propanoic acid; (b) **8**, 1-(4-iso-butylphynel)ethanol; (c) **10**, 4-isobutylacetophenone; (d) **12**, (2RS)-2-(4-formalphel) propionic acid;.(e) **15**, 4-acetylbenzoic acid and (f) **23**, 2-pheylpropionic acid.

## A3.2 Calibration curves ibuprofen oxidation intermediates

(a)

(b)
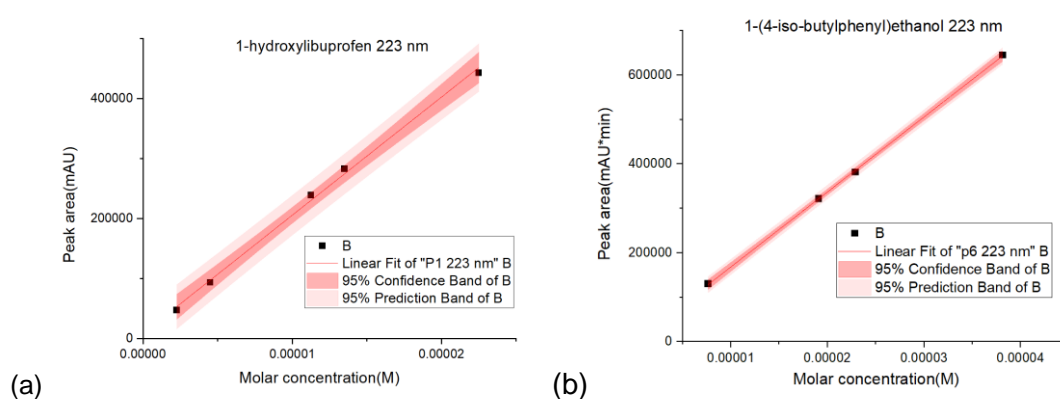
Figure A.2 Calibration curves of ibuprofen oxidation intermediates standard solutions obtained for (a) **1**, 1-hydroxyibuprofen/2-[4-(1-hydroxy-2-methylpropyl)phenyl]propanoic acid; (b) **8**, 1-(4-iso-butylphynel)ethanol; (c) **10**, 4-isobutylacetophenone; (d) **12**, (2RS)-2-(4-formalphel) propionic acid;.(e) **14.** 4-isobutylbenzoic acid (f) **15**, 4-acetylbenzoic acid and (g) **23**, 2-pheylpropionic acid.

Appendix

Table A.4 The chosen wavelength, interception, slop and R^2 of the ibuprofen intermediate calibration curves in Figure A.2.

Product entry	Intercept			Slope		Statistics
	λ	Value	SD	Value	SD	Adj R^2
1	223	8764	7749	1.97E+10	5.98E+08	0.99632
8	223	-149	3714	2E10	2E8	0.99976
10	250	5984	15433	178655	1784	0.9997
12	250	-407	8049	4.79E+10	4.98E+08	0.99957
14	223	19	851	2E10	4E7	0.99998
15	250	-2761	3781	308151	1309	1
23	223	-7	4997	5.06E+09	2.37E+07	0.99991

A4.1 Kinetic study of BnOH oxidation with different H_2O_2 dose
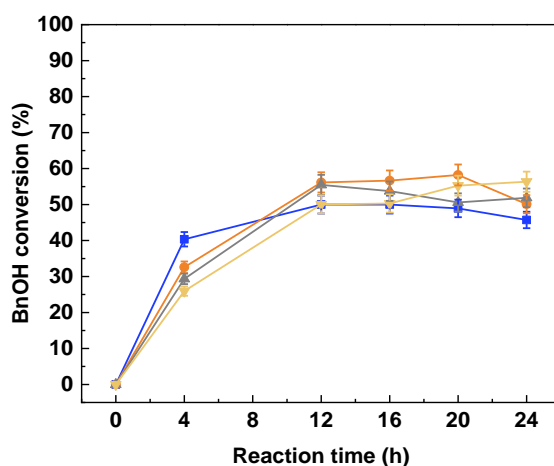
Figure A.3 Kinetic study of BnOH (1 g L^{-1}) oxidation after 4, 12, 16, 20 and 24 hours reaction. Reaction conditions: **G2** recycled glass (Fe: 0.3 wt.%), M:S=1:100, <0.1 (●), 0.1-0.2(●), 0.2-0.5(●) and 0.5-1(●) mm, BnOH:H_2O_2 molar ratio of 1:1, p = endogenous, 80 °C, 24 h, 500 rpm. 1gL^{-1} BnOH conversion after 4, 12, 16, 20 and 24 hours reaction with four different sizes of **G2** glass, with M:S ratio of 1:100, and molar ratio BnOH:H_2O_2 of 1:1, at 80 °C.
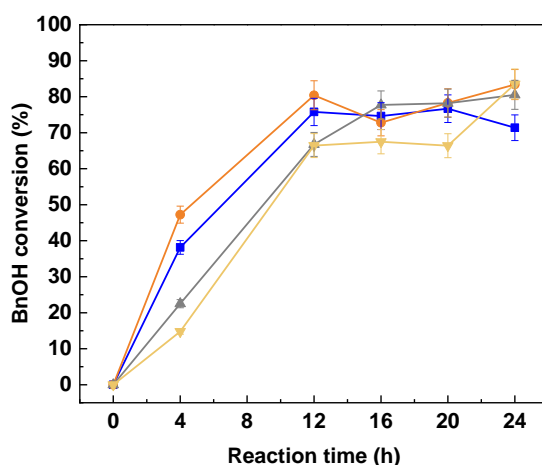
Figure A.4 Kinetic study of BnOH (1 g L^{-1}) oxidation after 4, 12, 16, 20 and 24 hours reaction. Reaction conditions: **G2** recycled glass (Fe: 0.3 wt.%), M:S=1:100, <0.1 (●), 0.1-0.2(●), 0.2-0.5(●) and 0.5-1(●) mm, BnOH:H$_2$O$_2$ molar ratio of 1:2, p = endogenous, 80 °C, 24 h, 500 rpm. 1gL^{-1} BnOH conversion after 4, 12, 16, 20 and 24 hours reaction with four different sizes of **G2** glass, with M:S ratio of 1:100, and molar ratio BnOH:H$_2$O$_2$ of 1:2, at 80 °C.
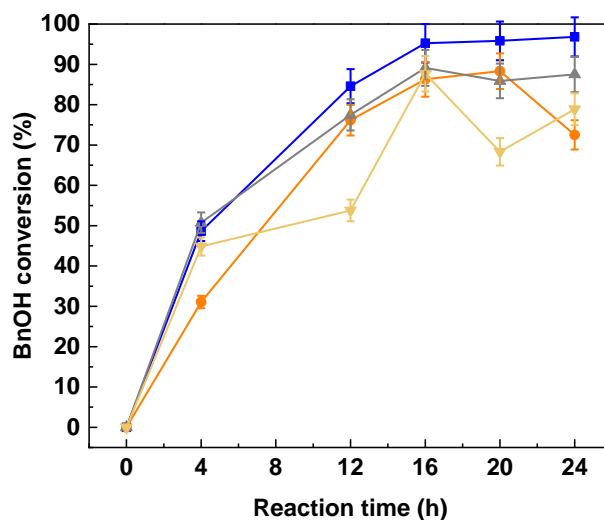
Figure A.5 Kinetic study of BnOH (1 g L^{-1}) oxidation after 4, 12, 16, 20 and 24 hours reaction. Reaction conditions: **G2** recycled glass (Fe: 0.3 wt.%), M:S=1:100, <0.1 (●), 0.1-0.2(●), 0.2-0.5(●) and 0.5-1(●) mm, BnOH:H$_2$O$_2$ molar ratio of 1:4, p = endogenous, 80 °C, 24 h, 500 rpm. 1gL^{-1} BnOH conversion after 4, 12, 16, 20 and 24 hours reaction with four different sizes of **G2** glass, with M:S ratio of 1:100, and molar ratio BnOH:H$_2$O$_2$ of 1:4, at 80 °C.

Appendix

A4.2 Calculation of reaction time for aerobic oxidation

As stirring-bubbling system is a dynamic system, reaction time and flow rate are important factor to consider when design an experiment so that oxygen will not be a limiting reagent.

With the current set-up (25 mL round bottom flask), 8 mL of BnOH water solution (1 g L⁻¹) were used to start the reaction. The minimum reaction time required will be calculated as follows:

If standard conditions and first-order reaction are assumed:

$$Required\ volume\ of\ O_2\ for\ benzyl\ alcohol\ to\ benzaldehyde$$

$$= 0.5 \times \frac{8\ mL \div 1000 \times 1g\ L^{-1}}{108.14\ g\ mol^{-1}} \times 24000\ mL\ mol^{-1}$$

$$= 0.888\ mL$$

$$Max\ volume\ of\ O_2\ can\ dissolve\ in\ 8\ mL$$

$$= \frac{\left(\frac{3}{1000}\right)g\ L^{-1} \times \left(\frac{8}{1000}\right)L}{32\ g\ mol^{-1}} \times 24000\ mL\ mol^{-1}$$

$$= 0.018\ mL$$

$$For\ first\ order\ reaction:$$

$$t\ ^1/_2 = \frac{\ln 2}{1 \times 10^{-3} s^{-1}} = 700\ s$$

$$\approx 12\ min$$

$$t = 24\ min$$

If oxygen can be activated, with the current reaction condition and a flow rate of 5 mL min⁻¹, a minimax of 24 min should be needed. However, based on the previous performance on iron catalyst with pressurized, a longer time such as 4 h was considered for the investigation to make sure that oxygen is not a limiting reagent.